



THE UNIVERSITY
of ADELAIDE

Soil erosion modelling as a tool for future land management and conservation planning

Thesis submitted for the degree of
Doctor of Philosophy

Amelie Jeanneau

School of Biological Sciences
The University of Adelaide

June 2020

Thesis declaration

I certify that this work contains no material which has been accepted for the award of any other degree or diploma in my name, in any university or other tertiary institution and, to the best of my knowledge and belief, contains no material previously published or written by another person, except where due reference has been made in the text. In addition, I certify that no part of this work will, in the future, be used in a submission in my name, for any other degree or diploma in any university or other tertiary institution without the prior approval of the University of Adelaide and where applicable, any partner institution responsible for the joint-award of this degree.

I acknowledge that copyright of published works contained within this thesis resides with the copyright holder(s) of those works.

I also give permission for the digital version of my thesis to be made available on the web, via the University's digital research repository, the Library Search and also through web search engines, unless permission has been granted by the University to restrict access for a period of time.

I acknowledge the support I have received for my research through the provision of an Australian Government Research Training Program Scholarship.

Amelie Jeanneau

June 2020

Acknowledgments

First and foremost, I would like to thank my supervisors Bertram Ostendorf and Tim Herrmann. Thank you for your guidance, encouragements and support throughout these four years. You helped me champion my ideas and develop a research project that was both innovative and highly applicable to current climate and environmental conditions and I am very grateful for this. I would also like to thank all the Spatial Sciences Group members, past and present, and the Oliphant Level 3 residents for their emotional support and guidance. I will always remember all the morning teas, lunches and after-work social events. From day one, I felt welcomed and included, although my French family was far away you helped to keep homesickness at bay.

I would also like to thank Craig Liddicoat, Trevor Hobbs and Giles Forward from the South Australian Department for Environment and Water (DEW) for their supportive ideas at the initial stage of the research and their valuable feedback to improve the quality of this manuscript.

I also wish to extend my gratitude to all my international friends from the University of Adelaide Waite campus. Being far from home is not always easy, but you have been part of my Australian family and provided an essential support system over the last few years.

A very special thanks to my partner Mathieu who encouraged me to pursue a research career, for bravely accompanying me through this journey and for giving me the energy to try my best every single day.

Finally, to my family and friends in France and Europe, thanks for your continuous support and encouragements. I know it would have been difficult to move further away from you, but you have always felt so close to me through this entire journey.

Publications arising from this thesis

Peer review journal articles:

Jeanneau, A., Ostendorf, B., Herrmann, T. (2019). Relative spatial differences in sediment transport in fire-affected agricultural landscapes: A field study. *Aeolian research* 39, 13-22, <https://doi.org/10.1016/j.aeolia.2019.04.002>

Articles written for publication:

Jeanneau, A., Herrmann, T., Ostendorf, B. (2020). Mapping the spatio-temporal variability of hillslope erosion with the G2 model and GIS: A case-study of the South Australian agricultural zone.

Jeanneau, A., Herrmann, T., Ostendorf, B. (2020). Assessing the spatio-temporal variability of extreme erosion events with a novel wind erosion model and GIS: A case-study of the South Australian agricultural zone.

Jeanneau, A., Herrmann, T., Ostendorf, B. (2020). An integrated modelling approach to estimate post-fire soil erosion by wind and water in the South Australian agricultural zone.

Conference presentations:

Jeanneau, A., Herrmann, T., Ostendorf, B., (2019). Climate change and soil security: An erosion modelling story. In, *23rd International Congress on Modelling and Simulation 2019*. Canberra, Australia

Jeanneau, A., Herrmann, T., Ostendorf, B., (2018). Once the dust settles – Assessing wind erosion after bushfires. In, *National Soils Conference 2018*. Canberra, Australia

Jeanneau, A., Herrmann, T., Ostendorf, B., (2018). Where has the soil gone? Soil erosion modelling case-study in agricultural landscapes of South Australia. In, *NRM Science Conference 2018*. Adelaide, Australia

“All models are wrong, but some are useful. The practical question is how wrong do they have to be to not be useful?”

Georges Box

Abstract

Maintaining future agricultural productivity and ensuring soil security is of global concern and requires evidence-based management practices. Moreover, understanding where and when land is at risk of erosion is a fundamental step to combatting future soil loss and reach Land Degradation Neutrality (LDN). However, this is a difficult task because of the high spatial and temporal variability of the controlling factors involved. Therefore, tools investigating the impact and frequency of extreme erosive events are crucial for land managers and policymakers to apply corrective measures for better erosion management in the future.

While the utility of using wind and water erosion models for management is well established, there is a paucity of work on the impact of climate change and extreme environmental conditions (e.g. wildfires) on soil erosion by wind and water simultaneously. Both erosion types are controlled by different environmental variable that vary highly in space and time. Therefore, the overarching aim of this study was to develop a joint wind-water erosion modelling method and demonstrate the utility of this approach to identify (1) the spatio-temporal variability of extreme erosion events in the South Australian agricultural zone (Australia) and (2) assess the likely increase of this variability in the face of climate change and the recurrence of wildfires.

To fulfil the aim of the research project, we adapted two state-of-the-art wind and water (hillslope) erosion models to integrate modern high-resolution datasets for spatial and temporal analysis of erosion. The adaptation of these models to local conditions and the use of high-resolution datasets was essential to ensure reliable erosion assessment.

First, we applied these models separately in the Eyre Peninsula and Mid-North agricultural regions. We evaluated the spatio-temporal variability of extreme erosion events between 2001 and 2017 and described the complex interactions between each erosional process and their influencing factors (e.g. soil types, climate conditions, and

vegetation cover). Hillslope erosion was very low for most of the Eyre Peninsula; however, a large proportion of the central Mid-North region frequently recorded severe erosion ($> 0.022 \text{ t ha}^{-1}$) two to three months per year, for most of the years in the time-series. The most severe erosion events were primarily driven by topography, low ground cover ($< 50\%$) and extreme rainfall erosivity ($> 500 \text{ MJ mm ha}^{-1} \text{ h}^{-1}$). Average annual wind erosion was very low and comparable in the two regions. Nonetheless, most of the west coast of the Eyre Peninsula frequently registered severe erosion ($> 0.000945 \text{ t ha}^{-1}$ or 0.945 kg ha^{-1}) two to three months per year, for most of the years. The most severe erosion events were largely driven by the soil type (sandy soils), recurring low ground cover ($< 50\%$) and extreme wind gusts ($> 68 \text{ km h}^{-1}$). We identified that erosion severity was low for the vast majority of the study area, while 4% and 9% of the total area suffered severe erosion by water and wind respectively, demonstrating an extreme spatial and temporal skewness of soil erosion processes.

Then we combined the modelling outputs from the wind and water erosion models and tested the models' response to major wildfire events. This research demonstrated how erosion modelling could be used to predict the impact of severe wildfire events on soil erosion. The two models satisfactorily captured the spatial and temporal variability of post-fire erosion. However, a very small fraction of the region (0.7%) was severely impacted by both wind and water erosion. We observed that soil erosion increased immediately after the wildfires or within the first six months for the ten fire-affected regions. For three of the wildfire events, the models showed an increase in wind and water erosion in consecutive months or at the same time. These results highlighted the importance to consider wind and water erosion simultaneously for post-fire erosion assessment in dryland agricultural regions.

Finally, we had the rare opportunity to assess the impact of a catastrophic wildfire event on wind erosion in an agricultural landscape by examining the influence of unburnt stubble patches on adjacent burnt or bare plots using a spatio-temporal sampling design. The field study allowed a quantitative assessment of spatial and temporal patterns of

wind erosion and sediment transport after a catastrophic wildfire event. It showed very high levels of spatial variability of erosion processes between burnt and bare patches and demonstrated how measuring field-scale sediment transport could complement fine-scale experimental studies to assess environmental processes at the field scale.

This research highlights the utility of erosion models to inform corrective measures for future land management. We have implemented tools that allow a realistic assessment of the influence of climate change and extreme environmental conditions scenarios on soil erosion for a wide range of land cover over large regions. Here, the models enabled the identification of the relative post-fire wind or water erosion risk in dryland agricultural landscapes, making them particularly useful for land management under future uncertainty. Spatial patterns compared well with previous modelling approaches and underpinned the benefit of erosion models to assess spatial differences in erosion risk and evaluate corrective measures at the regional scale. However, modelled soil erosion magnitudes strongly depend on how the influence of soils is implemented in the models, making it difficult to set absolute quantitative soil loss targets for land management.

The thesis has provided a proof of concept of the approach for South Australia. However, all input data can be freely sourced Australia-wide and similar dataset are available globally.

Table of Contents

Thesis declaration	i
Acknowledgments.....	iii
Publications arising from this thesis.....	v
Abstract.....	ix
List of Figures	xviii
List of Tables.....	xxii
Chapter 1	1
1.1 Introduction:	3
1.2 The processes	4
1.2.1 Water erosion	5
1.2.2 Wind erosion	6
1.2.3 The interaction of wind and water erosion.....	7
1.2.4 The influence of fires on erosion	8
1.3 Erosion modelling.....	10
1.3.1 Water erosion models.....	10
1.3.2 Wind erosion models.....	12
1.3.3 Integrated/Combination models.....	14
1.3.4 Post-fire erosion modelling	15
1.4 Aims and objectives of the project	18
1.5 Thesis structure.....	19
1.6 References	20
Chapter 2.....	35
Abstract	39

2.1	Introduction	39
2.2	Methods.....	43
2.2.1	The study area.....	43
2.2.2	Description of the data sources	45
2.2.3	The hillslope erosion model.....	47
2.3	Results and Discussion.....	56
2.3.1	Spatial variability of hillslope erosion	56
2.3.2	Temporal variation in hillslope erosion	58
2.3.3	Predicted hillslope erosion and “tolerable” soil loss.....	61
2.3.4	Comparison with previous soil erosion studies.....	63
2.4	Conclusions and further studies.....	65
2.5	References	67
	Appendix A.....	73
	Appendix B.....	75
	B.1 Introduction.....	75
	B.2 The effect of different rainfall time series on rainfall erosivity across South Australia	78
	B.2.1 Temporal aggregation types of rainfall time series and definition of rainfall events	78
	B.2.2 The effect of temporal aggregation types of rainfall time series on rainfall erosivity estimation	81
	B.3 References	84
	Appendix C.....	85
	C.1 Introduction.....	85

C.2 Testing of the Panagos et al. (2014) assumption to estimate the very fine sand fraction	86
C.2.1 The comparison datasets and testing methods	86
C.2.2 Results from the regression analysis.....	87
C.2.3 Comparison of the assumptions from Panagos et al. (2014) and the regression analysis results	88
C.3 References.....	90
Appendix D	91
D.1 The modelling parameters	91
D.2 Comparison of the modelled outputs with other modelling examples	96
D.3 References.....	97
Chapter 3.....	100
Abstract	104
3.1 Introduction	105
3.2 Methods.....	107
3.2.1 The study area.....	107
3.2.2 Description of the data sources	109
3.2.3 Modelling methods.....	110
3.2.4 Comparison of the wind erosion severity with the frequency of dust storms	
114	
3.2.5 Analysis of the model results	115
3.3 Results	116
3.3.1 Spatial variability of wind erosion.....	116
3.3.2 Temporal variability of wind erosion	121

3.3.3	Wind erosion influencing factors	124
3.3.4	Wind erosion and land use	127
3.4	Discussion	128
3.4.1	Comparison of the wind erosion model with the frequency of dust storms 128	
3.4.2	The model's response	130
3.4.3	Assessing the temporal variability in erosion.....	132
3.4.4	Regional land management	132
3.5	Conclusion.....	134
3.6	References	136
Chapter 4	143
Abstract	147
4.1	Introduction	148
4.2	Methods.....	152
4.2.1	The study area.....	152
4.2.2	Description of the data sources	154
4.2.3	The water erosion model	156
4.2.4	The wind erosion model	157
4.2.5	Description of the fire events.....	159
4.2.6	Analysis of the model results	161
4.3	Results	162
4.3.1	Spatial distribution of water and wind erosion	162
4.3.2	The impact of fires on erosion	165
4.3.3	Using AOD measurements for post-fire wind erosion monitoring	169

4.4	Discussion	170
4.4.1	The performance of the models	170
4.4.2	The opportunity of using AOD datasets for wind erosion monitoring.....	171
4.4.3	The implication of predicted soil erosion severity for land management..	172
4.5	Conclusion.....	173
4.6	References	174
Appendix E.....		183
Chapter 5.....		187
Abstract		191
5.1	Introduction	191
5.2	Material and Method.....	193
5.2.1	Site description	193
5.2.2	Monitoring design	195
5.2.3	Sediment analysis	197
5.3	Results.....	200
5.3.1	Meteorological conditions and surface cover	200
5.3.2	Spatial distribution of sediment flux.....	201
5.3.3	Factors influencing horizontal sediment flux.....	203
5.4	Discussion	206
5.5	Conclusion.....	208
5.6	References	210
Chapter 6.....		216
6.1	Key findings.....	219
6.2	Significance and broader implications.....	222

6.3	Key assumptions and limitations	223
6.4	Future research and general recommendations	224
6.5	References	227

List of Figures

Figure 1.1 Schematic diagram of the position of sheet, rill, and gully erosion on a simple hillslope system. Source: FAO (2019).	6
Figure 1.2 Schematic showing the physical processes influencing wind erosion and dust emissions. Source: Webb et al. (2017).....	7
Figure 1.3 Hypothesized trends of potential sediment transport capacity as a function of mean annual precipitation to highlight the potential total sediment transport for undisturbed environments. Adapted from Field et al. (2009)	8
Figure 1.4 a) Concept representation of the sheltering effect of vegetation from Raupach et al. (1993), b) concept of the shadow effect of vegetation proposed by Chappell et al. (2010) to derive vegetation structure from remote sensing. Source: Chappell et al. (2010).	14
Figure 2.1 Location map and presentation of the study area (Eyre Peninsula & Mid-North) within the South Australian agricultural zone.....	44
Figure 2.2 Land use classes for the Eyre Peninsula and Mid-North regions. Source: ABARES (2016).....	45
Figure 2.3 Dominant soil texture classes for the Eyre Peninsula and Mid-North regions. Source: DEW (2016).....	45
Figure 2.4 Modelled mean annual erosion severity across the Local Government Areas (LGA) of the Eyre Peninsula and Mid-North estimated with the G2 model. The LGAs represent a combination of environmental conditions, topography, climate with slightly different rainfall patterns and different farming systems.	56
Figure 2.5 Modelled average annual hillslope erosion per Local Government Area (LGA). The horizontal lines represent the regional average annual soil loss (Eyre Peninsula = $0.048 \text{ t ha}^{-1} \text{ yr}^{-1}$ – Mid-North = $0.114 \text{ t ha}^{-1} \text{ yr}^{-1}$).....	58
Figure 2.6 Temporal distribution of regional modelled annual hillslope erosion for the Eyre Peninsula and Mid-North region. The dashed line represents the Australian tolerable soil loss threshold of $0.2 \text{ t ha}^{-1} \text{ yr}^{-1}$ (source: Bui et al. (2011)).	59
Figure 2.7 Temporal distribution of predicted regional monthly hillslope erosion grouped by months between 2001 and 2017 for the Eyre Peninsula and Mid-North region.	60
Figure 2.8 Monthly percent distributions (ratio to total annual value) of modelled hillslope erosion (Erosion) and rainfall erosivity (Erosivity), compared with average monthly ground cover (Ground Cover), from 2001 to 2017 for the Eyre Peninsula and Mid-North region.....	61
Figure 2.9 Frequency distribution of predicted annual hillslope erosion above $0.2 \text{ t ha}^{-1} \text{ yr}^{-1}$	62
Figure 2.10 New predicted hillslope erosion severity map corroborated with the DEW inherent soil erosion susceptibility map. Note that the areas in grey represent zones where the classification of the DEW map did not overlap with the G2 model.....	65
Figure A.1 The BARRA domain map. The outer dashed outline represents the BARRA-R regional domain at 12km resolution. The inner solid lined domain represents the downscaled regional subdomains available	

at a spatial resolution of 1.5km. The regional subdomains are centred over some major cities of Australia, such as Perth, Adelaide, Hobart and Sydney.....	74
Figure B.1 Location of rain gauges within South Australia. Size of dots represents rainfall amount	76
Figure B.2 Mean annual rainfall of automatic rain gauges (full-quality-controlled daily data) compared with high-temporal pluviography data and BARRA rainfall extracts for time-periods after quality filtering	77
Figure B.3 Average number of rainfall periods per year, defined by Renard et al. (1997) as continuous periods of low rainfall < 0.13mm (0.05 in) during a period of 6 hours. Event numbers extracted from pluviographs and BARRA ('Type 3') are shown over reference pluviograph data at 30 minutes ('Type 2')..	81
Figure B.4 Evaluating the effect of rainfall aggregation on rainfall erosivity ($\text{MJ mm ha}^{-1} \text{h}^{-1} \text{yr}^{-1}$) for 47 rain gauges across South Australia.	82
Figure B.5 Evaluating the effect of rainfall aggregation on rainfall Erosivity ($\text{MJ mm ha}^{-1} \text{h}^{-1} \text{yr}^{-1}$). The x-axis represents mean annual rainfall erosivity of 41 stations in South Australia estimate from hourly gauge data and BARRA, respectively.....	82
Figure B.6 Comparison of patterns of erosivity when using 'Type 3' (Renard et al. (1997) definition of a storm event) and 'Type 4' (3-hour storm events) temporal rainfall aggregations.	83
Figure B.7 Evaluating the difference between rainfall Erosivity ($\text{MJ mm ha}^{-1} \text{h}^{-1} \text{yr}^{-1}$) using different rainfall data sources and temporal aggregation types. The x-axis represents the mean annual rainfall erosivity using 30-minute intensities from pluviograph data. BARRA 'Type 4' data has been used in this publication.	84
Figure C.1 Very fine sand fractions estimated with three regression analysis methods plotted against observed very fine sand fractions. The three methods are simple linear regression (Linear), simple linear regression with no intercept (Linear – no intercept), and second order polynomial regression (Polynomial).....	8
	8
Figure C.2 Soil erodibility factor (S) with the assumption of Panagos et al. (2014): %Very fine sand = 0.2 x %Total sand; and new Australian assumption: %Very fine sand = 0.44 x %Total sand.....	89
Figure 3.1 Location map and presentation of the study area (Eyre Peninsula & Mid-North) within the South Australian cropping region.	108
Figure 3.2 Land-use classes for the Eyre Peninsula and Mid-North regions. Source: ABARES (2016)....	109
Figure 3.3 Dominant soil texture classes for the Eyre Peninsula and Mid-North regions. Source: DEW (2016).....	109
Figure 3.4 a) Concept representation of the sheltering effect of vegetation from Raupach et al. (1993), b) concept of the shadow effect of vegetation proposed by Chappell et al. (2010) to derive vegetation structure from remote sensing. Source: Chappell and Webb (2016).....	111
Figure 3.5 Local Government Areas (LGA) represent a combination of environmental conditions, topography, climate with slightly different rainfall patterns and diverse farming systems.	116
Figure 3.6 Average annual soil loss per Local Government Area. The horizontal lines represent the regional average annual soil loss (Eyre Peninsula = $0.00258 \text{ t ha}^{-1} \text{y}^{-1}$ – Mid-North = $0.00243 \text{ t ha}^{-1} \text{y}^{-1}$).	117

Figure 3.7 Frequency of monthly erosion rate above 0.000945 t ha ⁻¹	118
Figure 3.8 Frequency of severe monthly erosion (> 0.000945 t ha ⁻¹) for each year in the study period. .	120
Figure 3.9 Long-term mean annual erosion rates in the Eyre Peninsula and Mid-North regions estimated from the “albedo” Wind Erosion Model.	121
Figure 3.10 Temporal distribution of monthly erosion records. Each data point represents the monthly soil loss for a single-pixel location grouped by month. The box-plots demonstrate high inter- and intra-seasonal variability.	122
Figure 3.11 Temporal distribution of annual soil loss. Each data point represents the annual soil erosion for a single-pixel location grouped by year. The box-plots demonstrate high inter- and intra-annual variability.....	123
Figure 3.12 Effect of wind speed and ground cover on daily soil erosion for the Eyre Peninsula and the Mid-North regions. The figure displays the proportion of daily erosion records (pixels) within each combination of wind speed and ground cover percentile classes for the entire space-time array (17 years of daily erosion records).These diagrams demonstrate that environmental conditions leading to erosion were very different for the two regions.	125
Figure 3.13 Effect of wind speed and ground cover on daily soil erosion for the Eyre Peninsula and the Mid-North regions. The figure displays the proportion of daily erosion records (pixels) within each combination of wind speed and ground cover percentile classes when selecting the most severe of daily erosion rates (> 61.9 g ha ⁻¹ day ⁻¹). These diagrams demonstrate that that high erosion events consistently occurred at high wind speed with a large range of ground cover levels.....	126
Figure 3.14 Long-term average annual wind erosion for the major agricultural land uses compared with natural environments.	128
Figure 3.15 Mean annual frequency of dust storms for the Eyre Peninsula and Mid-North regions derived from the MODIS MAIAC daily Aerosol Optical Depth (AOD) product (AOD > 0.3).	129
Figure 3.16 New erosion severity map corrected with MODIS MAIAC daily Aerosol Optical Depth (AOD) dataset. Note that the areas in grey represent zones where the classification of the AOD did not overlap with the “albedo” Wind Erosion Model.	130
Figure 4.1 Location map and presentation of the study area (Eyre Peninsula & Mid-North) within the South Australian cropping region.	153
Figure 4.2 Land-use classes for the Eyre Peninsula and Mid-North regions. Source: (ABARES, 2016) ..	153
Figure 4.3 Dominant soil texture classes for the Eyre Peninsula and Mid-North regions. Source: DEW (2016).	154
Figure 4.4 a) Concept representation of the sheltering effect of vegetation from Raupach et al. (1993), b) concept of the shadow effect of vegetation proposed by Chappell et al. (2010) to derive vegetation structure from remote sensing. Source: Chappell and Webb (2016)	157

Figure 4.5 Fire location map for the Eyre Peninsula and the Mid-North region. All the fire scar inserts are displayed at the same scale and the reference scale bar is located in the Wangary insert (bottom-left corner).	160
Figure 4.6 Modelled average annual water erosion severity (2001-2017)......	163
Figure 4.7 Modelled average annual wind erosion severity (2001-2017)......	164
Figure 4.8 Spatial distribution of the predicted most severe soil erosion classes (top decile) in the Eyre Peninsula and Mid-North regions and dominant erosion process.	165
Figure 4.9 Modelled monthly water erosion change for months m_0 (start of the fire) to $m + 6$ for each fire event. The y-axis represents the percent change in erosion for the month m_j compared to monthly averages. Bar graphs over the dotted line = increase in erosion compared to monthly averages, bar graphs below the dotted line = decrease in erosion compared to monthly averages.	167
Figure 4.10 Modelled monthly wind erosion change for months m_0 (start of the fire) to $m + 6$ for each fire event (bar graphs) and change in dust days from MODIS MAIAC (red dots). The y-axis represents the percent change in erosion for the month m_j compared to monthly averages. Bar graphs over the dotted line = increase in erosion compared to monthly averages, bar graphs below the dotted line = decrease in erosion compared to monthly averages.	168
Figure 5.1 Location map and extent of the Sherwood fire, Sherwood, South Australia. The imagery was sourced from the European Space Agency (ESA) Copernicus – Sentinel 2 imagery, 03 February 2018. Within the fire boundary, darker colours represent charred vegetation; lighter cream colour represents exposed bare sands. Sand drifts can be observed predominantly in the south-eastern corner of fire extent.	194
Figure 5.2 Dust samplers in the field, a) sediment sampler on unburnt wheat stubble, b) sediment sampler on the burnt bare ground, c) lower collecting cups filled with deposited sediment.	195
Figure 5.3 Experimental layout showing the spatial distribution of sampling masts and the position of the vegetation transects.	197
Figure 5.4 Wind roses representing wind speed and direction for the study area. a) collection weeks 1-3, b) collection weeks 4-6, c) collection weeks 7-9. Note the different frequency scale for collection week 7-9.	200
Figure 5.5 Vertically averaged horizontal sediment flux spatial distribution maps. a) collection weeks 1-3, b) collection weeks 4-6, c) collection weeks 7-9. The dots represent the MWAC dust sampler, and the two virtual sampling grids are outlined in grey.	202
Figure 5.6 Mean horizontal sediment flux for the study at a) 10cm, b) 25cm, c) 50cm and d) 85cm sampling height. The purple dots represent the position of each MWAC dust samplers. Note large differences in sediment flux with height as indicated by different colour scales, ranging from 0 to maximum value.	203
Figure 5.7 Observed horizontal sediment flux distribution with sampling distance from the burnt-unburnt boundary. 95% confidence interval of the LOESS regressions are shown as shaded grey bands.	204
Figure 5.8 Mean horizontal sediment flux derived from modelled estimated marginal means for the three collection periods on burnt and unburnt plots. Estimates are based on log-scale predictions from the model.	206

List of Tables

Table 2.1 Indicative examples of the conversion of EPM conservation coefficients into LU values. Source: Panagos et al. (2014a).....	50
Table 2.2 Correspondence table between the SA Land Cover dataset and the look-up table of Karydas and Panagos (2016, 2018)	51
Table 2.3 Soil permeability codes for corresponding soil hydraulic conductivity	52
Table 2.4 Constant values for $\xi_{i,j}$ parameter	54
Table 2.5 Modelled hillslope erosion severity classes and their area percentages for the study area.	57
Table 2.6 Comparison between G2 erosion estimates and previous studies conducted in South Australia	64
Table B.1 Sample calculations of storm EI (translated to metric from Renard et al. (1997), page 334. Total storm EI: 465 MJ mm ha ⁻¹ h ⁻¹ (“Type 1”)	79
Table B.2 Sample calculation for storm EI using regular 30-minute intervals. The example rainfall mimics the original example from Renard et al. (1997) (“Type 2”). Total storm EI: 417 MJ mm ha ⁻¹ h ⁻¹	80
Table B.3 Sample calculation for storm EI using regular 60-minute intervals, aggregated from table B2. This type of rainfall data is defined as “Type 3”. Total storm EI: 191 MJ mm ha ⁻¹ h ⁻¹	80
Table B.4 Sample calculations illustrating the approach taken here for BARRA hourly data defining each 3-hour period as an event (“Type 4”). Total storm EI: 191 MJ mm ha ⁻¹ h ⁻¹	80
Table C.1 Particle size analysis for a range of soil samples collected from the literature. *Note that the very fine sand content (%) is generally part of the fine sand fraction when estimating the total sand fraction..... Error! Bookmark not defined.	
Table C.2 Results from the regression analysis.....	88
Table D.1 Error matrix comparing the agreement (overlapping area in %, values in bold denote agreement) between wind erosion severity classes from the G2 model and the inherent water erosion potential.....	97
Table 3.1 Error matrix comparing the agreement (overlapping area in %, values in bold denote agreement) between wind erosion severity classes from the “albedo” Wind Erosion Model and the mean annual frequency of dust storms derived from the MODIS MAIAC daily Aerosol Optical Depth (AOD) product (AOD > 0.3).	129
Table 4.1 Description of the wildfire events used in the analysis.	159
Table 4.2 Modelled hillslope erosion severity classes by total land area.	164
Table 4.3 Modelled wind erosion severity classes by total land area.	164
Table 5.1 Summary of the soil surface conditions and vegetation states for the burnt and unburnt study plots, based on measurements collected	202

Table 5.2 Estimated effect of experimental variables on sediment transport, obtained from linear mixed-modelling and Anova Wald Chi-square test, type II. 205

Table E.1 Zonal stats results post-fire. The values in bold represent an increase in erosion compared to monthly averages. 183

Chapter 1

Introduction

1.1 Introduction:

Soil erosion is a natural process part of the soil and landscape formation; however, human activities have dramatically accelerated this phenomenon with the increasing removal of vegetation cover, expansion of farming onto marginal lands and overgrazing (Borrelli et al., 2017). According to FAO, soil erosion is the greatest challenge for sustainable soil management today (FAO, 2019). Soil erosion is of global concern because of its direct negative impact on ecosystem services, agricultural productivity and soil security. Local soil removal, generated by wind or water, induces the loss of fertile topsoil, containing vital nutrients and soil organic carbon, which further decreases soil fertility and ecosystem functions. On a larger scale, particles displaced by erosion can lead to pollution of water bodies through nutrient leaching, sedimentation of reservoirs and air pollution where airborne dust can lead to respiratory diseases (Flanagan et al., 2013).

Vegetation and ground cover are one of the most important controlling factors against erosion. However, changes in climate conditions and land uses have a direct impact on land cover and thus on soil erosion risk. A limited soil cover reduces protection against erosive forces such as rainfall and wind, and exposed soils become more susceptible to erosion. With the growing influence of climate change, soil erosion is expected to increase in frequency and severity in dryland regions of the world (Edwards et al., 2019; Nearing et al., 2004), and compound events are already major drivers of soil losses in Australia (Earl et al., 2019). With drier weather conditions, we are currently experiencing a reduction in soil cover and an increase in the number of extreme erosional events (Leys et al., 2018; Speer, 2013). 2019 was a record-breaking year for extreme environmental conditions around the globe (ECMWF, 2020; World Meteorological Organisation, 2019). As a result in Australia, low ground cover, dry conditions and strong wind gusts led to record-breaking frequencies of dust storms across the country (ABC News; DustWatch Australia). Scientists also predict a recurrence in such events with decreasing rainfall amounts (Edwards et al., 2019; Leys et al., 2018).

Current climate forecasts for Australia are predicting a reduction in annual rainfall, but more extreme precipitation events for dryland agricultural regions (CSIRO and Bureau of Meteorology, 2015). A recurrence in extreme precipitation events combined with low ground cover will potentially increase the risk of soil detachment and runoff. Drier overall conditions will also increase the risk of fire weather in the future (Bento-Gonçalves et al., 2012; Clarke et al., 2011; Williams et al., 2009). Fires have an adverse impact on soil erosion as they remove soil cover (vegetation and litter) and can modify the structure of the top-soil (e.g. water repellence). Therefore, an increase in fire risk will likely increase the risk of soil erosion as well. Future climate trends in low rainfall regions may also cause aeolian processes to be more prevalent than fluvial ones leading to more dust production (Field et al., 2011b). While dust storms are common in the Australian rangelands and grazing zone (Cattle, 2016; Shao et al., 2007) land-use intensification in the Australian cropping belt can also lead to increased dust emissions (Young and Herrmann, 2015).

Soil erosion processes have been well described through extensive fieldwork with wind tunnels, runoff plots, and sediment trough. A wide range of models have been developed to characterise and predict the extent and severity of erosion using the understanding of empirical processes from experimental data. The current erosion models differ in their applications based on the spatial or temporal scale of interest, region of the world and data availability. These models are extensively used by governments and decision-makers for policy development.

1.2 The processes

Soil erosion is a natural phenomenon contributing to the evolution of landscapes, characterised by the displacement of particles from the upper layer of soil, and can be induced by rainfall or wind (Lu et al., 2003). Erosion is influenced by soil properties, topography, vegetation cover, weather conditions, and land use/land management (Montgomery, 2007).

Soil weathering, whether it is wind- or water-induced, impacts the uppermost topsoil layer (upper 20 to 40 cm of the topsoil, called A-horizon). This layer stores the water available to plants and accumulates and cycles most of the vital nutrients for plant growth. If the A-horizon layer is reduced, even by a small fraction (few centimetres), this will lead to significant declines in agricultural productivity (Bui et al., 2011); therefore, the cost of production will be rising (Boardman, 2006). This assumption is particularly accurate for low rainfall regions where scarce water resources, often poor soil fertility and a thin A-horizon layer make agriculture more challenging. Hence the study of soil erosion in such areas represents a great interest for governmental agencies as well as the farming community.

1.2.1 Water erosion

Soil loss due to water erosion (from rainfall and surface runoff) is a one-dimensional process. Particles detached by raindrops are transported downhill by overland flow (sheet - interrill erosion) which form small and ephemeral concentrated flow paths (rill or channel erosion) and are deposited when the velocity of the flow decreases (Figure 1.1). These eroded channels, can later grow and develop into gullies from repeated runoff cycles and weathering of the drainage side walls (Vrieling, 2006). Water erosion and runoff remove fertile topsoil leading to a decline in nutrients, organic matter and soil carbon. These nutrients can either be deposited in nearby fields, thus enrich them, or be carried away until they reach rivers or reservoirs where nutrient leaching can lead to eutrophication. Sedimentation of reservoirs can also be a significant off-site consequence of water erosion, leading to a reduction of storage capacity and an increase in clean-up costs (Nearing et al., 2017). Water erosion is not considered as a reversible process because once the sediments are removed and transported downslope, they cannot be returned to their original location.

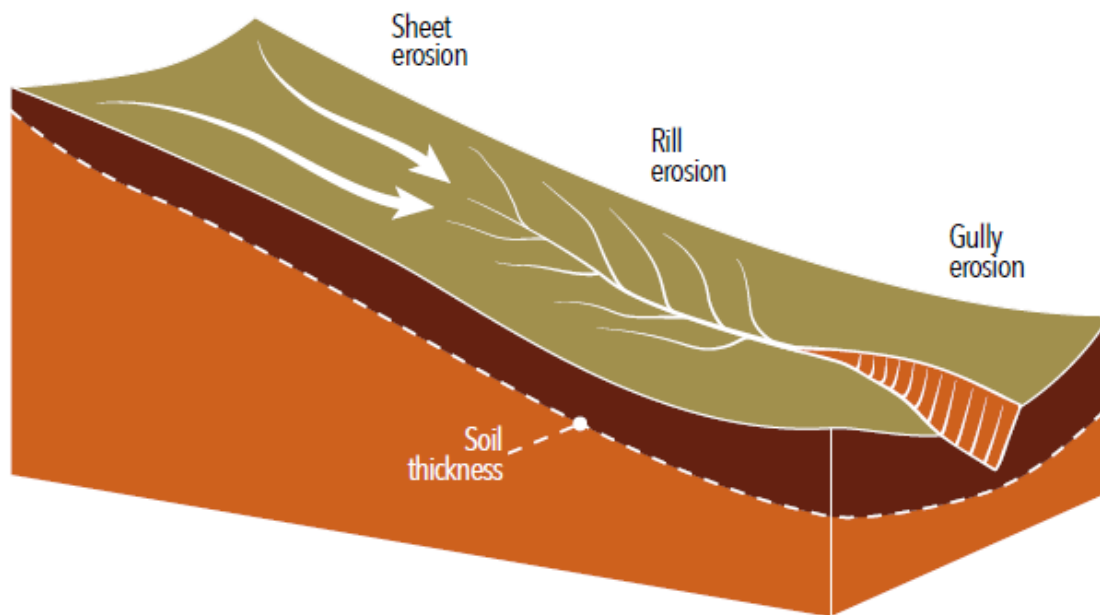


Figure 1.1 Schematic diagram of the position of sheet, rill, and gully erosion on a simple hillslope system. Source: FAO (2019).

1.2.2 Wind erosion

Wind erosion, on the other hand, is a two-dimensional process and does not necessarily lead to observable erosion features. Soil particles are conveyed in both vertical and horizontal directions, and sediment transport is omnidirectional as airborne material can be transported in all wind directions. As the wind sweeps the earth, coarser particles roll on the surface (saltation, creep) while finer particles like sands and clays are removed and transported vertically from one location and deposited away to another (horizontal displacement) (Figure 1.2). Even finer particles, such as clays and silts, are transported further and farther and generally remain in suspension in the air. When aggregated, these particles form dust clouds which can travel over very large scales and even across the globe (Field et al., 2009). As a result of erosion, coarse sand particles can damage crops and infrastructure through sandblasting and burial (Bennell et al., 2007; Panebianco et al., 2016), while fine particles suspended in the air (clays and silts), highly concentrated in vital nutrients, are depleting soils and reducing agricultural productivity (Tozer and Leys, 2013). Wind erosion, and more particularly dust storms, can also lead

to visibility reduction and damages to human health (respiratory conditions) (Baddock et al., 2014; Li et al., 2018; Seinfeld and Pandis, 2012). In some instances, wind erosion can be considered reversible as sediments and particles transported in one direction, can be re-deposited another time if the wind blows in the opposite direction. However, this does not resolve the problem of erosion of vital nutrients in the first place.

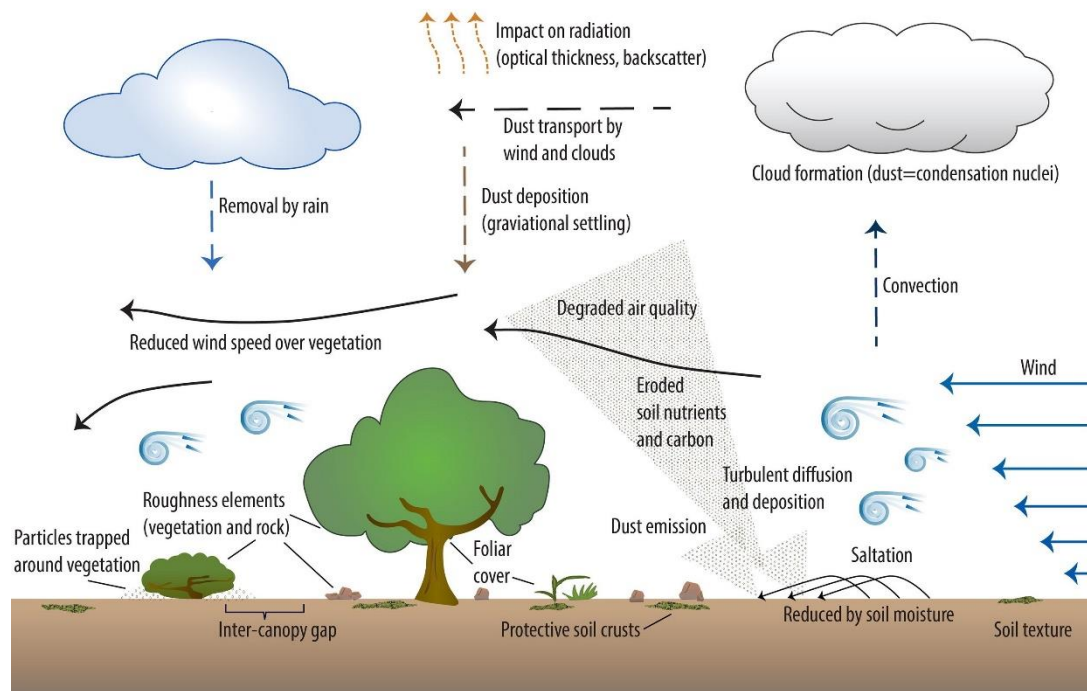


Figure 1.2 Schematic showing the physical processes influencing wind erosion and dust emissions. Source: Webb et al. (2017)

1.2.3 The interaction of wind and water erosion

Wind and water erosion affect a large proportion of arable lands around the globe (FAO, 2019; Field et al., 2009), and their combined effect can substantially contribute to total erosion rates in most dryland ecosystems (Field et al., 2011b). Depending on the regional climate, sediment transport capacity can be dominated by one process or the other. However for low rainfall regions, both phenomena are thought to co-exist (Figure 1.3), and these interactions can often go beyond the limit of the dryland ecosystem; therefore, increasing the need to consider the two erosional processes simultaneously. For instance, sediments transported by water in lake beds or floodplains

could be redistributed by wind over long distances during drier months, which could subsequently be carried again further by wind or water (Field et al., 2011b).

Although a growing body of research has compared the absolute and relative magnitude of wind and water erosion processes (Breshears et al., 2003; Du et al., 2016; Field et al., 2011a; Jiang et al., 2019; Wang et al., 2014), these two are generally studied individually (Belnap et al., 2011; Flanagan et al., 2013; Panagos et al., 2018). From these studies, significant uncertainty remains on the relative degree of wind and water erosion in dryland ecosystems and how the two processes interact in such environments. There is also ongoing uncertainty on how the interaction between the two processes changes with scale, and to what extent (Field et al., 2009; Field et al., 2011b). Moreover, integrated modelling approaches considering both processes simultaneously are still lacking (Flanagan et al., 2013).

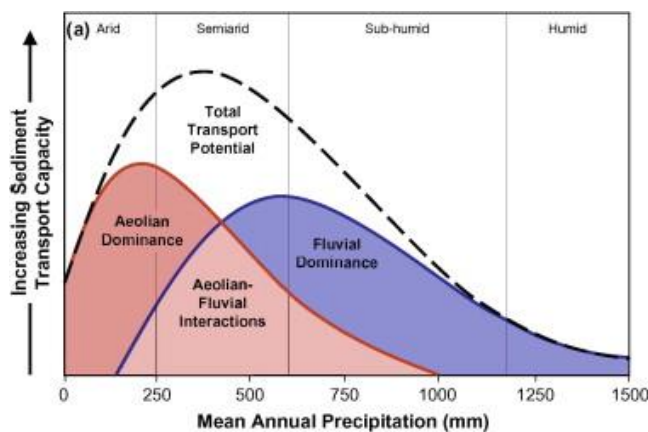


Figure 1.3 Hypothesized trends of potential sediment transport capacity as a function of mean annual precipitation to highlight the potential total sediment transport for undisturbed environments. Adapted from Field et al. (2009)

1.2.4 The influence of fires on erosion

Dryland ecosystems are highly sensitive to environmental disturbances (e.g. droughts, overgrazing, fires) which can dramatically increase soil erosion susceptibility. Out of these disturbing agents, wildfires are of particular concern because they are unpredictable, reduce or remove the protective ground cover, and can modify soil structure, thus increasing post-fire erosion risk.

With the reduction in aboveground biomass, raindrop kinetic energy is not captured by vegetation anymore which increases the splash impact, thus detaching more sediments and making them available for transportation (Lu et al., 2016). Under undisturbed conditions, above-ground biomass can trap sediments and soil particles, thus providing a protective barrier against weathering elements (e.g. wind and rainfall). However, the removal of vegetation by wildfires accelerates water runoff and reduces surface shear stress, therefore increasing soil erosion risk.

Fires can significantly impact soil structure. The destruction of organic and chemical bonds between soil particles and aggregates by wildfires can increase soil surface erodibility (Prats et al., 2016; Varela et al., 2010). Water repellence is also a significant driver of post-fire erosion (Neary, 2011; Shakesby, 2011) as it decreases water infiltration in the soil (DeBano and Neary, 2005). Therefore, a reduced water infiltrability will lead to more runoff events while a reduced soil particle cohesion will favour aeolian sediment transport.

Wildfires are likely to be more frequent and more intense for dryland agricultural regions (Clarke et al., 2011; Gonçalves et al., 2011) and drought conditions more recurrent in the future (CSIRO and Bureau of Meteorology, 2015). Therefore, soil erosion by wind or water is likely to increase too. With the recurrence in wildfires, soil surface will be more frequently exposed to commonly occurring storms, but it will also increase the probability that soils susceptible to erosion by wind or water will remain vulnerable when less frequent high-intensity events occur (Edwards et al., 2019). This information is of particular interest for dryland agricultural regions, where both aeolian and fluvial processes influence landscape formation, as wind and water erosion can be observed simultaneously or sequentially within months following major wildfire events (Shakesby et al., 2007; Shillito et al., 2012). The loss of fertile topsoil might also become more problematic if large fires are followed by drought conditions as vegetation and ground cover will take longer to recover leaving soils exposed for longer.

1.3 Erosion modelling

Environmental models can be considered as quantitative representations of complex environmental phenomena. Models are aimed at improving our understanding of environmental processes and enable us to test different scenarios (e.g. identify driving forces of change for specific environments, under various conditions). Models can be used to test hypotheses and make predictions on future changes in environmental conditions. Models are also attractive tools to summarise the state of knowledge of particular phenomena.

Technological advances in remote sensing, Geographic Information System (GIS) and spatial interpolation techniques, have contributed to the realism of erosion models applications. A growing number of models and model versions have been designed to integrate GIS, digital maps and satellite data. These advances have also been crucial to improving the policy relevance of erosion models. As a result, governments extensively use models predicting the extent of soil erosion for policy development and implementation of soil management and conservation strategies (Leys et al., 2017; Panagos et al., 2015). For example, in Europe, the European Commission derived a range of hillslope erosion maps from soil erosion modelling to set soil protection targets within the Common Agricultural Policy (CAP) (Panagos and Katsoyiannis, 2019). In Australia, the National Landcare Program used the Computational Environmental Management System model (CEMSYS) to assess the extent and severity of wind erosion and proposed guidelines to limit soil erosion risk in major Natural Resource Management eco-regions (Butler et al., 2007; Leys et al., 2017).

1.3.1 Water erosion models

Based on a comprehensive review of the literature, Borrelli et al., (2020) reported that water erosion was by far the most extensively studied process. Erosion is assessed using

a wide range of models which differ considerably in their objectives, spatio-temporal scales and their initial conceptualisation (Morgan, 2009).

Two of the most popular detailed process-based models are the Water Erosion Prediction Project (WEPP) (A. Nearing et al., 1990; Foster and Lane, 1987) and the European Soil Erosion Model (EUROSEM) (Morgan et al., 1998). The WEPP was designed to improve the empirically-based Universal Soil Loss Equation (USLE) to provide a continuous simulation of soil erosion predictions (rill and interrill) from distributed parameters. This model can simulate soil detachment and deposition over small catchments (< 260ha) for individual storms or longer periods. This model has been tested and calibrated on a wide range of environmental conditions (Morgan, 2009). The EUROSEM is an event-based model designed to estimate sediment transport, erosion and deposition over the land surface during a single storm. This model can be applied to individual fields or small catchments. Compared to other process-oriented models, EUROSEM is considered the most realistic as it simulates interrill erosion and deposition of sediments explicitly and contains a more thorough description of the protective effect of vegetation or crop cover in place. However, both models require high parameterisation effort and a large amount of input data, which might not always be readily available. They also require thorough knowledge of the local conditions and can only be applied over small areas.

The most popular models used at broad spatial scales are derived from the Universal Soil Loss Equation (USLE) (Wischmeier and Smith, 1978). The USLE is an empirical model derived from a correlation between erosion measured on experimental plots and environmental parameters such as topography, climate, soil properties and land use. The USLE was later improved (Revised USLE) to account for more modern farming practices and make use of computer technologies (Renard et al., 1997). Even though the RUSLE was developed initially to assess soil losses from plot-scale experiments, its large-scale application is becoming more and more common (Panagos et al., 2018). This interest is driven by the fact that the RUSLE derives soil erosion from a set of quantitative

environmental attributes used as input data, which are easily accessible across large regions. The model can also be used as a coherent baseline product to study the direct impact of changes in climate, vegetation, soil characteristics, and land use and land management operations on soil erosion. Most importantly, the RUSLE is presented in a simple numerical equation which can be easily integrated into a GIS environment and mapping software, and can assimilate large datasets when combined with computer programs.

More recently, Panagos et al. (2014) proposed a new perspective to the RUSLE modelling approach: the G2 model. G2 is a quantitative algorithm derived from the RUSLE and Gavrilovic (1988) concepts and quantifies hillslope erosion and sediment yield rates at monthly time intervals. Although quite similar to the RUSLE, this model proposed a new method to account for vegetation cover and management factor in a wide range of landscapes (Chapter 2). The authors also introduced a new parameter accounting for the effect of landscape alteration on soil erosion in a more recent manuscript (Karydas and Panagos, 2018). The G2 model has been successfully applied in several European countries and yielded good results (Karydas et al., 2020; Karydas and Panagos, 2016; Karydas et al., 2015; Panagos et al., 2012; Zdruli et al., 2016).

1.3.2 Wind erosion models

Although on-ground wind erosion monitoring with wind tunnel experiments sparked interest since the early 60s, wind erosion modelling is not as popular as water erosion modelling (Borrelli et al., 2020). The most common wind erosion models are the (Revised) Wind Erosion Equation ((R)WEQ; Fryrear et al. (2000); Woodruff and Siddoway (1965)), the Wind Erosion Prediction System (WEPS; Hagen (1991)) and the Integrated Wind Erosion Modelling System (IWEMS, Lu and Shao (2001)). The WEQ and RWEQ are empirical models with a similar structure to the USLE and predict potential average annual soil loss based on soil erodibility, wind energy, surface

roughness, length of wind fetch and vegetation cover. The revised version of WEQ allowed for the inclusion of advanced farming practices in the model, the simulation of erosion prediction over shorter periods and more detailed parameter accounting for erodible soil fraction and soil crusting.

Unlike WEQ and RWEQ, the WEPS and IWEMS are process-based models. The WEPS produces daily simulations of wind erosion at a field scale. It can also simulate the spatial and temporal variability of field conditions and soil loss/deposition within a field. This model has been developed for a wide range of scenarios in the USA, and has been applied with success in other parts of the world (Chen et al., 2017; Pi et al., 2019; Tatarko et al., 2016). One of the major limitations of the models mentioned above is that they require a large amount of detailed input data and can only be applied at the field scale. The IWEMS model is a combination of a sediment transport model and a dust emission model that can be used at a regional scale (Shao, 2001; Shao et al., 2002). However, this model requires an extensive range of input parameters that are not always readily available.

Using fundamental principles of aeolian sediment transport, Chappell and Webb (2016) redefined the approximation of aerodynamic roughness in the “albedo” Wind Erosion Model. The authors implemented and improved the characterisation of the lateral cover parameter (L) and surface roughness, and suggested that the values of L were about an order of magnitude smaller than field measurements. In addition, the authors argued that the sheltering effect from vegetation was not fully integrated into other wind erosion modelling approaches. For this reason, Chappell and Webb (2016) developed a new approach to wind erosion modelling by replacing the lateral cover parameters with a relationship between the sheltered area in the wake of objects and the proportion of shadow produced by the same object (Chappell et al., 2010) (Figure 1.4). The authors demonstrated that this proportion of shadow could be easily derived from MODIS Albedo products (MCD43A1 and MCD43A3) and designed regression relationships between aeolian sediment transport and shadow area (or black sky albedo). This new

method has now made it possible to fully integrate satellite imagery and remote sensing in complex wind erosion models. Therefore, the “albedo” Wind Erosion Model provides a dynamic (multi-temporal) global metric for wind erosion assessment at a moderate resolution. The model was successfully calibrated and tested the regression relationships with field data collected in Australia and in the US through a National Wind Erosion Research Network (Webb et al., 2016).

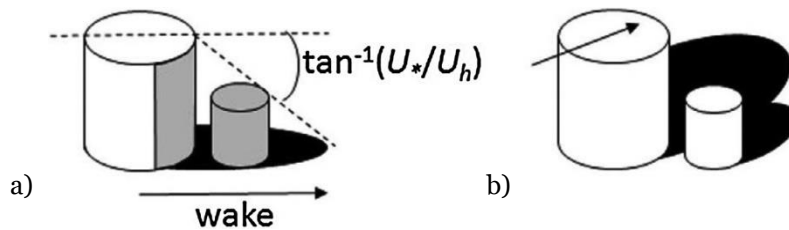


Figure 1.4 a) Concept representation of the sheltering effect of vegetation from Raupach et al. (1993), b) concept of the shadow effect of vegetation proposed by Chappell et al. (2010) to derive vegetation structure from remote sensing. Source: Chappell et al. (2010).

1.3.3 Integrated/Combination models

As wind- and water-borne erosion processes differ fundamentally, it is impossible to combine them into a single model. Fox et al. (2001) proposed coupling the WEPS and WEPP models to assess soil erosion in agricultural fields in the USA. The association of the two models was further discussed by Visser and Flanagan (2004), who defined the commonalities between the two approaches and illustrated how the two models could be combined. The authors suggested that a single erosion model would simplify reporting of erosional rates, offer consistent results, simplify computer programming and reduce the amount of database to maintain by government agencies. However, the creation of a common interface proved to be too complex leading to the development of the Object Modelling System (OMS) framework (OMSLab) and their Wind and Water Erosion Services (WWES) module (Ascough et al., 2011). The WWES module is composed of diverse sub-models that can estimate sheet/rill erosion (RUSLE2), tillage erosion (Soil Tillage, Intensity Rating, STIR), hillslope erosion (WEPP), and wind erosion (WEPS) for a given field in the US. The OMS framework can be accessed through a cloud-

based version or as a downloadable Java Graphical User Interface (GUI). This framework is the result from an extensive collaboration between the U.S Department for Agriculture and agro-environmental modelling organisation in the USA since the early 2000s. As a result, the OMS framework can only be accessed by partner organisations. Another shortcoming of this project is the fact that the OMS framework and the WWES module are only optimised for US conditions.

Outside of the US, a water erosion model is often coupled to a wind erosion model, and the outputs are summed to produce a total soil loss rate. The most popular water erosion model chosen for the task is the (R)USLE. This model is then combined with the (R)WEQ (Du et al., 2016; Hansen, 2007; Jiang et al., 2019; Jiang and Zhang, 2016; Miner et al., 2013; Zhang and McBean, 2016), a dust emission model (Al-Bakri et al., 2016; Santini et al., 2010), wind erosion susceptibility maps (Martínez-Graña et al., 2014) or radioelement measurements such as Cs¹³⁷ (Tuo et al., 2018). Other water erosion models such as the Rangeland Hydrology and Erosion Model (RHEM, Nearing et al., (2011)) or other hydrological models can be coupled with dust emission models to estimate the total contribution to wind and water erosion (Wang et al., 2014; Webb et al., 2014). The next most-preferred approach is the classification of images acquired by high-resolution satellite sensors or aerial photographs, combined with (Sankey et al., 2018; Sankey and Draut, 2014; Wang et al., 2019; Wang et al., 2016) or without field measurements (Al-Masrahy and Mountney, 2015; Liu and Coulthard, 2015). Other methods include Principal Component Analysis (PCA) or Multi-criteria Analysis on erosion controlling factors to predict soil erosion risk by wind and water over a region of interest (Bednář and Šarapatka, 2018; Šarapatka and Bednář, 2015).

1.3.4 Post-fire erosion modelling

Similar to erosion modelling under “undisturbed” conditions, water erosion models are by far the most popular approach to assess the impact of wildfires on soil erosion

(Borrelli et al., 2020). In general, water erosion models are used to predict post-fire erosion or estimate the effectiveness of rehabilitation treatments. For post-fire predictions, the RUSLE (Blake et al., 2020; Lanorte et al., 2019; Litschert et al., 2014; Zhu et al., 2019), MMF (Hosseini et al., 2018; Vieira et al., 2014; Vieira et al., 2018), WEPP (Fernández and Vega, 2018; Gould et al., 2016; Miller et al., 2011), PERSERA (Esteves et al., 2012; Fernández and Vega, 2016; Karamesouti et al., 2016) and SWAT (Basso et al., 2020; Carvalho-Santos et al., 2019; Havel et al., 2018; Rodrigues et al., 2019) models are the most common. However, these methods often yield very different results, and very limited studies validate their prediction outputs with field data (Vieira et al., 2018). Although there is a clear interest from the scientific community for post-fire erosion modelling, limited research has used erosion models to assess the efficacy of post-fire rehabilitation (Vieira et al., 2018). Nonetheless, the RUSLE (Fernández et al., 2010; Rulli et al., 2013; Vieira et al., 2018), MMF (Fernández et al., 2010; Vieira et al., 2014; Vieira et al., 2018; Zema et al., 2020) and WEPP (Robichaud et al., 2016; Robichaud et al., 2007) models have proven to be reliable operational tools. These approaches can then be used by land managers to prioritise treatment areas and optimise rehabilitation measures.

Traditional wind erosion models are not commonly used to assess the impact of fires on soil erosion. A couple of approaches have used sediment transport models combined with field measurements to predict post-fire dust emission (Shaw et al., 2008; Wagenbrenner et al., 2017), while others combined vegetation distribution and sediment transport models (Breshears et al., 2012; Mayaud et al., 2017; Michelotti et al., 2013). Wagenbrenner et al. (2017) used the WindNinja wind distribution model (Forthofer et al., 2014) in combination with field measurements to model PM₁₀ emissions post-fire. This model was initially developed for fire management and “fire weather” modelling, but it also contains a dust emission module (Wagenbrenner et al., 2010). The authors demonstrated that the model was able to capture a large post-fire dust event and identified dust emission hotspots in the Great Basin (USA) following a

large wildfire. Shaw et al. (2008) also used a dust transport model (DUSTRAN: Allwine et al. (2006)) and field measurements to monitor site recovery and predict dust emission following a large fire in the US (Washington State). The authors observed discrepancies between the observed and predicted dust emissions under wetter conditions. The DUSTRAN model also tends to overestimate PM₁₀ levels for low observed dust concentrations. Nonetheless, the model proved to be an effective tool for the prediction of post-fire dust events.

The Vegetation and Sediment TrAnsport (ViSTA) model was created from the combination of a vegetation distribution and a sediment transport model (Mayaud et al., 2017). Although this model was not primarily designed to assess the impact of wildfires on erosion, the vegetation module offers the possibility to add a “fire” disturbance. The ViSTA model can then compute the sediment transport and horizontal sediment flux after a wildfire occurred; however, this functionality has not been compared to ground measurements yet. The ViSTA approach is very similar to the Vegetation Moderated Transport (VMTran) model of Breshears et al. (2012) which also combines a vegetation and a sediment transport module to estimate the transport of contaminated soils by wind. The authors tested the VMTran model to predict sediment transport rates following drought, ground fire and crown fire disturbances over a 1000-year simulation. Overall, their method yielded good results when compared to ground-measurements. Still, sediment transport rates varied considerably in response to changes in the amount of woody plant cover due to underlying assumptions in the model. The VMTran model was used again to model the dispersal and deposition of windblown residual plutonium under environmental disturbances (drought, ground fire and crown fire) in a semi-arid region of the southwestern USA (Michelotti et al., 2013). The authors showed that accumulation rates of radionuclides after disturbances were about an order of magnitude faster than under undisturbed conditions. These results highlighted the need to apply more scrutiny to consider environmental disturbances in the assessment of long-term pollutant concentrations.

In conclusion, the vast majority of post-fire erosion modelling considers wind and water erosion processes separately even though evidence of wind redistribution of sediments have been reported in hydrological studies (Santín et al., 2015; Vega et al., 2020). Surprisingly, a very limited number of researchers have considered wind and water erosion simultaneously in post-fire studies (Shillito et al., 2012). There is, therefore, a need for more combined wind and water post-fire erosion assessment, especially in dryland ecosystems where the two processes can substantially contribute to total erosion rates under undisturbed conditions.

1.4 Aims and objectives of the project

The overarching aim of this study is to demonstrate the benefits of a joint wind-water-erosion modelling approach to identify the spatio-temporal variability of extreme erosion events in the South Australian agricultural zone and the likely increase of variability in the face of climate change and the recurrence of wildfires.

We give an example of how this approach can be used to inform corrective measures for future land management and test the influence of climate change and extreme environmental conditions scenarios on soil erosion for a wide range of land cover over large regions.

The specific objectives of this research were:

- To adapt two state-of-the-art wind and water erosion models to integrate modern high-resolution datasets for spatial and temporal analysis of erosion. The adaptation of these models to local conditions and the use of high-resolution datasets was crucial to ensure reliable erosion assessment.
- To identify sub-regions where wind and water erosion processes co-exist in the study area. This objective is of utmost importance for regional land management as no previous work has looked at the combined impact of wind and water erosion

in the South Australian agricultural zone. This knowledge would drive future policy development for soil conservation and inspire further work in this domain.

- To assess the impact of wildfires on wind and water erosion dynamics and test the capacity of the models to capture post-fire variability.
- To assess the impact of a catastrophic wildfire event on wind erosion in the field by examining the influence of unburnt stubble patches on adjacent burnt or bare plots.

1.5 Thesis structure

This thesis consists of six chapters; Chapter 5 was published in a peer-reviewed journal. The current chapter (Chapter 1) presents a general introduction to soil erosion processes and the diverse modelling approaches applied to study this phenomenon as well as the motivations behind the research. This chapter also presents the research objectives and the outline of the thesis. The following two sections describe the water and wind erosion models, define the adaptations of each model to local conditions, evaluate the spatio-temporal variability of extreme erosion events and describe the interaction between each erosional process and their influencing factors (Chapter 2 and 3). Chapter 4 identifies sub-regions where wind and water erosion processes co-exist and proposes to test the capacity of the wind and water erosion models to capture post-fire erosion variability. Chapter 5 presents a simple field-based method to monitor wind erosion after a catastrophic wildfire and demonstrates that unburnt stubble patches can greatly influence sediment transport to adjacent burnt or bare plots. Chapter 6 summarises the key findings, limitations and broader implication of the research and the recommendations for further exploration in the field.

1.6 References

- A. Nearing, M., Deer-Ascough, L., M. Laflen, J., 1990. SENSITIVITY ANALYSIS OF THE WEPP HILLSLOPE PROFILE EROSION MODEL. Transactions of the ASAE 33, 839-849, doi: <https://doi.org/10.13031/2013.31409>.
- ABC News, <https://www.abc.net.au/news/rural/2019-12-06/dust-storms-happening-with-record-breaking-frequency/11768306>
- Al-Bakri, J.T., Brown, L., Gedalof, Z., Berg, A., Nickling, W., Khresat, S., Salahat, M., Saoub, H., 2016. Modelling desertification risk in the north-west of Jordan using geospatial and remote sensing techniques. Geomatics Natural Hazards & Risk 7, 531-549, doi: <https://doi.org/10.1080/19475705.2014.945102>.
- Al-Masrahy, M.A., Mountney, N.P., 2015. A classification scheme for fluvial–aeolian system interaction in desert-margin settings. Aeolian Research 17, 67-88, doi: <https://doi.org/10.1016/j.aeolia.2015.01.010>.
- Allwine, K.J., Rutz, F.C., Shaw, W.J., Rishel, J.P., Fritz, B.G., Chapman, E.G., Hoopes, B.L., Seiple, T.E., 2006. DUSTRAN 1.0 User's Guide: A GIS-Based Atmospheric Dust Dispersion Modeling System. Pacific Northwest National Lab.(PNNL), Richland, WA (United States),
- Ascough, J.C., Flanagan, D.C., Truman, C.C., David, O., 2011. Development of a Combined Wind and Water Erosion Model (WWEM) for the Object Modeling System, International Symposium on Erosion and Landscape Evolution (ISELE), 18-21 September 2011, Anchorage, Alaska. American Society of Agricultural and Biological Engineers, p. 64, https://elibrary.asabe.org/pdfviewer.asp?param1=s:/8y9u8/q8qu/tq9q/5tv/H/y8uIIGHH/HHGMK_vy3q1.5tv¶m2=J/IP/IGIG¶m3=HIP.HIN.HKL.IIL¶m4=39260
- Baddock, M.C., Strong, C.L., Leys, J.F., Heidenreich, S.K., Tews, E.K., McTainsh, G.H., 2014. A visibility and total suspended dust relationship. Atmospheric Environment 89, 329-336, doi: <https://doi.org/10.1016/j.atmosenv.2014.02.038>.
- Basso, M., Vieira, D.C.S., Ramos, T.B., Mateus, M., 2020. Assessing the adequacy of SWAT model to simulate postfire effects on the watershed hydrological regime and water quality. Land Degradation & Development 31, 619-631, doi: <https://doi.org/10.1002/ldr.3476>.
- Bednář, M., Šarapatka, B., 2018. Relationships between physical-geographical factors and soil degradation on agricultural land. Environmental Research 164, 660-668, doi: <https://doi.org/10.1016/j.envres.2018.03.042>.
- Belnap, J., Munson, S.M., Field, J.P., 2011. Aeolian and fluvial processes in dryland regions: the need for integrated studies. Ecohydrology 4, 615-622, doi: <https://doi.org/10.1002/eco.258>.

- Bennell, M.R., Leys, J.F., Cleugh, H.A., 2007. Sandblasting damage of narrow-leaf lupin (*Lupinus angustifolius* L.): a field wind tunnel simulation. *Soil Research* 45, 119-128, doi: <https://doi.org/10.1071/SR06066>.
- Bento-Gonçalves, A., Vieira, A., Úbeda, X., Martin, D., 2012. Fire and soils: Key concepts and recent advances. *Geoderma* 191, 3-13, doi: <http://dx.doi.org/10.1016/j.geoderma.2012.01.004>.
- Blake, D., Nyman, P., Nice, H., D'Souza, F.M.L., Kavazos, C.R.J., Horwitz, P., 2020. Assessment of post-wildfire erosion risk and effects on water quality in south-western Australia. *International Journal of Wildland Fire* 29, 240-257, doi: <https://doi.org/10.1071/WF18123>.
- Boardman, J., 2006. Soil erosion science: Reflections on the limitations of current approaches. *Catena* 68, 73-86,
- Borrelli, P., Alewell, C., Alvarez, P., Anache, J.A.A., Baartman, J., Ballabio, C., Bezak, N., Biddoccu, M., Cerda, A., Chalise, D., Chen, S., Chen, W., Girolamo, A.M.D., Gessesse, G.D., Deumlich, D., Efthimiou, N., Erpul, G., Fiener, P., Freppaz, M., Gentile, F., Gericke, A., Haregeweyn, N., Hu, B., Jeanneau, A., Kaffas, K., Kiani-Harchegani, M., Villuendas, I.L., Li, C., Lombardo, L., López-Vicente, M., Lucas-Borja, M.E., Märker, M., Matjaž, M., Miao, C., Modugno, S., Möller, M., Naipal, V., Nearing, M., Owusu, S., Panday, D., Patault, E., Patriche, C.V., Poggio, L., Portes, R., Quijano, L., Rahdari, M.R., Renima, M., Ricci, G.F., Rodrigo-Comino, J., Saia, S., Samani, A.N., Schillaci, C., Syrris, V., Kim, H.S., Spinola, D.N., Oliveira, P.T., Teng, H., Thapa, R., Vantas, K., Vieira, D., Yang, J.E., Yin, S., Zema, D.A., Zhao, G., Panagos, P., 2020. Soil erosion modelling: A global review and statistical analysis, *Earth-Science Reviews*,
- Borrelli, P., Robinson, D.A., Fleischer, L.R., Lugato, E., Ballabio, C., Alewell, C., Meusburger, K., Modugno, S., Schütt, B., Ferro, V., Bagarello, V., Oost, K.V., Montanarella, L., Panagos, P., 2017. An assessment of the global impact of 21st century land use change on soil erosion. *Nature Communications* 8, 2013, doi: <https://doi.org/10.1038/s41467-017-02142-7>.
- Breshears, D.D., Kirchner, T.B., Whicker, J.J., Field, J.P., Allen, C.D., 2012. Modeling aeolian transport in response to succession, disturbance and future climate: Dynamic long-term risk assessment for contaminant redistribution. *Aeolian Research* 3, 445-457, doi: <https://doi.org/10.1016/j.aeolia.2011.03.012>.
- Breshears, D.D., Whicker, J.J., Johansen, M.P., Pinder, J.E., 2003. Wind and water erosion and transport in semi-arid shrubland, grassland and forest ecosystems: Quantifying dominance of horizontal wind-driven transport. *Earth Surface Processes and Landforms* 28, 1189-1209, doi: <https://doi.org/10.1002/esp.1034>.
- Bui, E.N., Hancock, G.J., Wilkinson, S.N., 2011. 'Tolerable' hillslope soil erosion rates in Australia: Linking science and policy. *Agriculture, Ecosystems & Environment* 144, 136-149, doi: <https://doi.org/10.1016/j.agee.2011.07.022>.

- Butler, H., Shao, Y., Leys, J., McTainsh, G., 2007. Modelling wind erosion at national & regional scales, Report to the National Land and Water Resources Audit (NLWRA)-National Monitoring and Evaluation Framework,
- Carvalho-Santos, C., Marcos, B., Nunes, J.P., Regos, A., Palazzi, E., Terzago, S., Monteiro, A.T., Honrado, J.P., 2019. Hydrological Impacts of Large Fires and Future Climate: Modeling Approach Supported by Satellite Data. *Remote Sensing* 11, 2832, doi: <https://doi.org/10.3390/rs11232832>.
- Cattle, S.R., 2016. The case for a southeastern Australian Dust Bowl, 1895-1945. *Aeolian Research* 21, 1-20, doi: <https://doi.org/10.1016/j.aeolia.2016.02.001>.
- Chappell, A., Van Pelt, S., Zobeck, T., Dong, Z., 2010. Estimating aerodynamic resistance of rough surfaces using angular reflectance. *Remote Sensing of Environment* 114, 1462-1470, doi: <https://doi.org/10.1016/j.rse.2010.01.025>.
- Chappell, A., Webb, N., 2016. Using albedo to reform wind erosion modelling, mapping and monitoring, doi: <https://doi.org/10.1016/j.aeolia.2016.09.006>.
- Chen, L., Zhao, H., Wang, W.X., Bai, Z.P., Wang, Z.L., Sun, F.J., Hou, L.J., Liu, G.H., Shi, M.S., Miao, Y.G., 2017. Effect of windblown dust from local and regional sources on the air quality of the central district in Jinan, China. *Atmospheric Research* 185, 44-52, doi: <https://doi.org/10.1016/j.atmosres.2016.10.026>.
- Clarke, H.G., Smith, P.L., Pitman, A.J., 2011. Regional signatures of future fire weather over eastern Australia from global climate models. *International Journal of Wildland Fire* 20, 550-562, doi: <https://doi.org/10.1071/WF10070>.
- CSIRO, Bureau of Meteorology, 2015. Climate Change in Australia Information for Australia's Natural Resource Management Regions: Technical Report. CSIRO and Bureau of Meteorology, Australia, https://www.climatechangeinaustralia.gov.au/media/ccia/2.1.6/cms_page_media/168/CCIA_2015_NRM_TechnicalReport_WEB.pdf
- DeBano, L.F., Neary, D.G., 2005. Part A—the soil resource: its importance, characteristics, and general responses to fire, In: *Wildland Fire in Ecosystems: Effects of Fire on Soil and Water*. Gen. Tech. Rep. , Fort Collins, pp. 21-28,
- Du, H.Q., Dou, S.T., Deng, X.H., Xue, X., Wang, T., 2016. Assessment of wind and water erosion risk in the watershed of the Ningxia-Inner Mongolia Reach of the Yellow River, China. *Ecological Indicators* 67, 117-131, doi: <https://doi.org/10.1016/j.ecolind.2016.02.042>.
- DustWatch Australia, Community DustWatch network, <https://www.dustwatch.edu.au/index.php/community-dustwatch/community-dw-network>

- Earl, N., Remenyi, T., Love, P., Harris, R., Rollins, D., Bindoff, N., 2019. Invited paper: Compound rainfall events in Tasmania, MODSIM2019, 23rd International Congress on Modelling and Simulation. Modelling and Simulation Society of Australia and New Zealand, Canberra, Australia,
- ECMWF, 2020. Copernicus: 2019 was the second warmest year and the last five years were the warmest on record, <https://climate.copernicus.eu/copernicus-2019-was-second-warmest-year-and-last-five-years-were-warmest-record>
- Edwards, B.L., Webb, N.P., Brown, D.P., Elias, E., Peck, D.E., Pierson, F.B., Williams, C.J., Herrick, J.E., 2019. Climate change impacts on wind and water erosion on US rangelands. *Journal of Soil and Water Conservation* 74, 405-418, doi: <https://doi.org/10.2489/jswc.74.4.405>.
- Esteves, T.C.J., Kirkby, M.J., Shakesby, R.A., Ferreira, A.J.D., Soares, J.A.A., Irvine, B.J., Ferreira, C.S.S., Coelho, C.O.A., Bento, C.P.M., Carreiras, M.A., 2012. Mitigating land degradation caused by wildfire: Application of the PESERA model to fire-affected sites in central Portugal. *Geoderma* 191, 40-50, doi: <https://doi.org/10.1016/j.geoderma.2012.01.001>.
- FAO, 2019. Soil erosion: the greatest challenge to sustainable soil management, Rome, p. 100 pp,
- Fernández, C., Vega, J.A., 2016. Evaluation of RUSLE and PESERA models for predicting soil erosion losses in the first year after wildfire in NW Spain. *Geoderma* 273, 64-72, doi: <https://doi.org/10.1016/j.geoderma.2016.03.016>.
- Fernández, C., Vega, J.A., 2018. Evaluation of the rusle and disturbed wepp erosion models for predicting soil loss in the first year after wildfire in NW Spain. *Environmental Research* 165, 279-285, doi: <https://doi.org/10.1016/j.envres.2018.04.008>.
- Fernández, C., Vega, J.A., Vieira, D.C.S., 2010. Assessing soil erosion after fire and rehabilitation treatments in NW Spain: Performance of rusle and revised Morgan–Morgan–Finney models. *Land Degradation & Development* 21, 58-67, doi: <https://doi.org/10.1002/ldr.965>.
- Field, J.P., Breshears, D.D., Whicker, J.J., 2009. Toward a more holistic perspective of soil erosion: Why aeolian research needs to explicitly consider fluvial processes and interactions. *Aeolian Research* 1, 9-17, doi: <http://dx.doi.org/10.1016/j.aeolia.2009.04.002>.
- Field, J.P., Breshears, D.D., Whicker, J.J., Zou, C.B., 2011a. Interactive effects of grazing and burning on wind- and water-driven sediment fluxes: rangeland management implications. *Ecological Applications* 21, 22-32, doi: <https://doi.org/10.1890/09-2369.1>.

- Field, J.P., Breshears, D.D., Whicker, J.J., Zou, C.B., 2011b. On the ratio of wind- to water-driven sediment transport: Conserving soil under global-change-type extreme events. *Journal of Soil and Water Conservation* 66, 51A-56A, doi: <https://doi.org/10.2489/jswc.66.2.51A>.
- Flanagan, D.C., Ascough, J.C., Nieber, J.L., Misra, D., Douglas-Mankin, K.R., 2013. *Advances in Soil Erosion Research: Processes, Measurement, and Modeling*. *Transactions of the ASABE* 56, 455-463, doi: <https://doi.org/10.13031/2013.42666>.
- Forthofer, J.M., Butler, B.W., Wagenbrenner, N.S., 2014. A comparison of three approaches for simulating fine-scale surface winds in support of wildland fire management. Part I. Model formulation and comparison against measurements. *International Journal of Wildland Fire* 23, 969-981, doi: <https://doi.org/10.1071/WF12089>.
- Foster, G.R., Lane, L.J., 1987. User requirements: USDA, water erosion prediction project (WEPP) Draft 6.3. NSERL report (USA),
- Fox, F.A., Flanagan, D.C., Wagner, L.E., Deer-Ascough, L., 2001. WEPS and WEPP science commonality project, in: Ascough, J.C., Flanagan, D.C. (Eds.), *Soil Erosion Research for the 21st Century*, Proceedings, pp. 375-379, doi: <https://doi.org/10.13031/2013.3286>.
- Fryrear, D.W., Bilbro, J.D., Saleh, A., Schomberg, H., Stout, J.E., Zobeck, T.M., 2000. RWEQ: Improved wind erosion technology. *Journal of Soil and Water Conservation* 55, 183-189, <http://www.jswconline.org/content/55/2/183.abstract>
- Gavrilovic, Z., 1988. Use of an Empirical Method(Erosion Potential Method) for Calculating Sediment Production and Transportation in Unstudied or Torrential Streams, *International Conference on River Regime*. Hydraulics Research Limited, Wallingford, Oxon UK. 1988. p 411-422, 5 fig, 4 tab, 8 ref.,
- Gonçalves, A.B., Vieira, A., Leite, F.F., Martins, J., Silva, D., Soares, V., 2011. ADAPTACLIMA: adaptation to the effects from climate change in the AVE, 3rd International Meeting of Fire Effects on Soil Properties. Nigp-Univ. Minho e Cegot, pp. 175-180, <http://hdl.handle.net/1822/19983>
- Gould, G.K., Liu, M., Barber, M.E., Cherkauer, K.A., Robichaud, P.R., Adam, J.C., 2016. The effects of climate change and extreme wildfire events on runoff erosion over a mountain watershed. *Journal of Hydrology* 536, 74-91, doi: <https://doi.org/10.1016/j.jhydrol.2016.02.025>.
- Hagen, L., 1991. A wind erosion prediction system to meet user needs. *Journal of Soil and Water Conservation* 46, 106-111,

- Hansen, L., 2007. Conservation Reserve Program: Environmental Benefits Update. *Agricultural and Resource Economics Review* 36, 267-280, doi: <https://doi.org/10.1017/S1068280500007085>.
- Havel, A., Tasdighi, A., Arabi, M., 2018. Assessing the hydrologic response to wildfires in mountainous regions. *Hydrol. Earth Syst. Sci.* 22, 2527-2550, doi: <https://doi.org/10.5194/hess-22-2527-2018>.
- Hosseini, M., Nunes, J.P., Pelayo, O.G., Keizer, J.J., Ritsema, C., Geissen, V., 2018. Developing generalized parameters for post-fire erosion risk assessment using the revised Morgan-Morgan-Finney model: A test for north-central Portuguese pine stands. *CATENA* 165, 358-368, doi: <https://doi.org/10.1016/j.catena.2018.02.019>.
- Jiang, C., Zhang, H.Y., Zhang, Z.D., Wang, D.W., 2019. Model-based assessment soil loss by wind and water erosion in China's Loess Plateau: Dynamic change, conservation effectiveness, and strategies for sustainable restoration. *Global and Planetary Change* 172, 396-413, doi: <https://doi.org/10.1016/j.gloplacha.2018.11.002>.
- Jiang, C., Zhang, L.B., 2016. Ecosystem change assessment in the Three-river Headwater Region, China: Patterns, causes, and implications. *Ecological Engineering* 93, 24-36, doi: <https://doi.org/10.1016/j.ecoleng.2016.05.011>.
- Karameouti, M., Petropoulos, G.P., Papanikolaou, I.D., Kairis, O., Kosmas, K., 2016. Erosion rate predictions from PESERA and RUSLE at a Mediterranean site before and after a wildfire: Comparison & implications. *Geoderma* 261, 44-58, doi: <https://doi.org/10.1016/j.geoderma.2015.06.025>.
- Karydas, C., Bouarour, O., Zdruli, P., 2020. Mapping Spatio-Temporal Soil Erosion Patterns in the Candelaro River Basin, Italy, Using the G2 Model with Sentinel2 Imagery. *Geosciences* 10, 89, <https://www.mdpi.com/2076-3263/10/3/89>
- Karydas, C.G., Panagos, P., 2016. Modelling monthly soil losses and sediment yields in Cyprus. *International Journal of Digital Earth*, 1-22, doi: <http://dx.doi.org/10.1080/17538947.2016.1156776>.
- Karydas, C.G., Panagos, P., 2018. The G2 erosion model: An algorithm for month-time step assessments. *Environmental Research* 161, 256-267, doi: <https://doi.org/10.1016/j.envres.2017.11.010>.
- Karydas, C.G., Zdruli, P., Koci, S., Sallaku, F., 2015. Monthly Time-Step Erosion Risk Monitoring of Ishmi-Erzeni Watershed, Albania, Using the G2 Model. *Environmental Modeling & Assessment* 20, 657-672, doi: <https://doi.org/10.1007/s10666-015-9455-5>.
- Lanorte, A., Cillis, G., Calamita, G., Nolè, G., Pilogallo, A., Tucci, B., De Santis, F., 2019. Integrated approach of RUSLE, GIS and ESA Sentinel-2 satellite data for post-fire soil erosion assessment in Basilicata region (Southern Italy). *Geomatics, Natural Hazards and Risk* 10, 1563-1595,

doi: <https://doi.org/10.1080/19475705.2019.1578271>.

- Leys, J., Chappell, A., Mewett, J., Barson, M., 2017. Wind Erosion Assessment for National Landcare Program. State of New South Wales and Office of Environment and Heritage, Sydney,
- Leys, J., Strong, C., Heidenreich, S., Koen, T., 2018. Where She Blows! A Ten Year Dust Climatology of Western New South Wales Australia. *Geosciences* 8, 232, <http://www.mdpi.com/2076-3263/8/7/232>
- Li, J., Kandakji, T., Lee, J.A., Tatarko, J., Blackwell, J., Gill, T.E., Collins, J.D., 2018. Blowing dust and highway safety in the southwestern United States: Characteristics of dust emission “hotspots” and management implications. *Science of The Total Environment* 621, 1023-1032, doi: <https://doi.org/10.1016/j.scitotenv.2017.10.124>.
- Litschert, S.E., Theobald, D.M., Brown, T.C., 2014. Effects of climate change and wildfire on soil loss in the Southern Rockies Ecoregion. *CATENA* 118, 206-219, doi: <https://doi.org/10.1016/j.catena.2014.01.007>.
- Liu, B.L., Coulthard, T.J., 2015. Mapping the interactions between rivers and sand dunes: Implications for fluvial and aeolian geomorphology. *Geomorphology* 231, 246-257, doi: <https://doi.org/10.1016/j.geomorph.2014.12.011>.
- Lu, H., Prosser, I.P., Moran, C.J., Gallant, J.C., Priestley, G., Stevenson, J.G., 2003. Predicting sheetwash and rill erosion over the Australian continent. *Soil Research* 41, 1037-1062, doi: <http://dx.doi.org/10.1071/SR02157>.
- Lu, H., Shao, Y.P., 2001. Toward quantitative prediction of dust storms: an integrated wind erosion modelling system and its applications. *Environmental Modelling & Software* 16, 233-249, doi: [https://doi.org/10.1016/s1364-8152\(00\)00083-9](https://doi.org/10.1016/s1364-8152(00)00083-9).
- Lu, J., Zheng, F., Li, G., Bian, F., An, J., 2016. The effects of raindrop impact and runoff detachment on hillslope soil erosion and soil aggregate loss in the Mollisol region of Northeast China. *Soil and Tillage Research* 161, 79-85,
- Martínez-Graña, A., Goy, J., Zazo, C., 2014. Water and Wind Erosion Risk in Natural Parks—A Case Study in “Las Batuecas–Sierra de Francia” and “Quilamas” Protected Parks (Central System, Spain). *International Journal of Environmental Research* 8, 61-68, doi: <https://doi.org/10.22059/ijer.2014.694>.
- Mayaud, J.R., Bailey, R.M., Wiggs, G.F.S., 2017. A coupled vegetation/sediment transport model for dryland environments. *Journal of Geophysical Research-Earth Surface* 122, 875-900, doi: <https://doi.org/10.1002/2016jf004096>.
- Michelotti, E.A., Whicker, J.J., Eisele, W.F., Breshears, D.D., Kirchner, T.B., 2013. Modeling aeolian transport of soil-bound plutonium: considering infrequent but

- normal environmental disturbances is critical in estimating future dose. *Journal of Environmental Radioactivity* 120, 73-80,
doi: <https://doi.org/10.1016/j.jenvrad.2013.01.011>.
- Miller, M.E., MacDonald, L.H., Robichaud, P.R., Elliot, W.J., 2011. Predicting post-fire hillslope erosion in forest lands of the western United States. *International Journal of Wildland Fire* 20, 982-999, doi: <https://doi.org/10.1071/WF09142>.
- Miner, G.L., Hansen, N.C., Inman, D., Sherrod, L.A., Peterson, G.A., 2013. Constraints of No-Till Dryland Agroecosystems as Bioenergy Production Systems. *Agronomy Journal* 105, 364-376, doi: <https://doi.org/10.2134/agronj2012.0243>.
- Montgomery, D.R., 2007. Soil erosion and agricultural sustainability. *Proceedings of the National Academy of Sciences* 104, 13268-13272,
doi: <https://doi.org/10.1073/pnas.0611508104>
- Morgan, R.P.C., 2009. *Soil erosion and conservation*. John Wiley & Sons,
- Morgan, R.P.C., Quinton, J.N., Smith, R.E., Govers, G., Poesen, J.W.A., Auerswald, K., Chisci, G., Torri, D., Styczen, M.E., 1998. The European Soil Erosion Model (EUROSEM): a dynamic approach for predicting sediment transport from fields and small catchments. *Earth Surface Processes and Landforms* 23, 527-544, doi: [https://doi.org/10.1002/\(SICI\)1096-9837\(199806\)23:6<527::AID-ESP868>3.0.CO;2-5](https://doi.org/10.1002/(SICI)1096-9837(199806)23:6<527::AID-ESP868>3.0.CO;2-5).
- Nearing, M., Lane, L.J., Lopes, V.L., 2017. Modeling soil erosion, *Soil erosion research methods*. Routledge, pp. 127-158,
- Nearing, M., Pruski, F.F., O'Neal, M.R., 2004. Expected climate change impacts on soil erosion rates: A review. *Journal of Soil and Water Conservation* 59, 43-50,
<http://www.jswnonline.org/content/59/1/43.abstract>
- Nearing, M., Wei, H., Stone, J., Pierson, F., Spaeth, K., Wertz, M., Flanagan, D., Hernandez, M., 2011. A rangeland hydrology and erosion model. *Transactions of the ASABE* 54, 901-908, doi: <https://doi.org/10.13031/2013.37115>.
- Near, D.G., 2011. Impacts of wildfire severity on hydraulic conductivity in forest, woodland, and grassland soils (Chapter 7), *Hydraulic Conductivity Issues, Determination, and Applications*, New York, NY, pp. 123-142,
https://www.fs.fed.us/rm/pubs_other/rmrs_2011_near_d006.pdf
- OMSLab, Object Modeling System (OMS), version 3 ed. U.S Department of Agriculture,
<https://alm.engr.colostate.edu/cb/wiki/17094>
- Panagos, P., Borrelli, P., Meusburger, K., Lugato, E., Ballabio, C., Poesen, J., Alewell, C., Montanarella, L., 2018. Soil erosion in Europe: current status, future climate and land use scenarios, in: Zlatic, M., Kostadinov, S. (Eds.), *Soil and Water Resources*

Protection in the Changing Environment, pp. 1-13, <Go to ISI>://WOS:000464898800001

- Panagos, P., Borrelli, P., Poesen, J., Ballabio, C., Lugato, E., Meusburger, K., Montanarella, L., Alewell, C., 2015. The new assessment of soil loss by water erosion in Europe. *Environmental Science & Policy* 54, 438-447, doi: <https://doi.org/10.1016/j.envsci.2015.08.012>.
- Panagos, P., Christos, K., Cristiano, B., Ioannis, G., 2014. Seasonal monitoring of soil erosion at regional scale: An application of the G2 model in Crete focusing on agricultural land uses. *International Journal of Applied Earth Observation and Geoinformation* 27, 147-155, doi: <https://doi.org/10.1016/j.jag.2013.09.012>.
- Panagos, P., Karydas, C.G., Gitas, I.Z., Montanarella, L., 2012. Monthly soil erosion monitoring based on remotely sensed biophysical parameters: a case study in Strymonas river basin towards a functional pan-European service. *International Journal of Digital Earth* 5, 461-487, doi: <https://doi.org/10.1080/17538947.2011.587897>.
- Panagos, P., Katsoyiannis, A., 2019. Soil erosion modelling: The new challenges as the result of policy developments in Europe. *Environmental Research* 172, 470-474, doi: <https://doi.org/10.1016/j.envres.2019.02.043>.
- Panebianco, J.E., Mendez, M.J., Buschiazzo, D.E., 2016. PM10 Emission, Sandblasting Efficiency and Vertical Entrainment During Successive Wind-Erosion Events: A Wind-Tunnel Approach. *Boundary-Layer Meteorology* 161, 335-353, doi: <https://doi.org/10.1007/s10546-016-0172-7>.
- Pi, H.W., Sharratt, B., Lei, J.Q., 2019. Wind erosion and dust emissions in central Asia: Spatiotemporal simulations in a typical dust year. *Earth Surface Processes and Landforms* 44, 521-534, doi: <https://doi.org/10.1002/esp.4514>.
- Prats, S.A., Malvar, M.C., Vieira, D.C.S., MacDonald, L., Keizer, J.J., 2016. Effectiveness of Hydromulching to Reduce Runoff and Erosion in a Recently Burnt Pine Plantation in Central Portugal. *Land Degradation & Development* 27, 1319-1333, doi: <https://doi.org/10.1002/ldr.2236>.
- Renard, K.G., Foster, G.R., Weesies, G., McCool, D., Yoder, D., 1997. Predicting soil erosion by water: a guide to conservation planning with the Revised Universal Soil Loss Equation (RUSLE). US Government Printing Office Washington, DC,
- Robichaud, P.R., Elliot, W.J., Lewis, S.A., Miller, M.E., 2016. Validation of a probabilistic post-fire erosion model. *International Journal of Wildland Fire* 25, 337-350, doi: <https://doi.org/10.1071/WF14171>.
- Robichaud, P.R., Elliot, W.J., Pierson, F.B., Hall, D.E., Moffet, C.A., 2007. Predicting postfire erosion and mitigation effectiveness with a web-based probabilistic erosion model. *CATENA* 71, 229-241, doi: <https://doi.org/10.1016/j.catena.2007.03.003>.

- Rodrigues, E.L., Jacobi, C.M., Figueira, J.E.C., 2019. Wildfires and their impact on the water supply of a large neotropical metropolis: A simulation approach. *Science of The Total Environment* 651, 1261-1271, doi: <https://doi.org/10.1016/j.scitotenv.2018.09.289>.
- Rulli, M.C., Offeddu, L., Santini, M., 2013. Modeling post-fire water erosion mitigation strategies. *Hydrol. Earth Syst. Sci.* 17, 2323-2337, doi: <https://doi.org/10.5194/hess-17-2323-2013>.
- Sankey, J.B., Caster, J., Kasprak, A., East, A.E., 2018. The response of source-bordering aeolian dunefields to sediment-supply changes 2: Controlled floods of the Colorado River in Grand Canyon, Arizona, USA. *Aeolian Research* 32, 154-169, doi: <https://doi.org/10.1016/j.aeolia.2018.02.004>.
- Sankey, J.B., Draut, A.E., 2014. Gully annealing by aeolian sediment: field and remote-sensing investigation of aeolian–hillslope–fluvial interactions, Colorado River corridor, Arizona, USA. *Geomorphology* 220, 68-80, doi: <https://doi.org/10.1016/j.geomorph.2014.05.028>.
- Santín, C., Doerr, Stefan H., Otero, Xosé L., Chafer, C.J., 2015. Quantity, composition and water contamination potential of ash produced under different wildfire severities. *Environmental Research* 142, 297-308, doi: <https://doi.org/10.1016/j.envres.2015.06.041>.
- Santini, M., Caccamo, G., Laurenti, A., Noce, S., Valentini, R., 2010. A multi-component GIS framework for desertification risk assessment by an integrated index. *Applied Geography* 30, 394-415, doi: <https://doi.org/10.1016/j.apgeog.2009.11.003>.
- Šarapatka, B., Bednář, M., 2015. Assessment of Potential Soil Degradation on Agricultural Land in the Czech Republic. *Journal of Environmental Quality* 44, 154-161, doi: <https://doi.org/10.2134/jeq2014.05.0233>.
- Seinfeld, J.H., Pandis, S.N., 2012. *Atmospheric chemistry and physics: from air pollution to climate change*. John Wiley & Sons,
- Shakesby, R.A., 2011. Post-wildfire soil erosion in the Mediterranean: Review and future research directions. *Earth-Science Reviews* 105, 71-100, doi: <http://dx.doi.org/10.1016/j.earscirev.2011.01.001>.
- Shakesby, R.A., Wallbrink, P.J., Doerr, S.H., English, P.M., Chafer, C.J., Humphreys, G.S., Blake, W.H., Tomkins, K.M., 2007. Distinctiveness of wildfire effects on soil erosion in south-east Australian eucalypt forests assessed in a global context. *Forest Ecology and Management* 238, 347-364, doi: <https://doi.org/10.1016/j.foreco.2006.10.029>.
- Shao, Y., 2001. A model for mineral dust emission. *Journal of Geophysical Research: Atmospheres* 106, 20239-20254, doi: <https://doi.org/10.1029/2001JD900171>.

- Shao, Y., Jung, E., Leslie, L.M., 2002. Numerical prediction of northeast Asian dust storms using an integrated wind erosion modeling system. *Journal of Geophysical Research: Atmospheres* 107, AAC 21-21-AAC 21-23, doi: <https://doi.org/10.1029/2001JD001493>.
- Shao, Y.P., Leys, J.F., McTainsh, G.H., Tews, K., 2007. Numerical simulation of the October 2002 dust event in Australia. *Journal of Geophysical Research-Atmospheres* 112, doi: <https://doi.org/10.1029/2006jd007767>.
- Shaw, W.J., Jerry Allwine, K., Fritz, B.G., Rutz, F.C., Rishel, J.P., Chapman, E.G., 2008. An evaluation of the wind erosion module in DUSTRAN. *Atmospheric Environment* 42, 1907-1921, doi: <http://dx.doi.org/10.1016/j.atmosenv.2007.11.022>.
- Shillito, R., Miller, J., Etyemezian, V., Mizell, S., 2012. Wind and Water Erosion Potential of Fire-Affected Soils: Immediate and Short-Term Effects in a Desert Ecosystem, *World Environmental and Water Resources Congress 2012*, pp. 1727-1736, doi: <https://doi.org/10.1061/9780784412312.171>.
- Speer, M.S., 2013. Dust storm frequency and impact over Eastern Australia determined by state of Pacific climate system. *Weather and Climate Extremes* 2, 16-21, doi: <https://doi.org/10.1016/j.wace.2013.10.004>.
- Tatarko, J., van Donk, S.J., Ascough, J.C., Walker, D.G., 2016. Application of the WEPS and SWEEP models to non-agricultural disturbed lands. *Heliyon* 2, 23, doi: <https://doi.org/10.1016/j.heliyon.2016.e00215>.
- Tozer, P., Leys, J., 2013. Dust storms – what do they really cost? *The Rangeland Journal* 35, 131-142, doi: <https://doi.org/10.1071/RJ12085>.
- Tuo, D., Xu, M., Gao, G., 2018. Relative contributions of wind and water erosion to total soil loss and its effect on soil properties in sloping croplands of the Chinese Loess Plateau. *Science of The Total Environment* 633, 1032-1040, doi: <https://doi.org/10.1016/j.scitotenv.2018.03.237>.
- Varela, M., Benito, E., Keizer, J., 2010. Wildfire effects on soil erodibility of woodlands in NW Spain. *Land degradation & development* 21, 75-82, doi: <https://doi.org/10.1002/ldr.896>
- Vega, S.P., Williams, C.J., Brooks, E.S., Pierson, F.B., Strand, E.K., Robichaud, P.R., Brown, R.E., Seyfried, M.S., Lohse, K.A., Glossner, K., Pierce, J.L., Roehner, C., 2020. Interaction of wind and cold-season hydrologic processes on erosion from complex topography following wildfire in sagebrush steppe. *Earth Surface Processes and Landforms* 45, 841-861, doi: <https://doi.org/10.1002/esp.4778>.
- Vieira, D.C.S., Prats, S.A., Nunes, J.P., Shakesby, R.A., Coelho, C.O.A., Keizer, J.J., 2014. Modelling runoff and erosion, and their mitigation, in burned Portuguese forest

- using the revised Morgan–Morgan–Finney model. *Forest Ecology and Management* 314, 150-165, doi: <https://doi.org/10.1016/j.foreco.2013.12.006>.
- Vieira, D.C.S., Serpa, D., Nunes, J.P.C., Prats, S.A., Neves, R., Keizer, J.J., 2018. Predicting the effectiveness of different mulching techniques in reducing post-fire runoff and erosion at plot scale with the RUSLE, MMF and PESERA models. *Environmental Research* 165, 365-378, doi: <https://doi.org/10.1016/j.envres.2018.04.029>.
- Visser, S.M., Flanagan, D.C., 2004. Commonalities in WEPP and WEPS and efforts towards a single erosion process model, in: Visser, S.M., Cornelis, W. (Eds.), *Wind and rain interaction in erosion*. Erosion & Soil and Water Conservation Group, Wageningen, pp. 15-30, <https://edepot.wur.nl/54153>
- Vrieling, A., 2006. Satellite remote sensing for water erosion assessment: A review. *Catena* 65, 2-18, doi: <http://dx.doi.org/10.1016/j.catena.2005.10.005>.
- Wagenbrenner, N., Chung, S., Lamb, B., 2017. A large source of dust missing in Particulate Matter emission inventories? Wind erosion of post-fire landscapes. *Elementa: Science of the Anthropocene*. 5: 2. 5, doi: <http://doi.org/10.1525/elementa.185>.
- Wagenbrenner, N.S., Lamb, B.K., Foltz, R.B., Robichaud, P.R., 2010. Modeling Post-Fire Ash and Dust Emissions in Complex Terrain, 2010 Pittsburgh, Pennsylvania, June 20 - June 23, 2010. ASABE, St. Joseph, MI, doi: <https://doi.org/10.13031/2013.31937>.
- Wang, J., Zhang, W., Zhang, Z., 2019. Impacts of Land-Use Changes on Soil Erosion in Water–Wind Crisscross Erosion Region of China. *Remote Sensing* 11, 1732, doi: <https://doi.org/10.3390/rs11141732>.
- Wang, X., Liu, T., Li, F., Gao, R., Yang, X., Duan, L., Luo, Y., Li, R., 2014. Simulated soil erosion from a semiarid typical steppe watershed using an integrated aeolian and fluvial prediction model. *Hydrological Processes* 28, 325-340, doi: <https://doi.org/10.1002/hyp.9579>.
- Wang, X., Zhao, X.L., Zhang, Z.X., Yi, L., Zuo, L.J., Wen, Q.K., Liu, F., Xu, J.Y., Hu, S.G., Liu, B., 2016. Assessment of soil erosion change and its relationships with land use/cover change in China from the end of the 1980s to 2010. *Catena* 137, 256-268, doi: <https://doi.org/10.1016/j.catena.2015.10.004>.
- Webb, N.P., Herrick, J.E., Duniway, M.C., 2014. Ecological site-based assessments of wind and water erosion: informing accelerated soil erosion management in rangelands. *Ecological Applications* 24, 1405-1420, doi: <https://doi.org/10.1890/13-1175.1>.
- Webb, N.P., Herrick, J.E., Van Zee, J.W., Courtright, E.M., Hugenholtz, C.H., Zobeck, T.M., Okin, G.S., Barchyn, T.E., Billings, B.J., Boyd, R., Clingan, S.D., Cooper, B.F.,

- Duniway, M.C., Derner, J.D., Fox, F.A., Havstad, K.M., Heilman, P., LaPlante, V., Ludwig, N.A., Metz, L.J., Nearing, M.A., Norfleet, M.L., Pierson, F.B., Sanderson, M.A., Sharratt, B.S., Steiner, J.L., Tatarko, J., Tedela, N.H., Toledo, D., Unnasch, R.S., Van Pelt, R.S., Wagner, L., 2016. The National Wind Erosion Research Network: Building a standardized long-term data resource for aeolian research, modeling and land management. *Aeolian Research* 22, 23-36, doi: <http://dx.doi.org/10.1016/j.aeolia.2016.05.005>.
- Webb, N.P., Van Zee, J.W., Karl, J.W., Herrick, J.E., Courtright, E.M., Billings, B.J., Boyd, R., Chappell, A., Duniway, M.C., Derner, J.D., Hand, J.L., Kachergis, E., McCord, S.E., Newingham, B.A., Pierson, F.B., Steiner, J.L., Tatarko, J., Tedela, N.H., Toledo, D., Scott Van Pelt, R., 2017. Enhancing Wind Erosion Monitoring and Assessment for U.S. Rangelands. *Rangelands* 39, 85-96, doi: <https://doi.org/10.1016/j.rala.2017.04.001>.
- Williams, R.J., Bradstock, R.A., Cary, G.J., Enright, N.J., Gill, A.M., Liedloff, A.C., Lucas, C., Whelan, R.J., Andersen, A.N., Bowman, D.M.J.S., Clarke, P.J., Cook, G.D., Hennessy, K.J., York, A., 2009. Interactions between climate change, fire regimes and biodiversity in Australia - a preliminary assessment. Department of Climate Change,
Department of the Environment, Water, Heritage and the Arts, Canberra, <http://researchrepository.murdoch.edu.au/id/eprint/14926>
- Wischmeier, W.H., Smith, D.D., 1978. Predicting rainfall erosion losses-A guide to conservation planning. *Predicting rainfall erosion losses-A guide to conservation planning*,
- Woodruff, N., Siddoway, F., 1965. A wind erosion equation. *Soil Science Society of America Journal* 29, 602-608,
- World Meteorological Organisation, 2019. United in Science. Science Advisory Group of the UN Climate Action Summit 2019, https://public.wmo.int/en/resources/united_in_science
- Young, M.-A., Herrmann, T., 2015. Celebrating 75 years of Soil-Care, 2015 State Community Landcare Conference. Government of South Australia, Department of Environment, Water and Natural Resources, Waikerie,
- Zdruli, P., Karydas, C.G., Dedaj, K., Salillari, I., Cela, F., Lushaj, S., Panagos, P., 2016. High resolution spatiotemporal analysis of erosion risk per land cover category in Korçe region, Albania. *Earth Science Informatics* 9, 481-495, doi: <https://doi.org/10.1007/s12145-016-0269-z>.
- Zema, D.A., Nunes, J.P., Lucas-Borja, M.E., 2020. Improvement of seasonal runoff and soil loss predictions by the MMF (Morgan-Morgan-Finney) model after wildfire and soil treatment in Mediterranean forest ecosystems. *CATENA* 188, 104415, doi: <https://doi.org/10.1016/j.catena.2019.104415>.

- Zhang, C., McBean, E.A., 2016. Estimation of desertification risk from soil erosion: a case study for Gansu Province, China. *Stochastic Environmental Research and Risk Assessment* 30, 2215-2229, doi: <https://doi.org/10.1007/s00477-015-1186-2>.
- Zhu, Q., Yang, X., Yu, B., Tulau, M., McInnes-Clarke, S., Nolan, R.H., Du, Z., Yu, Q., 2019. Estimation of event-based rainfall erosivity from radar after wildfire. *Land Degradation & Development* 30, 33-48, doi: <https://doi.org/10.1002/ldr.3146>.

Chapter 2

Mapping the spatio-temporal variability of hillslope erosion with the G2 model and GIS: A case-study of the South Australian agricultural zone

Statement of Authorship

Title of Paper	Mapping the spatio-temporal variability of hillslope erosion with the G2 model and GIS: A case-study of the South Australian agricultural zone
Publication Status	<input type="checkbox"/> Published <input type="checkbox"/> Accepted for Publication <input checked="" type="checkbox"/> Unpublished and Unsubmitted work written in manuscript style <input type="checkbox"/> Submitted for Publication
Publication Details	Jeanneau, A., Herrmann, T. & Ostendorf, B (2020). Assessing the spatio-temporal variability of extreme erosion events with the G2 water erosion model and GIS: A case-study of the South Australian agricultural zone (unpublished)

Principal Author


Name of Principal Author (Candidate)	Amelie Jeanneau	
Contribution to the paper	Conceptualization, methodology, data curation, formal analysis, writing – original draft preparation, writing – review and editing.	
Overall percentage (%)	70%	
Certification	This paper reports on original research I conducted during the period of my Higher Degree by Research candidature and is not subject to any obligations or contractual agreements with a third party that would constrain its inclusion in this thesis. I am the primary author of this paper.	
Signature		Date: 04/06/2020

Co-author Contributions

By signing the Statement of Authorship, each author certifies that:

- i. the candidate's stated contribution to the publication is accurate (as detailed above);
- ii. permission is granted for the candidate to include the publication in the thesis; and
- iii. the sum of all co-author contributions is equal to 100% less the candidate's stated contribution.

Name of Co-Author	Tim Herrmann	
Contribution to the Paper	Methodology, formal analysis, writing – review and editing.	
Signature		Date: 04/06/2020

Name of Co-Author	Bertram Ostendorf	
Contribution to the Paper	Methodology, formal analysis, writing – review and editing.	
Signature		Date: 04/06/2020

Abstract

Soil erosion is a major cause of land degradation globally and requires consistent and continuous monitoring methods to ensure future agricultural productivity and soil security. Therefore, tools to investigate the impact and frequency of erosive events are crucial for land managers and policymakers in order to apply corrective measure for better erosion management in the future. Here we applied the G2 erosion model to two agricultural regions of South Australia, Australia (the Eyre Peninsula and Mid-North) to predict and monitor monthly hillslope erosion. We also explored the use of a high spatio-temporal resolution rainfall product combined with other high-resolution datasets to develop a model that realistically represents the complex combination of critical drivers of erosion. The modelling outputs were used to identify the spatial and temporal variation of hillslope erosion in South Australia to support cost-effective soil and land-management strategies. The average annual hillslope erosion was relatively low, but regional erosion estimates were about two times higher for the Eyre Peninsula ($0.048 \text{ t ha}^{-1} \text{ y}^{-1}$) compared to the Mid-North region ($0.114 \text{ t ha}^{-1} \text{ y}^{-1}$). The Flinders Ranges and Orroroo/Carrieton Local Government Areas (LGAs) were predicted to be the most impacted by erosion between 2001 and 2017 (0.19 and $0.21 \text{ t ha}^{-1} \text{ y}^{-1}$ respectively). On the other hand, hillslope erosion estimates were very low for most of the Eyre Peninsula and the Adelaide Plains LGA. The model presented in this paper could be applied elsewhere as the input data can be downloaded through open access platforms Australia-wide, and similar datasets are available globally.

2.1 Introduction

Soil erosion, more particularly sheet and rill (hillslope) erosion, is a major cause of land degradation globally and is listed as one of the top priority in the Land Degradation Neutrality (LDN) framework (FAO, 2011, 2019). Hillslope erosion removes topsoil containing vital nutrients, organic matter and soil carbon, therefore, leading to a decrease in soil productivity and biodiversity (Baumhardt et al., 2015; Montgomery,

2007). This erosion process can also lead to off-site consequences like pollution through nutrient leaching to water bodies and sedimentation of reservoirs (Rickson, 2014).

Measurements of soil erosion in the field with rainfall simulators and standardised plots provided the foundation for the development of models used in risk assessment and regional management of the soil resource. However, measurements are restricted to fine-scales and extrapolation to regional- or continental-scale applications is challenging. Thus, empirical and physical models have been developed to describe erosional processes. Recent technological advances in remote sensing and Geographic Information System (GIS), have substantially contributed to the development and application of erosion models as a growing number of them were designed to integrate GIS, digital maps and satellite data (Flanagan et al., 2013; Panagos and Katsoyiannis, 2019). Advances in spatial technologies have also been crucial to improving the management relevance of erosion models. As a result, governments increasingly rely on models to assess soil erosion for policy development. For example, in Europe, the European Commission derived a range of hillslope erosion maps from soil erosion modelling to set soil protection targets within the Common Agricultural Policy (CAP) (Panagos and Katsoyiannis, 2019).

Prediction models generally differ in their definition of the processes causing erosion, their underlying theory and the type of input data required. The most commonly used models include the (Revised) Universal Soil Loss Equation (R/USLE) (Renard et al., 1997; Wischmeier and Smith, 1978), the Water Erosion Prediction Project (WEPP) (Foster and Lane, 1987; Nearing et al., 1989), and the European Soil Erosion Model (EUROSEM) (Morgan et al., 1998). The RUSLE-derived models are the most popular for soil erosion prediction at large scales over a diverse range of ecosystems (Panagos et al., 2018) due to the simplicity of the models, the availability of data and their easy integration in GIS and mapping software. In Australia, the SOILOSS program was developed in 1992 to model hillslope erosion at the farm scale (Rosewell, 1993). SOILOSS follows similar USLE principles, but some of the parameters were adapted to local conditions through field measurements in NSW (e.g. *R*-, *C*-, *K*- factors). However, one of

the major limitations of this program is that it relies on information from look-up tables, particularly for estimation of the *C*- and *K*-factors, and does not make use of the most recent remote sensing and digital soil mapping products for Australia (Grundy et al., 2015; Guerschman et al., 2015).

The RUSLE approach has also been used in Australia to predict hillslope erosion at the continental scale (Lu et al., 2003; Teng et al., 2016). These two studies estimated the long-term annual sheet and rill erosion based on national soils and land use datasets. However, these approaches are not suitable for regional assessment of hillslope erosion. Although the model of Lu et al. (2003) made use of remote sensing technology to estimate the monthly vegetation cover (*C-factor*), the spatial resolution of some of the input parameters was too coarse to capture the spatial variability of erosion patterns (e.g. NDVI: 1km; DEM: 250m). Another limitation of this approach was the misclassification of dry or dead vegetation as bare soil, increasing overall erosion predictions. Teng et al. (2016), on the other hand, didn't use a seasonal cover management factor. Instead, they assigned annual *C-factor* values to a range of land cover classes from the Dynamic Land Cover Dataset (DLCD) (Lymburner et al., 2011). This approach has been criticised by McKenzie et al. (2017) who suggested that using fractional vegetation cover would be more appropriate to describe seasonal vegetation dynamics than the DLCD. The authors also highlighted that fractional vegetation cover could prevent misclassification of dry vegetation as bare soil, as seen in the model of Lu et al. (2003). To make better use of the emerging fractional vegetation cover product for Australia (Guerschman et al., 2015) and alleviate the issues abovementioned, Yang (2014) developed a regression relationship between ground cover (photosynthetic (PV) + non-photosynthetic (NVP) vegetation), and the cover and management factor (*C-factor*). This new equation is well adapted for landscapes with zero disturbances, such as rangelands and natural vegetation landscapes. However, the author cautioned not to use the regression relationship for agricultural landscapes as it does not take into account the influence of different land management and treatments on land cover. An alternative approach proposed by the G2 model (Panagos et al., 2014a) could be applied to

agricultural landscapes of Australia to combine the use of fractional vegetation products and land use and land cover classifications (ABARES, 2016; Willoughby et al., 2018). G2 is a quantitative algorithm derived from the RUSLE and Gavrilovic (1988) concepts, and quantifies hillslope erosion and sediment yield rates at monthly time intervals. The authors also introduced a new parameter accounting for the effect of landscape alteration on soil erosion in a more recent manuscript (Karydas and Panagos, 2018). The G2 model has been successfully applied in several European countries and yielded good results (Karydas et al., 2020; Panagos et al., 2014a; Zdruli et al., 2016).

Erosion is a complex process, influenced by a combination of factors (e.g. soil properties, landscape, climate) which vary strongly in space and time. Thus, to better represent these complex interactions and the spatio-temporal variability in erosion, we need to use high-resolution input datasets. For example, rainfall erosivity is a key driver of erosion and is highly variable in space and time (Nearing et al., 2017). Climate change will also likely increase the spatio-temporal variability of rainfall patterns, making the estimation of trends even more difficult. Therefore, to deal with this uncertainty, we need access to localised rainfall data at a high temporal resolution to better predict relative erosion patterns. The Australian Bureau of Meteorology Atmospheric high-resolution Regional Reanalysis dataset for Australia (BARRA) can deal with some of this uncertainty (Su et al., 2019). It provides spatially explicit hourly precipitation accumulation data for each pixel in the study area, which enables a better characterisation of erosive rainfall events. The use of hourly rainfall intensity is also more in line with the original USLE approach and the latest recommendations from Nearing et al. (2017). With this approach, we can then identify where and when high erosive events occur, and also estimate the frequency distribution of these erosive rainfall events. Combining the BARRA hourly rainfall data with the most recent remote sensing and digital soil mapping products for Australia will improve the level of details and accuracy of hillslope erosion estimates for South Australia (SA) compared to the previous modelling approaches.

Therefore, the aims of this study are i) to explore the use of BARRA combined with other high-resolution datasets to develop a model that realistically represents the complex

combination of critical drivers of erosion, and ii) to identify the spatial and temporal variation of hillslope erosion in South Australia to support cost-effective soil and land-management strategies. For this reason, we will use the Eyre Peninsula and Mid-North regions of South Australia as a case-study application.

2.2 Methods

2.2.1 *The study area*

Our study focusses on two dryland agricultural regions of South Australia, Australia: Eyre Peninsula (EP – 33°568'S 135°755'E – 4.7x10⁴ km²) and the Mid-North (MidN – 33°376'S 138°723'E – 3,4x10⁴ km², Figure 2.1). These two regions are major contributors to agricultural production in South Australia (ABARES, 2018) and part of these regions are historically prone to hillslope erosion, therefore representing an essential interest for food and soil security. Agricultural land uses represent the majority of the regional land uses (Figure 2.2) with cereal cropping representing 50% and 33% of the land surface for the Eyre Peninsula and Mid-North respectively, followed by grazing (modified) pastures, representing 11% and 54% of the total regional land use for the regions, respectively (ABARES, 2016).

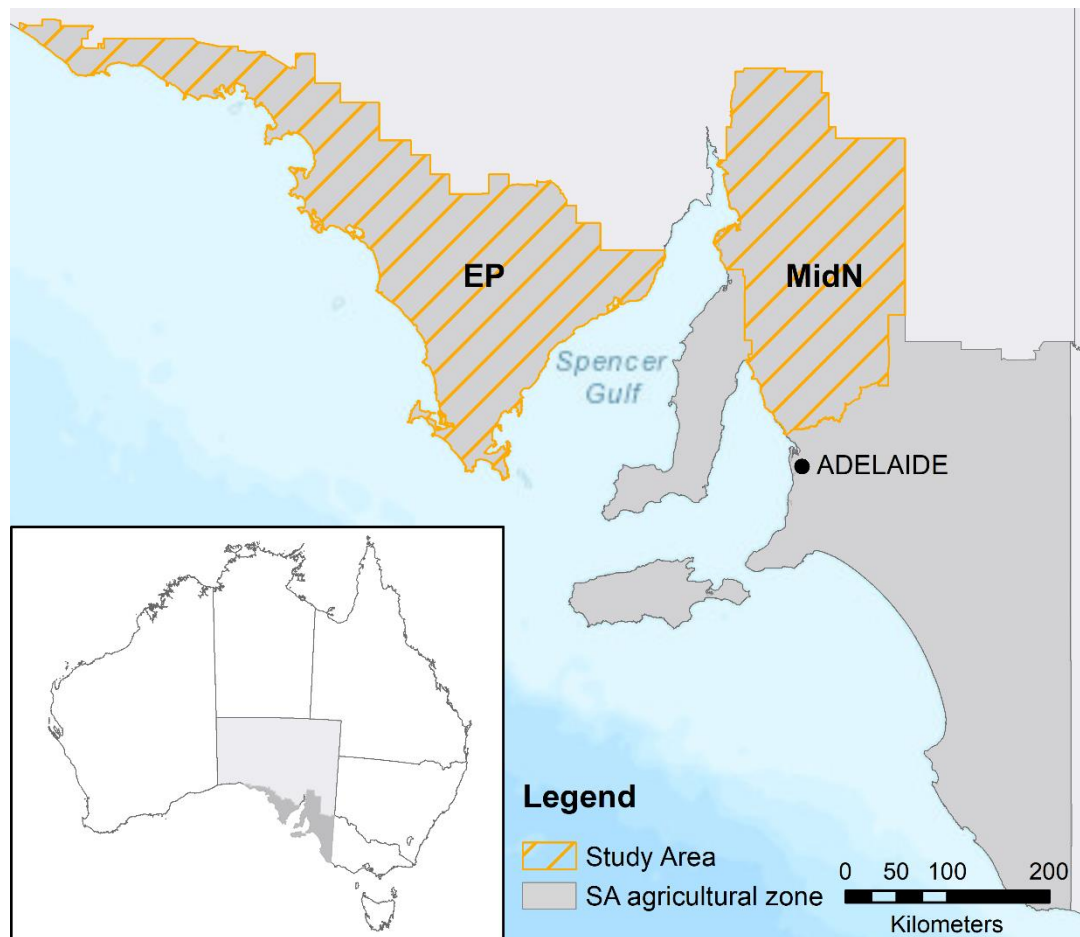


Figure 2.1 Location map and presentation of the study area (Eyre Peninsula & Mid-North) within the South Australian agricultural zone.

The two regions are characterised by a Mediterranean climate, with cool wet winters and hot dry summers with occasional summer storms and exhibit diverse soils and land uses, providing an excellent study site to demonstrate the utility of erosion modelling for land management. Mean annual rainfall ranges from 200mm in the north to 500mm in the south, with a mean of 350mm (BoM, 2016a). The average daily temperature varies between 12 and 19°C (BoM, 2016b). The agricultural region of Eyre Peninsula has a range of sandy to clay-loam soils (Figure 2.3). On the other hand, dominant soil types throughout the Mid-North region are more diverse and predominantly loam or clay-loam soils, with some sandy-loam patches (Figure 2.3). Elevation in the Eyre Peninsula region ranges between 0m and 480m, and from south-west to north-east. For the Mid-North region, altitude ranges between 0m and 950m above sea level with the highest elevations found in the centre of the region. The topography is complex in this area, and some parts have very steep slopes with gradients ranging from 0% to 60%.

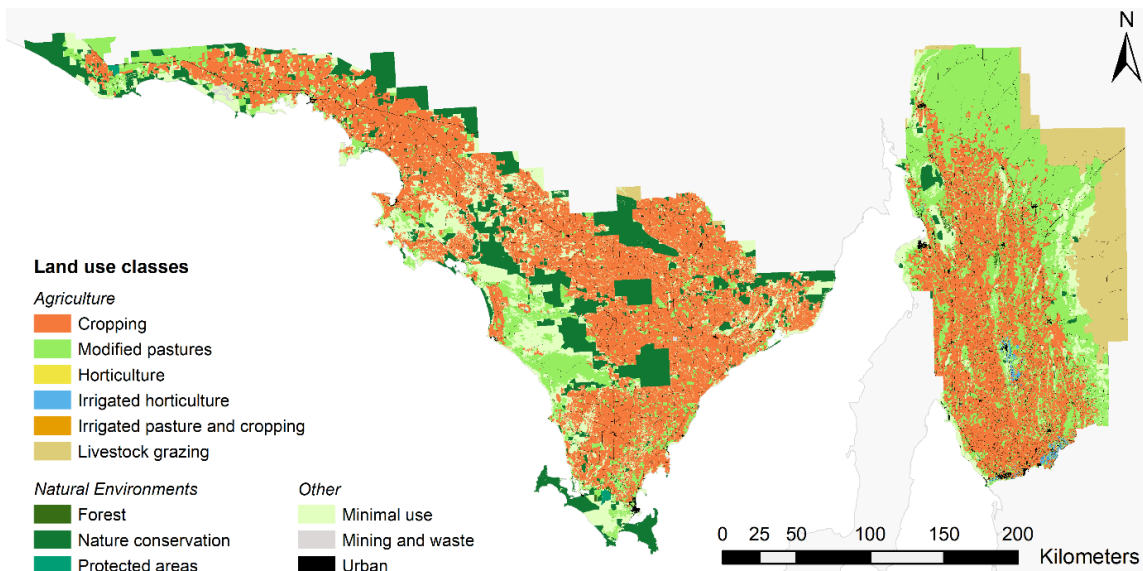


Figure 2.2 Land use classes for the Eyre Peninsula and Mid-North regions. Source: ABARES (2016).

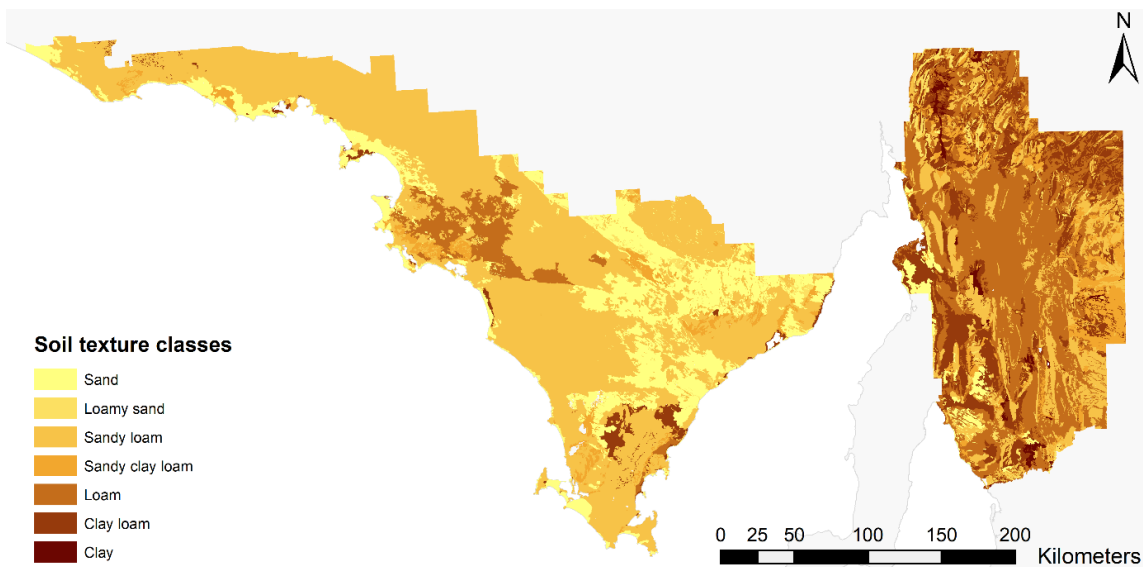


Figure 2.3 Dominant soil texture classes for the Eyre Peninsula and Mid-North regions. Source: DEW (2016)

2.2.2 Description of the data sources

All the datasets used in this study have been acquired from open-source databases. Data description (e.g. type, resolution, sources) can be found in Appendix A – Table A.1. Climate and weather data were obtained from the Australian Bureau of Meteorology Atmospheric high-resolution Regional Reanalysis dataset for Australia (BARRA) (Su et al., 2019). This reanalysis dataset compiles all available observations and uses weather models to fill in the fine details of atmospheric and land surface conditions. The BARRA dataset covers the Australian continent and the surrounding regions, including parts of

south-east Asia, New Zealand and south to the ice of the Antarctic continent Appendix A – Figure A.1. This dataset also offers hourly spatial resolution for about 100 parameters including temperature, precipitation accumulation, wind speed and direction, humidity, evapotranspiration and soil moisture. The spatial resolutions are 12km at the continental scale and additional model run at 1.5km resolution for spatial subsets, including South Australia. Here we used the 1.5km resolution data.

Land use and land cover were derived from the South Australian Land Cover dataset (Willoughby et al., 2018). This dataset modelled land cover throughout the State of South Australia based on a combination of satellite imagery (Landsat), aerial photography and land use classification from National inventory (ABARES, 2016). This dataset classified the landscape in 17 ‘most likely’ land cover classes (Appendix A – Table A.1) and is available for six epochs (1987-1990, 1990-95, 1995-2000, 2000-05, 2005-10, 2010-15) at a spatial resolution of 25m. In the G2 model, the effect of landscape alterations on erosion can be derived from high-resolution satellite imagery (Karydas and Panagos, 2018). The authors have shown that a non-directional edge filter (i.e. Sobel filter) applied on the Near-Infrared (NIR) band of high-resolution imagery can capture landscape features intercepting slope and limiting hillslope erosion (e.g. roads, fences, hedges, terraces). For this reason, we used the NIR band of Landsat 7 imagery (accessed from the Google Earth Engine platform) for the period 2001 2017 at a resolution of 30m.

Ground cover was derived from Moderate Resolution Imaging Spectroradiometer (MODIS) fractional cover dataset for Australia (Guerschman et al., 2015). Guerschman et al. (2015) extracted three fractions representing the proportion of photosynthetic vegetation (PV), non-photosynthetic vegetation (NPV) and bare soil (BS) at monthly and 8-day time intervals. This product has significantly improved the mapping of ground cover for diverse uses and particularly for soil erosion modelling (Yang, 2014).

Topography was derived from the Advanced Land Observing Satellite (ALOS) Digital Surface Model (DSM) version 2.1 at a resolution of 30m (Tadono et al., 2014). The Soil and Landscape Grid of Australia (SLGA) digital soil property maps were used to extract

soils information necessary for erosion modelling (e.g. clay, silt and sand fractions; soil organic carbon (SOC) and coarse fragment content). The SLGA dataset is available at a resolution of 90m for the whole continent and can be programmatically downloaded through the *slga*:: R package (O'Brien, 2019), more information about the range of soil properties and landscape attributes can also be found at www.csiro.au/soil-and-landscape-grid. We also downloaded additional soil properties datasets from the Australian Soil Resource Information System (ASRIS) (ASRIS, 2011) such as hydraulic conductivity and surface stone cover for the refinement of the soil erodibility factor.

2.2.3 The hillslope erosion model

To estimate sheet and rill (hillslope) erosion, we adapted the G2 model of Panagos et al. (2014a) to Australian conditions. The structure of the G2 model is derived from the RUSLE with five input parameters combined in a multiplicative equation as

$$E_m = \frac{R_m}{V_m} \times S \times \frac{T}{L}, \quad (1)$$

where E_m is the soil loss for month m (t ha^{-1}), R_m is the total rainfall erosivity for each month ($\text{MJ mm ha}^{-1} \text{ h}^{-1} \text{ month}^{-1}$), V_m is the vegetation retention for month m (dimensionless), S represents the soil erodibility ($\text{t ha h ha}^{-1} \text{ MJ}^{-1} \text{ mm}^{-1}$), T is the terrain influence (dimensionless), and L represents the landscape effect (dimensionless).

Rainfall erosivity (R)

The rainfall erosivity factor represents the kinetic energy of raindrops and their capacity to detach and transport soil particles. Therefore, it is a function of rainstorm intensity and duration. In this study, we estimated R using 17 years (2001-2017) of hourly precipitation accumulation data. The R -factor was calculated by combining the approach from Vrieling et al. (2010) and standard procedures of Renard et al. (1997). As we are dealing with a considerable amount of spatio-temporal data, it would be inconvenient to use event-based processing on a pixel basis. Temporal aggregation (i.e. to average over months and years) is very difficult using true events because events span temporal

intervals that differ for every single pixel. We therefore suggest to use storm events defined as regular 3-hour time intervals but use the hourly intensity to most closely resemble the estimation of rainfall erosivity from original empirical relationships found from rainfall simulations (Wischmeier and Smith, 1978). See also Nearing et al. (2017) for a strong argument to acknowledge the vast empirical knowledge derived from these early studies. Furthermore, 3-hour time intervals are the highest temporal resolution of TRMM rainfall dataset, which is widely used to estimate the R-factor. Appendix B shows a critical appraisal for the comparability of different rainfall datasets interacting with a range of rainfall intensity-kinetic energy ($R-ek$) relationships.

First, we estimated the rainfall kinetic energy for each hour (e_{k_h}) from the rainfall intensity (I_h) following the empirical relationship proposed by van Dijk et al. (2002) and Nearing et al. (2017), based on extensive volume-specific rainfall energy-intensity relationship reviews across the globe

$$e_{k_h} = 0.283 \times [1 - 0.52 \times \exp^{-0.042 \times I_h}] \quad (2)$$

where e_{k_h} is expressed in MJ ha⁻¹ mm⁻¹ and I_h is expected in units of mm h⁻¹. Values for I_h were derived from the hourly precipitation of the BARRA dataset. Then, we estimated the total kinetic energy for each 3-hour storm (E_{3h}),

$$E_{3h} = \sum_{h=1}^3 (e_{k_h} \times p_h) \quad (3)$$

where E_{3h} is in MJ ha⁻¹ and p_h is the precipitation (mm) measured in an hour. The monthly and annual R-factor is then calculated as follow:

$$R = \sum_{k=1}^N (E_{3h})_k \times (I_{30})_k \quad (4)$$

where R is in MJ mm ha⁻¹ h⁻¹ y⁻¹, N is the total number of 3-hour storms in a year or a month, I_{30} is the maximum 30-min rainfall intensity scaled to mm h⁻¹. As suggested by Vrieling et al. (2010), we assumed I_{30} to be equivalent to the maximum rainfall intensity in a 3-hour storm (but see Appendix B for biases introduced by this assumption). The

R-factor was calculated for each month and year from 2001 to 2017 and resampled to 90m to be combined with the other G2 factors.

Vegetation retention (V)

In the RUSLE model, the cover management factor (*C-factor*) assesses the combined effect of surface vegetation and canopy cover as well as surface roughness, crop management and soil organic matter content. It is characterised as the ratio of soil loss from land cultivated under particular conditions to the equivalent loss from continuous tilled fallow conditions. Depending on the level of information available, we can find many ways to estimate the *C-factor*, which offer various levels of accuracy (Panagos et al., 2015b; Yang, 2014). In Australia, Yang (2014) proposed an exponential regression relationship between ground cover (PV+NPV) and the *C-factor* instead of using long-term annual values derived from look-up tables. This method significantly improved the estimation of the cover management factor and allowed a seasonal assessment of soil erosion. However, the authors cautioned to only apply this method for landscapes with zero disturbance, such as rangelands and natural vegetation because it does not take into account the influence of different land management and treatments on land cover.

In the original USLE model, the *C-factor* is reduced non-linearly with increasing ground cover and differs to different degrees for a variety of tillage practices (Wischmeier and Smith, 1978). For this reason, Panagos et al. (2014a) introduced a new parameter: the retention effect of vegetation (*V*). Similarly to the *C-factor*, the values of *V* are different for comparable ground cover fractions to emphasise the influence of different land uses for the same vegetation coverage. The authors thus proposed an exponential curve to correlate the fraction of ground cover and the *V-factor* to satisfy the non-linear variability of the *C-factor* and introduced a land-use parameter (*LU*) to represent the influence of different land management and treatments on land cover. The authors also defined the *V-factor* as inversely analogous to the USLE *C-factor* to highlight the protective effect of ground cover and land use against erosion. The form of this function

is very similar to previous Australian studies (Webb et al., 2009; Yang, 2014), but has the advantage of taking into account the effect of land use and land management in the calculations of V and is not restricted to non-disturbed landscapes (e.g. rangelands and natural vegetation).

In the G2 model, V is a dynamic factor which combines time-series of ground cover (PV+NPV) and a constant empirical land-use parameter (LU). This factor is defined by the following expression

$$V_{mj} = e^{(LU_j \times FC_m)} \quad (5)$$

where V_{mj} is the vegetation retention for month m and land use j (normalised $[1 - +\infty]$, dimensionless), with $V = 1$ for bare or heavily managed agricultural land and $V > 1$ for land with better land management practices; FC_m is the monthly fraction of the ground covered by photosynthetic and non-photosynthetic vegetation (normalised $[0-1]$); LU_j is an empirical land-use parameter for a particular land use j ranging from 1 to 10, lower values represent intensive land management or unprotected land uses. In comparison, a higher LU represents better land-management conditions.

Panagos et al. (2014a) developed a look-up table derived from the CORINE Land Cover classification database and interpretation of the Gavrilovic model dataset (or Erosion Potential Method, EPM) (Gavrilovic, 1988) to define the values of LU for a range of land uses. The Gavrilovic model contains information about the influence of land use and land management on erosion control: X_a parameter (analogous to the C-factor). To satisfy the conditions of the V -factor in equation (5), the X_a values (ranging from 0 to 1) were converted to LU (ranging from 1 to 10) with a simple linear inversion (indicative examples in Table 2.1)

$$LU = \begin{cases} -10 \times X_a + 11, & X_a \geq 0.1 \\ 10, & X_a < 0.1 \end{cases} \quad (6)$$

Table 2.1 Indicative examples of the conversion of EPM conservation coefficients into LU values. Source: Panagos et al. (2014a)

Gavrilovic land-use categories	Conservation coefficient (X_a)	Corresponding CORINE LC codes	LU
Forestation	0.600	3111/312/313/323	5.0

Orchards and vineyards	0.315	221/222/223	7.9
Contour farming strip cultivation with crop rotation	0.450	211/212/213	6.5
Meadows and similar perennial crops	0.400	-	7.0
Grazing, meadows amelioration	0.300	231	8.0
Mountain pastures	0.600	321	5.0
Ploughed field up and down a slope	0.900	-	2.0
Barren untilled soil	1.000		1.0

Table 2.2 Correspondence table between the SA Land Cover dataset and the look-up table of Karydas and Panagos (2016, 2018)

SA Land Cover Dataset	Classes from Karydas and Panagos (2016, 2018)	LU
Woody Native Vegetation	Sclerophyllous vegetation	9
Mangrove Vegetation	NA	9
Non-Woody Native Vegetation	Natural grasslands	7
Saltmarsh Vegetation	Salt marshes/salines	10
Wetland Vegetation	Inland marshes	10
Natural Low Cover	Natural grasslands	7
Salt Lake/ Saltpan	Salines	10
Dryland Agriculture	Non-irrigated arable land	5.5
Exotic Vegetation	Moors and heathland	7
Irrigated Non-Woody	Annual crops associated with permanent crops	5.5
Orchards/ Vineyards	Vineyards/Fruit trees/Olive groves	7.8
Plantation (Softwood)	Coniferous forest	10
Plantation (Hardwood)	Broad-leaved forest	10
Urban Area	Discontinuous urban fabric	10
Built-up Area	Industrial or commercial units	10
Disturbed Ground / Outcrop	Mineral extraction sites	1
Water Unspecified	Water bodies	10

The look-up table for *LU* values was later updated to include a broader range of land uses (Karydas and Panagos, 2016, 2018). In our study, we used this reference set and expert knowledge from the Department for Environment and Water (DEW) to obtain *LU* values adapted to the South Australian Land Cover dataset classification (Table 2.2).

We estimated the *V-factor* for each month and year from 2001 to 2017 by applying equation (5) with the MODIS fractional cover dataset and the *LU* parameter from Table 2.2. The *V-factor* was resampled to 90m resolution to match the resolution of the other G2 factors.

Soil erodibility (S)

The soil erodibility factor (S in $\text{t ha h ha}^{-1} \text{ MJ}^{-1} \text{ mm}^{-1}$), represents the susceptibility of the soil to erosion as measured in standard unit plot conditions. Because direct measurements of S -factor are impossible at broad spatial scales, the soil erodibility nomograph (Wischmeier and Smith, 1978) is the most commonly used and cited tool for soil erodibility estimation. The nomograph is a representation of the soil aggregate size distribution and properties (clay sand, silt and organic carbon content, soil structure and profile permeability) adopting the following expression

$$S = 2.766 \times M^{1.14} \times 10^{-7} \times (12 - OM) + 4.28 \times 10^{-3} \times (ss - 2) + 3.28 \times 10^{-3} \times (pp - 3) \quad (7)$$

where M is the textural factor defined as the percentage of silt + fine sand fraction times (100 – clay fraction); OM is the organic matter content defined as 1.72 times the organic carbon content (%), ss is the soil structure class ($ss = 1$: very fine granular, $ss = 2$: fine granular, $ss = 3$, medium or coarse granular, $ss = 4$: blocky, platy or massive); pp is the soil permeability class (Table 2.3).

As there was no sufficient information to reliably estimate the spatial distribution of soil structure in our study area, we used a uniform value of $ss = 2$ as recommended by Rosewell (1993) and Teng et al. (2016). We defined the soil permeability classes following the recommendations of Panagos et al. (2014b) associated with hydraulic conductivity information from the ASRIS database (ASRIS, 2011).

Table 2.3 Soil permeability codes for corresponding soil hydraulic conductivity

Permeability class (pp)	Hydraulic conductivity
1 (fast and very fast)	> 130 mm/h
2 (moderate fast)	60 – 130 mm/h
3 (moderate)	20 – 60 mm/h
4 (moderate low)	5 – 20 mm/h
5 (slow)	1 – 5 mm/h
6 (very slow)	< 1 mm/h

The nomograph expression is only valid if the organic matter content is known and the silt fraction is lower than 70%, which is the case for soils of Southern South Australia. The estimation of the S -factor using this methodology required two adaptations, relating to the organic matter content and the very fine sand fraction.

The nomograph equation presented above is only applicable for soils with organic matter content below 4%; therefore, we applied an upper limit of 4% to soils in our region of interest. This limit is designed to reduce an underestimation of soil erodibility for soils which are rich in organic matter.

Sand content is generally classified into five categories of sand: very fine, fine, medium, coarse, very coarse in the literature. If no information about the very fine sand fraction was available, Panagos et al. (2014b) proposed to define the very fine sand fraction as 20% of the total sand. According to Loch and Rosewell (1992), the particle size parameter M explains up to 85% of the variability in soil erodibility (S-factor). The higher the fraction of particles in the 0.002 - 0.10 mm range, the higher the soil erodibility. It is therefore important to ensure that the fraction of very fine sand and silt particles is well defined for a more reliable estimation of soil erodibility. Unfortunately, there currently is no continental-scale spatial dataset containing information about the very fine sand fraction in Australia. We tested the application of the assumption from Panagos et al. (2014b) and found that this assumption did not hold for Australian soils where the fine and very fine sand fractions can represent up to 40-50% of the total sand fraction. Appendix C shows a comprehensive comparison of different assumptions to estimate the very fine sand fraction and provides details on the regression analysis conducted to derive a new relationship for the definition of the very fine sand fraction in Australia.

Topographic influence (T)

In the G2 model, the influence of topography on soil erosion (T) follows the approach of Desmet and Govers (1996) using the concept of unit contributing area

$$T = T_L \times T_S \quad (8)$$

with

$$T_L = \frac{(A_{i,j-in} + D^2)^{m+1} - A_{i,j-in}^{m+1}}{x_{i,j}^m \times D^{m+2} \times 22.13^m} \quad (9)$$

where T_L represents a slope length parameter, $A_{i,j-in}$ is the contributing area at the inlet of a grid cell (i, j) , or flow accumulation (m^2). D is the grid cell size (m), $x_{i,j}$ is a parameter influenced by the aspect direction of the grid cell (i, j) (Table 2.4).

Table 2.4 Constant values for $x_{i,j}$ parameter

Values for $x_{i,j}$	Aspect direction
1	N, E, S, W
1.4	NE, SE, SW, NW

m is related to the ratio β of rill to interill erosion.

$$m = \frac{\beta}{(1 + \beta)} \quad (10)$$

where,

$$\beta = \frac{(\sin \alpha / 0.0896)}{(3(\sin \alpha)^{0.8} + 0.56)} \quad (11)$$

α is the slope angle in degrees. The ratio m ranges between 0 and 1 and approaches 0 when the ratio of rill to interill erosion is close to 0.

The estimation of slope influence (T_S) is based on the slope gradient s and is calculated using

$$T_S = \begin{cases} 10.8 \sin \alpha + 0.03, & s < 9\% \\ 16.8 \sin \alpha - 0.5, & s \geq 9\% \end{cases} \quad (12)$$

This methodology has shown the ability to capture the influence of complex topography on soil erosion (Desmet and Govers, 1996; Panagos et al., 2015a). However, to limit accuracy errors inherent to Digital Elevation Models (DEMs), Panagos et al. (2014a) suggested to only use DEMs with a spatial resolution of 30m or higher.

The T-factor was then derived from the 30m ALOS DSM for the Eyre Peninsula and Mid-North regions with *LS-factor field-based* topographic indices from the hydrology module contained in SAGA (System for Automated Geoscientific Analyses) software, which incorporates the multi-flow algorithm described above (Pilesjö and Hasan, 2014). The *T-factor* was then resampled to 90m to match the resolution of the other model parameters.

Landscape alteration effect (L)

The *L-factor* represents the effect of land use and land cover alterations on soil erosion. This parameter can capture landscape features intercepting rainfall runoff, thus limiting hillslope erosion. The landscape alteration factor can also be considered to have a compensating effect on the topography influence factor (*T*), in the sense that can reduce slope length (T_L).

The L-factor is calculated using a 3x3 Sobel filter (non-directional edge-detection filter) applied on the NIR band of satellite imagery with a similar or greater resolution to that of the DEM used for T. For this reason, we applied this filter on Landsat 7 imagery with the `spatialEco::R`-package (Evans, 2018). The Sobel filter aims to highlight 'edge' features such as roads, terraces, contour ridges. The L-factor can then be estimated as follow

$$L = 1 + \sqrt{S_f / DN_{max}} \quad (13)$$

where *L* is the landscape effect in range (ranging from 1 to 2), S_f is the Sobel filter value (ranging from 0 to DN_{max}), and DN_{max} is the theoretic maximum digital number of the image (e.g. 255 for 8-bit recording systems, 1 for 32-bit imagery). We estimated the *L-factor* on monthly sets of Landsat imagery than averaged the value for each pixel over a year and repeated the process for the period 2001-2017. The *L-factor* was then resampled to 90m and used along other G2 model factors to estimate soil loss over the study area.

Monthly and annual hillslope erosion rates between 2001 and 2017 were estimated across the Eyre Peninsula and Mid-North region at a cell size of 90m. Spatial distribution maps and frequency distribution histograms for each of the parameters are reported in Appendix D.

2.3 Results and Discussion

2.3.1 Spatial variability of hillslope erosion

Figure 2.4 presents the spatial variability in modelled annual hillslope erosion across the Eyre Peninsula and the Mid-North region between 2001 - 2017. The majority of the study area (c.a. 90%) was predicted to have a very low erosion susceptibility, below the “tolerable” hillslope erosion rate for Australia (c.a. $0.2 \text{ t ha}^{-1} \text{ y}^{-1}$) (Bui et al., 2011). At the same time, only 9.6% of the study area was estimated to be within the slight to moderate erosion severity category (0.2 to $2 \text{ t ha}^{-1} \text{ y}^{-1}$) (Table 2.5). Most of the moderately impacted land was in the Mid-North region and is characterised by steeper slopes (higher T) and higher rainfall erosivity (higher R).

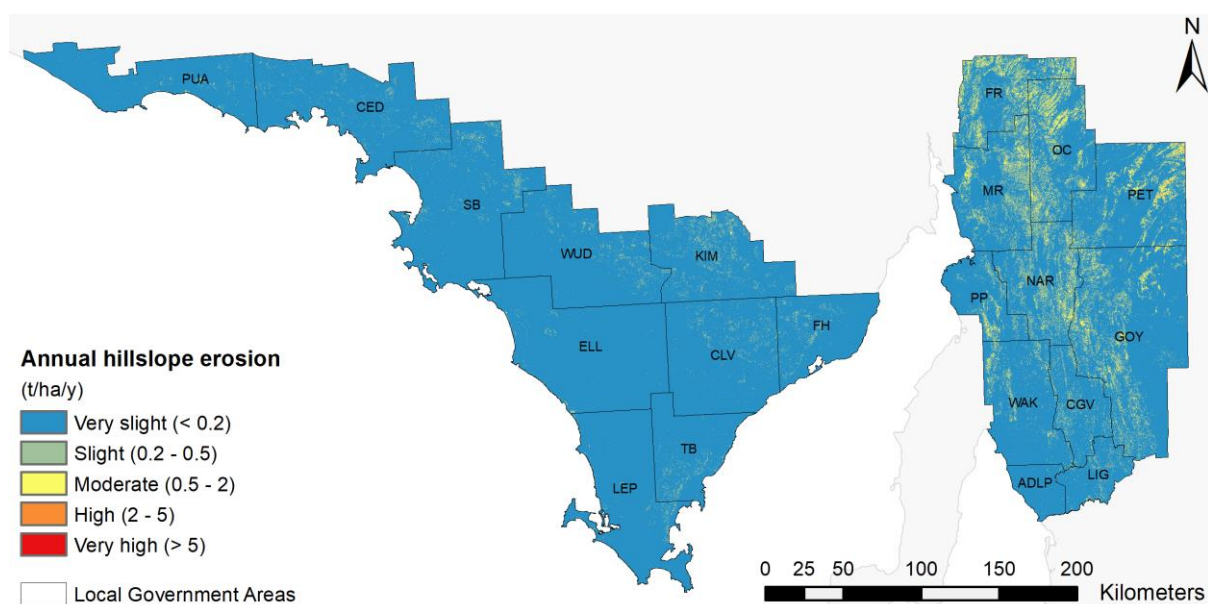


Figure 2.4 Modelled mean annual erosion severity across the Local Government Areas (LGA) of the Eyre Peninsula and Mid-North estimated with the G2 model. The LGAs represent a combination of environmental conditions, topography, climate with slightly different rainfall patterns and different farming systems.

Eyre Peninsula: PUA: Pastoral Unincorporated Area; CED: Ceduna; SB: Streaky Bay; WUD: Wudinna; KIM: Kimba; ELL: Elliston; CLV: Cleve; FH: Franklin Harbour; LEP: Lower Eyre Peninsula; TB: Tumby Bay.

Mid-North: FR: Flinders Ranges; MR: Mount Remarkable; OC: Orroroo/Carrieton; PET: Peterborough; PP: Port Pirie; NAR: Northern Areas; WAK: Wakefield; CGV: Claire Gilbert Valley; GOY: Goyder Regional Council; ADLP: Adelaide Plain; LIG: Light Regional Council

Conservation farming and the adoption of no-tillage has considerably improved land conditions across South Australia over the past decade (Young and Herrmann, 2015).

As a result, the number of observations of dust events and rill erosion has dramatically reduced (DEW, 2017; Hancock et al., 2015). These observations corroborate well with the spatial distribution patterns presented in Figure 2.4 and the low erosion rates predicted by the G2 model.

Table 2.5 Modelled hillslope erosion severity classes and their area percentages for the study area.

Erosion severity	Class range (t ha⁻¹ y⁻¹)	Area (km²)	Percent Area
Very slight	< 0.2	73,471	90.41
Slight	0.2 – 0.5	6,632	8.16
Moderate	0.5 – 2.0	1,134	1.40
High	2.0 – 5.0	27	0.034
Very high	> 5.0	5	0.006

Regional soil erosion estimates also differed substantially between the two regions of interest (Figure 2.5). The annual hillslope erosion in the Mid-North region was predicted to be about two and a half times larger than on the Eyre Peninsula during the period 2001-2017 (0.048 vs 0.114 t ha⁻¹ y⁻¹ respectively). This difference can be explained by the topography of the Mid-North region (higher *T*) as well as the dominant soil texture (higher *S*) and higher rainfall erosivity (higher *R*).

Regional soil erosion estimates also differed substantially between the two regions of interest (Figure 2.5). The annual hillslope erosion in the Mid-North region was predicted to be about two and a half times larger than on the Eyre Peninsula during the period 2001-2017 (0.048 vs 0.114 t ha⁻¹ y⁻¹ respectively). This difference can be explained by the topography of the Mid-North region (higher *T*) as well as the dominant soil texture (higher *S*) and higher rainfall erosivity (higher *R*).

On average, the highest predicted erosion rates in the Mid-North region were in the Flinders Ranges and the Orroroo/Carrieton LGAs (0.19 to 0.21 t ha⁻¹ y⁻¹), while Kimba, in the northern fringes of the Eyre Peninsula, appeared to be the most impacted (0.08 t ha⁻¹ y⁻¹) for this region. On the other hand, hillslope erosion estimates were very low for most of the Eyre Peninsula and the Adelaide Plains LGA.

The Local Government Areas in this study were characterised by different environmental conditions, topography, climate with slightly different rainfall patterns and different

farming systems. This combination of factors affected the modelled regional and sub-regional erosion susceptibility and resulted in observed inter- and intra-regional differences.

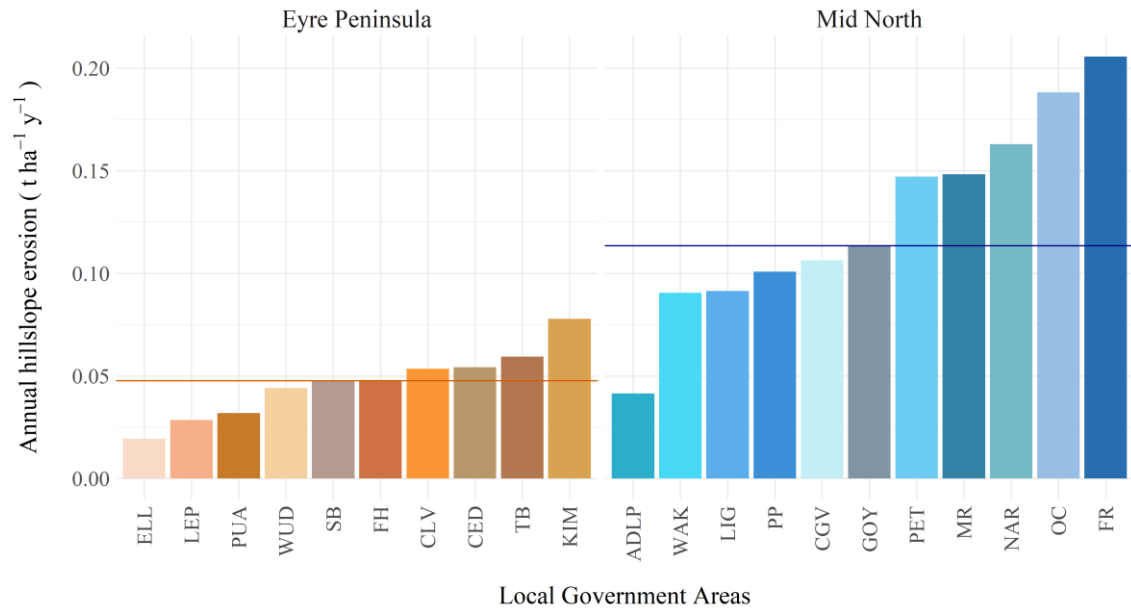


Figure 2.5 Modelled average annual hillslope erosion per Local Government Area (LGA). The horizontal lines represent the regional average annual soil loss (Eyre Peninsula = 0.048 t ha⁻¹ yr⁻¹ – Mid-North = 0.114 t ha⁻¹ yr⁻¹)

Eyre Peninsula: PUA: Pastoral Unincorporated Area; CED: Ceduna; SB: Streaky Bay; WUD: Wudinna; KIM: Kimba; ELL: Elliston; CLV: Cleve; FH: Franklin Harbour; LEP: Lower Eyre Peninsula; TB: Tumby Bay

Mid-North: FR: Flinders Ranges; MR: Mount Remarkable; OC: Orroroo/Carrieton; PET: Peterborough; PP: Port Pirie; NA: Northern Areas; WAK: Wakefield; CGV: Claire Gilbert Valley; GOY: Goyder Regional Council; ADLP: Adelaide Plain; LIG: Light Regional Council.

2.3.2 Temporal variation in hillslope erosion

Although annual erosion rates were predicted to be relatively low, Figure 2.6 shows high inter-annual variability in modelled hillslope erosion between 2001 and 2017 for both regions. Hillslope erosion was at its lowest between 2002 and 2006 for the Eyre Peninsula and Mid-North region, while the highest values were predicted for 2007 (EP: 0.11 t ha⁻¹ y⁻¹; MidN: 0.57 t ha⁻¹ y⁻¹) and 2011 (EP: 0.08 t ha⁻¹ y⁻¹; MidN: 0.17 t ha⁻¹ y⁻¹). Between 2001 and 2010, Southern Australia experienced a wide-spread drought (known

as the Australian ‘Millennium Drought’). During this period, ground cover and soil moisture were very low, leading to an increase in erosion susceptibility. This information could explain the increase in predicted hillslope erosion rates across the study area in 2007. A combination of very low ground cover and extreme rainstorm events (in January-February) likely led to more severe annual erosion in the study area, exceeding the recommended “tolerable” hillslope erosion threshold for Australia ($0.2 \text{ t ha}^{-1} \text{ y}^{-1}$) (Bui et al., 2011).

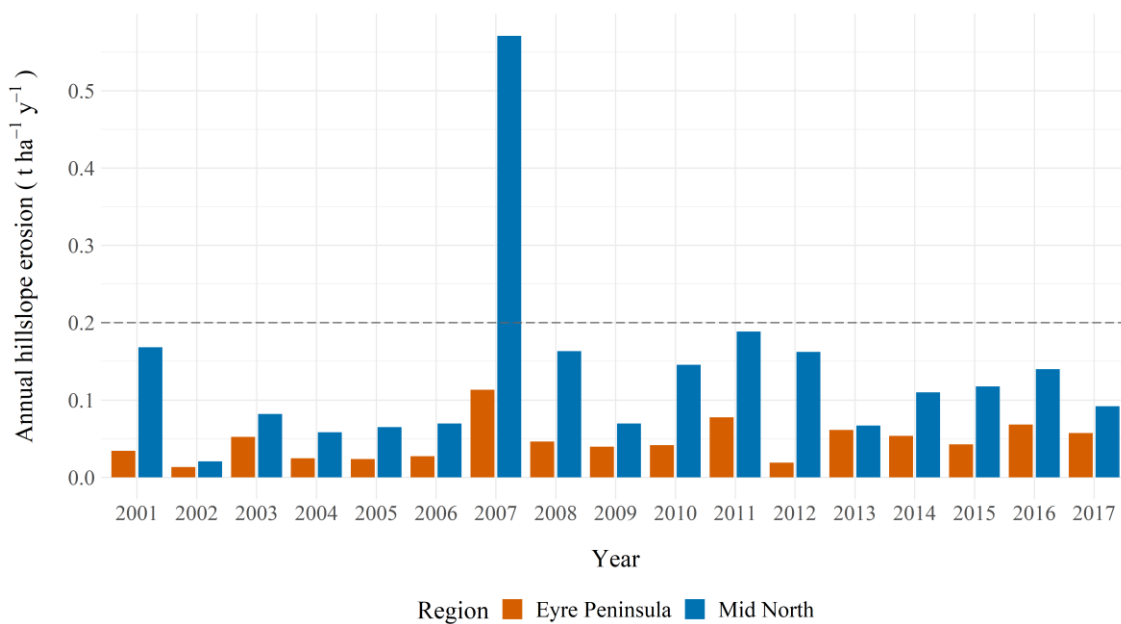


Figure 2.6 Temporal distribution of regional modelled annual hillslope erosion for the Eyre Peninsula and Mid-North region. The dashed line represents the Australian tolerable soil loss threshold of $0.2 \text{ t ha}^{-1} \text{ y}^{-1}$ (source: Bui et al. (2011)).

The G2 model predicted a strong seasonal and inter-annual variability in hillslope erosion for the Eyre Peninsula and Mid-North region (Figure 2.7). Summer (December to February) appeared to have the highest erosion rates. Modelled hillslope erosion in January was about 15 times higher than in August for the Mid-North region, whereas on the Eyre Peninsula, March erosion rates were about six times higher than the lowest predicted erosion risk in August. These patterns are likely driven by a combination of low ground cover (grazed stubble), drier soils (increased erodibility: S), and stronger rainfall events (increased R) (Figure 2.8). Summer rainstorms in southern Australia are generally more intense and isolated than winter rainfall leading to a higher erosion risk (Yang and Yu, 2015).

Overall, regional variations in predicted monthly hillslope erosion correlated well with variations in rainfall erosivity and seemed to coincide with low average monthly ground cover (c.a. 50-60%) (Figure 2.8). Figure 2.8 also highlights that summer hillslope erosion accounts for 40 to 50% of the total annual erosion for both regions. For instance, predicted erosion in January 2007, 2009 and 2012 represented about 70 to 80% of the total annual erosion for the Mid-North region.

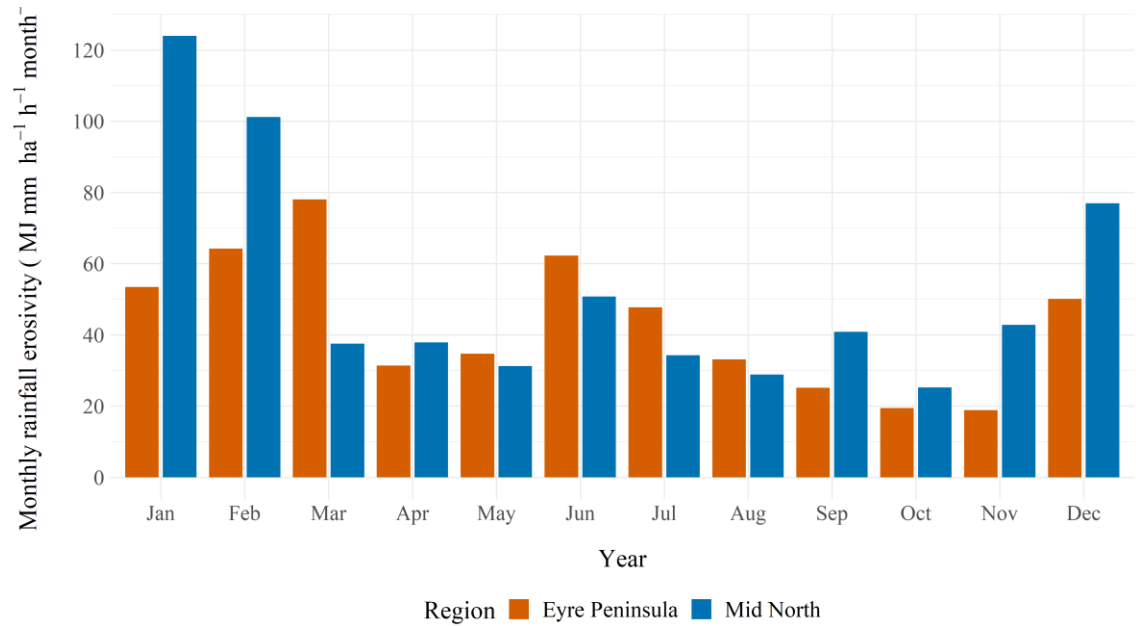


Figure 2.7 Temporal distribution of predicted regional monthly hillslope erosion grouped by months between 2001 and 2017 for the Eyre Peninsula and Mid-North region.

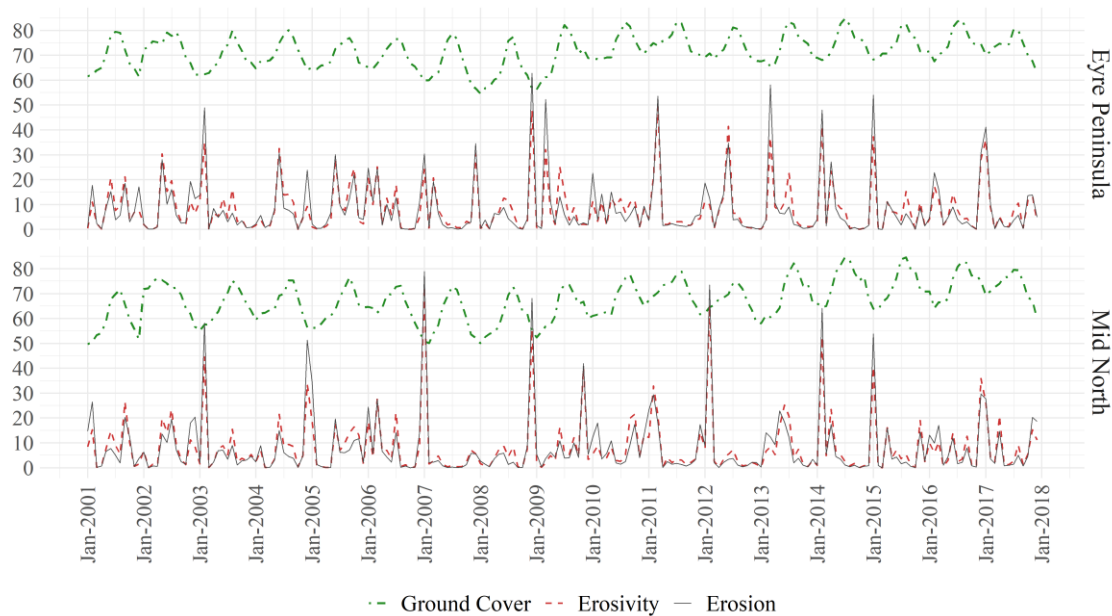


Figure 2.8 Monthly percent distributions (ratio to total annual value) of modelled hillslope erosion (Erosion) and rainfall erosivity (Erosivity), compared with average monthly ground cover (Ground Cover), from 2001 to 2017 for the Eyre Peninsula and Mid-North region.

2.3.3 Predicted hillslope erosion and “tolerable” soil loss

Soil weathering, whether it is wind- or water-induced, impacts the uppermost topsoil layer (upper 20 to 40 cm of the topsoil, called A-horizon), where water available to plants is stored and where most nutrients are accumulated and cycled. If the A-horizon layer is reduced, even by a small fraction (few centimetres), this will lead to significant declines in agricultural productivity (Bui et al., 2010) therefore the cost of production will be rising (Boardman, 2006). This is particularly true for low rainfall regions where scarce water resources, often poor soil fertility and a thin A-horizon layer make agriculture more challenging. For this reason, Bui et al. (2011) proposed a “tolerable” soil loss threshold for hillslope erosion in Australia. The proposed value of $0.2 \text{ t ha}^{-1} \text{ y}^{-1}$ represents the equilibrium between soil production rate and soil erosion rate, based on long-term studies on soil production and denudation rates in Australia (Leaman et al., 2003; Loughran et al., 2004). The authors also suggest that a more conservative value of $0.1 \text{ t ha}^{-1} \text{ y}^{-1}$ could be proposed for areas more susceptible to hillslope erosion.

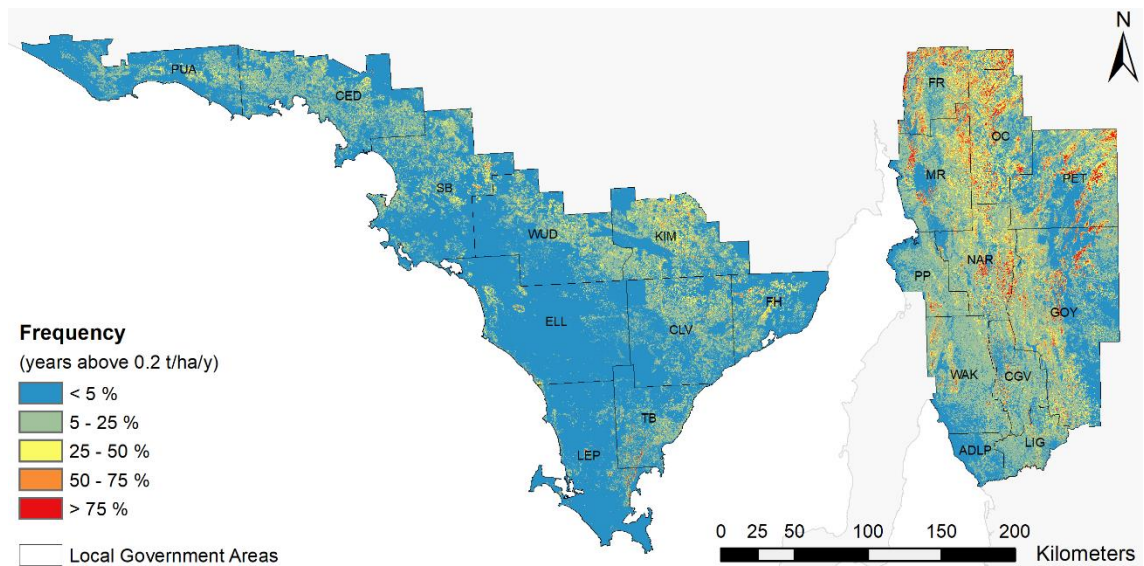


Figure 2.9 Frequency distribution of predicted annual hillslope erosion above $0.2 \text{ t ha}^{-1} \text{ y}^{-1}$

Between 2001 and 2017, the Australian “tolerable” soil loss was predicted to be exceeded less than 25% of the time for most of the Eyre Peninsula (Figure 2.9). On the other hand, the Flinders Ranges, Orroroo/Carrieton and Northern Areas LGAs, in the Mid-North region, were predicted to exceed the Australian “tolerable” soil loss more than 50% of the time period (Figure 2.9). Even if the predicted hillslope erosion was around $0.2 \text{ t ha}^{-1} \text{ y}^{-1}$ in the districts frequently exceeding this threshold, this could potentially have high implications for agricultural productivity and land management in the region. Our results could then serve as a guide to inform land managers about potential erosion severity under a range of environmental conditions. Other stakeholders involved with policies and programs relating to sustainable agricultural land management and land use planning (e.g. the agricultural industry, local and State governments, and research organisations) could also use these results to inform strategic changes and future decisions in regards to erosion management.

Today, land managers control the risk of erosion by managing the ground cover with the use of minimum tillage and cover crops. Still, even with the best management practices, land managers might have little control to prevent erosion with a recurrence in extreme events such as extended droughts, wildfires or extreme precipitation events. Nonetheless, farming systems and land management options such as greater use of

perennial plants (including pasture species, fodder shrubs and trees) could help to mitigate erosion risk with increasing dry seasonal conditions in lower rainfall areas.

2.3.4 Comparison with previous soil erosion studies

Our modelling exercise was not destined to model localised hillslope erosion, but rather to identify the spatial and temporal variation of hillslope erosion in South Australia to support cost-effective soil and land-management strategies. This study demonstrated that the G2 model was well suited for the task. Although we didn't validate the model outputs against on-ground measurements, we compared the predicted hillslope erosion with previous studies conducted in South Australia. The most comprehensive comparison dataset was reported in the study of Loughran and Elliott (1996) and Loughran et al. (2004) who estimated net soil loss from Caesium-137 (^{137}Cs) measurements. In this study, eight of the ten South Australian samples were located within the study area, and the comparison between their results and our modelling outputs are presented in . Overall the G2 model predictions correlated well the measurements from Loughran and Elliott (1996) and were within the same order of magnitude. Another study conducted within the Mount Lofty Ranges and Fleurieu Peninsula (Wilkinson et al., 2005) reported hillslope erosion rates within the same order of magnitude than the ones presented in this study (0 – 0.1 t ha⁻¹ y⁻¹ on floodplains and flatter land; 0.5 – 5 t ha⁻¹ y⁻¹ on steeper slopes).

To increase our confidence in spatial distribution patterns of predicted hillslope erosion, we also corroborated the map presented in Figure 2.4 inherent soil erosion susceptibility datasets created by the South Australian Government (Figure D.6). This susceptibility map represents the potential for hillslope erosion in the event that vegetation and other ground cover has been removed. The assessment was based on the mapping of slope and the spatial prediction of inherent soil erodibility characteristics.

Table 2.6 Comparison between G2 erosion estimates and previous studies conducted in South Australia

Town	Long. (E)	Lat. (S)	Estimated soil loss from previous studies (t ha ⁻¹ y ⁻¹)	Estimated hillslope erosion from G2 model (t ha ⁻¹ y ⁻¹)	Source
Bundaleer	138° 29'00"	33° 18'00"	0.26	0.25	
Cleve	136° 29'29"	33° 42'34"	0.4 - 1.48 - 8.16	0.43	
Jamestown	138° 36'29"	33° 12'34"	0.01 - 0.2 - 0.72	0.13	
Kapunda	138° 54'44"	34° 20'47"	1.98	3.91	
Mintaro	138° 43'1"	33° 55'31"	1.34	0.22	
Saddleworth	138° 46'28"	34° 5'15"	1.25	0.54	Loughran and Elliott (1996)
Spalding	138° 36'24"	33° 30'24"	0.57	0.50	
Whyte Yarcowie	138° 53'05"	33° 14'17"	0.64	0.48	
Strathalbyn	138° 53'22"	35° 15'51"	3	NA	
Woodside	138° 52'00"	34° 57'00"	2.56 - 12.8	NA	
Mount Lofty Ranges (steep slopes)			0.5 - 5	NA	
Mount Lofty Ranges (flats)			0 - 0.1	NA	Wilkinson et al. (2005)

More details about the corroboration methods are presented in Appendix D. Even if this comparison did not allow us to validate the actual amount of erosion predicted by the G2 model, the long-term spatial and temporal distribution of predicted hillslope erosion corroborated well with this previous approach (Figure 2.10). It also demonstrates that the erosion severity predicted by the G2 model in the study area was not only driven by inherent soil erosion susceptibility (i.e. soil properties and terrain), but also climatic conditions (i.e. intense storms) and environmental factors (i.e. ground cover, land management). For example, districts or local government areas with a high inherent erosion susceptibility might not be at risk of erosion if a reasonable amount of ground cover is maintained and no extreme climatic event occurs. On the other hand, districts with low inherent soil erosion susceptibility might be at higher risk of erosion if ground cover is very low (e.g. during a drought period) and coincide with extreme weather events, such as the year 2007 for both region (Figure 2.7 and Figure 2.8).

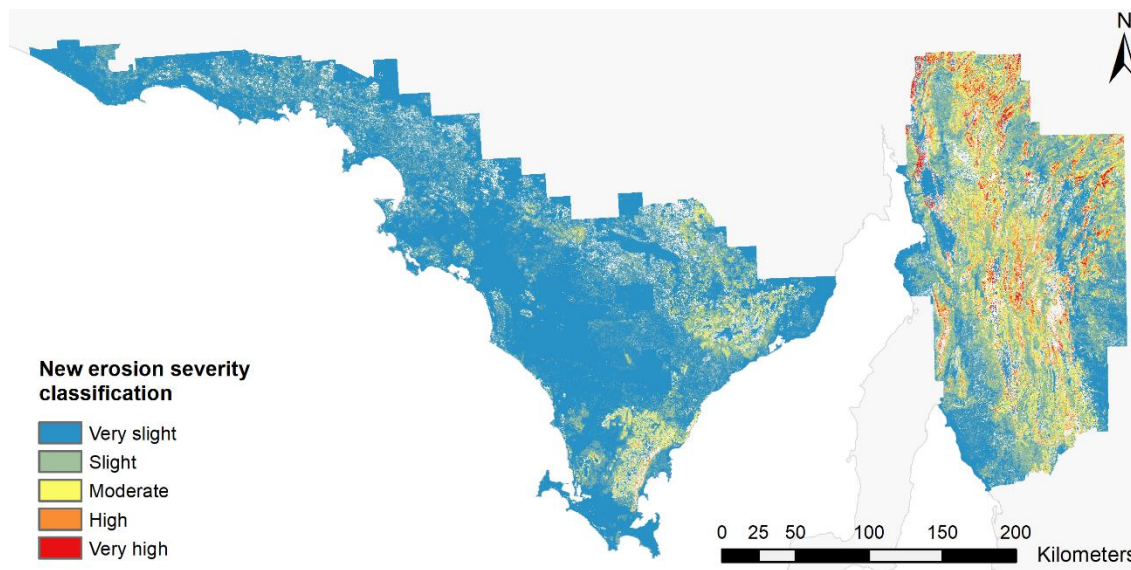


Figure 2.10 New predicted hillslope erosion severity map corroborated with the DEW inherent soil erosion susceptibility map. Note that the areas in grey represent zones where the classification of the DEW map did not overlap with the G2 model.

2.4 Conclusions and further studies

This study demonstrated that erosion models could be used to inform corrective measures for future land management and provide a valuable tool for assessing the

spatio-temporal variability of hillslope erosion. Here we applied the G2 erosion model to two agricultural regions of South Australia, Australia (the Eyre Peninsula and Mid-North). We also explored the use of high spatio-temporal resolution BARRA rainfall product combined with other high-resolution datasets to develop a model that realistically represented the complex combination of critical drivers of erosion.

Although the erosion rates predicted by G2 were not validated with direct measurements, the spatial patterns of modelled erosion corroborated well with previous studies. The consistency and continuity of the time series produced in this study could also allow us to understand the spatial distribution of erosion risk and monitor hillslope erosion within the agricultural districts of South Australia. The time series of rainfall erosivity (R) and vegetation retention (V) could also be used to evaluate the influence of changes in land management or climate on soil erosion predictions.

The application of the G2 model to the study area demonstrated that this model was well suited for the assessment of hillslope erosion over a large area. The model consists of automated scripts which can process a large amount of high spatio-temporal resolution dataset very efficiently. Although the focus of this study was on the Eyre Peninsula and Mid-North agricultural regions, the model could be extended to the rest of the State or across all the Australian agricultural zone, given sufficient computing power. The input data can be downloaded through open access platforms Australia-wide (Table A.1), and similar datasets are available globally.

Even if we proposed some changes to the original G2 model to better suit Australian conditions and the datasets available (e.g soil erodibility and V -factor), further improvements could be introduced. As presented in section 2.2.3, the fraction of the finest soil particles (0.002 – 0.10 mm) can explain up to 85% of the variability in soil erodibility (S). It is therefore critical to ensure that the soil erodibility parameter is calibrated for a specific region rather than using crude assumptions. Digital soil mapping techniques could be applied to derive a new very fine sand dataset for South Australia based on the analysis of soil samples and local geomorphological information (Gray et

al., 2016). New data fusion techniques could also help to improve the spatial resolution of the fractional vegetation cover dataset. Such techniques could be used to blend Moderate Resolution Imaging Spectroradiometer (MODIS) and Landsat imagery to obtain monthly fractional vegetation cover composites at a finer resolution (30m vs 500m). The use of higher resolution datasets will, therefore, improve the model accuracy and provide modelling outputs at a scale more meaningful for soil and land management. A new generation of climate projections (NSW and Australian Capital Territory (ACT) Regional Climate Modelling: NARClIM-2 project) will be available in about two years (Yang, 2020). This new set of climate projections will provide maps of daily rainfall projections at a resolution of 1km (vs 10km presently) for a continuous period of 100 years (2020 – 2100) (Evans et al., 2014). This new dataset could be incorporated in the G2 model to test the influence of a range of possible climate scenarios on future soil losses and provide detailed information for soil and land management options in the future.

2.5 References

- ABARES, 2016. The Australian Land Use and Management Classification Version 8. Australian Bureau of Agricultural and Resource Economics and Sciences (ABARES), http://data.daff.gov.au/anrdl/metadata_files/pe_alumc9aal20161017.xml?convertrlinks=0
- ABARES, 2018. Catchment scale land use of Australia - Commodities - Version 2. Australian Bureau of Agricultural and Resource Economics and Sciences (ABARES), <https://www.agriculture.gov.au/abares/aclump/land-use/catchment-scale-land-use-of-australia-commodities-update-december-2018>
- ASRIS, 2011. ASRIS - Australian Soil Resource Information System, <http://www.asris.csiro.au>
- Baumhardt, R.L., Stewart, B.A., Sainju, U.M., 2015. North American Soil Degradation: Processes, Practices, and Mitigating Strategies. *Sustainability* 7, 2936-2960, doi: <https://doi.org/10.3390/su7032936>.
- Boardman, J., 2006. Soil erosion science: Reflections on the limitations of current approaches. *Catena* 68, 73-86,

- BoM, 2016a. Average annual, seasonal and monthly rainfall. Bureau of Meteorology, http://www.bom.gov.au/jsp/ncc/climate_averages/rainfall/index.jsp?period=an&area=sa#maps
- BoM, 2016b. Decadal and multi-decadal temperature. Bureau of Meteorology, http://www.bom.gov.au/jsp/ncc/climate_averages/decadal-temperature/index.jsp?maptype=6&period=7605&product=max#maps
- Bui, E.N., Hancock, G.J., Chappell, A., Gregory, L.J., 2010. Evaluation of tolerable erosion rates and time to critical topsoil loss in Australia. Caring for our Country publication, Commonwealth of Australia, Canberra [nrmonline. nrm. gov. au/catalog/mql: 2237] 3,
- Bui, E.N., Hancock, G.J., Wilkinson, S.N., 2011. 'Tolerable' hillslope soil erosion rates in Australia: Linking science and policy. *Agriculture, Ecosystems & Environment* 144, 136-149, doi: <https://doi.org/10.1016/j.agee.2011.07.022>.
- Desmet, P.J.J., Govers, G., 1996. A GIS procedure for automatically calculating the USLE LS factor on topographically complex landscape units. *Journal of Soil and Water Conservation* 51, 427-433, [Go to ISI>://WOS:A1996WC48400014](https://www.researchgate.net/publication/235419960)
- DEW, 2016. Surface Soil Texture. Government of South Australia, Department for Environment and Water, <https://data.sa.gov.au/data/dataset/3ee7c63d-cae6-4076-a394-4db4a158e740>
- DEW, 2017. Soil protection from erosion. Government of South Australia, Department for Environment and Water, https://www.environment.sa.gov.au/Knowledge_Bank/Science_research/land-condition-sustainable-management/soil-protection-from-erosion
- Evans, J.P., Ji, F., Lee, C., Smith, P., Argüeso, D., Fita, L., 2014. Design of a regional climate modelling projection ensemble experiment – NARClIM. *Geosci. Model Dev.* 7, 621-629, doi: <https://doi.org/10.5194/gmd-7-621-2014>.
- Evans, J.S., 2018. spatialEco-package, R package version 0.1.1-1 ed, <https://github.com/jeffrejevans/spatialEco>
- FAO, 2011. The state of the world's land and water resources for food and agriculture (SOLAW) - Managing systems at risk. Food and Agriculture Organization of the United Nations, Rome and Earthscan, London,
- FAO, 2019. Soil erosion: the greatest challenge to sustainable soil management, Rome, p. 100 pp,
- Flanagan, D.C., Ascough, J.C., Nieber, J.L., Misra, D., Douglas-Mankin, K.R., 2013. Advances in Soil Erosion Research: Processes, Measurement, and Modeling. *Transactions of the ASABE* 56, 455-463, doi: <https://doi.org/10.13031/2013.42666>.
- Foster, G.R., Lane, L.J., 1987. User requirements: USDA, water erosion prediction project (WEPP) Draft 6.3. NSERL report (USA),

- Gavrilovic, Z., 1988. Use of an Empirical Method(Erosion Potential Method) for Calculating Sediment Production and Transportation in Unstudied or Torrential Streams, International Conference on River Regime. Hydraulics Research Limited, Wallingford, Oxon UK. 1988. p 411-422, 5 fig, 4 tab, 8 ref.,
- Gray, J.M., Bishop, T.F.A., Wilford, J.R., 2016. Lithology and soil relationships for soil modelling and mapping. *CATENA* 147, 429-440, doi: <https://doi.org/10.1016/j.catena.2016.07.045>.
- Grundy, M.J., Rossel, R.A.V., Searle, R.D., Wilson, P.L., Chen, C., Gregory, L.J., 2015. Soil and Landscape Grid of Australia. *Soil Research* 53, 835-844, doi: [10.1071/sr15191](https://doi.org/10.1071/sr15191).
- Guerschman, J.P., Scarth, P.F., McVicar, T.R., Renzullo, L.J., Malthus, T.J., Stewart, J.B., Rickards, J.E., Trevithick, R., 2015. Assessing the effects of site heterogeneity and soil properties when unmixing photosynthetic vegetation, non-photosynthetic vegetation and bare soil fractions from Landsat and MODIS data. *Remote Sensing of Environment* 161, 12-26, doi: <https://doi.org/10.1016/j.rse.2015.01.021>.
- Hancock, G.R., Wells, T., Martinez, C., Dever, C., 2015. Soil erosion and tolerable soil loss: Insights into erosion rates for a well-managed grassland catchment. *Geoderma* 237-238, 256-265, doi: <https://doi.org/10.1016/j.geoderma.2014.08.017>.
- Karydas, C., Bouarour, O., Zdruli, P., 2020. Mapping Spatio-Temporal Soil Erosion Patterns in the Candelaro River Basin, Italy, Using the G2 Model with Sentinel2 Imagery. *Geosciences* 10, 89, doi: <https://doi.org/10.3390/geosciences10030089>.
- Karydas, C.G., Panagos, P., 2016. Modelling monthly soil losses and sediment yields in Cyprus. *International Journal of Digital Earth*, 1-22, doi: <http://dx.doi.org/10.1080/17538947.2016.1156776>.
- Karydas, C.G., Panagos, P., 2018. The G2 erosion model: An algorithm for month-time step assessments. *Environ Res* 161, 256-267, doi: <https://doi.org/10.1016/j.envres.2017.11.010>.
- Leaman, D.E., Kohn, B.P., O'Sullivan, P.B., Gleadow, A.J.W., Brown, R.W., Gallagher, K., Foster, D.A., 2003. Discussion and Reply: Shaping the Australian crust over the last 300 million years: Insights from fission track thermotectonic imaging and denudation studies of key terranes. *Australian Journal of Earth Sciences* 50, 645-650, doi: [10.1046/j.1440-0952.2003.01006.x](https://doi.org/10.1046/j.1440-0952.2003.01006.x).
- Loch, R., Rosewell, C., 1992. Laboratory methods for measurement of soil erodibilities (K-factors) for the universal soil loss equation. *Soil Research* 30, 233-248,
- Loughran, R., Elliott, G., McFarlane, D., Campbell, B., 2004. A survey of soil erosion in Australia using caesium-137. *Australian Geographical Studies* 42, 221-233,
- Loughran, R.J., Elliott, G.L., 1996. Rates of soil erosion in Australia determined by the caesium-137 technique: a national reconnaissance survey. IAHS Publications-

Series of Proceedings and Reports-Intern Assoc Hydrological Sciences 236, 275-282,

- Lu, H., Prosser, I.P., Moran, C.J., Gallant, J.C., Priestley, G., Stevenson, J.G., 2003. Predicting sheetwash and rill erosion over the Australian continent. *Soil Research* 41, 1037-1062, doi: <http://dx.doi.org/10.1071/SR02157>.
- Lymburner, L., Tan, P., Mueller, N., Thackway, R., Thankappan, M., Islam, A., Lewis, A., Randall, L., Senarath, U., 2011. The national dynamic land cover dataset—technical report, National Earth Observation Group. Geoscience Australia, Symonston, ACT, <http://pid.geoscience.gov.au/dataset/ga/71069>
- McKenzie, N., Hairsine, P., Gregory, L.J., Austin, J., Baldock, J., Webb, M., Mewett, J., Cresswell, H., Welti, N., Thomas, M., 2017. Priorities for improving soil condition across Australia's agricultural landscapes, Report prepared for the Australian Government Department of Agriculture and Water Resources. CSIRO, Australia,
- Montgomery, D.R., 2007. Soil erosion and agricultural sustainability. *Proceedings of the National Academy of Sciences* 104, 13268-13272, doi: <https://doi.org/10.1073/pnas.0611508104>
- Morgan, R.P.C., Quinton, J.N., Smith, R.E., Govers, G., Poesen, J.W.A., Auerswald, K., Chisci, G., Torri, D., Styczen, M.E., 1998. The European Soil Erosion Model (EUROSEM): a dynamic approach for predicting sediment transport from fields and small catchments. *Earth Surface Processes and Landforms* 23, 527-544, doi: [https://doi.org/10.1002/\(SICI\)1096-9837\(199806\)23:6<527::AID-ESP868>3.0.CO;2-5](https://doi.org/10.1002/(SICI)1096-9837(199806)23:6<527::AID-ESP868>3.0.CO;2-5).
- Nearing, M., Foster, G., Lane, L., Finkner, S., 1989. A process-based soil erosion model for USDA-Water Erosion Prediction Project technology. *Transactions of the ASAE* 32, 1587-1593,
- Nearing, M.A., Yin, S.-q., Borrelli, P., Polyakov, V.O., 2017. Rainfall erosivity: An historical review. *Catena* 157, 357-362, doi: <https://doi.org/10.1016/j.catena.2017.06.004>.
- O'Brien, L., 2019. slga: Data Access Tools for the Soil and Landscape Grid of Australia, R package version 1.0.1 ed, <https://github.com/obrl-soil/slga>
- Panagos, P., Borrelli, P., Meusburger, K., 2015a. A New European Slope Length and Steepness Factor (LS-Factor) for Modeling Soil Erosion by Water. *Geosciences* 5, 117, <http://www.mdpi.com/2076-3263/5/2/117>
- Panagos, P., Borrelli, P., Meusburger, K., Alewell, C., Lugato, E., Montanarella, L., 2015b. Estimating the soil erosion cover-management factor at the European scale. *Land Use Policy* 48, 38-50, doi: <https://doi.org/10.1016/j.landusepol.2015.05.021>.
- Panagos, P., Borrelli, P., Meusburger, K., Lugato, E., Ballabio, C., Poesen, J., Alewell, C., Montanarella, L., 2018. Soil erosion in Europe: current status, future climate and land use scenarios, in: Zlatic, M., Kostadinov, S. (Eds.), *Soil and Water Resources*

Protection in the Changing Environment, pp. 1-13, <Go to ISI>://WOS:000464898800001

- Panagos, P., Christos, K., Cristiano, B., Ioannis, G., 2014a. Seasonal monitoring of soil erosion at regional scale: An application of the G2 model in Crete focusing on agricultural land uses. *International Journal of Applied Earth Observation and Geoinformation* 27, 147-155, doi: <https://doi.org/10.1016/j.jag.2013.09.012>.
- Panagos, P., Katsoyiannis, A., 2019. Soil erosion modelling: The new challenges as the result of policy developments in Europe. *Environmental Research* 172, 470-474, doi: <https://doi.org/10.1016/j.envres.2019.02.043>.
- Panagos, P., Meusburger, K., Ballabio, C., Borrelli, P., Alewell, C., 2014b. Soil erodibility in Europe: A high-resolution dataset based on LUCAS. *Science of The Total Environment* 479-480, 189-200, doi: <https://doi.org/10.1016/j.scitotenv.2014.02.010>.
- Pilesjö, P., Hasan, A., 2014. A Triangular Form-based Multiple Flow Algorithm to Estimate Overland Flow Distribution and Accumulation on a Digital Elevation Model. *Transactions in GIS* 18, 108-124, doi: <https://doi.org/10.1111/tgis.12015>.
- Renard, K.G., Foster, G.R., Weesies, G., McCool, D., Yoder, D., 1997. Predicting soil erosion by water: a guide to conservation planning with the Revised Universal Soil Loss Equation (RUSLE). US Government Printing Office Washington, DC,
- Rickson, R.J., 2014. Can control of soil erosion mitigate water pollution by sediments? *Science of The Total Environment* 468-469, 1187-1197, doi: <https://doi.org/10.1016/j.scitotenv.2013.05.057>.
- Rosewell, C., 1993. SOILOSS: a program to assist in the selection of management practices to reduce erosion. Soil Conservation Service of NSW, Sydney, NSW,
- Su, C.-H., Eizenberg, N., Steinle, P., Jakob, D., Fox-Hughes, P., White, C., Rennie, S., Franklin, C., Dharssi, I., Zhu, H., 2019. BARRA v1.0: The Bureau of Meteorology Atmospheric high-resolution Regional Reanalysis for Australia. *Geoscientific Model Development* 12, 2049-2068, doi: <https://doi.org/10.5194/gmd-12-2049-2019>.
- Tadono, T., Ishida, H., Oda, F., Naito, S., Minakawa, K., Iwamoto, H., 2014. Precise Global DEM Generation by ALOS PRISM. *ISPRS Ann. Photogramm. Remote Sens. Spatial Inf. Sci.* II-4, 71-76, doi: <https://doi.org/10.5194/isprsannals-II-4-71-2014>.
- Teng, H., Viscarra Rossel, R.A., Shi, Z., Behrens, T., Chappell, A., Bui, E., 2016. Assimilating satellite imagery and visible–near infrared spectroscopy to model and map soil loss by water erosion in Australia. *Environmental Modelling & Software* 77, 156-167, doi: <https://doi.org/10.1016/j.envsoft.2015.11.024>.
- van Dijk, A.I.J.M., Bruijnzeel, L.A., Rosewell, C.J., 2002. Rainfall intensity–kinetic energy relationships: a critical literature appraisal. *Journal of Hydrology* 261, 1-23, doi: [https://doi.org/10.1016/S0022-1694\(02\)00020-3](https://doi.org/10.1016/S0022-1694(02)00020-3).

- Vrieling, A., Sterk, G., de Jong, S.M., 2010. Satellite-based estimation of rainfall erosivity for Africa. *Journal of hydrology* 395, 235-241, doi: <https://doi.org/10.1016/j.jhydrol.2010.10.035>.
- Webb, N.P., McGowan, H.A., Phinn, S.R., Leys, J.F., McTainsh, G.H., 2009. A model to predict land susceptibility to wind erosion in western Queensland, Australia. *Environmental Modelling & Software* 24, 214-227, doi: <https://doi.org/10.1016/j.envsoft.2008.06.006>.
- Wilkinson, S.N., Jansen, A., Watts, R., Read, A.M., Davey, B., 2005. Techniques for targeting erosion control and riparian rehabilitation in the Mount Lofty Ranges, Canberra, p. 48p, doi: <https://doi.org/10.4225/08/58694496485e7>.
- Willoughby, N., Thompson, D., Royaland, M., Miles, M., 2018. South Australian Land Cover Layers: an Introduction and Summary Statistics. Government of South Australia, Department for Environment and Water (DEW), Adelaide, Australia, <https://data.environment.sa.gov.au/Content/Publications/SA-Land-Cover-Layers-1987-2015-Technical-Summary.pdf>
- Wischmeier, W.H., Smith, D.D., 1978. Predicting rainfall erosion losses-A guide to conservation planning. *Predicting rainfall erosion losses-A guide to conservation planning*,
- Yang, X., 2014. Deriving RUSLE cover factor from time-series fractional vegetation cover for hillslope erosion modelling in New South Wales. *Soil Research* 52, 253-261, doi: <http://dx.doi.org/10.1071/SR13297>.
- Yang, X., 2020. State and trends of hillslope erosion across New South Wales, Australia. *Catena* 186, 104361, doi: <https://doi.org/10.1016/j.catena.2019.104361>.
- Yang, X., Yu, B., 2015. Modelling and mapping rainfall erosivity in New South Wales, Australia. *Soil Research* 53, 178-189, doi: <http://dx.doi.org/10.1071/SR14188>.
- Young, M.-A., Herrmann, T., 2015. Celebrating 75 years of Soil-Care, 2015 State Community Landcare Conference. Government of South Australia, Department of Environment, Water and Natural Resources, Waikerie,
- Zdruli, P., Karydas, C.G., Dedaj, K., Salillari, I., Cela, F., Lushaj, S., Panagos, P., 2016. High resolution spatiotemporal analysis of erosion risk per land cover category in Korçë region, Albania. *Earth Science Informatics* 9, 481-495, doi: <https://doi.org/10.1007/s12145-016-0269-z>.

Appendix A

Chapter 2 to 4 – Supplementary material

This supplementary material includes a table describing the input datasets accessed to run the G2 and “albedo” erosion models in this study as well as links to download the raw data.

Table A.1 Description of the datasets used for the modelling with sources and resolution.

Data type	Dataset name and specific information	source
Weather data	Hourly precipitation accumulation Hourly maximum wind speed Hourly soil moisture (0 - 10cm layer) (1.5x1.5km)	BARRA-AD
Land use	Australian Land Use and Management Classification Version 8	ABARES
Land cover	South Australian Land Cover dataset Three epochs (2000-05, 2005-10, 2010-15) (25mx25m)	Enviro Data SA
Ground cover	MODIS 8-day Fractional Cover (v6) 2001-2017 (500mx500m)	TERN- Auscover
	MODIS BRDF/Albedo model parameters daily (MCD43A1) (v6) 2001-2017 (500mx500m) MODIS Albedo daily (MCD43A3) (v6) 2001-2017 (500mx500m)	rOpenSci MODISrsp R-package
Landscape alteration	Landsat 7 NIR-band; 14-days (30x30m)	Goolge Eearth Engine
Topography	ALSO DSM (30x30m)	JAXA - EORC
Soil data	Clay, sand, silt fractions, SOC, coarse fragments, bulk density (90x90m)	Soil Landscape Grid Australia <i>slga::</i> R-package
	Hydraulic conductivity, surface stone cover (90mx90m)	ASRIS webportal

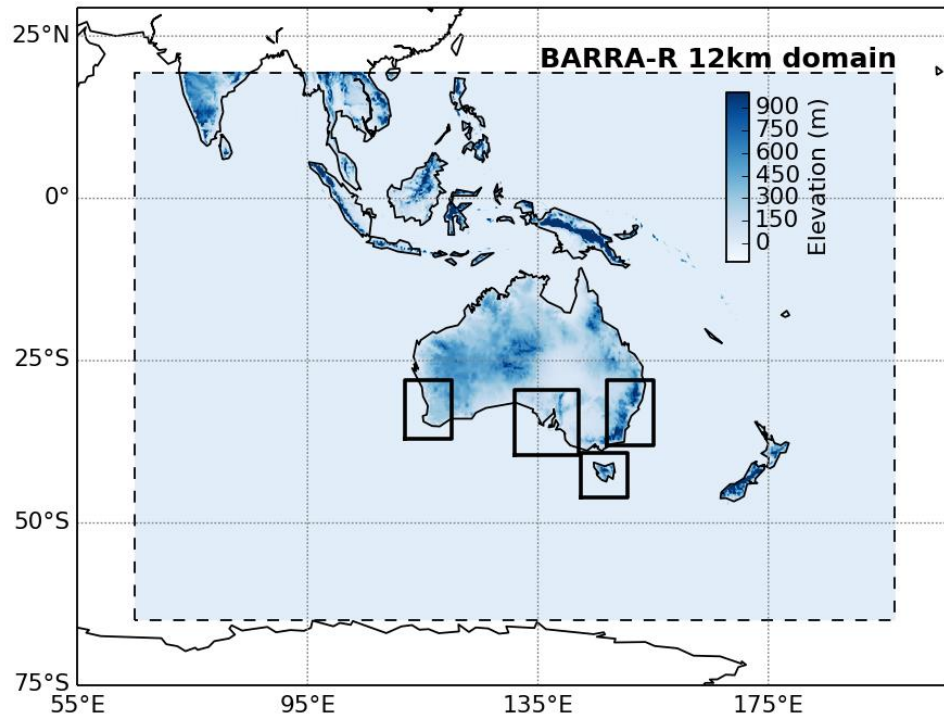


Figure A.1 The BARRA domain map. The outer dashed outline represents the BARRA-R regional domain at 12km resolution. The inner solid lined domain represents the downscaled regional subdomains available at a spatial resolution of 1.5km. The regional subdomains are centred over some major cities of Australia, such as Perth, Adelaide, Hobart and Sydney.

Appendix B

Chapter 2 – Supplementary material

Assumptions in using BARRA rainfall data for estimates of rainfall erosivity

B.1 Introduction

Rainfall erosivity is a key variable in erosion models. It is ultimately based on models relating the energy from rain events to erosion magnitude. Comprehensive field studies conducted in the 1950s (Wischmeier and Smith, 1978) are still the foundation of modern erosion models (Nearing et al., 2017). These early studies showed that rainfall intensity sustained over 30-minute time intervals best predicted soil loss. However, at broad spatial scales, relevant to land management, this data is unavailable. Rainfall data used in erosion modelling is spatially interpolated with crude implicit assumptions. Gauge data is generally accepted as truth, although for spatial modelling one needs to acknowledge that the meteorological world standard opening of rain gauges (203mm) only represents a minute spatial sample of 0.0000023% of a square kilometre.

Because of the high spatio-temporal variability of rainfall, it is important to understand how differences in rainfall data carry through to estimates of rainfall erosivity. BARRA provides a unique opportunity to source spatio-temporal rainfall information. The BARRA dataset was generated by using the best available data and models to represent the magnitude and distribution of gauged rainfall. However, the use of BARRA data for soil erosion is new and needs to be scrutinised. Below we, therefore, show a comparison of BARRA based rainfall and rainfall erosivity at rain gauge locations within South Australia.

There are 61 automatic rain gauges (pluviographs) within South Australia (Figure B.1) maintained by the Bureau of Meteorology (BOM) and conform to standards of the World Meteorological Organisation. While daily data for these stations is available from the

BOM at high quality, raw pluviography data (tipping bucket events) is considered experimental and does not contain a full quality check. This data was purchased from the BOM.

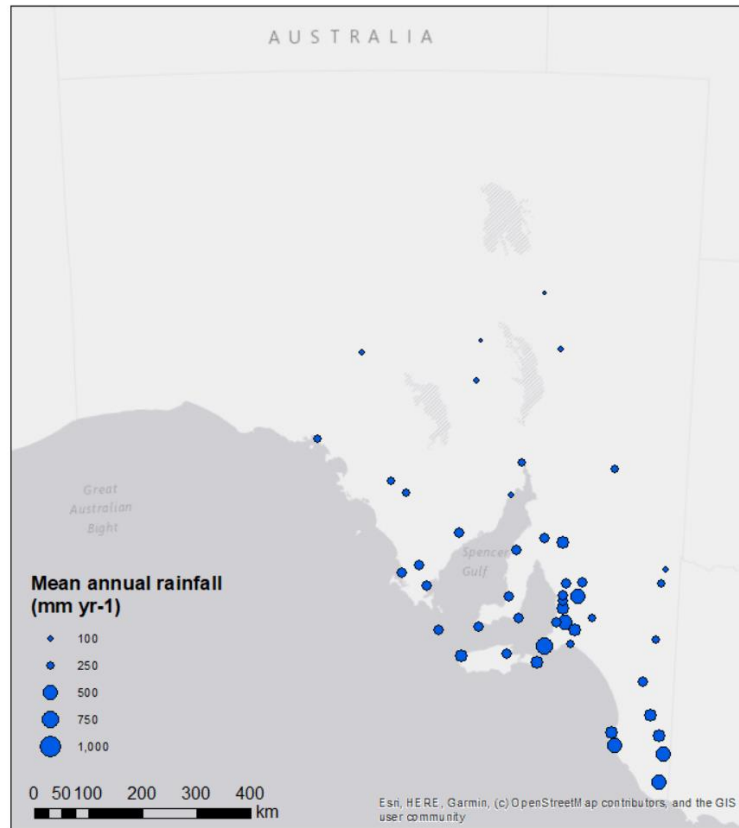


Figure B.1 Location of rain gauges within South Australia. Size of dots represents rainfall amount

Potential errors in tipping-bucket rain gauges are numerous and quality-checked sub-daily rainfall is extremely difficult to come by. False negatives (missing rainfall, i.e. power failure or equipment failures) are generally only detected during rain events, hence potentially biasing any analysis. False positives are possible (i.e. strong winds) but are not of high concern in our analysis. The quality checks done for this study were kept as simple and conservative as possible. We initially aggregated minute-data to daily periods from 9 am to 9 am of the following day and compared daily sums with higher quality daily rainfall. A discrepancy of 5mm per day was used as an exclusion criterion. The differences in data recording posed a significant problem. In some years for most stations, pluviograph time series were aggregated to hourly records, prohibiting estimates of 30-minute rainfall intensities. These periods were identified by evaluating

if rainfall rates above 0.2mm were recorded for time differences longer than 30 minutes. If such periods represented more than 90% of the available time-periods of any year (24x365 for hourly data and 48x365 for 30-minute data), the entire year was excluded.

This quality check reduced the number of stations available to 47 with a median number of 8 years per station and a total of 426 station-years. Having less than ten years for most stations implied a small sample, but the sampled years represented well long-term rainfall statistics (Figure B.2). The high correspondence between long-term gauge data and daily aggregates of 30-minute data was expected as it showed the same data, albeit for different time epochs. BARRA estimates exhibit a slight overestimation of rainfall in the BARRA data, hence producing comparable rainfall time series.

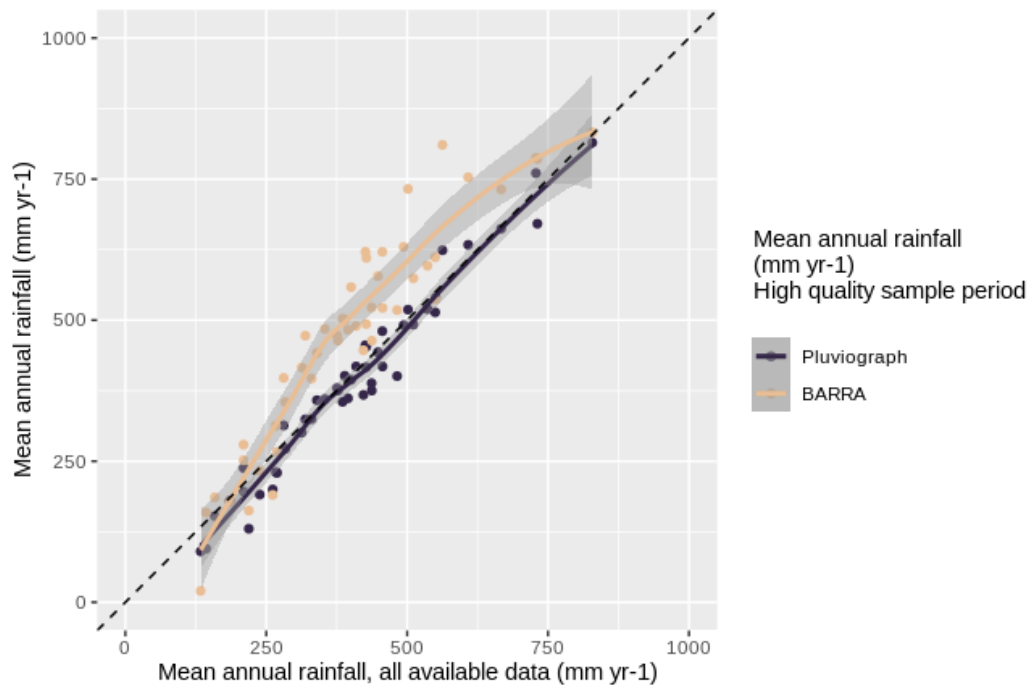


Figure B.2 Mean annual rainfall of automatic rain gauges (full-quality-controlled daily data) compared with high-temporal pluviography data and BARRA rainfall extracts for time-periods after quality filtering

In this analysis, we used the average rainfall intensity-kinetic energy ($R-ek$) relationships from van Dijk et al. (2002) (also used by Teng et al. (2016), Chapter 2 equation 2) to test the applicability of gridded products such as BARRA for rainfall erosivity calculations.

B.2 The effect of different rainfall time series on rainfall erosivity across South Australia

Following the argument of Nearing et al. (2017), we need to link our models as closely as possible to the original erosivity-rainfall energy relationships. These equations summarise the comprehensive erosion experiments conducted in the 1950s and to date still represent the best empirical links available between rainfall and soil erosion. These empirical relationships are based on detailed rainfall records and estimates of peak rainfall intensities sustained over 30 minutes in events. Events are defined as rain periods separated by at least 6 hours below a small rainfall threshold.

However, such detailed rainfall information is not always readily available for long time-series that allow long-term averages and when there are large distances between pluviographs. Therefore, it is imperative to use broad-scale products. Nonetheless, gridded spatio-temporal data is only available at hourly (BARRA) or 3-hourly (TRMM) time intervals. Furthermore, gridded products are very different in spatial scales from rainfall used in the original ($R-ek$) models. We thus need to scrutinise the effect of assumptions inherent to the different types of rainfall data for erosion studies.

B.2.1 Temporal aggregation types of rainfall time series and definition of rainfall events

Here we define four temporal rainfall aggregation types and we will test below how these differences influence estimates of rainfall erosivity. ‘Type 1’ denotes the original raw rainfall records, grouped into events; ‘Type 2’ is high temporal rainfall at regular 30-minute intensities for events; ‘Type 3’ is using hourly rainfall aggregates for events, and ‘Type 4’ groups rainfall into simple, regular 3-hour rainstorms, using peak hourly rates of this period to estimate total storm energy. Types 1-3 follow the original definition of events as being divided by 6-hour periods of low rainfall sums ($< 1.3\text{mm}$ or 0.05in). This processing is computationally difficult as events are of different length and span across irregular time intervals. High rain intensities usually occur during small time-

periods and most events are of low intensity. Defining regular periods (i.e. 3 hours for ‘Type 4’) substantially simplifies computation.

Table B.1 shows example calculations of total storm EI30 (**EI**: storm event Energy x Intensity using 30-minute peak rainfall intensities). Using the original example from Renard et al. (1997) (page 334) Table B2-B4 explain the equivalent calculations for ‘Type 2’ to ‘Type 4’ aggregations and show substantial differences. The storm event in Table B.1 has a maximum 30-minute rainfall of 27.4 mm (54.9 mm h⁻¹). Total energy amounts to 8.47 MJ ha⁻¹ (1271 ft tonf acre⁻¹) with a total storm EI of 465 = 8.47 MJ ha⁻¹ x 54.9 mm h⁻¹ (or 27.5 ft tonf inch acre⁻¹ h⁻¹). Similar results are obtained after converting rainfall to 30-minute intervals with a peak intensity of 52.0 mm h⁻¹ and total storm EI of 417 MJ mm ha⁻¹ h⁻¹ (Table B.2). Using regular 60-minute intervals reduces the ability to estimate sub-hour intensities. Peak intensity is reduced to 27mm h⁻¹ and the estimate of total storm EI is reduced to 191 MJ mm ha⁻¹ h⁻¹.

The data was processed at the different levels represented in Table B.2 (Type 2-4). Automatic gauge rainfall was used to estimate rainfall erosivity for Types 2-4 and BARRA for Types 3 and 4, respectively. A total of 23,000 rainfall events were found in the rainfall time series with very similar results for both pluviography and BARRA data. The number of rainfall events per year for each station ranges from 24 in the desert regions to 105 in the higher rainfall regions and corresponds well (Table B.3) for all rainfall data sources.

Table B.1 Sample calculations of storm EI (translated to metric from Renard et al. (1997), page 334. Total storm EI: 465 MJ mm ha⁻¹ h⁻¹ (‘Type 1’)

Chart readings		For each increment			Energy (MJ ha ⁻¹)	
Time (min)	Amount (mm)	Duration (min)	Depth (mm)	Intensity (mm h ⁻¹)	Per mm	Total
20	1.3	20	1.3	3.8	0.158	0.200
27	3.0	7	1.8	15.2	0.205	0.365
36	8.9	9	5.8	38.9	0.254	1.486
50	26.7	14	17.8	76.2	0.277	4.925
57	30.5	7	3.8	32.7	0.246	0.936
65	31.8	8	1.3	9.5	0.184	0.234
75	31.8	10	0.0	0.0	0.136	0.000
90	33.0	15	1.3	5.1	0.164	0.208
Totals:		90	33.0			8.35

Table B.2 Sample calculation for storm EI using regular 30-minute intervals. The example rainfall mimics the original example from Renard et al. (1997) ("Type 2"). Total storm EI: 417 MJ mm ha⁻¹ h⁻¹.

For each increment			Energy (MJ ha ⁻¹)	
Duration (min)	Depth(mm)	Intensity (mm h ⁻¹)	Per mm	Total
30	0.2	0.4	0.138	0.028
30	0.4	0.8	0.141	0.056
30	1.0	2.0	0.148	0.148
30	4.0	8.0	0.178	0.711
30	26.0	52.0	0.266	6.927
30	1.0	2.0	0.148	0.148
30	0.0	0.0	0.136	0.000
30	0.4	0.8	0.141	0.056
Totals:	33.0			8.07

Table B.3 Sample calculation for storm EI using regular 60-minute intervals, aggregated from table B2. This type of rainfall data is defined as "Type 3". Total storm EI: 191 MJ mm ha⁻¹ h⁻¹.

For each increment			Energy (MJ ha ⁻¹)	
Duration (min)	Depth(mm)	Intensity (mm h ⁻¹)	Per mm	Total
60	0.6	0.6	0.140	0.084
60	5.0	5.0	0.164	0.819
60	27.0	27.0	0.236	6.363
60	0.4	0.4	0.138	0.055
Totals:	33.0			7.32

Table B.4 Sample calculations illustrating the approach taken here for BARRA hourly data defining each 3-hour period as an event ("Type 4"). Total storm EI: 191 MJ mm ha⁻¹ h⁻¹.

For each increment			Energy (MJ ha ⁻¹)		3-hour events	
Duration (min)	Depth (mm)	Intensity (mm h ⁻¹)	Per mm	Total	peak int. (mm h ⁻¹)	3h-storm EI (MJ ha ⁻¹)
60	0.6	0.6	0.14	0.084		
60	5.0	5.0	0.16	0.819		
60	27.0	27.0	0.24	6.363	27.0	196.15
60	0.4	0.4	0.14	0.055		
60	0	0	0	0		
60	0	0	0	0	0.4	0.02
Totals:	33.0					196.2

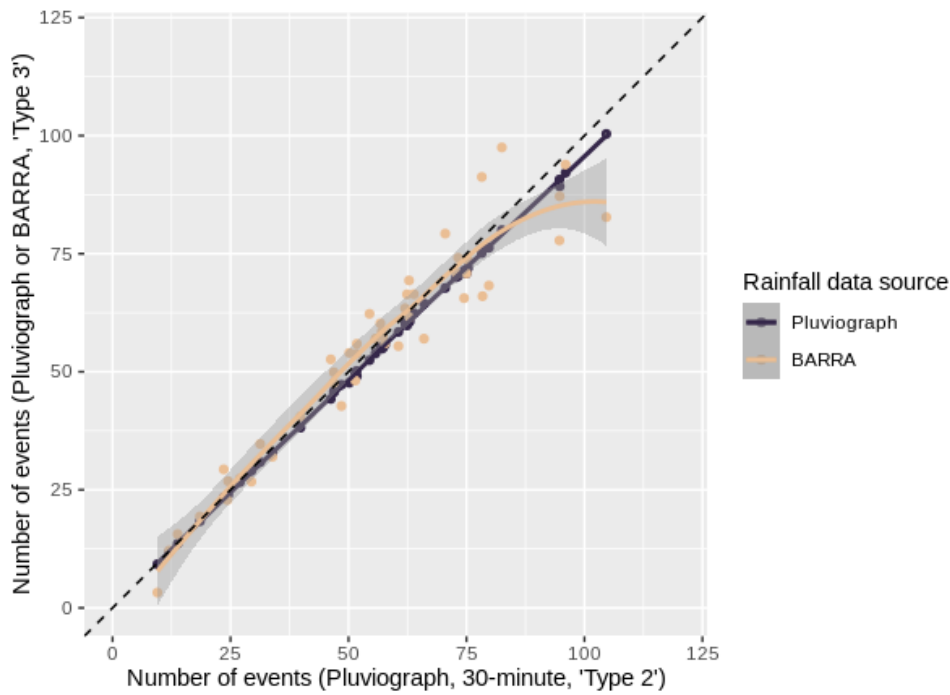


Figure B.3 Average number of rainfall periods per year, defined by Renard et al. (1997) as continuous periods of low rainfall < 0.13mm (0.05 in) during a period of 6 hours. Event numbers extracted from pluviographs and BARRA (“Type 3”) are shown over reference pluviograph data at 30 minutes (“Type 2”)

B.2.2 The effect of temporal aggregation types of rainfall time series on rainfall erosivity estimation

We can now iteratively test how rainfall erosivity is affected by (i) changing the temporal aggregation type of rainfall events, (ii) changing from point-based gauge data to gridded BARRA data, and (iii) by combining temporal aggregation and gridding.

As expected, there is a substantial difference in rainfall erosivity between different temporal aggregation types (Figure B.4). Aggregation from 30-minute to 1 hour time steps (“Type 2” compared with “Type 3”) substantially reduces R estimates. This is due to higher intensities in the 30-minute data that are not sustained over an hour period (compare Table B.2 and B3). The slope between “Type 2’ and “Type 3’ is 0.63 and 0.52 when comparing “Type 4’ with “Type 2’ ($R^2 = 0.99$ for both regressions, linear models).

Changing from “Type 3’ to “Type 4’ does not substantially change rainfall erosivity estimates (slope = 0.83 for gauge data and slope = 0.84 for BARRA data). This relationship is consistent for gauge and BARRA data (Figure B.5). Furthermore, spatial

patterns are consistent when changing from 'Type 3' to 'Type 4' (Figure B.6). This observation supports the approach of using simplified 3-hour events.

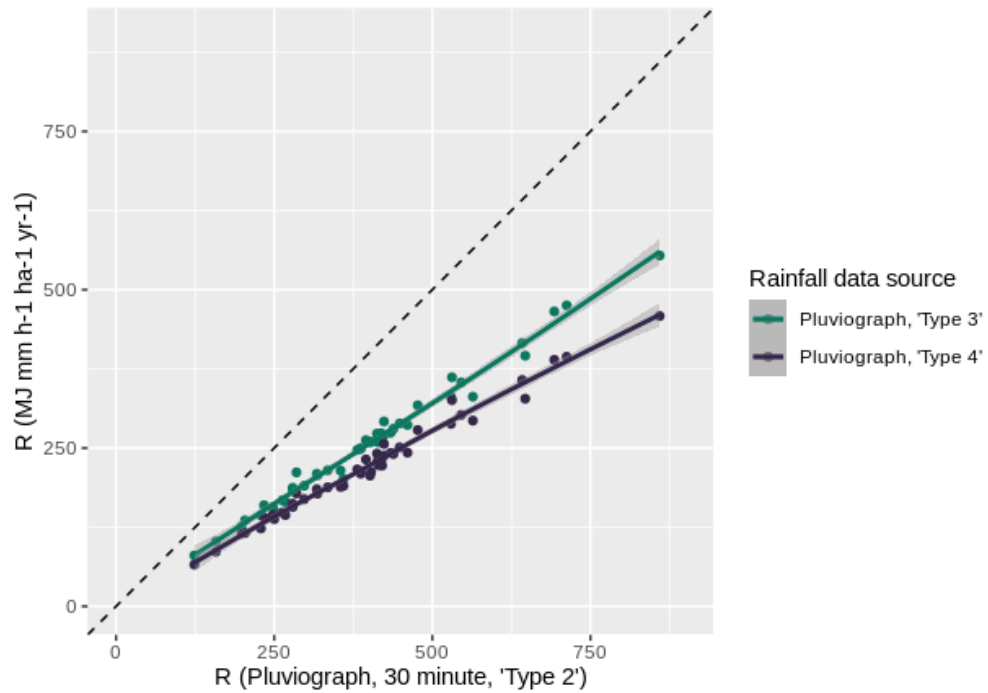


Figure B.4 Evaluating the effect of rainfall aggregation on rainfall erosivity ($\text{MJ mm ha}^{-1} \text{h}^{-1} \text{yr}^{-1}$) for 47 rain gauges across South Australia.

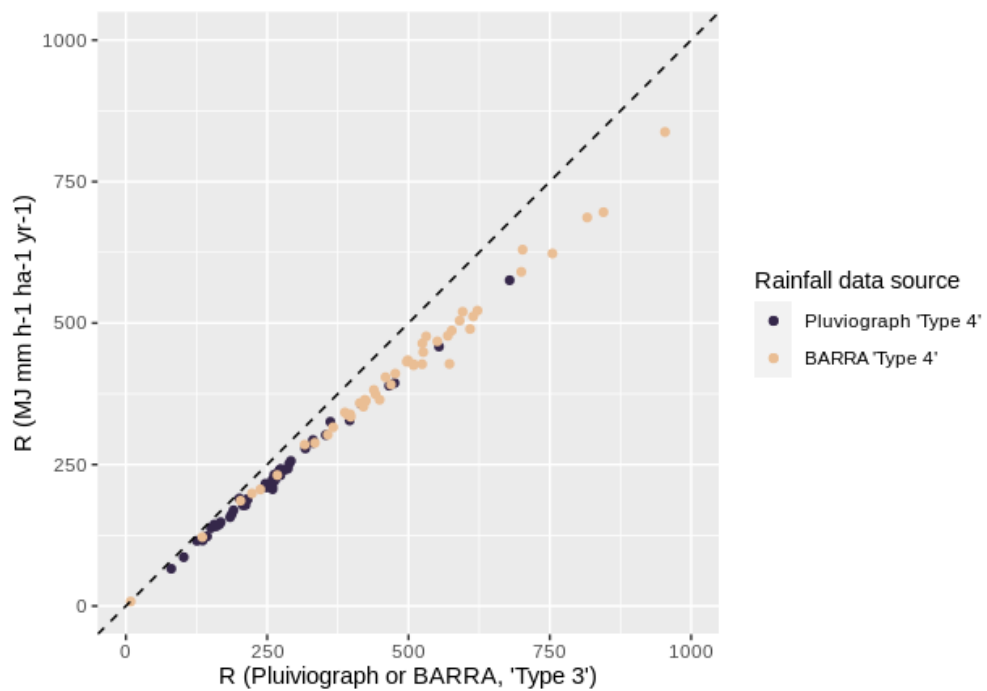


Figure B.5 Evaluating the effect of rainfall aggregation on rainfall Erosivity ($\text{MJ mm ha}^{-1} \text{h}^{-1} \text{yr}^{-1}$). The x-axis represents mean annual rainfall erosivity of 41 stations in South Australia estimate from hourly gauge data and BARRA, respectively.

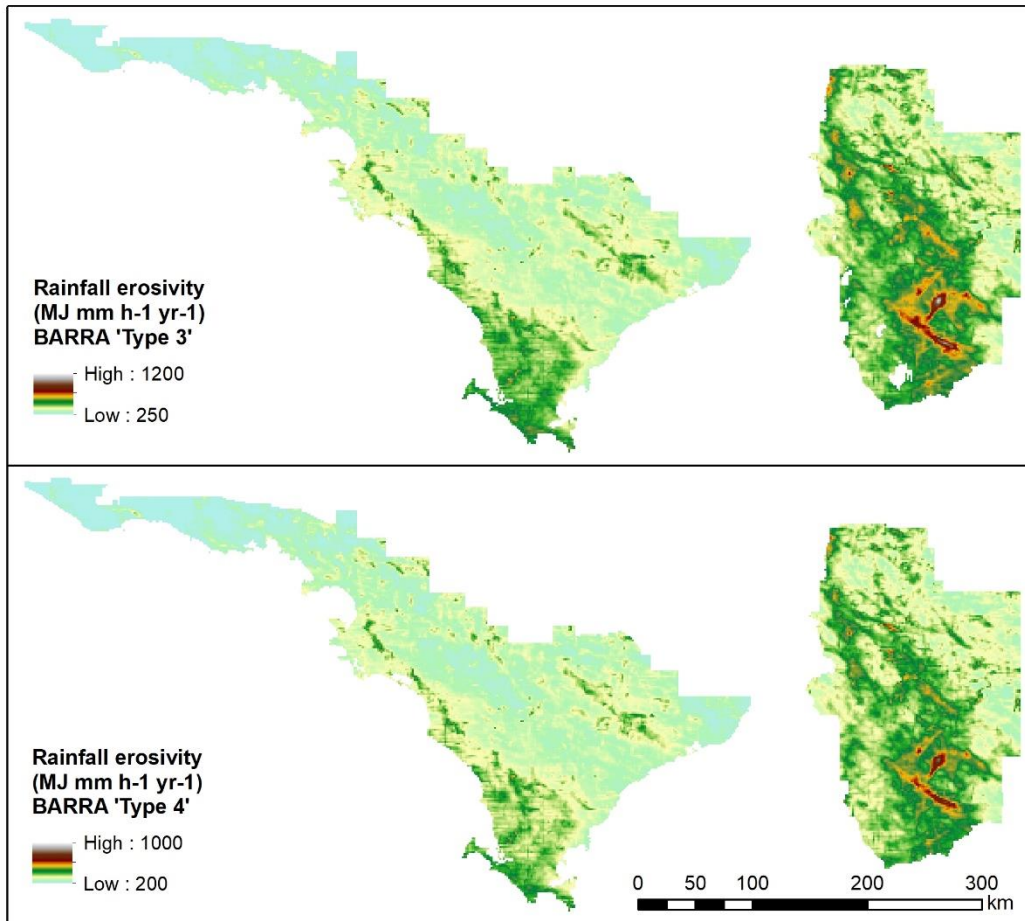


Figure B.6 Comparison of patterns of erosivity when using ‘Type 3’ (Renard et al. (1997) definition of a storm event) and ‘Type 4’ (3-hour storm events) temporal rainfall aggregations.

Further comparing gauge and BARRA data, we find more pronounced differences (Figure B.7). This is expected as gauge data is point data with a very small spatial footprint and BARRA data indicates sustained hourly rates over 1.5km x 1.5km. Using BARRA data produces higher erosivity compared to 30-minute gauge-based rainfall. Overall, these effects compensate and the ‘Type 4’ BARRA erosivity compares well with 30-minute gauge data.

The most critical observation for our analysis is that spatial patterns of erosivity and pluviograph data using the original event analysis algorithm (Renard et al., 1997) compared well with ‘Type 3’ and ‘Type 4’ BARRA erosivity estimates ($R^2=0.47$, with $p < 10^{-6}$ for both models; using generalised linear modelling ‘gam’ from the *mgcv* package (Wood, 2019)).

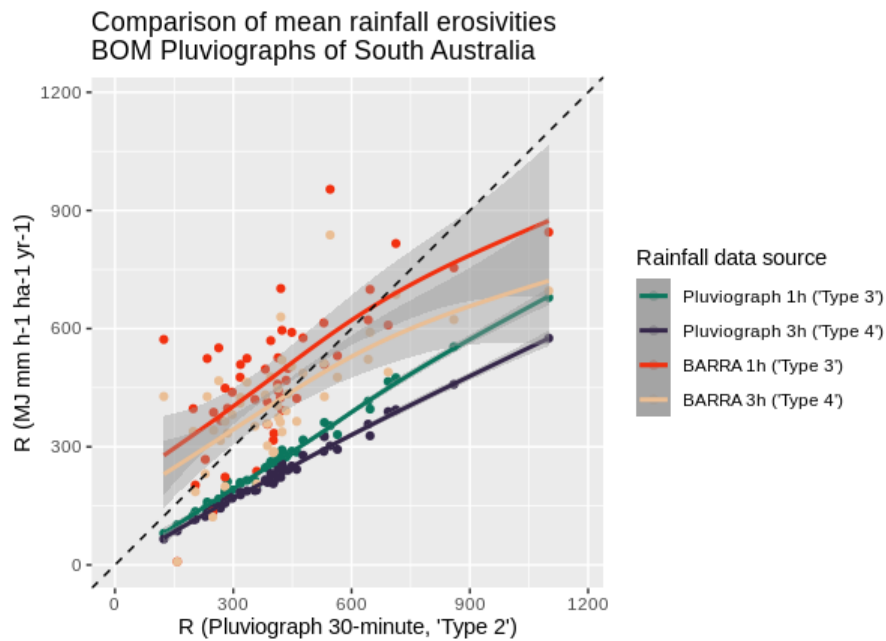


Figure B.7 Evaluating the difference between rainfall Erosivity ($\text{MJ mm ha}^{-1} \text{h}^{-1} \text{yr}^{-1}$) using different rainfall data sources and temporal aggregation types. The x-axis represents the mean annual rainfall erosivity using 30-minute intensities from pluviograph data. BARRA 'Type 4' data has been used in this publication.

B.3 References

- Nearing, M.A., Yin, S.-q., Borrelli, P., Polyakov, V.O., 2017. Rainfall erosivity: An historical review. *Catena* 157, 357-362, doi: <https://doi.org/10.1016/j.catena.2017.06.004>.
- Renard, K.G., Foster, G.R., Weesies, G., McCool, D., Yoder, D., 1997. Predicting soil erosion by water: a guide to conservation planning with the Revised Universal Soil Loss Equation (RUSLE). US Government Printing Office Washington, DC,
- Teng, H., Viscarra Rossel, R.A., Shi, Z., Behrens, T., Chappell, A., Bui, E., 2016. Assimilating satellite imagery and visible–near infrared spectroscopy to model and map soil loss by water erosion in Australia. *Environmental Modelling & Software* 77, 156-167, doi: <https://doi.org/10.1016/j.envsoft.2015.11.024>.
- van Dijk, A.I.J.M., Bruijnzeel, L.A., Rosewell, C.J., 2002. Rainfall intensity–kinetic energy relationships: a critical literature appraisal. *Journal of Hydrology* 261, 1-23, doi: [https://doi.org/10.1016/S0022-1694\(02\)00020-3](https://doi.org/10.1016/S0022-1694(02)00020-3).
- Wischmeier, W.H., Smith, D.D., 1978. Predicting rainfall erosion losses-A guide to conservation planning. Predicting rainfall erosion losses-A guide to conservation planning,
- Wood, S., 2019. Mixed GAM Computation Vehicle with Automatic Smoothness Estimation, doi: <https://doi.org/10.1201/9781315370279>.

Appendix C

Chapter 2 – Supplementary material

Assumptions to define the very fine sand fraction from total sand content

C.1 Introduction

Being able to predict where and when agricultural regions are at risk of hillslope erosion will become paramount to ensure future agricultural productivity and soil security. Soil erosion is highly variable through space and time and is driven by key influencing factors such as rainfall erosivity, cover management, topography and inherent soil erodibility. Soil erodibility has a critical influence on total soil erosion estimates and contains a lot of uncertainty. According to Loch and Rosewell (1992), the particle size parameter M (%silt + %very-fine-sand) explains up to 85% of the total variability in soil erodibility (K-factor). The higher the fraction of particles in the 0.002 - 0.10 mm range, the higher the soil erodibility. It is therefore important to ensure that the fraction of very fine sand and silt particles is well defined for a more reliable estimation of soil erodibility. However, there is a lack of readily available information about the fine and very fine sand fractions and a lack of soil information directly relevant for the estimation of soil erodibility. If no information about the very fine sand fraction was available, Panagos et al. (2014) proposed to define the very fine sand fraction as 20% of the total sand. But, this general assumption might not be applicable to regional conditions with specific soils properties (e.g. sandy soils of South Australia). Therefore, we need to evaluate the correctness of such assumption for Australian soils. For this reason, we tested the assumption from Panagos et al. (2014) to estimate the very fine sand fraction and compared the results with previous soil erodibility studies conducted in Australia. This case-study will give us a better definition of inherent soil erodibility for South Australia and will have implications for global models as well.

C.2 Testing of the Panagos et al. (2014) assumption to estimate the very fine sand fraction

C.2.1 The comparison datasets and testing methods

We conducted a review of the literature to compile information about Particle Size Analysis (PSA) from a range of soil samples collected in Australia. We collated 65 records from distinct soil samples from four published studies (Loch and Rosewell, 1992; Loch et al., 1998; Rosewell, 1993; Yang et al., 2017). The records are presented in Table C.2. We then ran three regression analysis to define a new correlation between the total sand fraction (i.e. fine + coarse sand) and the very fine sand fraction for the sample dataset. The first two were simple linear regression models with (equation C.1) and without intercept (equation C.2), the third one was a second order polynomial regression (equation C.3). The regression analysis was run in R (R Development Core Team, 2010) and the accuracy of the models was tested with the Nash-Sutcliffe model efficiency coefficient (NSE) (*hydroGOF::* package, (Zambrano-Bigiarini, 2020)). The NSE coefficient is an indicator of how close the values in a scatter plot are from the 1:1 line, and can be considered as a measure of model efficiency. The values of this coefficient vary between $-\infty$ and 1. The closer the NSE values are to 1, the better the model.

$$\%VeryFineSand = \%Sand \times \alpha + \beta \quad (C.1)$$

$$\%VeryFineSand = \%Sand \times \alpha \quad (C.2)$$

$$\%VeryFineSand = \%Sand \times \alpha + \%Sand^2 \times \beta + \gamma \quad (C.3)$$

Table C1 Particle size analysis for a range of soil samples collected from the literature. *Note that the very fine sand content (%) is generally part of the fine sand fraction when estimating the total sand fraction.

Location	Clay (%)	Silt (%)	Very fine sand (%)*	Fine sand (%)	Coarse sand (%)	Source
Cowra (NSW)	8	7	25	40	45	Rosewell (1993)
Cowra (NSW)	13	14	38	50	23	Rosewell (1993)
Cowra (NSW)	6	10	24	37	47	Rosewell (1993)
Cowra (NSW)	5	10	27	40	45	Rosewell (1993)
Gunnedah (NSW)	23	20	27	38	19	Rosewell (1993)
Gunnedah (NSW)	30	18	24	32	20	Rosewell (1993)
Gunnedah (NSW)	28	20	34	35	17	Rosewell (1993)
Inverell (NSW)	51	22	16	20	7	Rosewell (1993)
Inverell (NSW)	26	18	45	54	2	Rosewell (1993)
Inverell (NSW)	61	20	12	16	3	Rosewell (1993)
Inverell (NSW)	38	33	18	24	5	Rosewell (1993)
Inverell (NSW)	78	20	0	0	2	Loch and Rosewell (1992)
Scone (NSW)	28	11	26	37	24	Rosewell (1993)
Scone (NSW)	20	9	30	40	31	Rosewell (1993)
Wagga Wagga (NSW)	19	14	39	49	18	Rosewell (1993)
Wagga Wagga (NSW)	8	10	48	62	20	Rosewell (1993)
Wagga Wagga (NSW)	9	27	27	37	27	Rosewell (1993)
Wellington (NSW)	25	17	31	40	18	Rosewell (1993)
Wellington (NSW)	24	11	35	46	19	Rosewell (1993)
Gundee Moorook (NSW)	27	10	21	30	28	Yang et al. (2017)
North Fitzroy (NSW)	18	25	25	36	19	Yang et al. (2017)
Blackman (NSW)	14	9	20	29	45	Yang et al. (2017)
Acland (QLD)	40	17	27	33	10	Loch and Rosewell (1992)
Acland (QLD)	43	12	27	38	7	Loch et al. (1998)
Greenmount (WA)	62	30	7	7	1	Loch and Rosewell (1992)
Kholo (QLD)	32	24	21	30	14	Loch et al. (1998)
Brown's Plains (QLD)	39	41	6	9	11	Loch et al. (1998)
Atherton (QLD)	62	13	11	16	9	Loch et al. (1998)
Toowoomba (QLD)	53	17	13	19	11	Loch et al. (1998)
Kingaroy (QLD)	58	21	12	17	4	Loch et al. (1998)
Kingaroy (QLD)	62	21	10	14	3	Loch et al. (1998)
Gin Gin (QLD)	13	2	55	78	6	Loch et al. (1998)
Gin Gin (QLD)	12	21	32	46	21	Loch et al. (1998)
Gin Gin (QLD)	13	1	40	57	28	Loch et al. (1998)
Gin Gin (QLD)	11	11	34	48	30	Loch et al. (1998)
Gin Gin (QLD)	8	6	23	33	52	Loch et al. (1998)
Gin Gin (QLD)	14	9	36	52	25	Loch et al. (1998)
Gin Gin (QLD)	9	18	48	68	5	Loch et al. (1998)
Roma - Ardrossie (QLD)	21	7	20	29	42	Loch et al. (1998)
Roma - Holyrood (QLD)	18	12	39	55	17	Loch et al. (1998)
Roma - Dalmainly (QLD)	28	24	28	40	12	Loch et al. (1998)
Roma (QLD)	57	19	15	21	3	Loch et al. (1998)
Pinnarandi (QLD)	20	6	16	23	51	Loch et al. (1998)
Bundaberg (QLD)	15	13	42	60	12	Loch et al. (1998)
Bundaberg (QLD)	23	22	18	25	30	Loch et al. (1998)
Bundaberg (QLD)	9	5	18	25	61	Loch et al. (1998)
Bundaberg (QLD)	19	9	34	48	24	Loch et al. (1998)
Tent Hill (QLD)	41	28	21	30	1	Loch et al. (1998)
Gatton (QLD)	13	10	37	53	24	Loch et al. (1998)
Ryeford - Clifton (QLD)	19	7	33	47	28	Loch et al. (1998)
Brigalow (QLD)	32	7	23	33	29	Loch et al. (1998)
Billa Billa (QLD)	24	16	39	55	6	Loch et al. (1998)
Pittsworth (QLD)	66	18	8	12	4	Loch et al. (1998)
Pittsworth (QLD)	64	16	13	19	1	Loch et al. (1998)
Warwick/Hermitage (QLD)	70	19	6	9	2	Loch et al. (1998)
Darling Downs (QLD)	68	13	13	18	1	Loch et al. (1998)
Darling Downs (QLD)	57	17	18	26	0	Loch et al. (1998)
Lawes (QLD)	46	23	19	27	4	Loch et al. (1998)
Biloela (QLD)	37	24	26	37	5	Loch et al. (1998)
Warra (QLD)	52	16	16	23	9	Loch et al. (1998)
Gatton-Esk Rd (QLD)	35	6	20	28	31	Loch et al. (1998)
Plainlands (QLD)	38	11	25	35	16	Loch et al. (1998)
Hatton Vale (QLD)	42	19	23	33	6	Loch et al. (1998)

C.2.2 Results from the regression analysis

The three regression models fitted the observations reasonably well when the observed very fine sand fraction was between 0 and 30% (Figure C.1). However, all three models did not seem to perform very well beyond 30%. The three methods display a similar distribution of values along the 1:1 line between the observed and predicted very fine sand fractions and their NSE coefficient are very similar. The predicted values fall within similar ranges to that of observed values and present strong positive correlations

(Table C.2). Overall, the polynomial regression seemed to better fit the observed values, but to be more comparable to the assumption of Panagos et al. (2014), we will select the results from the linear regression with no intercept for the second part of this analysis.

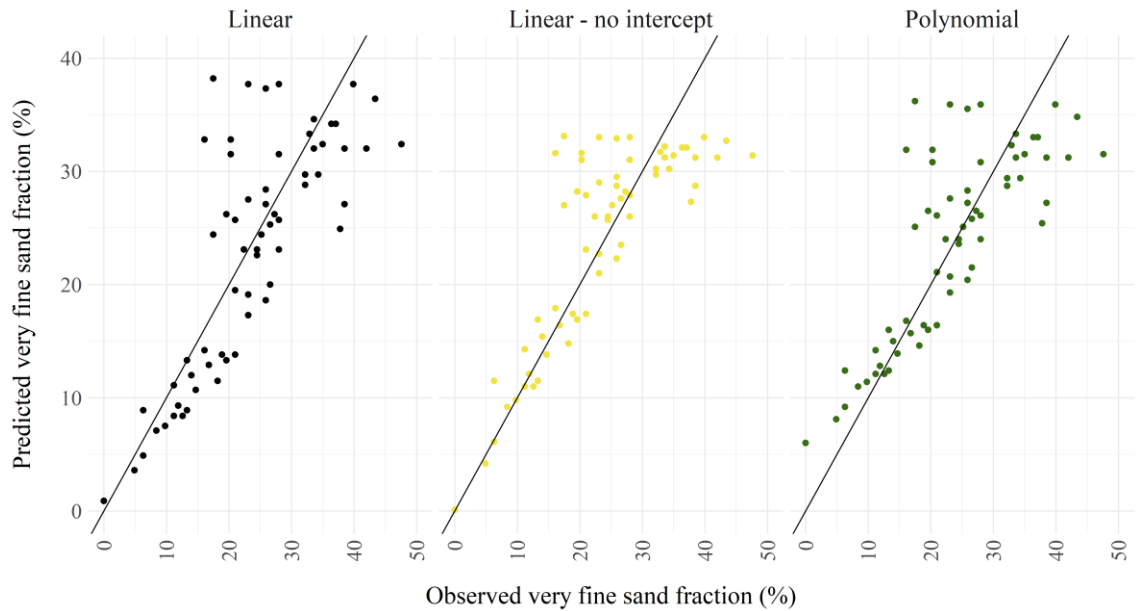


Figure C.1 Very fine sand fractions estimated with three regression analysis methods plotted against observed very fine sand fractions. The three methods are simple linear regression (Linear), simple linear regression with no intercept (Linear – no intercept), and second order polynomial regression (Polynomial).

Table C.2 Results from the regression analysis

Model	NSE coefficient	New equation
Linear regression with intercept	0.43	$\%VeryFineSand = \%Sand \times 0.36 + 5.32$
Linear regression, no intercept	0.39	$\%VeryFineSand = \%Sand \times 0.44$
Second order polynomial	0.46	$\%VeryFineSand = \%Sand \times 68 - \%Sand^2 \times 14.5 + 24.1$

C.2.3 Comparison of the assumptions from Panagos et al. (2014) and the regression analysis results

With a simple regression analysis based on 65 soil samples collected in Australia (NSW and QLD), we demonstrated that general assumptions might not be applicable to regional conditions with specific soils properties. Here, the very fine sand fraction could be estimated as about 44% of the total sand fraction as opposed to 20% recommended by Panagos et al. (2014). We then estimated the soil erodibility factor (S) with the two assumptions and compared their respective frequency distributions.

Figure C.2 demonstrates that the assumption from Panagos et al. (2014) highly underestimated the soil erodibility in the region. The value range was about half of the new soil erodibility distribution. The value ranges of the new soil erodibility maps for the study area is more in line with soil erodibility measured in Australia (Rosewell, 1993).

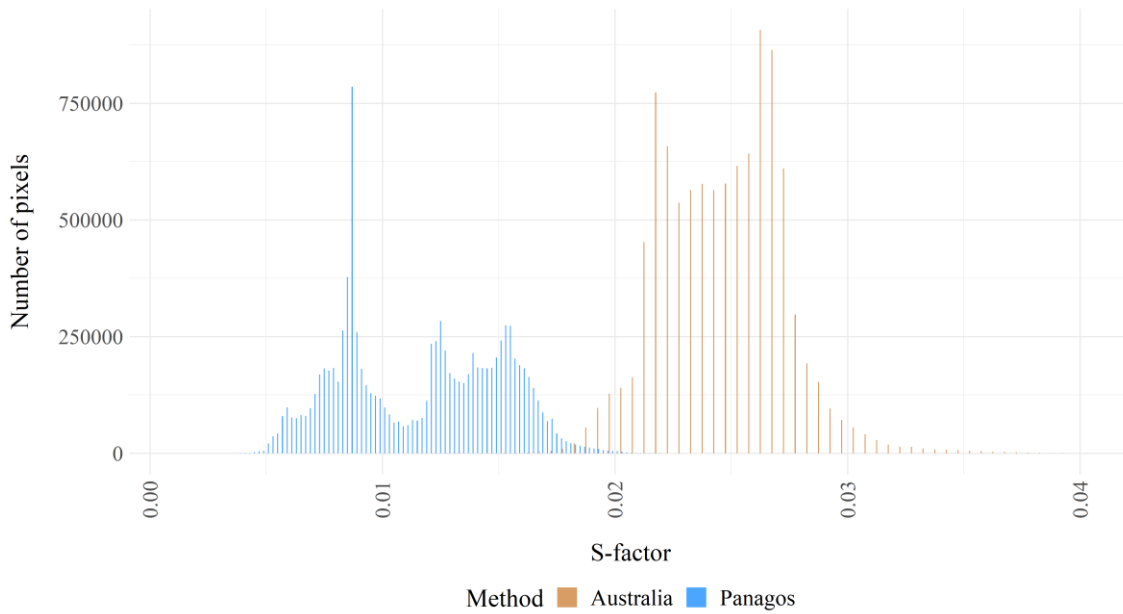


Figure C.2 Soil erodibility factor (S) with the assumption of Panagos et al. (2014): %Very fine sand = 0.2 x %Total sand; and new Australian assumption: %Very fine sand = 0.44 x %Total sand.

C.3 References

- Loch, R., Rosewell, C., 1992. Laboratory methods for measurement of soil erodibilities (K-factors) for the universal soil loss equation. *Soil Research* 30, 233-248,
- Loch, R.J., Slater, B.K., Devoil, C., 1998. Soil erodibility Km values for some Australian soils. *Soil Research* 36, 1045-1056, doi: <http://dx.doi.org/10.1071/S97081>.
- Panagos, P., Meusburger, K., Ballabio, C., Borrelli, P., Alewell, C., 2014. Soil erodibility in Europe: A high-resolution dataset based on LUCAS. *Science of The Total Environment* 479-480, 189-200, doi: <https://doi.org/10.1016/j.scitotenv.2014.02.010>.
- R Development Core Team, 2010. R: A Language and Environment for Statistical Computing. R Foundation for Statistical Computing, Vienna, Austria, <http://www.R-project.org>
- Rosewell, C., 1993. SOILOSS: a program to assist in the selection of management practices to reduce erosion. Soil Conservation Service of NSW, Sydney, NSW,
- Yang, X., Gray, J., Chapman, G., Zhu, Q., Tulau, M., McInnes-Clarke, S., 2017. Digital mapping of soil erodibility for water erosion in New South Wales, Australia. *Soil Research* 56, 158-170, doi: <https://doi.org/10.1071/SR17058>.
- Zambrano-Bigiarini, M., 2020. hydroGOF: Goodness-of-fit functions for comparison of simulated and observed hydrological time series, R package version 0.4-0 ed, doi: <https://doi.org/10.5281/zenodo.839854>.

Appendix D

Chapter 2 – Supplementary material

Corroboration of the modelled outputs with other examples and individual maps for the G2 model parameters and frequency distributions

D.1 The modelling parameters

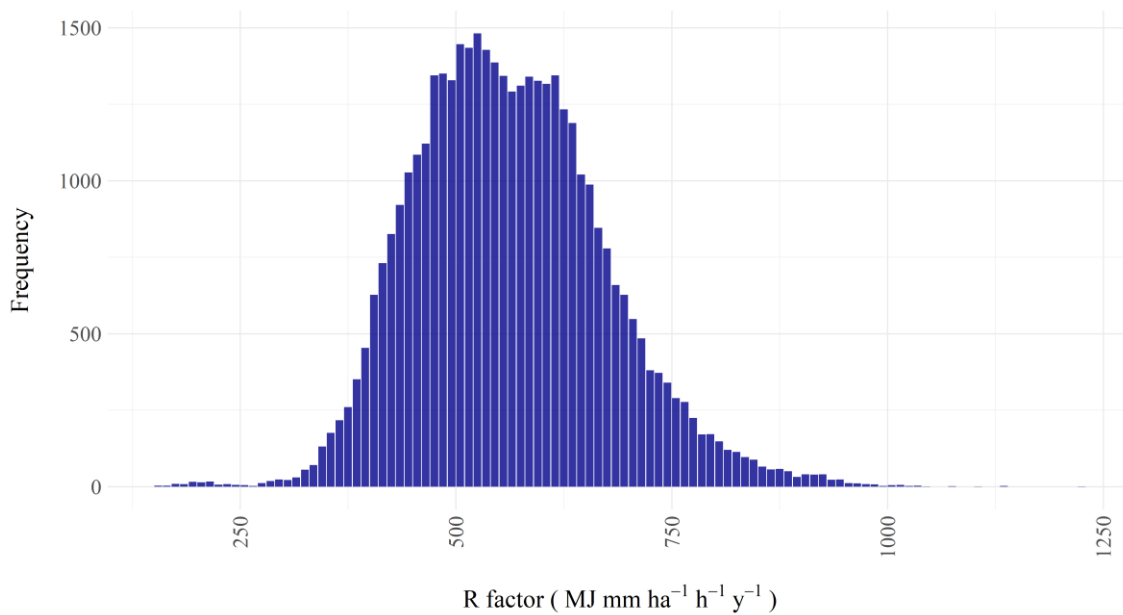


Figure D.1.a Average annual rainfall erosivity distribution.

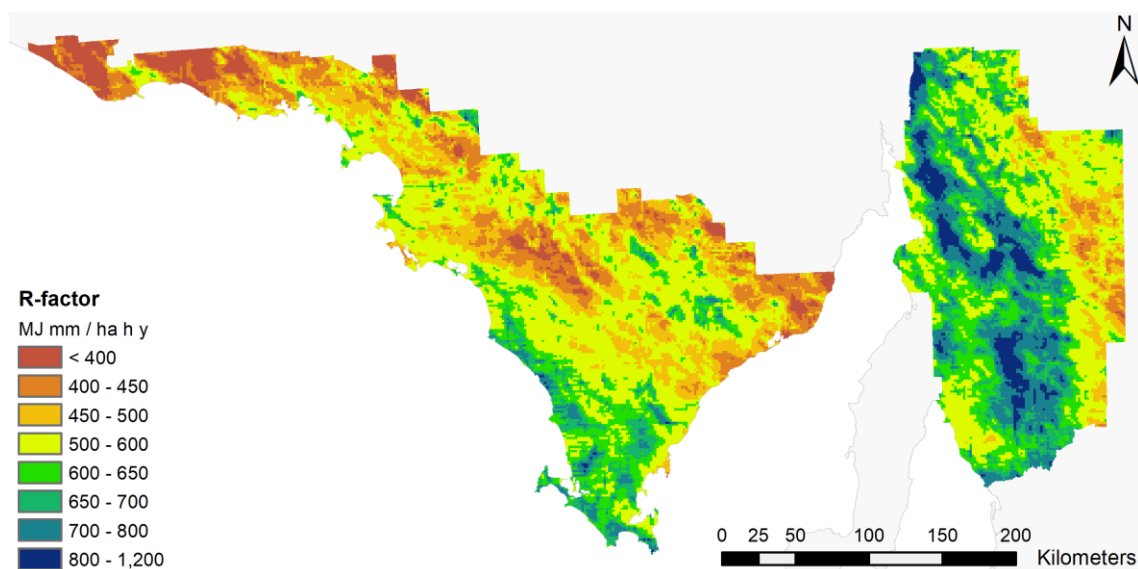


Figure D.1.b Average annual rainfall erosivity spatial distribution.

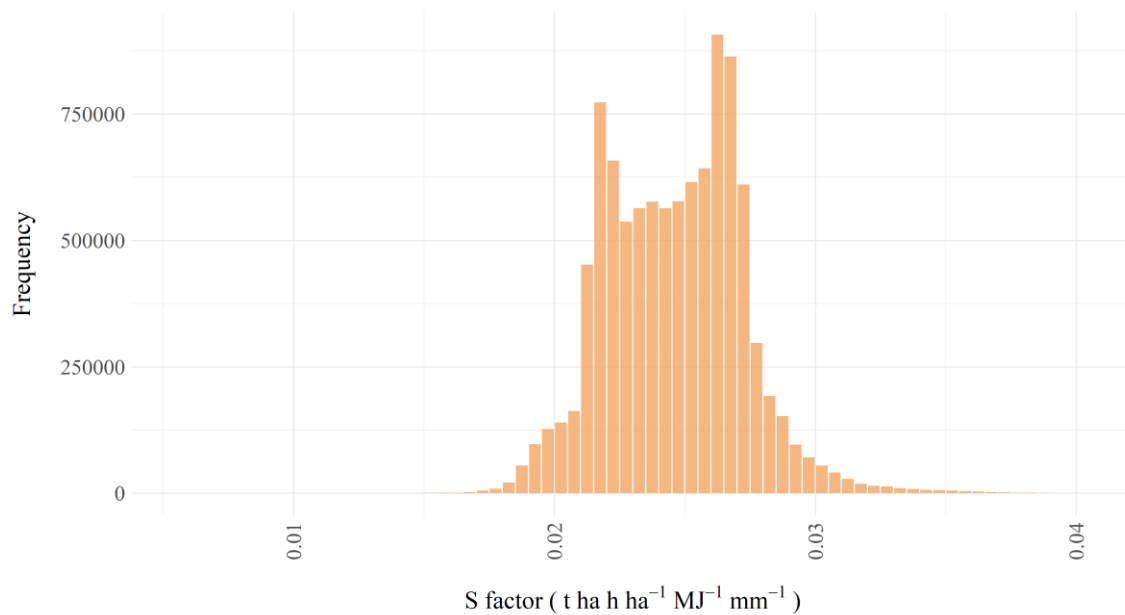


Figure D.2.a Soil erodibility distribution.

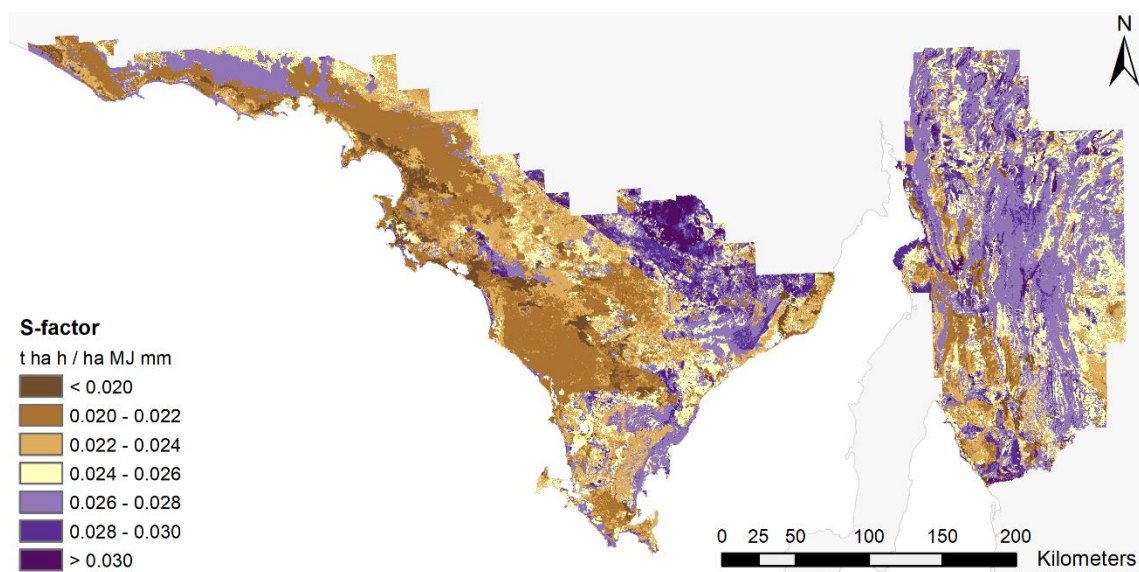


Figure D.2.b Soil erodibility spatial distribution.

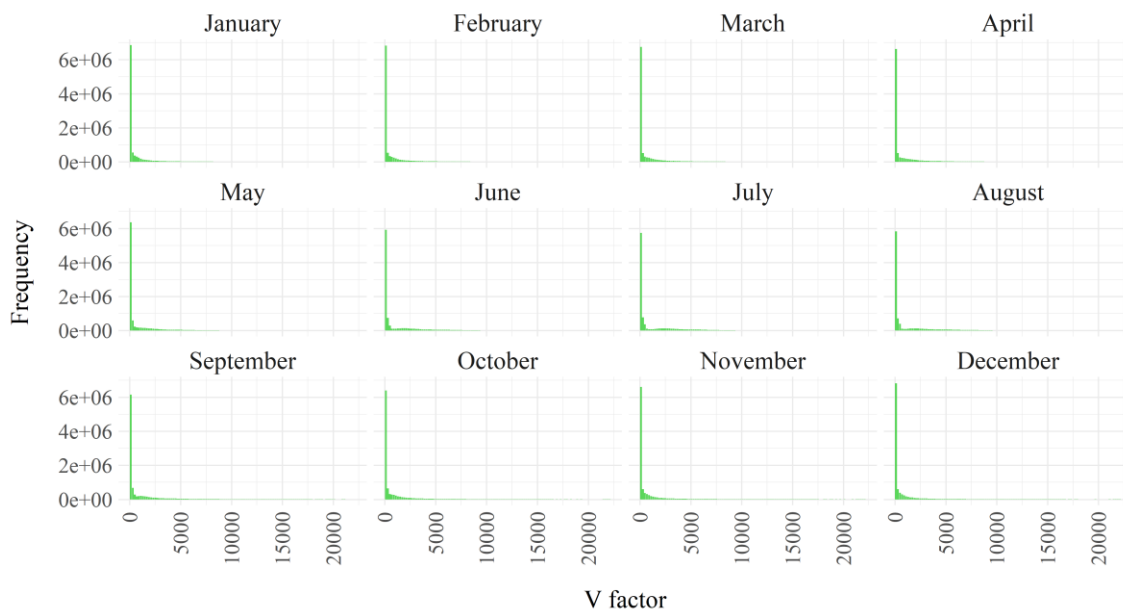


Figure D.3.a Average monthly vegetation cover retention distribution.

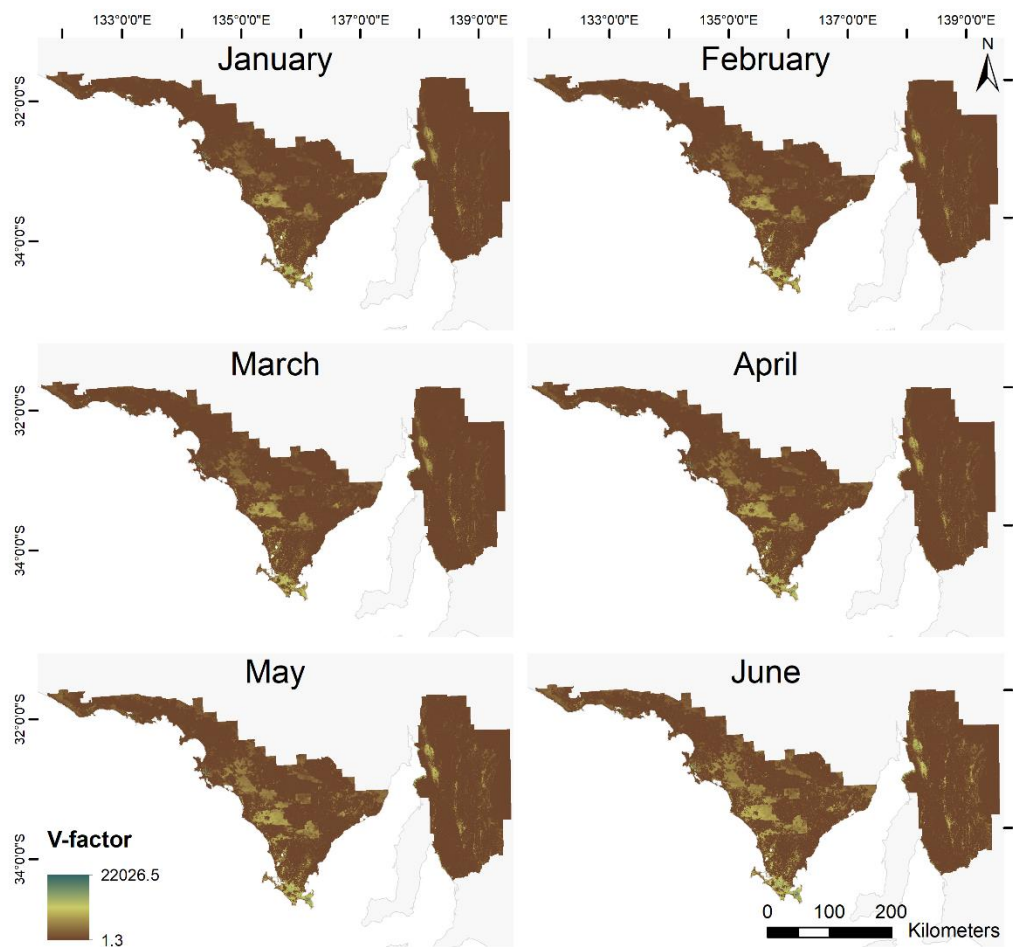


Figure D.3.b Average monthly vegetation cover retention spatial distribution.

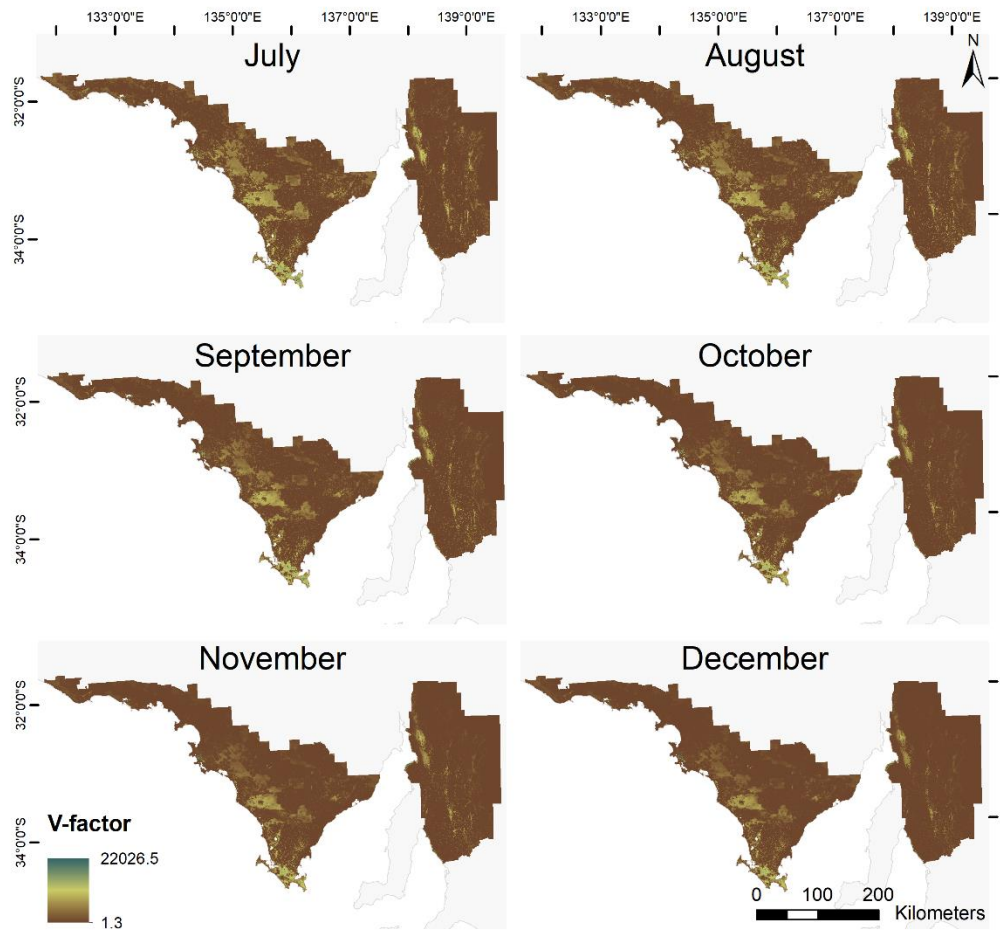


Figure D.3.c Average monthly vegetation cover retention spatial distribution.

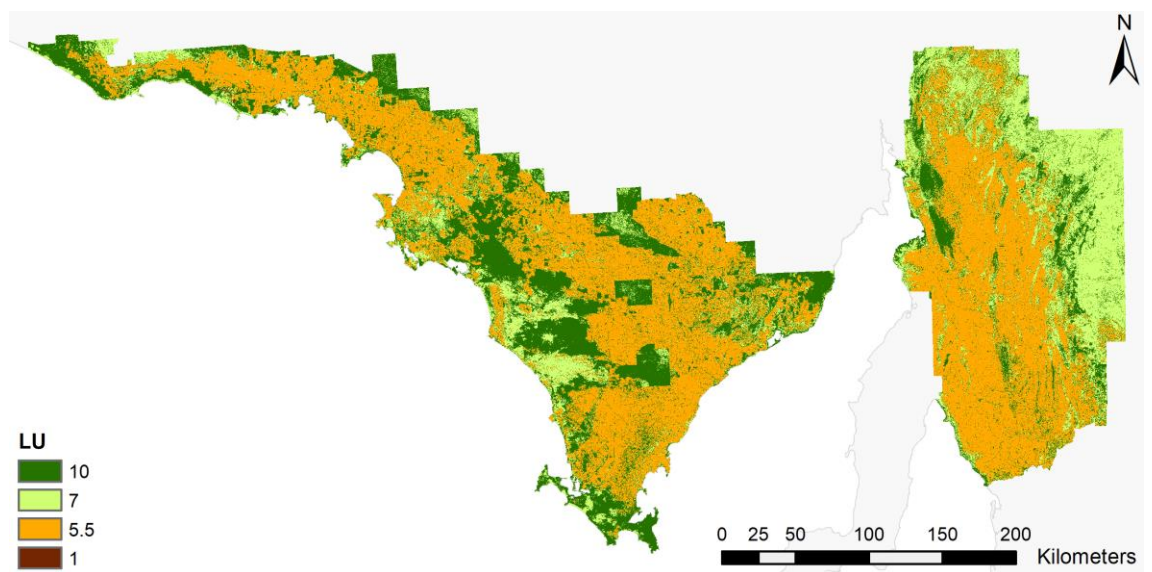


Figure D.4 Land Use parameter spatial distribution

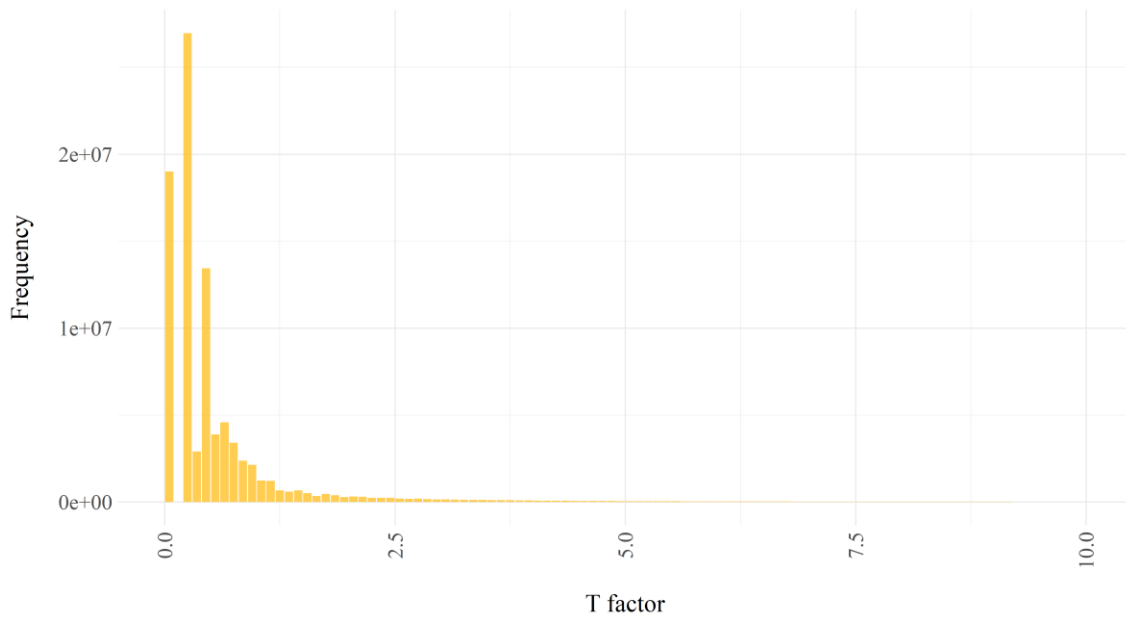


Figure D.5.a Topography factor distribution.

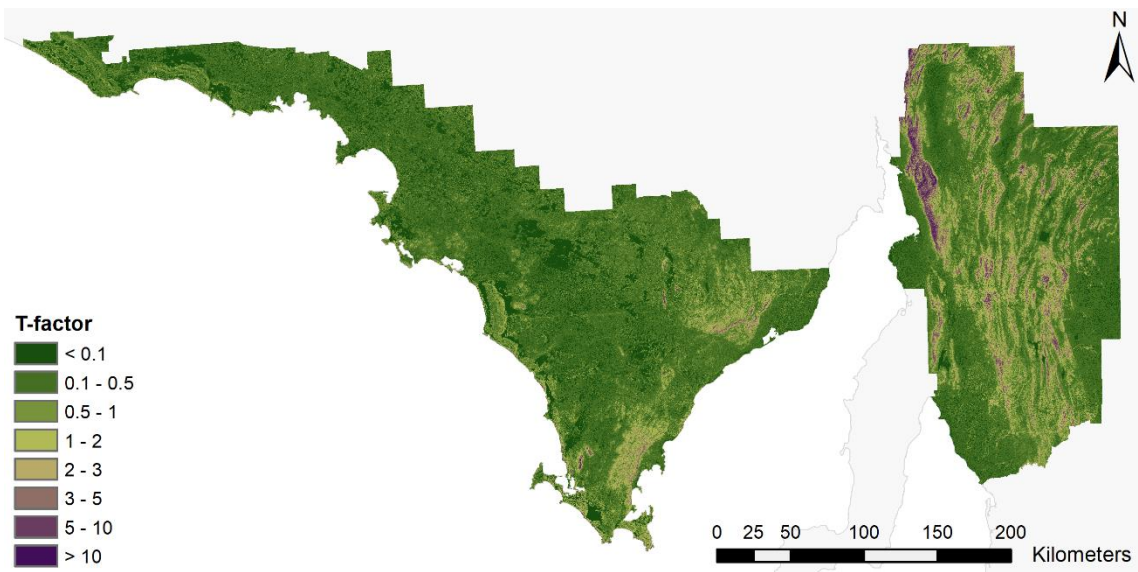


Figure D.5.b Topography factor spatial distribution.

D.2 Comparison of the modelled outputs with other modelling examples

We corroborated the results from our modelling approach with the Department for Environment and Water inherent water erosion potential maps (Figure D.6). We estimated the long-term average annual hillslope erosion and ranked the resulting map into five classes using a Jenks natural breaks classification method (Jenks and Caspall, 1971). We then ran an overlay analysis between the average annual soil loss predicted by the G2 model and inherent soil erodibility map to create an error matrix and we evaluated our results based on overall accuracy.

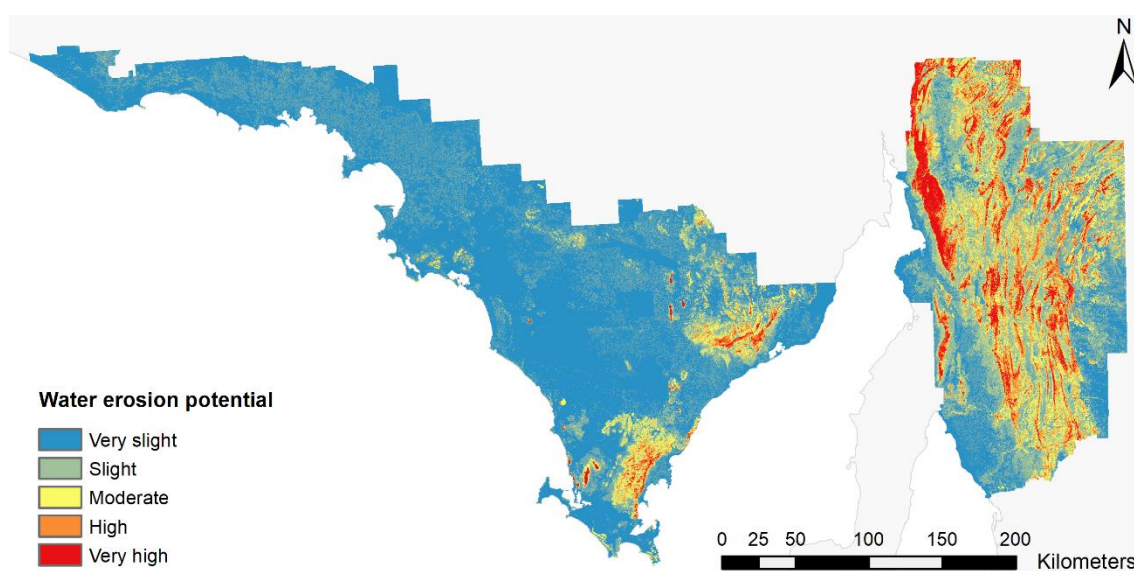


Figure D.6 Water erosion potential (source: DEW (2017))

Each element in Table D.1 represents the number of observations (pixels) within each class intersection divided by the total number of pixels and expressed as a percentage. The overall accuracy was then estimated by the sum of the diagonal elements.

If we assume that the classification of the hillslope severity and the inherent erosion susceptibility maps were comparable, then the overall accuracy of the model was 58.2%, which is reasonable. However, if we assume that a one-class difference is acceptable because the classes were not defined on a nominal scale but an ordinal-scale (Vrieling et al., 2006), then the accuracy of the wind erosion model increases to 90.1% which is reasonably satisfactory (Figure D.7).

Table D.1 Error matrix comparing the agreement (overlapping area in %, values in bold denote agreement) between wind erosion severity classes from the G2 model and the inherent water erosion potential.

Water erosion model	Soil Water erosion Potential				
	Very slight	Slight	Moderate	High	Very high
Very slight	44.9	6.2	1.7	0.6	0.2
Slight	14.4	8.9	4.0	1.4	0.5
Moderate	3.5	3.6	2.8	1.7	0.7
High	0.4	0.7	0.9	1.0	0.7
Very high	0.1	0.1	0.2	0.4	0.6
Overall accuracy	58.2%				

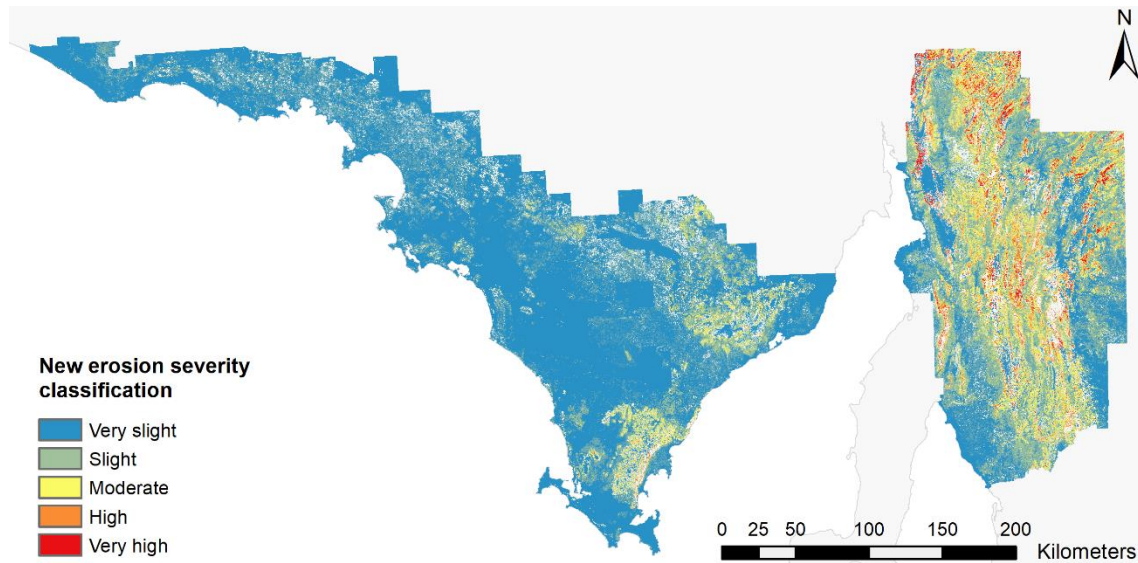


Figure D.7 New predicted hillslope erosion severity map corroborated with the DEW inherent soil erosion susceptibility map. Note that the areas in grey represent zones where the classification of the DEW map did not overlap with the G2 model.

D.3 References

- DEW, 2017. Soil Water Erosion Potential. Government of South Australia, Department for Environment and Water, <https://data.sa.gov.au/data/dataset/water-erosion-grid>
- Jenks, G.F., Caspall, F.C., 1971. Error on choroplethic maps: Definition, measurement, reduction. *Annals of the Association of American Geographers* 61, 217-244, doi: <https://doi.org/10.1111/j.1467-8306.1971.tb00779.x>.
- Vrieling, A., Sterk, G., Vigiak, O., 2006. Spatial evaluation of soil erosion risk in the West Usambara Mountains, Tanzania. *Land Degradation & Development* 17, 301-319, doi: <https://doi.org/10.1002/ldr.711>.

Chapter 3

Assessing the spatio-temporal variability of extreme erosion events with a novel wind erosion model and GIS: A case-study of the South Australian agricultural zone

Statement of Authorship

Title of Paper	Assessing the spatio-temporal variability of extreme erosion events with a novel wind erosion model and GIS: A case-study of the South Australian agricultural zone
Publication Status	<input type="checkbox"/> Published <input type="checkbox"/> Accepted for Publication <input checked="" type="checkbox"/> Unpublished and <input type="checkbox"/> Submitted for Publication Unsubmitted work written in manuscript style
Publication Details	Jeanneau, A., Herrmann, T. & Ostendorf, B (2020). Assessing the spatio-temporal variability of extreme erosion events with a novel wind erosion model and GIS: A case-study of the South Australian agricultural zone (unpublished)

Principal Author

Name of Principal Author (Candidate)	Amelie Jeanneau	
Contribution to the paper	Conceptualization, methodology, data curation, formal analysis, writing – original draft preparation, writing – review and editing.	
Overall percentage (%)	70%	
Certification	This paper reports on original research I conducted during the period of my Higher Degree by Research candidature and is not subject to any obligations or contractual agreements with a third party that would constrain its inclusion in this thesis. I am the primary author of this paper.	
Signature		Date: 04/06/2020

Co-author Contributions

By signing the Statement of Authorship, each author certifies that:

- i. the candidate's stated contribution to the publication is accurate (as detailed above);
- ii. permission is granted for the candidate to include the publication in the thesis; and
- iii. the sum of all co-author contributions is equal to 100% less the candidate's stated contribution.

Name of Co-Author	Tim Herrmann	
Contribution to the Paper	Methodology, formal analysis, writing – review and editing.	
Signature		Date: 04/06/2020

Name of Co-Author	Bertram Ostendorf	
Contribution to the Paper	Methodology, formal analysis, writing – review and editing.	
Signature		Date: 04/06/2020

Abstract

Soil erosion is highly variable through space and time. Therefore being able to identify when and under which conditions erosive events occur will produce critical information for land managers and policymakers to apply corrective measures for better erosion management in the future.

Here, we adapted a state-of-the-art wind erosion model (“albedo” Wind Erosion Model) to integrate modern high-resolution datasets for spatial and temporal analysis of erosion. We assessed the spatio-temporal variability of erosion events in two dryland agricultural regions of South Australia, Australia, between 2001 and 2017. We described the complex interactions between wind erosion and influencing factors (e.g. climate conditions and vegetation cover), and defined the relative contribution of a range of land uses to erosion for the Eyre Peninsula (EP) and Mid-North (MidN) agricultural regions of South Australia.

This study demonstrated the utility of soil erosion modelling for land management and agricultural development. The model identified the very high spatial as well as seasonal and inter-annual variability in wind erosion in the study area. Average annual erosion was very low and comparable in both regions (EP: $0.00258 \text{ t ha}^{-1} \text{ y}^{-1}$; MidN: $0.00243 \text{ t ha}^{-1} \text{ y}^{-1}$). However, most of the west coast of the Eyre Peninsula frequently recorded severe erosion ($> 0.000945 \text{ t ha}^{-1} \text{ month}^{-1}$ or $0.945 \text{ kg ha}^{-1} \text{ month}^{-1}$). The most severe erosion events in both regions were primarily driven by the soil type (sandy soils), recurring low ground cover ($< 50 \%$) and extreme wind gusts ($> 68 \text{ km h}^{-1}$). Agricultural land uses were significant contributors to total regional erosion (EP: $0.007 \text{ t ha}^{-1} \text{ y}^{-1}$; MidN: $0.008 \text{ t ha}^{-1} \text{ y}^{-1}$), with dryland cropping, modified pastures and livestock grazing representing the greatest proportion.

This study provides a proof of concept of how erosion models could be used to inform corrective measures for future land management through improved understanding of how different land uses and management affect regional wind erosion severity.

3.1 Introduction

Soil erosion is a significant cause of land degradation globally. The United Nations Convention to Combat Desertification (UNCCD) and their Land Degradation Neutrality (LDN) framework listed soil erosion as one of their top priority (FAO, 2011, 2017), and target 15.3 of the UN Sustainable Development Goals (SDG) emphasises the need to combat desertification and land degradation. Wind erosion is particularly of global concern as it strongly impacts agricultural productivity and public health. Wind erosion processes generate on-site disturbances such as the loss of topsoil leading to a decline in nutrients, organic matter and soil carbon, but can also damage crops and infrastructure through sand-blasting and burial (Baumhardt et al., 2015; Bennell et al., 2007; Panebianco et al., 2016). The cost of nutrient replacement, purchase of new grain seeds and loss of productivity can be a substantial burden for agriculture (Montgomery, 2007). Wind erosion also generates off-site damages such as visibility limitation leading to road safety and transport issues, health impacts including asthma and other respiratory problems (Baddock et al., 2014; Seinfeld and Pandis, 2012) as well as cleaning costs due to dust deposition and road maintenance.

Measurements of wind erosion in the field with wind tunnel experiments and standardised plots have contributed significantly to the development of prediction models. However, such measurements are not sustainable when considering regional- or continental-scale applications. Thus, empirical and physical models have been developed to describe erosional processes. Recent technological advances in remote sensing and Geographic Information System (GIS), have also contributed to the popularity of erosion models as a growing number of models were designed to integrate GIS, digital maps and satellite data.

Models commonly used for broad-scale wind erosion assessment often use the Normalized Difference Vegetation Index (NDVI) and Leaf Area Index (LAI) vegetation indices to represent plant phenological effects. However, these indices often misrepresent land surface aerodynamic roughness as they fail to characterise the

sheltering effect of vegetation and do not capture changes in land use and land cover very well (Chappell and Webb, 2016; Webb et al., 2020). For this reason, Chappell and Webb (2016) redefined the approximation of aerodynamic roughness using fundamental principles of aeolian sediment transport and developed a new approach to wind erosion modelling: the “albedo” Wind Erosion Model. They replaced the lateral cover parameters (L) with a relationship between the sheltered area in the wake of objects and the proportion of shadow produced by the same object (Chappell et al., 2010). The authors demonstrated that this proportion of shadow could be easily derived from MODIS Albedo products (MCD43A1 and MCD43A3) and designed regression relationships between aeolian sediment transport and the shadow area (or black sky albedo). This new method has now made it possible to fully integrate satellite imagery and remote sensing in complex wind erosion models. Therefore, the “albedo” Wind Erosion Model provides a dynamic (multi-temporal) global metric for wind erosion assessment at a moderate resolution. Chappell and Webb (2016) successfully calibrated and tested the regression relationships with field data collected in Australia and the US through a National Wind Erosion Research Network (Webb et al., 2016).

Vegetation cover plays a significant role in erosion control, especially in dryland agricultural landscapes (Chappell et al., 2019; Jeanneau et al., 2019; McKenzie and Dixon, 2006; Shao, 2008; Vacek et al., 2018). These regions are already vulnerable to changes in land conditions (e.g. droughts, wildfires) and are expected to sustain a recurrence in extreme environmental conditions and compound events (McKenzie et al., 2017). These compound events are also likely to increase future soil erosion risk (Bardsley et al., 2008; Earl et al., 2019; Li and Fang, 2016). Hence, investigating the impact and frequency of extreme erosive events will produce vital information for land managers and policymakers to apply corrective measure for better erosion management in the future.

Even though wind erosion processes have been well described, the high spatial and temporal variability in erosion makes the prediction of erosion trends very difficult. To

overcome these limitations, we need detailed data and access to high spatio-temporal datasets to be able to give the best assessment of soil losses and identify regions at risk of erosion in the future.

Therefore, this paper aims to demonstrate the utility of soil erosion modelling for the management of natural and agricultural environments by identifying the spatio-temporal variability of erosion events. The specific objectives of this research are twofold. First, to adapt a state-of-the-art wind erosion model to integrate modern high-resolution datasets for spatial-and temporal analysis. And second, to use the model to describe the complex interactions between wind erosion and influencing factors (e.g. land use, climate conditions, and vegetation cover) for two agricultural regions of South Australia.

3.2 Methods

3.2.1 *The study area*

Our study focusses on two dryland agricultural regions of South Australia, Australia: Eyre Peninsula (EP – 33° 568'S 135° 755'E – 4.7x10⁴ km²) and the Mid-North (MidN – 33° 376'S 138° 723'E – 3,4x10⁴ km², Figure 3.1). These two regions are significant contributors to agricultural production in South Australia (ABARES, 2018) and part of these regions are historically prone to wind erosion, therefore representing a vital interest for food and soil security. Agricultural land-uses represent the majority of the regional land-uses (Figure 3.2) with cereal cropping representing 50% and 33% of the land surface for the Eyre Peninsula and Mid-North respectively, followed by grazing (modified) pastures, representing 11% and 54% of the total regional land-use for each region (ABARES, 2016).



Figure 3.1 Location map and presentation of the study area (Eyre Peninsula & Mid-North) within the South Australian cropping region.

The study area is characterised by a Mediterranean climate, with cool wet winters and hot dry summers with occasional summer storms and exhibit diverse soils and land uses, providing an excellent study site to demonstrate the utility of erosion modelling for land management. Mean annual rainfall ranges from 200mm in the north to 500mm in the south, with a mean of 350mm (BoM, 2016a). The average daily temperature varies between 12 and 19°C (BoM, 2016b). The agricultural region of Eyre Peninsula has a range of sandy to clay-loam soils (Figure 3.3). On the other hand, dominant soil types throughout the Mid-North region are more diverse and predominantly loam or clay-loam soils, with some sandy-loam patches (Figure 3.3). Elevation in the Eyre Peninsula region ranges between 0m and 480m, and from south-west to north-east. For the Mid-North region, altitude ranges between 0m and 950m above sea level with the highest elevations found in the centre of the region. The topography is complex in this area, and some parts have very steep slopes with gradients ranging from 0% to 60%.

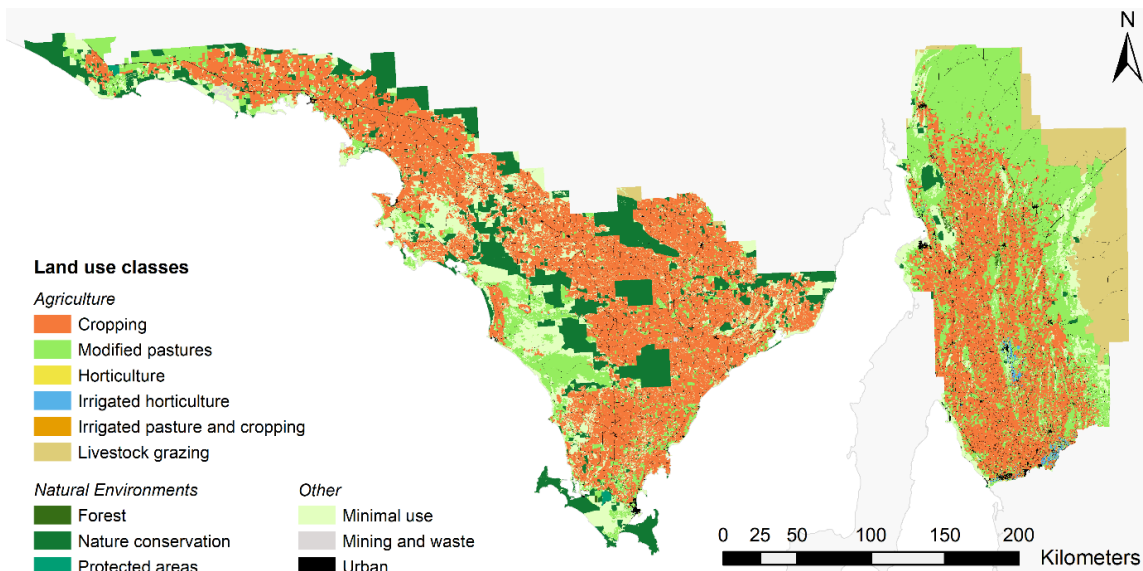


Figure 3.2 Land-use classes for the Eyre Peninsula and Mid-North regions. Source: ABARES (2016).

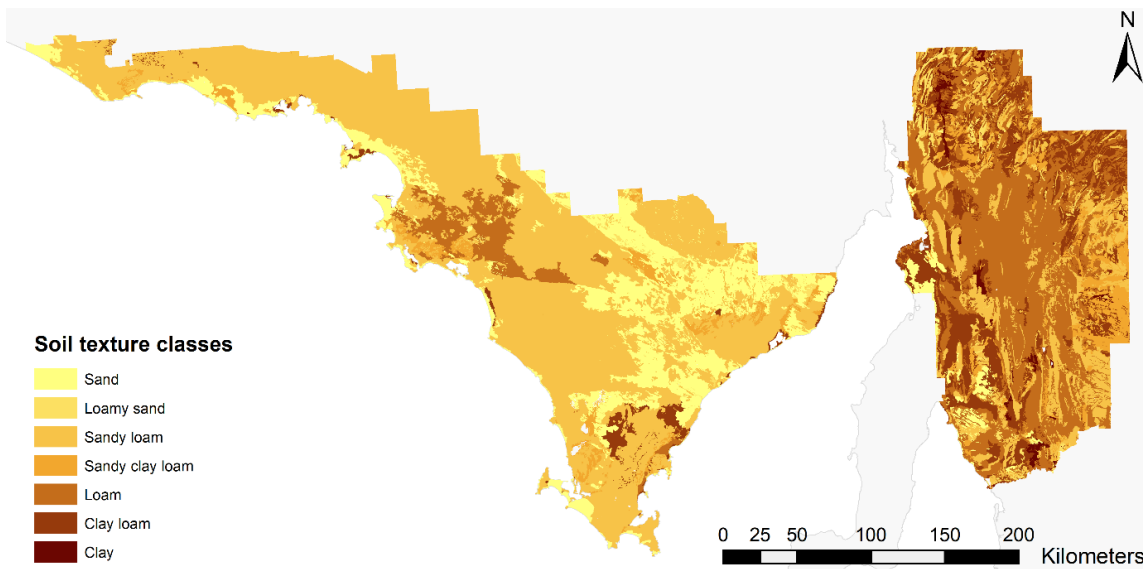


Figure 3.3 Dominant soil texture classes for the Eyre Peninsula and Mid-North regions. Source: DEW (2016).

3.2.2 Description of the data sources

All the datasets used in this study have been acquired from open-source databases. Data description (e.g. type, resolution, sources) can be found in Appendix A - Table A.1. . Climate and weather data were obtained from the Australian Bureau of Meteorology Atmospheric high-resolution Regional Reanalysis dataset for Australia (BARRA) (Su et al., 2019). The spatial resolution of the dataset is 12km at the continental scale and additional model run at 1.5km resolution for spatial subsets, including South Australia. Here we used the 1.5km resolution data.

Ground cover was derived from Moderate Resolution Imaging Spectroradiometer (MODIS) fractional cover dataset for Australia (Guerschman et al., 2015), accessed from the Terrestrial Ecosystem Research Network (TERN) archive (CSIRO, 2019). The MODIS BRDF/albedo products (MCD43A1 and MCD43A3, band 1) were programmatically downloaded with the *MODISrsp*: R package (Busetto and Ranghetti, 2016) to extract the isotropic (f_{iso}) and directional hemispherical reflectance (or black-sky albedo ω) parameters required to derive the normalised albedo factor for the wind erosion model. More details about the datasets can be found in Chappell and Webb (2016) and Chappell et al. (2018). Both MODIS datasets (Fractional Cover and MODIS BRDF/albedo) provide daily data available at 500m resolution from the year 2000.

We extracted soil properties information from the Soil and Landscape Grid of Australia (SLGA) digital soil maps to estimate the ideal threshold friction velocity. This dataset contains information about soil texture composition as a mass fraction at a depth of 0-5cm (clay < 2 μ m, silt < 50 μ m, sand < 2000 μ m, coarse fragments > 2000 μ m) and bulk density of the soil. The SLGA dataset is available at a resolution of 90m for the whole continent and can be automatically downloaded through the *slga*: R package (O'Brien, 2019), more information about the range of soil properties and landscape attributes can also be found at www.csiro.au/soil-and-landscape-grid.

3.2.3 Modelling methods

Ground cover plays a critical role in erosion control. However, considering the ground cover alone is not enough to describe all the protective effect of vegetation against wind erosion. Many authors have highlighted that surface roughness and particularly lateral vegetation cover (L) or frontal area index (LAI) is the most influential erosion control parameter (Leys et al., 2017b; Okin, 2008). Therefore, it is essential to fully describe vegetation structure, density and distribution as vegetation extracts wind momentum and applies a sheltering effect to adjacent and downstream areas (Jeanneau et al., 2019; Vacek et al., 2018).

Chappell and Webb (2016) proposed a new approach for wind erosion modelling simplifying the drag partition scheme of Raupach et al. (1993) while combining the use of remote sensing satellite imagery. The authors established a relationship between the sheltered area and the proportion of shadow over a given area (Figure 3.4).

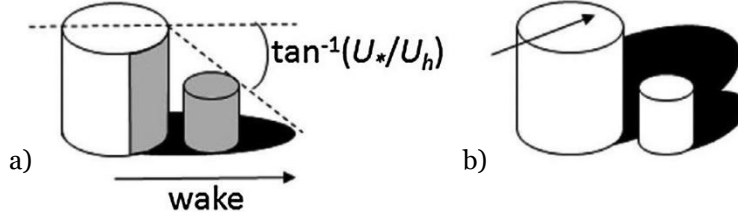


Figure 3.4 a) Concept representation of the sheltering effect of vegetation from Raupach et al. (1993), b) concept of the shadow effect of vegetation proposed by Chappell et al. (2010) to derive vegetation structure from remote sensing. Source: Chappell and Webb (2016).

This proportion of shadow can be derived from the inverse of the direct beam directional hemispherical reflectance (or black sky albedo, ω) viewed at nadir. This approach preserves the principles of previous wind erosion models, and the horizontal sediment flux can then be expressed as follow

$$Q_h = c_{shao} \times \frac{\rho_a \times u_{S*}^3}{g} \times \left(1 - \frac{u_{*ts}^2 \times H(w)^2}{u_{S*}^2} \right) \quad (14)$$

where c_{shao} (0.006) represents a tuning factor adjusted to the magnitude of the model output, ρ_a is the density of the air (1.23 kg m^{-3}), g is the acceleration due to gravity (9.81 m s^{-1}), u_{*ts} is the soil threshold shear stress of bare soil below which sediment transport does not occur (Shao et al., 1996), and $H(w)$ is a soil moisture correction function which reduces sediment transport through the increase of cohesive forces in the soil (Fecan et al., 1999). The model is also adjusted by the influence of the total wind energy (shear stress) that is applied at the soil surface (u_{S*}).

The bare soil threshold friction velocity (u_{*ts}) for a particle size D can be defined as follow

$$u_{*ts}(D) = \sqrt{A_N \times \left(\frac{\rho_p}{\rho_a} \times g \times D + \frac{\gamma}{\rho_a \times D} \right)} \quad (15)$$

with A_N is as a scaling coefficient (0.0123), ρ_p is the density of particles (2650 kg m^{-3}), ρ_a is the density of the air (1.23 kg m^{-3}), g is the acceleration due to gravity (9.81 m s^{-1}),

and γ represents a parameter accounting for cohesive forces of the particles $((1.65/5) \times 10^{-4} \text{ kg s}^{-2})$ (Darmenova et al., 2009).

The soil moisture correction function used in this approach followed the principles of Fecan et al. (1999)

$$H(w) = \begin{cases} 1, & w < w' \\ (1 + 1.21 \times (w - w')^{0.68})^{0.5}, & w \geq w' \end{cases} \quad (16)$$

where w is the gravimetric soil moisture (%), and w' is the limit value of soil moisture in a soil layer (%). The latter depends on the clay content in percent ($\%clay$) in the soil and can be defined by

$$w' = 0.0014 \times (\%clay)^2 + 0.17 \times \%clay \quad (17)$$

The gravimetric soil moisture can be derived from volumetric soil moisture (w_v , in %) with the following expression

$$w = \frac{\rho_w}{\rho_b} \times w_v \quad (18)$$

where ρ_w is the density of water (1000 kg m^{-3}) and ρ_b is the soil bulk density derived from the Soil Landscape Grid of Australia dataset. This soil moisture correction function was developed from wind tunnel experiments where soil moisture was only changed in the top 1-2cm layer of the soil. Soil moisture in the “surface layer” can sometimes significantly differ from the “topmost layer” relevant to dust generation. To reduce the overestimation of soil moisture in the “surface layer”, Darmenova et al. (2009) proposed to apply a corrective factor of 0.1 when using a soil moisture dataset with a “surface layer” of 10cm. In this study, we applied this correction factor to the BARRA hourly (0-10cm) soil moisture dataset to calculate equation (18).

Although the equations (14) to (18) are drawn from classical wind erosion modelling approaches, the definition of shear stress at the soil surface (u_{s*}) is where the improvements of Chappell and Webb (2016) occur. The authors demonstrated a strong correlation between the rescaled normalised albedo (ω_{ns}) and u_{s*} scaled by freestream wind speed at 10 meters (U_f). This relationship can be described as follow

$$\frac{u_{S^*}}{U_f} = 0.0306 \times \left(\frac{\exp^{-\omega_{ns}^{1.1202}}}{0.0125} \right) + 0.0072 \quad (19)$$

Chappell and Webb (2016) defined the normalised albedo parameter (ω_n) as the ratio between the shadow effect of the black sky albedo ($1 - \omega$) and the weighted sum of an isotropic weighting parameter (f_{iso}), which represents the spectral contribution. Dividing $(1 - \omega)$ by f_{iso} removed the influence of surface reflectance. Both spectral parameters can be derived from MODIS Albedo products (f_{iso} : MCD43A1, value range [0 - 1]; ω : MCD43A4, value range [0 - 1]). The normalised albedo can be obtained with the following expression

$$\omega_n = \frac{(1 - \omega)}{f_{iso}} \quad (20)$$

The parameter ω_n is then rescaled from the normalised range ($\omega_{n \min}$; $\omega_{n \max}$) of a given waveband (v) to that of the calibration data ($a = 0.0001$ to $b = 0.1$).

$$\omega_{ns} = \frac{(a - b) \times (\omega_n(v) - \omega_n(v)_{\max})}{(\omega_n(v)_{\min} - \omega_n(v)_{\max})} + b \quad (21)$$

Following recommendations from Chappell and Webb (2016), we used the band 1 for each MODIS products as this band introduced the least bias when compared to wind tunnel experiments. We set the values of the normalised range to $\omega_{n \min} = 0$ and $\omega_{n \max} = 35$ to avoid the results being dominated by extremes based on the recommendation from Adrian Chappell (*pers.com*). Chappell and Webb (2016) defined these values from an assessment of global ω_n estimates of the MODIS archive and $\omega_{n \max} = 35$ represented the value of the 95th percentile.

To estimate wind erosion for the two regions of interest, we converted the horizontal sediment flux (Q_h , $\text{g m}^{-1} \text{s}^{-1}$), representing transport in one dimension, to an areal quantity (E , $\text{t ha}^{-1} \text{y}^{-1}$). First, we estimated the horizontal sediment flux on an hourly basis (finest temporal resolution) for each pixel in the archive (2001-2017). Then, we calculated the median value of daily horizontal sediment flux for each day in the time-series. Finally, we converted the median daily horizontal flux to an areal quantity to obtain the daily erosion rate (E_{day} , $\text{t ha}^{-1} \text{day}^{-1}$). To apply the conversion, we drew inspiration from

Chappell et al. (2019) and used similar assumptions. We assumed that (i) the area of transport was defined by the size of a pixel (500m) and (ii) heterogeneity of transport within a pixel was captured by the albedo response of each pixel. Based on these assumptions, the median daily sediment transport in one dimension (Q_{h_day} , $\text{g m}^{-1} \text{s}^{-1}$) was converted to a surface quantity by dividing Q_{h_day} with the MODIS pixel size of 500m ($\text{g m}^{-2} \text{s}^{-1}$). We further assumed wind erosion to be non-selective over a day and multiplied this quantity by the number of seconds in one day ($\text{g m}^{-2} \text{day}^{-1}$) and then divided by 100 to convert the units to $\text{t ha}^{-1} \text{day}^{-1}$. The daily erosion rate (E_{day}) was then summed by months and years for the analysis.

3.2.4 Comparison of the wind erosion severity with the frequency of dust storms

A lack of measured wind erosion data precluded the direct validation of the wind erosion model outputs. A growing number of satellite sensors can now retrieve Aerosol Optical Depth (AOD) with better accuracy than ever before, and researchers have used them to locate natural dust sources over arid and semi-arid regions (Chudnovsky et al., 2014; Fenta et al., 2020; Moridnejad et al., 2015). These AOD measurements can then be used as a proxy to estimate the frequency of dust storms. Fenta et al. (2020) demonstrated that the prevalence of dust storms estimated from AOD measurements could be used to validate wind erosion susceptibility maps in eastern Africa with an accuracy of about 70%. Here, we estimated the frequency of dust storms from the MODIS Multi-Angle Implementation of Atmospheric Correction (MAIAC) algorithm dataset (Lyapustin et al., 2011a; Lyapustin et al., 2011b; Lyapustin et al., 2012). The annual frequency of dust storms was then calculated as the number of days in a year for which $\text{AOD} > 0.30$. This threshold value is characteristic of freshly emitted dust particles and is representative of dust storm days in dryland environments (Ginoux et al., 2010; Moridnejad et al., 2015). We calculated the long-term average annual frequency of dust storms for the Eyre Peninsula and Mid-North regions and ranked the resulting map into five classes using a Jenks natural breaks classification method (Jenks and Caspall, 1971) to be comparable

with the approach of Fenta et al. (2020). We then ran an overlay analysis between the average annual soil loss predicted by the “albedo” Wind Erosion Model and the annual frequency of dust storms map to create an error matrix and we evaluated our results based on overall accuracy.

We also compared relative patterns of erosion severity with local historical observations and previous erosion susceptibility maps developed by the South Australian Government.

3.2.5 Analysis of the model results

The main focus of this study is to assess the spatial and temporal variability of erosion events in our two regions of interest. For this reason, we extracted the pixel values of the monthly and annual raster time-series. Here, we defined extreme erosion events as falling within the 99th percentile based on 17 years of monthly and annual erosion rates (204 months, 17 years). We then estimated the frequency of these highly erosive events in space and time.

To analyse the influence of ground cover and weather conditions on soil erosion, we estimated the joint distribution of extreme erosion events for daily ground cover and wind velocity percentiles.

In order to exemplify application and flow of evidence derived from the “albedo” Wind Erosion Model for decision support of soil management, we estimated the median annual wind erosion for each land use (Figure 3.2) and Local Government Areas (LGAs) (Figure 3.5) within the two regions of interest.

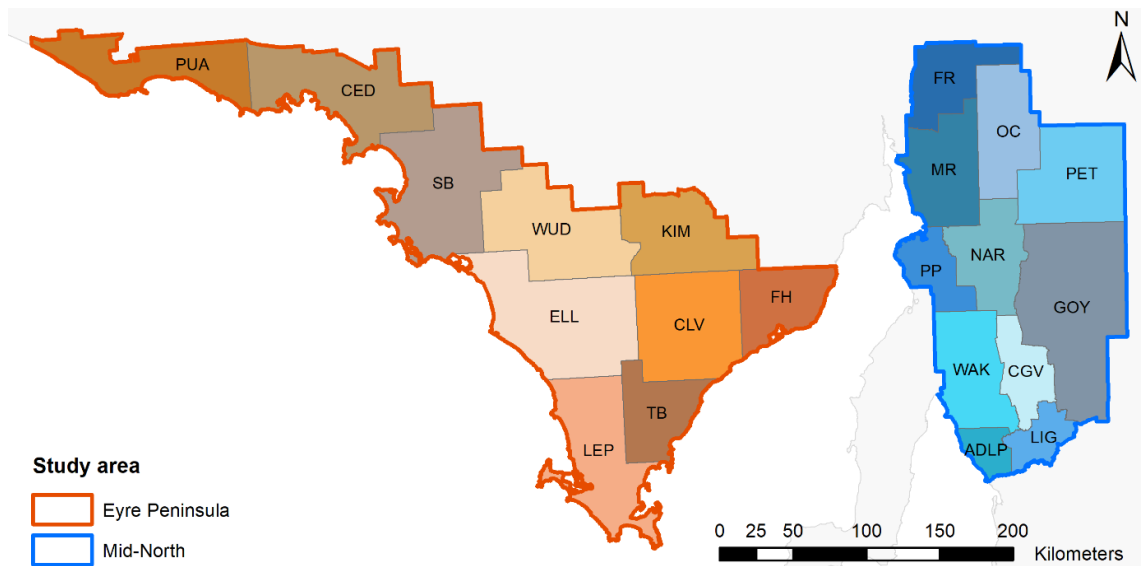


Figure 3.5 Local Government Areas (LGA) represent a combination of environmental conditions, topography, climate with slightly different rainfall patterns and diverse farming systems.

Eyre Peninsula: PUA: Pastoral Unincorporated Area; CED: Ceduna; SB: Streaky Bay; WUD: Wudinna; KIM: Kimba; ELL: Elliston; CLV: Cleve; FH: Franklin Harbour; LEP: Lower Eyre Peninsula; TB: Tumby Bay.

Mid-North: FR: Flinders Ranges; MR: Mount Remarkable; OC: Orroroo/Carrieton; PET: Peterborough; PP: Port Pirie; NAR: Northern Areas; WAK: Wakefield; CGV: Claire Gilbert Valley; GOY: Goyder Regional Council; ADLP: Adelaide Plain; LIG: Light Regional Council

3.3 Results

3.3.1 Spatial variability of wind erosion

Modelled regional wind erosion was extremely low across most of the study area ($\ll 1 \text{ t ha}^{-1} \text{ y}^{-1}$). Long term median annual erosion estimates were very similar in the Eyre Peninsula and Mid-North regions between 2001 and 2017 ($0.00258 \text{ vs } 0.00243 \text{ t ha}^{-1} \text{ y}^{-1}$ respectively). However, we identified strong inter- and intra-regional patterns (Figure 3.6). LGAs in the Eyre Peninsula region presented considerable differences in erosion susceptibility. Western LGAs (Pastoral Unincorporated Area, Ceduna, and Streaky Bay) had estimated average erosion rates between 1.2 and 1.5 times higher than the regional average (up to $0.00382 \text{ t ha}^{-1} \text{ y}^{-1}$), while the central LGAs experiences very low erosion (Elliston, Lower Eyre peninsula, Wudinna). These differences can be explained by the nature of the soils in these districts (sandy soils) and the influence of strong coastal winds on the west coast of the Eyre Peninsula. In contrast, modelled average annual soil loss

between LGAs in the Mid-North region remained relatively consistent. The Port Pirie LGA represented the most significant contribution to regional erosion with $0.00288 \text{ t ha}^{-1} \text{ y}^{-1}$.

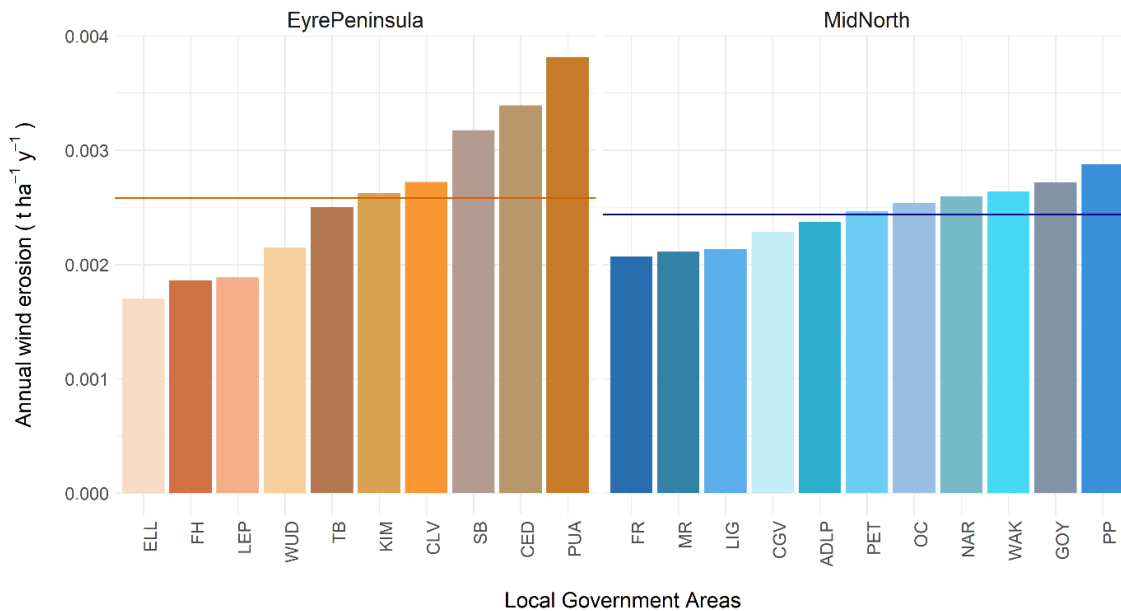


Figure 3.6 Average annual soil loss per Local Government Area. The horizontal lines represent the regional average annual soil loss (Eyre Peninsula = $0.00258 \text{ t ha}^{-1} \text{ y}^{-1}$ – Mid-North = $0.00243 \text{ t ha}^{-1} \text{ y}^{-1}$).

One of the main aims of this modelling exercise was to characterise the patterns of extreme erosion rates in space and time. Understanding the high spatio-temporal variability of factors influencing erosion is challenging for policy development and evaluation. It is also essential to evaluate if erosion trends are due to climatic (i.e. rainfall) or human changes (i.e. land-use) or their interactions (i.e. cover). As erosion rates in the region are very low, we defined the most severe monthly erosion as falling within the top percentile (99th) based on 17 years of monthly erosion records (204 layers). This threshold ($0.000945 \text{ t ha}^{-1} \text{ month}^{-1}$ or $0.945 \text{ kg ha}^{-1} \text{ month}^{-1}$) was then used to count the number of months with the most severe monthly soil loss (Figure 3.7).

The results indicate that the west coast of the Eyre Peninsula region potentially recorded severe monthly erosion between 8 and 20 months out of 204 during the study period. Parts of the Pastoral Unincorporated Area, Ceduna, and Streaky Bay LGAs were predicted to be the most severely affected 40 months out of 204. Large parts of the Cleve, Kimba and Tumby Bay LGAs also possibly experienced severe erosion with a frequency between 8

and 20 months out of 204. The most impacted areas were characterised by sandier hills and were regularly exposed to strong coastal wind gusts. On the other hand, most of the Mid-North region did not appear to be frequently impacted by intense erosion except the Port Pirie area and the Barunga Range (north-western part of the Wakefield LGA) where monthly soil loss estimates exceeded the 99th percentile threshold over 40 months out of 204. Some parts of the central ranges of the Mid-North region also experienced a higher frequency of severe erosion (8-20 months out of 204).

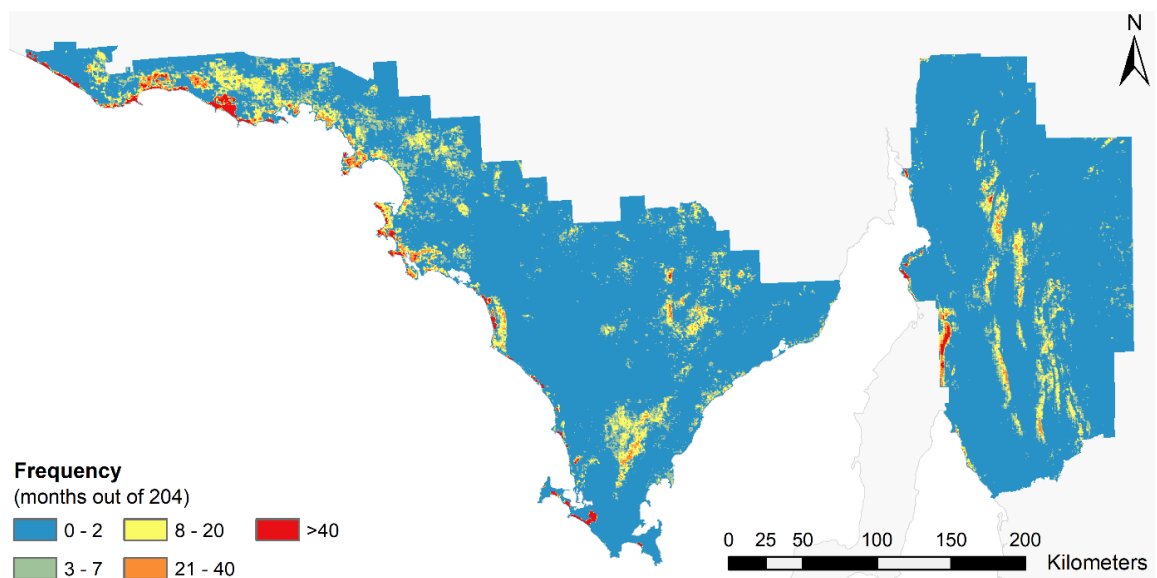


Figure 3.7 Frequency of monthly erosion rate above $0.000945 \text{ t ha}^{-1}$.

Spatial patterns of modelled soil erosion varied strongly in time (Figure 3.8). The results demonstrate that extreme monthly erosion possibly took place in the same areas over multiple years for two to three months each year and highlights the high temporal variability of extreme erosion events across the years.

Between 2001 and 2010, Southern Australia experienced a wide-spread drought (known as the 'Millennium Drought'). During this period, ground cover and soil moisture were very low, which led to an increase in soil erosion susceptibility in these regions. Here we identified that both regions possibly experienced a recurrence in extreme monthly erosion ($> 0.000945 \text{ t ha}^{-1}$) during this period, especially in 2003, 2004 and 2006. Outside of the Australian 'Millennium Drought', 2013 appeared to record the most significant proportion of severe monthly erosion, with a large part of the Eyre Peninsula

impacted by extreme erosion between 3 and 4 months out of 12. The higher recurrence in monthly erosion for these years is likely linked to a combination of sparse ground cover and extreme wind gusts (see also Figure 3.13 below).

This information is critical evidence for management actions because this high variability makes it extremely difficult to compare erosion between periods, i.e. before and after policy changes. The high temporal variability in erosion was mainly driven by extreme erosion events in some of the years within the study period; therefore, preventing the assessment of long-term erosion trend. Even though we can't assert that erosion severity increased over the modelling period, we could argue that a recurrence in compound events (e.g. extended drought and intense storms with strong wind gusts) would likely increase the risk of extreme erosion events in the future.

Although average annual erosion estimates can seem to be very low (Figure 3.9), the erosion patterns and LGAs predicted to be the most frequently impacted by extreme erosion (Figure 3.7 and 3.8) corroborated well with previous predictions of erosion severity at the continental scale (Leys et al., 2017; Leys et al., 2010; Leys et al., 2009).

The last continental-scale wind erosion assessment for the National Landcare program classified the west coast and northern parts of the Eyre Peninsula as well as the Port Pirie LGA and the Barunga Range in the Mid-North region as high and moderately high wind erosion severities (Leys et al., 2017b). This report also introduced a new indicator to assess wind erosion susceptibility with the fraction of bare ground exposed to wind (FEW). For our study area, this assessment identified that on average, between 2000 and 2010, the fraction of bare soil for the Pastoral Unincorporated Area and Ceduna LGAs was high enough (thus low surface roughness) to expose the soil to wind erosion. This information corroborates well with results from Figure 3.8, where parts of these LGAs exceeded the monthly 99th percentile threshold between 3 and 6 months out of 12. Even though the zones predicted to be the most severely impacted by erosion in the study area concur with previous reports, the “albedo” Wind Erosion Model was able to identify when and how often these areas exceeded the erosion severity threshold. This observation,

therefore, supports the utility of erosion modelling to assess the spatio-temporal variability of erosion extremes.

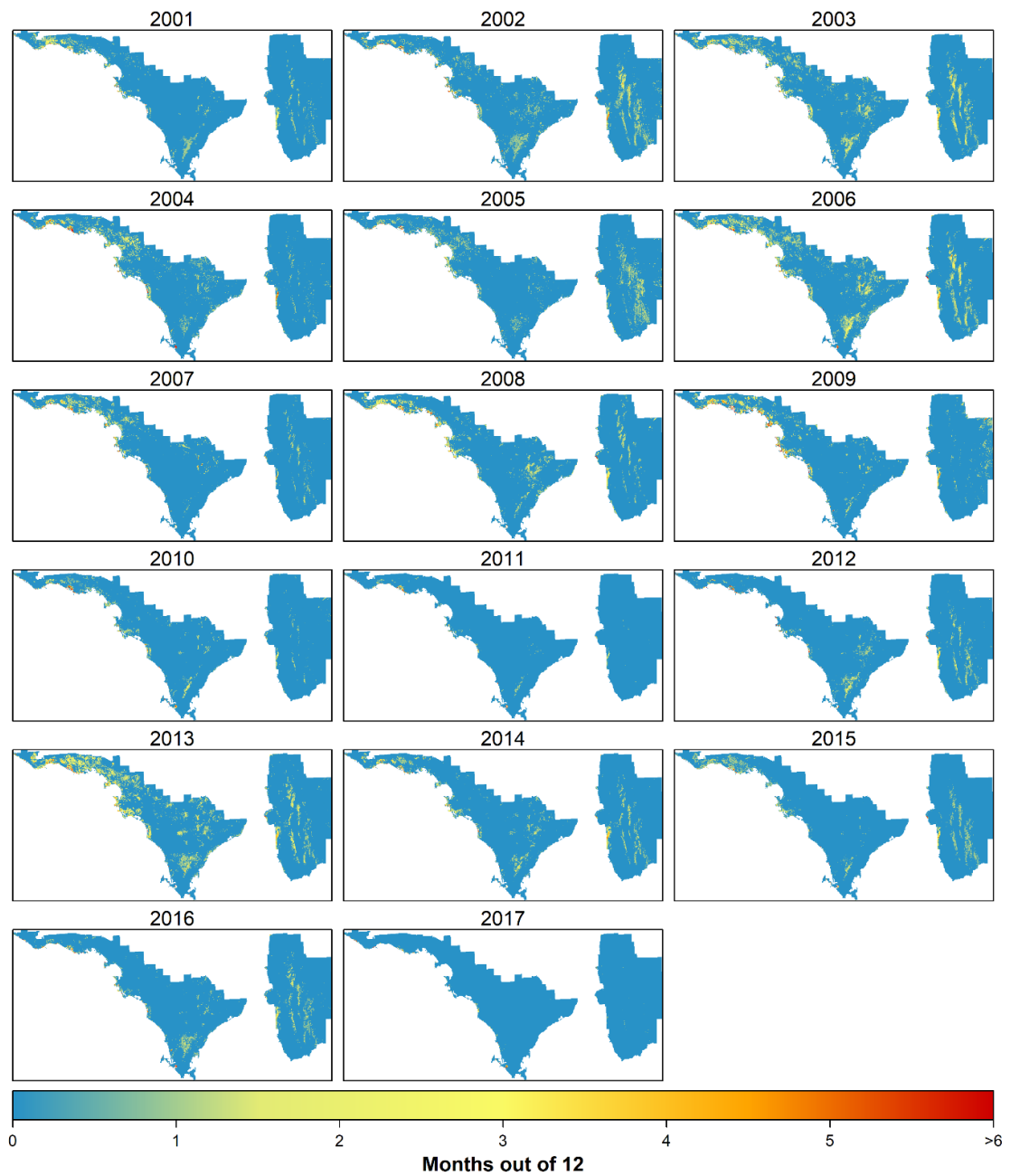


Figure 3.8 Frequency of severe monthly erosion ($> 0.000945 \text{ t ha}^{-1}$) for each year in the study period.

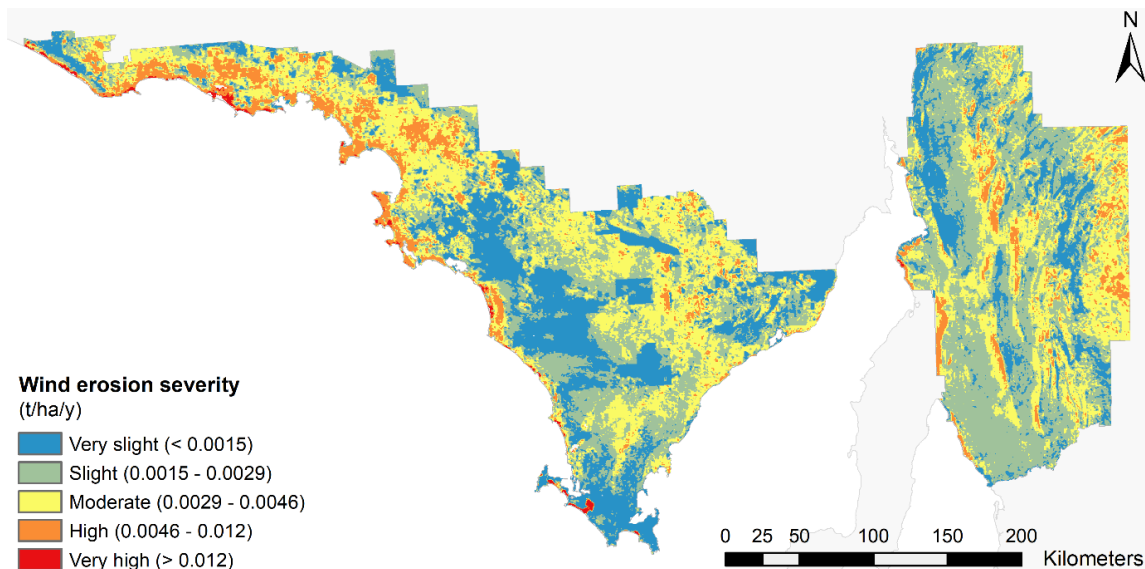


Figure 3.9 Long-term mean annual erosion rates in the Eyre Peninsula and Mid-North regions estimated from the “albedo” Wind Erosion Model.

3.3.2 Temporal variability of wind erosion

To examine the temporal variability of erosion, we extracted the monthly erosion estimates for each pixel in the time-series, then grouped them by month to generate box-plots. Each box-plot represents the distribution of monthly erosion for the two regions separately and each month of a calendar year (Figure 3.10).

We demonstrated in Section 3.3.1 that records of extreme monthly soil loss were highly variable in space throughout the study area. But the box-plots presented in Figure 3.10 indicate that monthly erosion was also highly variable through time, as shown by the variable box sizes and very long tails.

Regional averages were very comparable for the Eyre Peninsula and Mid-North regions across the seasons. Average monthly wind erosion was higher in summer (December - February), spring (October - November) and early autumn (March) for both regions with median values up to 0.0004 t ha^{-1} and recorded a lot of extreme erosion (long whiskers and presence of outliers). However, monthly erosion was more variable on the Eyre Peninsula than in the Mid-North as shown by larger boxes.

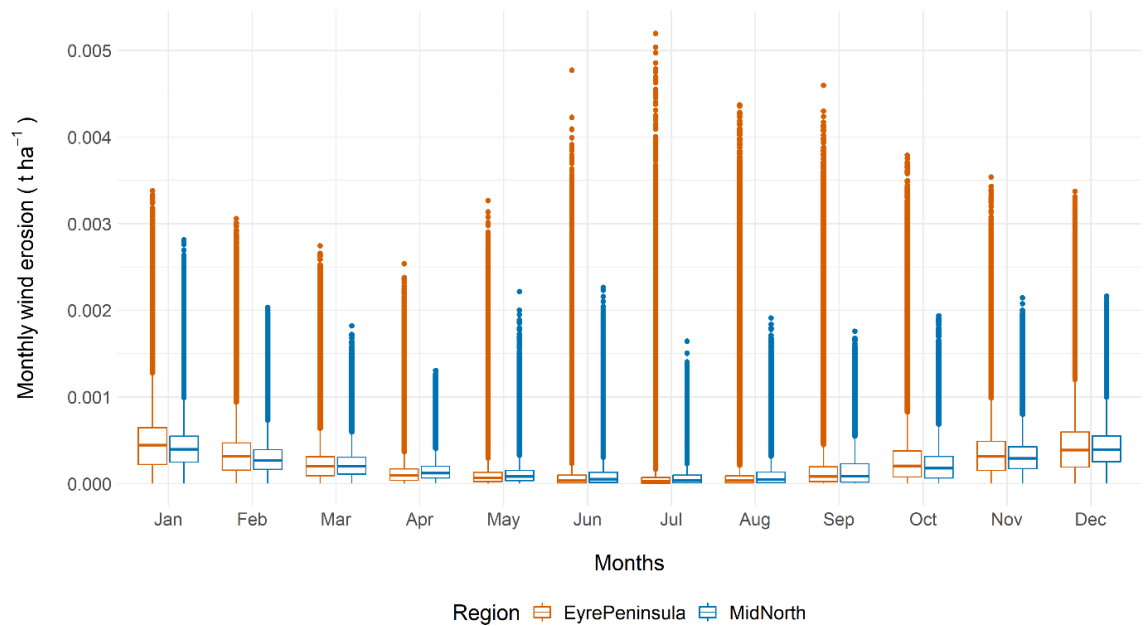


Figure 3.10 Temporal distribution of monthly erosion records. Each data point represents the monthly soil loss for a single-pixel location grouped by month. The box-plots demonstrate high inter- and intra-seasonal variability.

Although average erosion was very low in late autumn (May - June) and during winter (July - September), the variability in extreme monthly soil loss on the Eyre Peninsula was very high (as shown by the number of outliers). These skewed patterns could be explained by the fact that ground cover can become very low at the end of summer on the west coast of the Eyre Peninsula. For instance, crop stubble is often grazed by stock and used as fodder before sowing the next crop. New crops also establish later in the season in this region due to the limited or late availability of opening season rainfall.

In contrast, in the Mid-North region, the distribution of extreme monthly erosion was smaller and more uniform throughout the year, which correlated well with spatial patterns from Figure 3.8 and the fact that this region is less susceptible to wind erosion (DEW, 2017b). Nonetheless, the highest erosion rates occurred in summer (December - February) and late autumn (May - June). These patterns could be explained by a combination of very sparse ground cover (just after harvest) and higher regional wind gusts during these months. Post-harvest ground cover is in general comparable to that of the Eyre Peninsula, except that more land is sown with pulse and legume crops (e.g. peas, lentils, chickpeas). These crop types have minimal stubble quantity compared

to cereals. The ground cover would then be further reduced where land managers graze the legume stubbles, leaving susceptible soils more exposed to wind erosion.

To analyse the temporal variability of erosion between different years, we extracted the annual erosion estimates for each pixel in the time-series, then grouped them by years to generate box-plots. Each box-plot represents the distribution of annual erosion estimates for the two regions separately and each year of the study period.

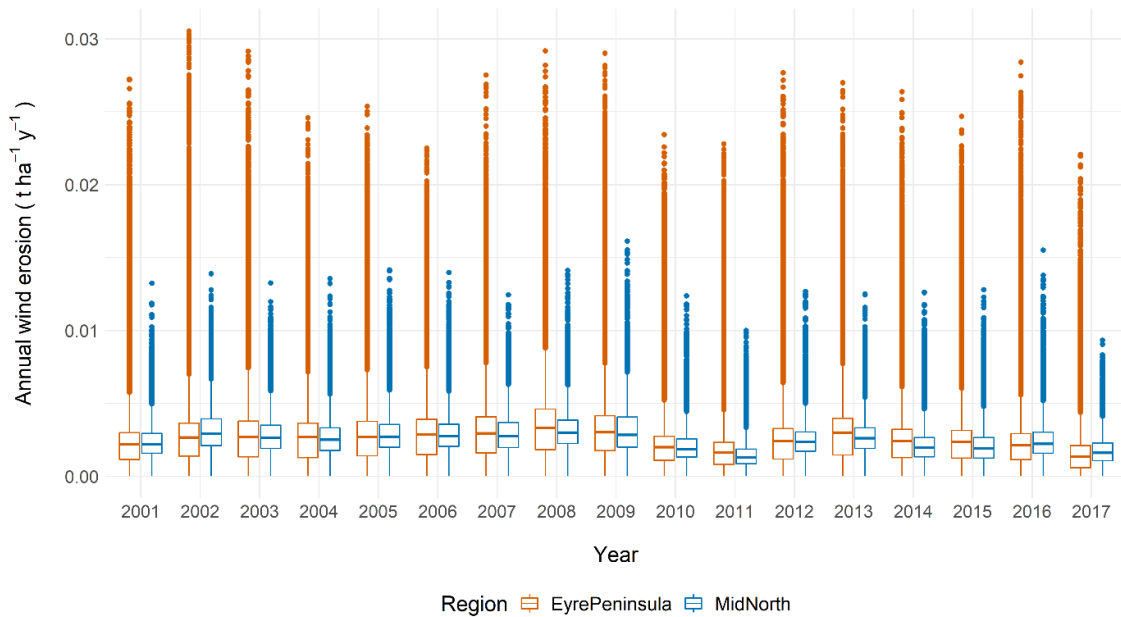


Figure 3.11 Temporal distribution of annual soil loss. Each data point represents the annual soil erosion for a single-pixel location grouped by year. The box-plots demonstrate high inter- and intra-annual variability.

The distribution of annual soil loss displayed high inter- and intra-variability across our study period (Figure 3.11). Average regional erosion was comparable between the two regions throughout the study period and was the highest during the Australian ‘Millennium Drought’ (2002-2009) (c.a. $0.003 \text{ t ha}^{-1} \text{y}^{-1}$). In contrast, lower regional soil loss was recorded in 2010 and 2011 for the two regions, which coincided with the end of the “drought”.

Even though regional erosion was comparable between the two regions, the distribution of annual soil loss was more variable on the Eyre Peninsula represented by the wider boxes. Parts of this region also experienced a greater recurrence in extreme annual soil loss (i.e. large number of outliers). This observation supports the argument that the two

regions responded differently to extreme environmental conditions, and highlights the inter- and intra-regional differences between the two areas.

3.3.3 Wind erosion influencing factors

Horizontal sediment flux and wind erosion are driven by soil type, surface roughness and wind velocity. Understanding the influence of ground cover in the regional context is critical for soil conservation as this is partly within the control management through land-use policy such as incentives for land use or the support of conservation tillage. However, while policy or incentives play a key role, the adoption of improved management practices by land managers is more important (i.e. practices such as no-till seeding, stubble retention, grazing management, maintaining windbreaks, revegetation/vegetation management). This also extends to adapting management techniques to suit changing seasonal variation and other conditions from year to year. In light of this, it is thus essential to know how combinations of ground cover and wind velocities influence extreme erosion events so that land managers can make informed decisions in the future.

The spatio-temporal model allowed us to produce a regional fingerprint of environmental conditions and the resulting soil erosion. Here we visually compared the joint frequency distribution of raster stack pixels falling into daily wind speed and ground cover percentiles. In order to compare regions with different sizes, we presented the proportion of the total number of records, or in other words the number of pixels falling into each of the 100x100 percentile combinations as a fraction of the total number of raster stack pixels; 1,162,542,027 and 841,425,051 records for the Eyre Peninsula and Mid-North, respectively (Figure 3.12). To describe the environmental conditions leading to extreme daily events, we repeated the process but only selected records falling within the 99th percentile of daily erosion ($6.19 \times 10^{-5} \text{ t ha}^{-1} \text{ day}^{-1}$ or $61.9 \text{ g ha}^{-1} \text{ day}^{-1}$) (Figure 3.13).

Environmental conditions leading to erosion were very different between the two regions and throughout the study period (Figure 3.12a and b). On the Eyre Peninsula, daily

erosion events occurred with a combination of medium to high ground cover with a wide range of wind speed classes as represented by the higher density of daily erosion records in these categories (Figure 3.12a). These conditions concur with regional observations and conclusions from the latest National Landcare Program report (Leys et al., 2017). This report mentioned that wind erosion was wide-spread in the region and was threatening the long-term viability of agricultural businesses and reducing the ecosystem services of clean air. Results from Figure 3.12a also highlight that daily erosion on the Eyre Peninsula can occur under any combination of ground cover and wind velocity, which makes it even more relevant to land managers. This observation could also be related to the nature of the soils in this region. Indeed, a large proportion of the soils on the Eyre Peninsula are sandier soil types (Figure 3.3), which are more susceptible to wind erosion.

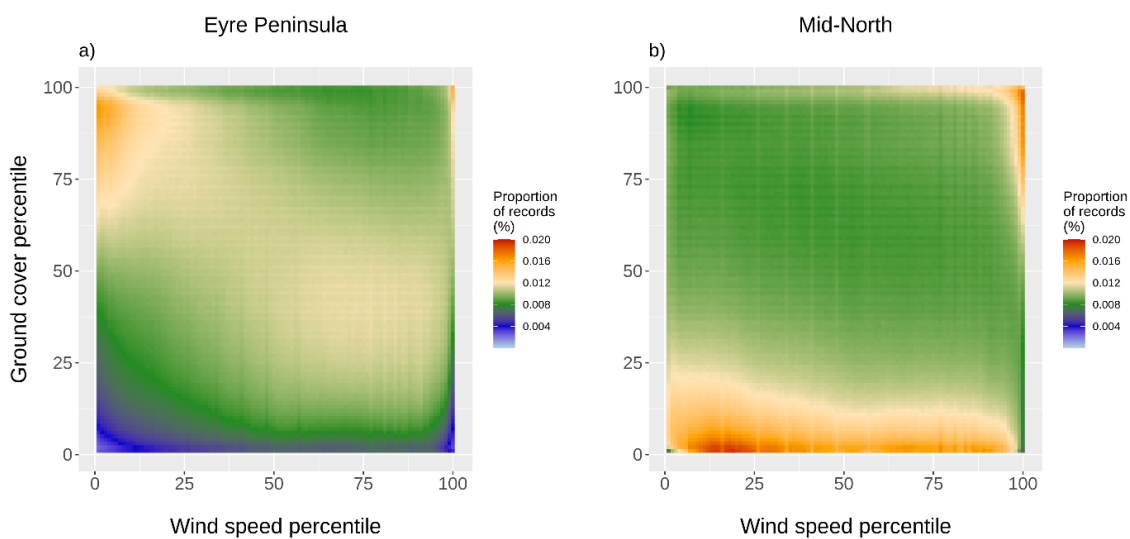


Figure 3.12 Effect of wind speed and ground cover on daily soil erosion for the Eyre Peninsula and the Mid-North regions. The figure displays the proportion of daily erosion records (pixels) within each combination of wind speed and ground cover percentile classes for the entire space-time array (17 years of daily erosion records). These diagrams demonstrate that environmental conditions leading to erosion were very different for the two regions.

In contrast, daily erosion events in the Mid-North region mainly occurred with a combination of low to medium ground cover and a broad range of wind velocity classes (Figure 3.12b). However, local observations and the National Landcare Program report specified that erosion events were very localised and of very low intensity throughout the

region. They also report that the fraction of bare ground exposed to wind was low to moderate across most of the area, therefore limiting the risk of wind erosion.

Although regional environmental conditions leading to erosion were very different, both regions displayed a similar distribution of extreme daily erosion ($> 61.9 \text{ g ha}^{-1} \text{ day}^{-1}$). These severe daily erosive events consistently occurred with a combination of strong wind speed (100th percentile: 19 to 41 m s^{-1} or 68 to 148 km h^{-1}) and low to moderate ground cover (0-10th percentile: 0 to 51.5% ground cover) (Figure 3.13a and b). These observations concur with published literature and highlight the influence of ground cover and wind velocity on extreme soil losses within our two regions of interest.

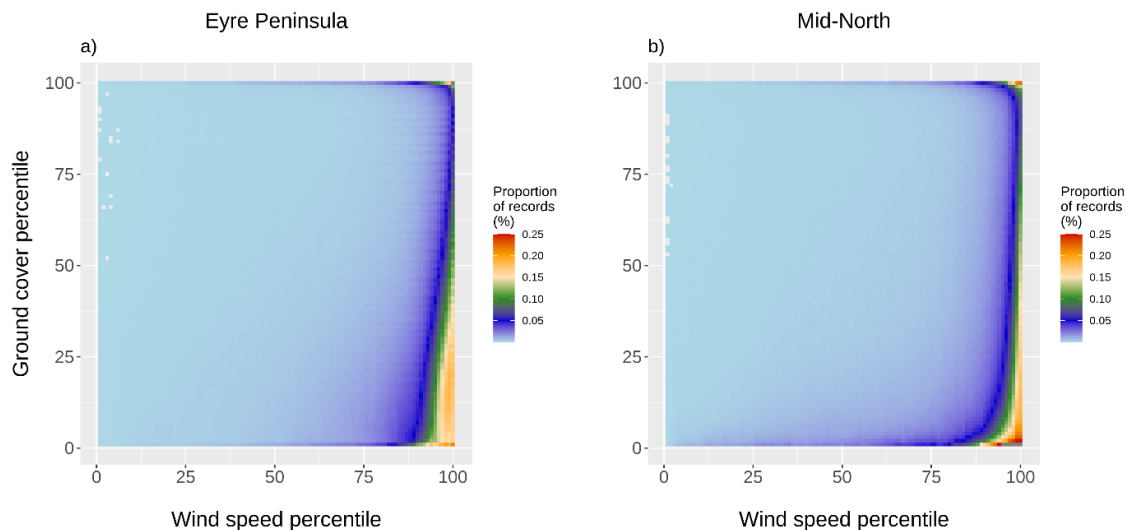


Figure 3.13 Effect of wind speed and ground cover on daily soil erosion for the Eyre Peninsula and the Mid-North regions. The figure displays the proportion of daily erosion records (pixels) within each combination of wind speed and ground cover percentile classes when selecting the most severe of daily erosion rates ($> 61.9 \text{ g ha}^{-1} \text{ day}^{-1}$). These diagrams demonstrate that that high erosion events consistently occurred at high wind speed with a large range of ground cover levels.

Our results can be significant for land managers as we described the environmental conditions leading to extreme erosive events in the Mid-north and Eyre Peninsula regions. As supported by previous studies, maintaining adequate ground cover is paramount to limit wind erosion and reduce wind velocity (Leys et al., 2017). Even sparse vegetation or crop stubble can act as a windbreak and mitigate the impact of wind erosion on adjacent bare or overgrazed paddocks (Jeanneau et al., 2019). Here we proposed new targets for ground cover management to improve preventive erosion control in dryland

agricultural regions. Land managers should then aim to maintain a ground cover over 50% to limit the risk of erosion with extreme weather events. It might not be practical to meet this target every year when environmental conditions are not optimal for crops growth or if a wildfire rages through the region, but it can often be recovered the following year. However, land managers would have little control over ground cover management when experiencing two or more successive seasons with well below average rainfall, as we have seen during the Australian 'Millennium Drought'. With the impact of a changing climate, farmers are likely to be exposed to a higher recurrence in low-yielding years, which would lead to a higher frequency of erosion risk.

3.3.4 Wind erosion and land use

Agriculture was the dominant land-use type in both regions representing 60% and 88% of the surface of the Eyre Peninsula and the Mid-North respectively (Figure 3.2). On the Eyre Peninsula, agricultural land-uses (i.e. cropping, modified pastures and livestock grazing) represented 73% of the total regional annual contribution ($0.007 \text{ t ha}^{-1} \text{ y}^{-1}$) (Figure 3.14). Dryland cropping had the highest contribution to total regional erosion ($0.0034 \text{ t ha}^{-1} \text{ y}^{-1}$), followed by modified pastures ($0.0026 \text{ t ha}^{-1} \text{ y}^{-1}$). The other agricultural land uses and natural environments did not significantly contribute to regional wind erosion.

Agricultural land uses also contributed significantly to total annual erosion with 92% in the Mid-North region ($0.008 \text{ t ha}^{-1} \text{ y}^{-1}$) (Figure 3.14). Livestock grazing and dryland cropping represented the principal contribution to the annual regional erosion with 0.003 and $0.0028 \text{ t ha}^{-1} \text{ y}^{-1}$ respectively, followed by modified pastures ($0.0023 \text{ t ha}^{-1} \text{ y}^{-1}$). Natural land uses in the Mid-North region had a small contribution to total regional erosion ($< 0.0008 \text{ t ha}^{-1} \text{ y}^{-1}$).

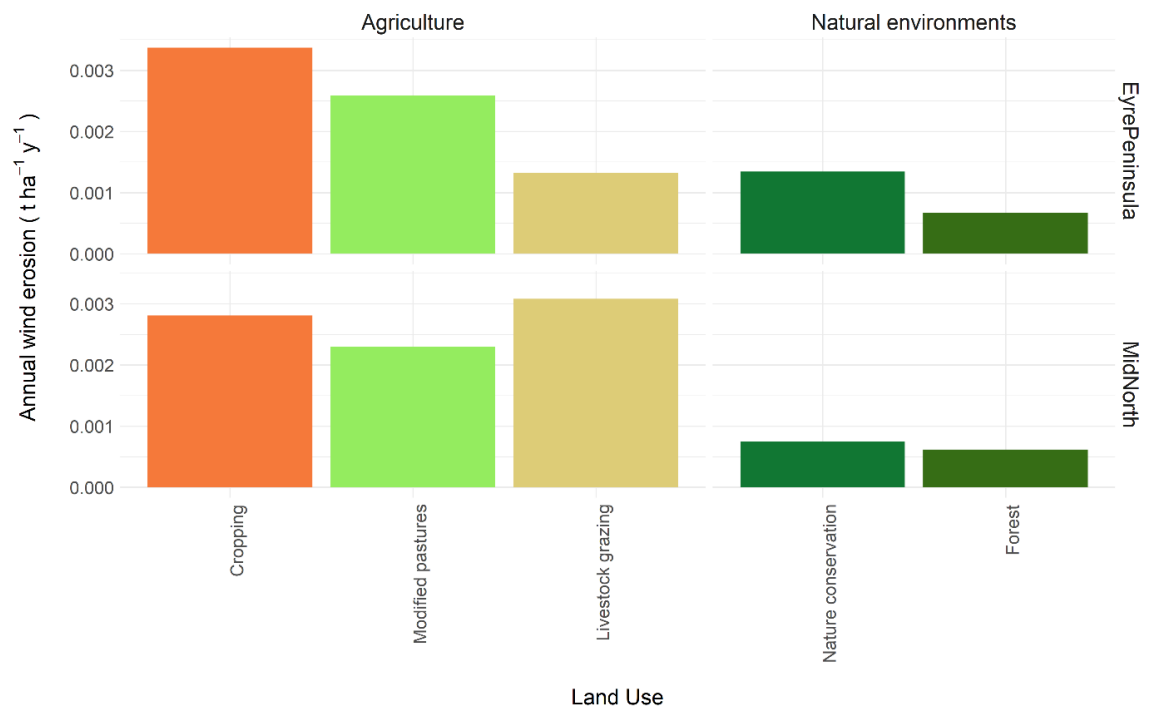


Figure 3.14 Long-term average annual wind erosion for the major agricultural land uses compared with natural environments.

3.4 Discussion

3.4.1 Comparison of the wind erosion model with the frequency of dust storms

We were not able to directly compare our wind erosion estimates with quantitative measurements as there were no recent ground-based observations for wind erosion in the Eyre Peninsula and Mid-North regions. Therefore, we produced a map of mean annual frequency of dust storms (Figure 3.15) from MODIS MAIAC daily gridded data to evaluate the credibility of our wind erosion severity maps (Figure 3.9) and locate potential dust sources in the two regions of interest. We produced an error matrix (Table 3.1), based on an overlay analysis between Figure 3.9 and Figure 3.15, to compare the agreement between the “albedo” Wind Erosion Model and the frequency of dust storms. Each element in Table 3.1 represents the number of observations (pixels) within each class intersection divided by the total number of pixels and expressed as a percentage. The overall accuracy was then estimated by the sum of the diagonal elements.

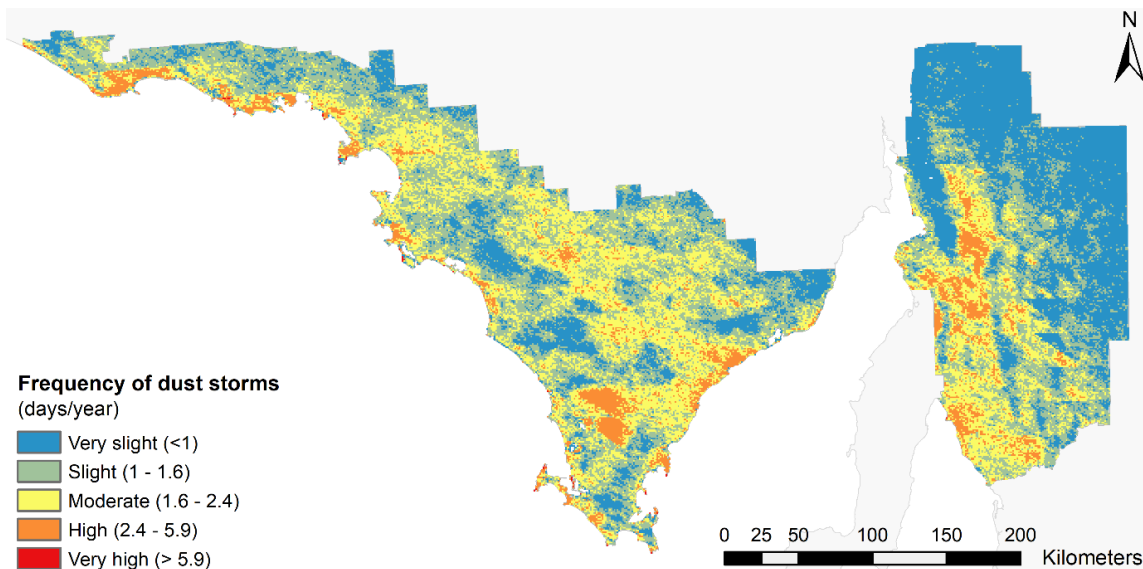


Figure 3.15 Mean annual frequency of dust storms for the Eyre Peninsula and Mid-North regions derived from the MODIS MAIAC daily Aerosol Optical Depth (AOD) product (AOD > 0.3).

Table 3.1 Error matrix comparing the agreement (overlapping area in %, values in bold denote agreement) between wind erosion severity classes from the “albedo” Wind Erosion Model and the mean annual frequency of dust storms derived from the MODIS MAIAC daily Aerosol Optical Depth (AOD) product (AOD > 0.3).

Wind erosion model	Frequency of dust storms				
	Very slight	Slight	Moderate	High	Very high
Very slight	10.1	8.8	2.6	0.3	0.0
Slight	9.7	13.4	12.1	2.9	0.0
Moderate	7.3	11.2	10.7	2.6	0.0
High	1.7	2.7	2.7	1.2	0.0
Very high	0.0	0.1	0.1	0.1	0
Overall accuracy	35.4%				

If we assume that the classification of the wind erosion severity and the frequency of dust storm maps were comparable, then the overall accuracy of the model was 35.4%, which is very low. However, if we assume that a one-class difference is acceptable because the classes were not defined on a nominal scale but an ordinal-scale (Vrieling et al., 2006), then the accuracy of the wind erosion model increases to 82.6% which is reasonably satisfactory (Figure 3.16). The results from Figure 3.16 correlated well with historical data and local observations as well as wind erosion susceptibility maps produced by the South Australian Government (DEW, 2017b). This validation attempt is quite unique and

proved that we could be confident in the erosion severity patterns predicted by the “albedo” Wind Erosion Model.

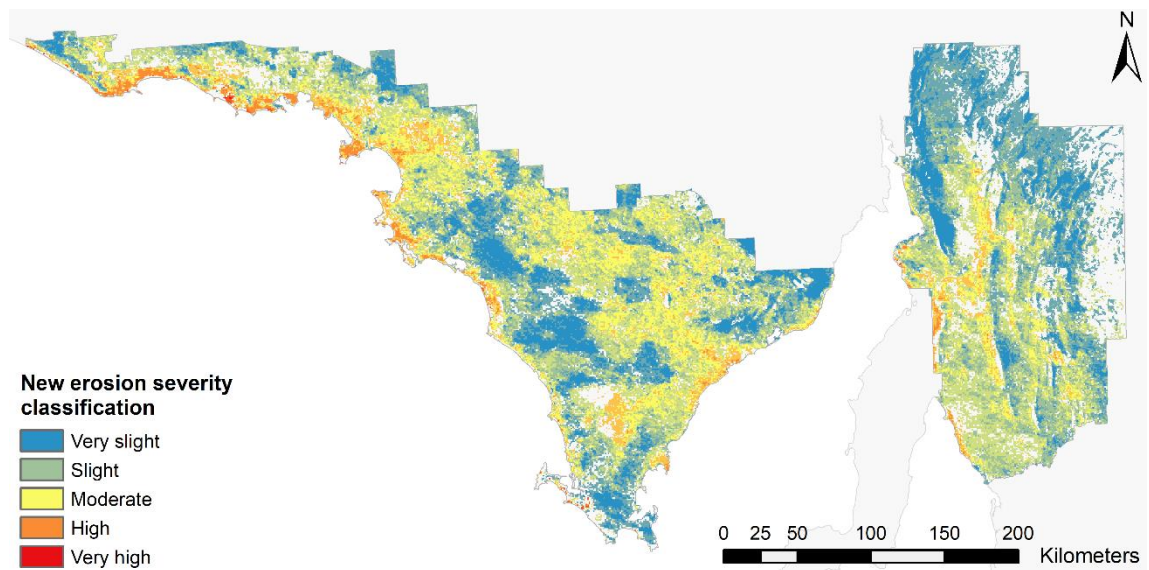


Figure 3.16 New erosion severity map corrected with MODIS MAIAC daily Aerosol Optical Depth (AOD) dataset. Note that the areas in grey represent zones where the classification of the AOD did not overlap with the “albedo” Wind Erosion Model.

3.4.2 The model’s response

Our modelling exercise aimed to identify the relative spatio-temporal variability of extreme erosion events for land management and demonstrated that the “albedo” Wind Erosion Model was well suited for the task. However, the wind erosion severity was probably misclassified in some parts of the study area, especially in the central ranges and eastern parts of the Mid-North, and the central part of the Eyre Peninsula as shown by the empty pixels in Figure 3.16. This misclassification could be correlated with the way we estimated the bare soil threshold friction velocity (u_{*ts}). To estimate this parameter, we relied on information about the soil particle diameter (D), which was not available at a regional scale in our study area due to the lack of field measurements. We drew on the experience from previous modelling approaches (Chappell and Webb, 2016; Chappell et al., 2019) to derive this information and used the Soil and Landscape Grid of Australia (SLGA) digital soil dataset. We estimated the ideal threshold friction velocity from the fraction of sand, silt and clay in the topmost soil layer and their relative particle

size diameter (clay < 2 μ m, silt < 50 μ m, sand < 2000 μ m). We also applied a correction to the soil texture fractions with the coarse fragment content (> 2000 μ m) to prevent the misclassification of non-erodible soil fractions (denser soils and rocky outcrops). This correction significantly improved our predictions; however, some foothills in the Mid-North region were still considered as potentially erodible when local observations did not concur with these results. Even though our approach could lead to potential misclassification or overestimation of erosion in some parts of the study area, Chappell and Webb (2016) demonstrated that modifying the soil particle size D (between 50 and 500 μ m) did not result in significant changes in predicted erosion patterns.

The moderate resolution of the model (500m) might not reflect the diversity of land-uses and vegetation cover classes present within a single MODIS pixel and the albedo parameters might not be able to assimilate this complex landscape. South Australian authorities currently recommend that standing crop residue is probably more important than ground cover for controlling wind erosion in this region. Jeanneau et al. (2019) demonstrated that even shallow vegetation (crop stubble) could protect adjacent burnt or bare paddocks against wind erosion. Although the “albedo” Wind Erosion Model takes into account vegetation height, it might not entirely capture the structure of crop residues anchored in the soil. This information is critical and might have led to misclassification of local erosion severity as well, especially in the Mid-North region where the agricultural landscape is more fragmented (Figure 3.2). However, this study intended to characterise erosion patterns at a regional scale and was not designed to identify wind erosion severity at the field scale.

The “albedo” Wind Erosion Model managed to capture regional variability and enabled the identification of regions the most frequently impacted by erosion in the study area. Overall, spatial patterns of erosion severity compared well with previous modelling approaches (DEW, 2017b; Leys et al., 2017a) and underpin the value of erosion models to assess spatial differences and evaluate corrective measures. However, our results were

untested against erosion measurements, making it difficult to set absolute quantitative soil loss targets for land management.

3.4.3 Assessing the temporal variability in erosion

The selection of reference periods for baseline studies is critical to evaluate long-term trends in soil erosion and should be selected carefully. It is very easy to skew analysis if a one-in-50-years dust storm rages through a region of interest during the study period and drives extreme erosion rates. Therefore, any trends observed in this case would not be representative of the long-term distribution of erosion in this region. Here we conducted our study with the best spatio-temporal datasets currently available, but we could only access 17 years of reliable data. For this reason, our work focussed on assessing the frequency and recurrence of severe monthly erosion records to identify the spatio-temporal variability of erosion extremes in agricultural zones of South Australia for the reference period 2001-2017. The “albedo” Wind Erosion Model efficiently captured this variability, thus proving the value of erosion modelling for the assessment of regional erosion severity through time. Some of the years in our archive could then be used as a surrogate to test different climate change scenario for future land management.

Even though our modelling period included the Australian ‘Millennium Drought’ (2001-2010) and very wet years (2016, 2015), we couldn’t reliably assess long-term trends in erosion severity for the Eyre Peninsula and Mid-North regions. Further work should be implemented in the future when the archives will contain 30 to 50 years of spatio-temporal data to estimate relative trends in erosion for the agricultural zone of South Australia.

3.4.4 Regional land management

The large spatial and temporal variability observed between the Local Government Areas (LGAs) of the Eyre Peninsula and Mid-North regions demonstrated the difficulty to set absolute Federal or State-based land management targets. As each State is characterised

by a wide range of landscapes, environmental conditions and erosion susceptibility, land management targets need to be tailored to each Local Government Area or district individually and be adapted to the capacity of each locality.

We also identified that ground cover and wind velocity had a strong influence on erosion regardless of the region. Intense wind gusts ($> 19 \text{ m s}^{-1}$, c.a. 68 km h^{-1}) dramatically increased erosion severity with a ground cover below 50%, but management practices could potentially influence ground cover protection. For this reason, land managers need to be conscious of the zones the most susceptible to erosion in their region to leave room for improvement and support conservation practices. Therefore, our results and the wind erosion severity map (Figure 3.9) could serve as a guide to inform land managers about potential erosion severity under a range of environmental conditions. Other stakeholders involved with policies and programs relating to sustainable agricultural land management and land use planning (e.g. the agricultural industry, local and state governments, and research organisations) could also use these results to inform strategic changes and future decisions in regards to erosion management.

Since the early 2000s, the Eyre Peninsula and Mid-North regions have recorded an overall reduction of erosion risk (from 85 days to 25 days at risk per year) with the adoption of conservation tillage (Young and Herrmann, 2015). This effort has dramatically reduced the number of observed dust events and rill erosion (DEW, 2017a; Hancock et al., 2015; Young and Herrmann, 2015). However, even with the best management practices, land managers might have little ability to prevent erosion with a recurrence in extreme events such as extended droughts, wildfires or extreme precipitation events. Nonetheless, farming systems and land management options such as greater use of perennial plants (including pasture species, fodder shrubs and trees) could help to mitigate erosion risk with increasing dry seasonal conditions in lower rainfall areas.

Low rainfall regions are highly sensitive to future climate change. Current climate models for Australia predict less reliable rainfall but more intense rainfall events; hotter and

extended periods of heatwaves; more frequent droughts; and increased risks of fire events (Bardsley, 2006; CSIRO & BoM, 2015). All these climatic variables are directly influencing soil erosion. Compound events such as extended drought periods and extreme wind gusts are likely to increase soil losses (Leys et al., 2018). During a prolonged drought period, soil moisture which is the primary water source available for plants and contributes to soil aggregate stability will be very limited. As a result, biomass production will become more variable and is likely to decline. Lower production will lead to less protective cover and reduced soil stability; therefore, soils will be more exposed to erosion with the next intense storm event.

Our results showed that a combination of extended droughts, thus very low ground cover, and extreme wind gusts ($> 68 \text{ km h}^{-1}$) led to a sharp increase in daily, monthly and annual soil loss during the Australian 'Millennium Drought' across a large proportion of the Eyre Peninsula and in coastal areas in the Mid-North region. Therefore, maintaining a reasonable ground cover in the future will become paramount to prevent extreme erosional events.

3.5 Conclusion

This study demonstrated that erosion models could be used to inform corrective measures for future land management and provides a valuable tool for assessing the spatio-temporal variability of wind erosion. Here, we adapted a state-of-the-art wind erosion model ("albedo" Wind Erosion Model) to integrate modern high-resolution datasets for spatial and temporal analysis of erosion. This study characterised spatial patterns of erosion severity at a regional scale by identifying when and how often extreme erosion events occurred between 2001 and 2017 in the Eyre Peninsula and Mid-North agricultural zones of South Australia. We also described the influence of wind velocity and ground cover on extreme daily erosion events and differentiated erosion figures for a range of land-uses in the study area.

Average regional erosion was comparable between the Eyre Peninsula and Mid-North regions (0.00258 and 0.00243 t ha⁻¹ y⁻¹ respectively). However, most of the west coast of the Eyre Peninsula frequently experienced severe erosion (above 0.000945 t ha⁻¹ month⁻¹ or 0.945 kg ha⁻¹ month⁻¹). The high erosion severity was primarily driven by the soil type (sandy soils), recurring low ground cover and extreme wind gusts.

We identified that average monthly wind erosion was the highest in summer (December - February), spring (October - November) and early autumn (March) for both regions with median values up to 0.0004 t ha⁻¹ month⁻¹. Although average erosion was very low in late autumn (May - June) and during winter (July - September), the variability in extreme monthly soil loss on the Eyre Peninsula was very high. Average regional annual erosion was also comparable between the two regions throughout the study period and was the highest during the Australian 'Millennium Drought' (2002-2009) (c.a. 0.003 t ha⁻¹ y⁻¹).

Overall, agricultural land-uses produced higher erosion rates than natural environments and contributed to c.a. 40% of the total annual regional contributions for both regions (EP: 0.007 t ha⁻¹ y⁻¹; MidN: 0.008 t ha⁻¹ y⁻¹). We identified that ground cover was a critical controlling factor to limit the impact of wind velocity on erosion. Severe daily erosive events consistently occurred with a combination of strong wind gusts (100th percentile: 19 to 41 m s⁻¹ or 68 to 148 km h⁻¹) and low to moderate ground cover (0-10th percentile: 0 to 52% ground cover). As a result, land management actions could be taken to maintain a reasonable ground cover all year round (e.g. conservation agriculture and no-tillage), most particularly for the dryland cropping or grazing pasture sector.

To the best of our knowledge, this study is the first one to examine the relative assessment of wind erosion frequency for the agricultural zone of Southern Australia. It provides valuable insight regarding erosion severity for the management of natural and dryland agricultural environments. Our results can now be used to set land management targets tailored to specific Local Government Areas of South Australia.

Although the focus of this study was on the Eyre Peninsula and Mid-North agricultural regions, the model could be extended to the rest of the State or across all the Australian agricultural zone, given sufficient computing power. The input data can be downloaded through open access platforms Australia-wide (Table A.1), and similar datasets are available globally.

3.6 References

- ABARES, 2016. The Australian Land Use and Management Classification Version 8. Australian Bureau of Agricultural and Resource Economics and Sciences (ABARES), http://data.daff.gov.au/anrdl/metadata_files/pe_alumc9aal20161017.xml?convertrlinks=0
- ABARES, 2018. Catchment scale land use of Australia - Commodities - Version 2. Australian Bureau of Agricultural and Resource Economics and Sciences (ABARES), <https://www.agriculture.gov.au/abares/aclump/land-use/catchment-scale-land-use-of-australia-commodities-update-december-2018>
- Baddock, M.C., Strong, C.L., Leys, J.F., Heidenreich, S.K., Tews, E.K., McTainsh, G.H., 2014. A visibility and total suspended dust relationship. *Atmospheric Environment* 89, 329-336, doi: <https://doi.org/10.1016/j.atmosenv.2014.02.038>.
- Bardsley, D.K., Sweeny, S., Rogers, G., 2008. A regional climate change decision framework for natural resource management. Department of Water, Land and Biodiversity Conservation,
- Baumhardt, R.L., Stewart, B.A., Sainju, U.M., 2015. North American Soil Degradation: Processes, Practices, and Mitigating Strategies. *Sustainability* 7, 2936-2960, doi: <https://doi.org/10.3390/su7032936>.
- Bennell, M.R., Leys, J.F., Cleugh, H.A., 2007. Sandblasting damage of narrow-leaf lupin (*Lupinus angustifolius* L.): a field wind tunnel simulation. *Soil Research* 45, 119-128, doi: <https://doi.org/10.1071/SR06066>.
- BoM, 2016a. Average annual, seasonal and monthly rainfall. Bureau of Meteorology, http://www.bom.gov.au/jsp/ncc/climate_averages/rainfall/index.jsp?period=an&area=sa#maps
- BoM, 2016b. Decadal and multi-decadal temperature. Bureau of Meteorology, http://www.bom.gov.au/jsp/ncc/climate_averages/decadal-temperature/index.jsp?maptype=6&period=7605&product=max#maps

- Busetto, L., Ranghetti, L., 2016. MODISstp: An R package for automatic preprocessing of MODIS Land Products time series. *Computers & Geosciences* 97, 40-48, doi: <https://doi.org/10.1016/j.cageo.2016.08.020>.
- Chappell, A., Van Pelt, S., Zobeck, T., Dong, Z., 2010. Estimating aerodynamic resistance of rough surfaces using angular reflectance. *Remote Sensing of Environment* 114, 1462-1470, doi: <https://doi.org/10.1016/j.rse.2010.01.025>.
- Chappell, A., Webb, N., 2016. Using albedo to reform wind erosion modelling, mapping and monitoring. *Aeolian Research* 23, 63-78, doi: <https://doi.org/10.1016/j.aeolia.2016.09.006>.
- Chappell, A., Webb, N.P., Guerschman, J.P., Thomas, D.T., Mata, G., Handcock, R.N., Leys, J.F., Butler, H.J., 2018. Improving ground cover monitoring for wind erosion assessment using MODIS BRDF parameters. *Remote Sensing of Environment* 204, 756-768, doi: <https://doi.org/10.1016/j.rse.2017.09.026>.
- Chappell, A., Webb, N.P., Leys, J.F., Waters, C.M., Orgill, S., Eyres, M.J., 2019. Minimising soil organic carbon erosion by wind is critical for land degradation neutrality. *Environmental Science & Policy* 93, 43-52, doi: <https://doi.org/10.1016/j.envsci.2018.12.020>.
- Chudnovsky, A.A., Koutrakis, P., Kloog, I., Melly, S., Nordio, F., Lyapustin, A., Wang, Y.J., Schwartz, J., 2014. Fine particulate matter predictions using high resolution Aerosol Optical Depth (AOD) retrievals. *Atmospheric Environment* 89, 189-198, doi: <https://doi.org/10.1016/j.atmosenv.2014.02.019>.
- Cornelis, W.M., Gabriels, D., 2005. Optimal windbreak design for wind-erosion control. *Journal of Arid Environments* 61, 315-332, doi: <https://doi.org/10.1016/j.jaridenv.2004.10.005>.
- CSIRO, 2017. Global Rangelands Monitoring, <https://www.csiro.au/en/Research/LWF/Areas/Landscapes/Earth-observation/RAPP-Map-GEOGLAM>
- Darmenova, K., Sokolik, I.N., Shao, Y., Marticorena, B., Bergametti, G., 2009. Development of a physically based dust emission module within the Weather Research and Forecasting (WRF) model: Assessment of dust emission parameterizations and input parameters for source regions in Central and East Asia. *Journal of Geophysical Research: Atmospheres* 114, doi: <https://doi.org/10.1029/2008JD011236>.
- DEW, 2016. Surface Soil Texture. Government of South Australia, Department for Environment and Water, <https://data.sa.gov.au/data/dataset/3ee7c63d-cae6-4076-a394-4db4a158e740>
- DEW, 2017a. Soil protection from erosion. Government of South Australia, Department for Environment and Water,

https://www.environment.sa.gov.au/Knowledge_Bank/Science_research/land-condition-sustainable-management/soil-protection-from-erosion

- DEW, 2017b. Soil Wind Erosion Potential. Government of South Australia, Department for Environment and Water, <https://data.sa.gov.au/data/dataset/wind-erosion-grid>
- Earl, N., Remenyi, T., Love, P., Harris, R., Rollins, D., Bindoff, N., 2019. Invited paper: Compound rainfall events in Tasmania, MODSIM2019, 23rd International Congress on Modelling and Simulation. Modelling and Simulation Society of Australia and New Zealand,, Canberra, Australia,
- FAO, 2011. The state of the world's land and water resources for food and agriculture (SOLAW) - Managing systems at risk. Food and Agriculture Organization of the United Nations, Rome and Earthscan, London,
- FAO, 2017. Voluntary Guidelines for Sustainable Soil Management. Food and Agriculture Organization of the United Nations, Rome, Italy,
- Fecan, F., Marticorena, B., Bergametti, G., 1999. Parametrization of the increase of the aeolian erosion threshold wind friction velocity due to soil moisture for arid and semi-arid areas. *Annales Geophysicae-Atmospheres Hydrospheres and Space Sciences* 17, 149-157, doi: <https://doi.org/10.1007/s005850050744>.
- Fenta, A.A., Tsunekawa, A., Haregeweyn, N., Poesen, J., Tsubo, M., Borrelli, P., Panagos, P., Vanmaercke, M., Broeckx, J., Yasuda, H., Kawai, T., Kurosaki, Y., 2020. Land susceptibility to water and wind erosion risks in the East Africa region. *Science of The Total Environment* 703, 135016, doi: <https://doi.org/10.1016/j.scitotenv.2019.135016>.
- Fryrear, D.W., Bilbro, J.D., Saleh, A., Schomberg, H., Stout, J.E., Zobeck, T.M., 2000. RWEQ: Improved wind erosion technology. *Journal of Soil and Water Conservation* 55, 183-189, <http://www.jswconline.org/content/55/2/183.abstract>
- Ginoux, P., Garbuzov, D., Hsu, N.C., 2010. Identification of anthropogenic and natural dust sources using Moderate Resolution Imaging Spectroradiometer (MODIS) Deep Blue level 2 data. *Journal of Geophysical Research: Atmospheres* 115, doi: <https://doi.org/10.1029/2009jd012398>.
- Guerschman, J.P., Scarth, P.F., McVicar, T.R., Renzullo, L.J., Malthus, T.J., Stewart, J.B., Rickards, J.E., Trevithick, R., 2015. Assessing the effects of site heterogeneity and soil properties when unmixing photosynthetic vegetation, non-photosynthetic vegetation and bare soil fractions from Landsat and MODIS data. *Remote Sensing of Environment* 161, 12-26, doi: <https://doi.org/10.1016/j.rse.2015.01.021>.
- Hagen, L., 1991. A wind erosion prediction system to meet user needs. *Journal of Soil and Water Conservation* 46, 106-111,

- Hancock, G.R., Wells, T., Martinez, C., Dever, C., 2015. Soil erosion and tolerable soil loss: Insights into erosion rates for a well-managed grassland catchment. *Geoderma* 237-238, 256-265, doi: <https://doi.org/10.1016/j.geoderma.2014.08.017>.
- Jeanneau, A.C., Ostendorf, B., Herrmann, T., 2019. Relative spatial differences in sediment transport in fire-affected agricultural landscapes: A field study. *Aeolian Research* 39, 13-22, doi: <https://doi.org/10.1016/j.aeolia.2019.04.002>.
- Jenks, G.F., Caspall, F.C., 1971. Error on choroplethic maps: Definition, measurement, reduction. *Annals of the Association of American Geographers* 61, 217-244, doi: <https://doi.org/10.1111/j.1467-8306.1971.tb00779.x>.
- Leys, J., Chappell, A., Mewett, J., Barson, M., 2017. Wind Erosion Assessment for National Landcare Program. State of New South Wales and Office of Environment and Heritage, Sydney,
- Leys, J., Strong, C., Heidenreich, S., Koen, T., 2018. Where She Blows! A Ten Year Dust Climatology of Western New South Wales Australia. *Geosciences* 8, 232, <http://www.mdpi.com/2076-3263/8/7/232>
- Leys, J.F., Butler, H.J., Yang, X., Heidenreich, S., 2010. CEMSYS modelled wind erosion.
- Leys, J.F., Smith, J., MacRae, C., Rickards, J., Yang, X., Randall, L., Hairsine, P., Dixon, J., McTainsh, G., 2009. Improving the capacity to monitor wind and water erosion: a review. DAFF,
- Li, Z., Fang, H., 2016. Impacts of climate change on water erosion: A review. *Earth-Science Reviews* 163, 94-117, doi: <http://dx.doi.org/10.1016/j.earscirev.2016.10.004>.
- Lu, H., Shao, Y.P., 2001. Toward quantitative prediction of dust storms: an integrated wind erosion modelling system and its applications. *Environmental Modelling & Software* 16, 233-249, doi: [https://doi.org/10.1016/s1364-8152\(00\)00083-9](https://doi.org/10.1016/s1364-8152(00)00083-9).
- Lyapustin, A., Korkin, S., Wang, Y., Quayle, B., Laszlo, I., 2012a. Discrimination of biomass burning smoke and clouds in MAIAC algorithm. *Atmos. Chem. Phys.* 12, 9679-9686, doi: <https://doi.org/10.5194/acp-12-9679-2012>.
- Lyapustin, A., Martonchik, J., Wang, Y., Laszlo, I., Korkin, S., 2011a. Multiangle implementation of atmospheric correction (MAIAC): 1. Radiative transfer basis and look-up tables. *Journal of Geophysical Research: Atmospheres* 116, doi: <https://doi.org/10.1029/2010JD014985>.
- Lyapustin, A., Wang, Y., Frey, R., 2008. An automatic cloud mask algorithm based on time series of MODIS measurements. *Journal of Geophysical Research: Atmospheres* 113, doi: <https://doi.org/10.1029/2007JD009641>.

- Lyapustin, A., Wang, Y., Laszlo, I., Kahn, R., Korkin, S., Remer, L., Levy, R., Reid, J.S., 2011b. Multiangle implementation of atmospheric correction (MAIAC): 2. Aerosol algorithm. *Journal of Geophysical Research: Atmospheres* 116, doi: <https://doi.org/10.1029/2010JD014986>.
- Lyapustin, A.I., Wang, Y., Laszlo, I., Hilker, T., G.Hall, F., Sellers, P.J., Tucker, C.J., Korkin, S.V., 2012b. Multi-angle implementation of atmospheric correction for MODIS (MAIAC): 3. Atmospheric correction. *Remote Sensing of Environment* 127, 385-393, doi: <https://doi.org/10.1016/j.rse.2012.09.002>.
- McKenzie, N., Dixon, J., 2006. Monitoring soil condition across Australia. Recommendations from expert panels. Prepared for the National Committee on Soil and Terrain for the National Land and Water Resources Audit, <http://lwa.gov.au/products/pn21340>
- Montgomery, D.R., 2007. Soil erosion and agricultural sustainability. *Proceedings of the National Academy of Sciences* 104, 13268-13272, doi: <https://doi.org/10.1073/pnas.0611508104>
- Moridnejad, A., Karimi, N., Ariya, P.A., 2015. A new inventory for middle east dust source points. *Environmental Monitoring and Assessment* 187, 582, doi: <https://doi.org/10.1007/s10661-015-4806-x>.
- O'Brien, L., 2019. slga: Data Access Tools for the Soil and Landscape Grid of Australia, R package version 1.0.1 ed, <https://github.com/obrl-soil/slga>
- Okin, G.S., 2008. A new model of wind erosion in the presence of vegetation. *Journal of Geophysical Research: Earth Surface* 113, doi: <https://doi.org/10.1029/2007JF000758>.
- Panebianco, J.E., Mendez, M.J., Buschiazzo, D.E., 2016. PM10 Emission, Sandblasting Efficiency and Vertical Entrainment During Successive Wind-Erosion Events: A Wind-Tunnel Approach. *Boundary-Layer Meteorology* 161, 335-353, doi: <https://doi.org/10.1007/s10546-016-0172-7>.
- Raupach, M., Gillette, D., Leys, J., 1993. The effect of roughness elements on wind erosion threshold. *Journal of Geophysical Research: Atmospheres* 98, 3023-3029,
- Seinfeld, J.H., Pandis, S.N., 2012. Atmospheric chemistry and physics: from air pollution to climate change. John Wiley & Sons,
- Shao, Y., 2008. Physics and modelling of wind erosion. Springer Science & Business Media,
- Shao, Y., Raupach, M., Leys, J., 1996. A model for predicting aeolian sand drift and dust entrainment on scales from paddock to region. *Soil Research* 34, 309-342, doi: <http://dx.doi.org/10.1071/SR9960309>.

- Su, C.-H., Eizenberg, N., Steinle, P., Jakob, D., Fox-Hughes, P., White, C., Rennie, S., Franklin, C., Dharssi, I., Zhu, H., 2019. BARRA v1.0: The Bureau of Meteorology Atmospheric high-resolution Regional Reanalysis for Australia. *Geoscientific Model Development* 12, 2049-2068, doi: <https://doi.org/10.5194/gmd-12-2049-2019>.
- Vacek, Z., Rehacek, D., Cukor, J., Vacek, S., Khel, T., Sharma, R.P., Kucera, J., Kral, J., Papaj, V., 2018. Windbreak Efficiency in Agricultural Landscape of the Central Europe: Multiple Approaches to Wind Erosion Control. *Environmental Management* 62, 942-954, doi: <https://doi.org/10.1007/s00267-018-1090-x>.
- Vrieling, A., Sterk, G., Vigiak, O., 2006. Spatial evaluation of soil erosion risk in the West Usambara Mountains, Tanzania. *Land Degradation & Development* 17, 301-319, doi: <https://doi.org/10.1002/ldr.711>.
- Webb, N.P., Herrick, J.E., Van Zee, J.W., Courtright, E.M., Hugenholtz, C.H., Zobeck, T.M., Okin, G.S., Barchyn, T.E., Billings, B.J., Boyd, R., Clingan, S.D., Cooper, B.F., Duniway, M.C., Derner, J.D., Fox, F.A., Havstad, K.M., Heilman, P., LaPlante, V., Ludwig, N.A., Metz, L.J., Nearing, M.A., Norfleet, M.L., Pierson, F.B., Sanderson, M.A., Sharratt, B.S., Steiner, J.L., Tatarko, J., Tedela, N.H., Toledo, D., Unnasch, R.S., Van Pelt, R.S., Wagner, L., 2016. The National Wind Erosion Research Network: Building a standardized long-term data resource for aeolian research, modeling and land management. *Aeolian Research* 22, 23-36, doi: <http://dx.doi.org/10.1016/j.aeolia.2016.05.005>.
- Yang, X., 2014. Deriving RUSLE cover factor from time-series fractional vegetation cover for hillslope erosion modelling in New South Wales. *Soil Research* 52, 253-261, doi: <http://dx.doi.org/10.1071/SR13297>.
- Young, M.-A., Herrmann, T., 2015. Celebrating 75 years of Soil-Care, 2015 State Community Landcare Conference. Government of South Australia, Department of Environment, Water and Natural Resources, Waikerie,

Chapter 4

An integrated modelling approach to estimate
post-fire soil erosion by wind and water in the South
Australian agricultural zone

Statement of Authorship

Title of Paper	An integrated modelling approach to estimate post-fire soil erosion by wind and water in the South Australian agricultural zone
Publication Status	<input type="checkbox"/> Published <input type="checkbox"/> Accepted for Publication <input type="checkbox"/> Submitted for Publication <input checked="" type="checkbox"/> Unpublished and Unsubmitted work written in manuscript style
Publication Details	Jeanneau, A., Herrmann, T. & Ostendorf, B (2020). An integrated modelling approach to estimate post-fire soil erosion by wind and water in the South Australian agricultural zone (unpublished)

Principal Author

Name of Principal Author (Candidate)	Amelie Jeanneau	
Contribution to the paper	Conceptualization, methodology, data curation, formal analysis, writing – original draft preparation, writing – review and editing.	
Overall percentage (%)	70%	
Certification	This paper reports on original research I conducted during the period of my Higher Degree by Research candidature and is not subject to any obligations or contractual agreements with a third party that would constrain its inclusion in this thesis. I am the primary author of this paper.	
Signature		Date: 04/06/2020

Co-author Contributions

By signing the Statement of Authorship, each author certifies that:

- i. the candidate's stated contribution to the publication is accurate (as detailed above);
- ii. permission is granted for the candidate to include the publication in the thesis; and
- iii. the sum of all co-author contributions is equal to 100% less the candidate's stated contribution.

Name of Co-Author	Tim Herrmann	
Contribution to the Paper	Conceptualization, methodology, formal analysis, writing – review and editing.	
Signature		Date: 04/06/2020

Name of Co-Author	Bertram Ostendorf	
Contribution to the Paper	Conceptualization, methodology, formal analysis, writing – review and editing.	
Signature		Date: 04/06/2020

Abstract

The combined effect of wind and water erosion can substantially contribute to total erosion rates in most dryland ecosystems. However, the impact of these two processes is still widely assessed separately. Dryland ecosystems are highly sensitive to environmental disturbances (e.g. droughts, overgrazing, fires) which can dramatically increase soil erosion susceptibility. Unfortunately, these threats, particularly wildfires, are likely to be more frequent in the future due to climate change, land management practices and planning. While fires are recognised as a major driver of erosion, there is a strong demand for model-based tools for predicting post-fire erosion response.

In this study, we applied two state-of-the-art water and wind erosion model (G2 and “albedo” Wind Erosion Model) to identify regions that were the most severely affected by wind, water or both erosion types in the Eyre Peninsula and Mid-North agricultural zones of South Australia. We also tested the applicability of a joint wind-water erosion approach to assessing post-fire erosion after ten catastrophic wildfires. Finally, we investigated whether Aerosol Optical Depth (AOD) products could provide complementary information to post-fire wind erosion assessment.

Erosion severity was low for the vast majority of the study area, while 4% and 9% of the total area suffered severe erosion by water and wind respectively. However, a very small fraction of the region (0.7%) was severely impacted by both wind and water erosion. The two erosion models satisfactorily captured the spatial and temporal variability of post-fire erosion. All fire-affected regions suffered an increase in erosion either immediately after the wildfires or within the first six months. For some of the wildfire events, an increase in both wind and water erosion was predicted in consecutive months or at the same time. Therefore, this information highlights the importance to consider wind and water erosion simultaneously for post-fire erosion assessment in dryland agricultural regions. Although this work was preliminary, the MODIS AOD dataset complemented well wind erosion predictions for post-fire erosion assessment.

However, more validation and correlation work is needed to apply this technique with more confidence.

Overall, this research demonstrated the importance of using an integrated modelling approach to estimate the impact of wind and water erosion in dryland agricultural regions under undisturbed conditions as well as post-fire erosion assessment. This method could then be used to target remedial (on-ground) activities to reduce soil loss and protect watercourses, dams, and livelihood of the community.

4.1 Introduction

Soil erosion is a natural process part of the soil and landscape formation; however, human activities have dramatically accelerated this phenomenon with the increasing removal of vegetation cover, expansion of farming onto marginal lands and overgrazing (Borrelli et al., 2017). According to FAO, soil erosion is the greatest challenge for sustainable soil management today (FAO, 2019). Soil erosion is of global concern because of its direct negative impact on ecosystem services, agricultural productivity and soil security. Local soil removal, generated by wind or water, induces the loss of fertile topsoil, containing vital nutrients and soil organic carbon, which further decreases soil fertility and ecosystem functions. On a larger scale, particles displaced by erosion can lead to pollution of water bodies through nutrient leaching, sedimentation of reservoirs and air pollution where airborne dust can lead to respiratory diseases (Flanagan et al., 2013).

Soil erosion can be generated by two main forces: wind and water and can be characterised as aeolian and fluvial processes. Transport characteristics of the two processes are very distinct and operate in different direction and dimensions, which makes direct comparison difficult. Aeolian transport is two dimensional as sediments are conveyed in both vertical and horizontal directions, and omnidirectional as airborne material can be transported in all wind directions. On the contrary, fluvial transport is mainly unidimensional, as sediments are transported downslope in a single direction.

Wind and water erosion affect a large proportion of arable lands around the globe (FAO, 2019), and their combined effect can substantially contribute to total erosion rates in most dryland ecosystems (Field et al., 2011b). It has been observed that these interactions can often go beyond the limit of the dryland ecosystem. For instance, sediments transported by water in lake beds or floodplains could be redistributed by wind over long distances during drier months, which could subsequently be carried again further by wind or water (Field et al., 2011b).

Dryland ecosystems are highly sensitive to environmental disturbances (e.g. droughts, overgrazing, fires) which can dramatically increase soil erosion susceptibility. Out of these disturbing agents, wildfires are of particular concern because they are unpredictable, reduce or eliminate protective ground cover, and can modify soil structure, thus increasing post-fire erosion risk. With the likely increase in the frequency and intensity of wildfires in dryland agricultural regions (Clarke et al., 2011; Gonçalves et al., 2011) and more recurring drought conditions (CSIRO and Bureau of Meteorology, 2015), soil erosion by wind or water is likely to increase too. With the recurrence in wildfires, soil surface will be more frequently exposed to commonly occurring storms, but it will also increase the probability that soils susceptible to erosion by wind or water will remain vulnerable when less frequent high-intensity events occur (Edwards et al., 2019). This information is of particular interest for dryland agricultural regions, where both aeolian and fluvial processes influence landscape formation, as wind and water erosion can be observed simultaneously or sequentially within months following major wildfire events (Shakesby et al., 2007; Shillito et al., 2012). The loss of fertile topsoil might also become more problematic if large fires are followed by drought conditions as vegetation and ground cover will take longer to recover leaving soils exposed for longer.

A growing body of research has compared the absolute and relative magnitude of wind and water erosion processes (Breshears et al., 2003; Du et al., 2016; Field et al., 2011a; Jiang et al., 2019; Wang et al., 2014). Nonetheless, these two are generally studied individually and integrated modelling approaches considering both processes

simultaneously are lacking (Belnap et al., 2011; Flanagan et al., 2013; Panagos et al., 2018). From existing modelling researches, significant uncertainty remains on the relative degree of wind and water erosion in dryland ecosystems and how the two processes interact in such environments (Flanagan et al., 2013). There is also ongoing uncertainty on how the interaction between the two processes changes with scale, and to what extent (Field et al., 2009; Field et al., 2011b), and how changes in fire regimes and frequency will impact the balance between wind and water erosion susceptibility in dryland ecosystems (Edwards et al., 2019). Post-fire erosion assessment has prompted significant interest in the past decades (Blake et al., 2020; Dukes et al., 2018; Fernández and Vega, 2018; Wagenbrenner et al., 2013), and evidence of wind redistribution of sediments has been reported in hydrological studies (Santín et al., 2015; Vega et al., 2020). However, a very limited number of researchers have considered wind and water erosion simultaneously in post-fire studies (Shillito et al., 2012).

Measurements of wind and water erosion in the field with wind tunnel experiments and standardised runoff plots have contributed significantly to the development of prediction models. However, such measurements are not sustainable when considering regional or continental scales applications. Thus, empirical and physical models have been developed to describe erosional processes. Recent technological advances in remote sensing and Geographic Information System (GIS), have also contributed to the popularity of erosion models as a growing number of models were designed to integrate GIS, digital maps and satellite data. These advances have also been crucial to improving the policy relevance of erosion models. As a result, authorities extensively use models predicting the extent of soil erosion for policy development. For instance, in Australia, the New South Wales government is using the CEMSYS wind erosion model (Leys et al., 2010) in combination with on-ground dust monitoring stations (DustWatch project, Leys et al. (2008)) to predict wind erosion and dust concentration over large areas (catchments and continent) and long time-periods (years). In Europe, the European Commission created a range of hillslope erosion maps from soil erosion

modelling to set soil protection targets within the Common Agricultural Policy (CAP) (Panagos and Katsoyiannis, 2019).

However, prediction models generally differ in the complexity of the processes examined and the type of input data required. For water erosion modelling (sheet and rill), RUSLE-derived models are the most popular (Borrelli et al., 2020; Panagos et al., 2018). This interest could be explained by the simplicity of the models, the availability of data and their simple integration in GIS and mapping software. For wind erosion modelling, the most commonly employed models are the (Revised) Wind Erosion Equation ((R)WEQ; Fryrear et al. (2000); Woodruff and Siddoway (1965)), the Wind Erosion Prediction System (WEPS; Hagen (1991)) and the Integrated Wind Erosion Modelling System (IWEMS, Lu and Shao (2001)) (Borrelli et al., 2020). The WEQ and RWEQ are empirical models with a similar structure to the USLE and predict potential average annual soil loss at the field scale, while WEPS and IWEMS models are process-based models. One of the major limitations of these models is that they require a large amount of detailed input data that might not always be readily available at larger scales and the WEQ, RWEQ and WEPS can only be applied at the field scale.

Besides the models mentioned above, two novel methods for water and wind erosion have increasingly drawn attention. The first one is the G2 model proposed by Panagos et al. (2014). G2 is a quantitative algorithm derived from the RUSLE approach, which quantifies hillslope erosion and sediment yield rates at monthly time intervals. Although quite similar to the RUSLE, this model proposed a new method to account for vegetation cover and management factor in a wide range of landscapes (see section 4.2.3). The second model is Chappell and Webb (2016) “albedo” Wind Erosion Model. The authors redefined the approximation of aerodynamic roughness using fundamental principles of aeolian sediment transport and made it possible to fully integrate satellite imagery and remote sensing in complex wind erosion models (see section 4.2.4).

Even though erosion processes have been well described, the high spatial and temporal variability in erosion makes the prediction of erosion trends very difficult. To overcome

these limitations, we need detailed data and access to high spatio-temporal datasets to be able to give the best assessment of soil losses and identify regions at risk of erosion in the future.

This study aims to identify regions that were the most severely affected by wind, water or both erosion types in the Eyre Peninsula and Mid-North agricultural zones of South Australia between 2001 and 2017. We also tested the applicability of a joint wind-water erosion approach to assessing post-fire erosion in the region and investigated whether AOD products could provide complementary information to post-fire wind erosion assessment.

4.2 Methods

4.2.1 The study area

Our study focusses on two dryland agricultural regions of South Australia, Australia: Eyre Peninsula (EP – 33°568'S 135°755'E – 4.7x10⁴ km²) and the Mid-North (MidN – 33°376'S 138°723'E – 3,4 x10⁴ km²) (Figure 4.1). These two regions are significant contributors to agricultural production in South Australia (ABARES, 2018) and parts of these regions are historically prone to wind and water erosion, therefore representing a vital interest for food and soil security. Agricultural land-uses represent the majority of the regional land-uses (Figure 4.2) with cereal cropping representing 50% and 33% of the land surface for the Eyre Peninsula and Mid-North respectively, followed by grazing (modified) pastures, representing 11% and 54% of the total regional land-use for each district (ABARES, 2016).

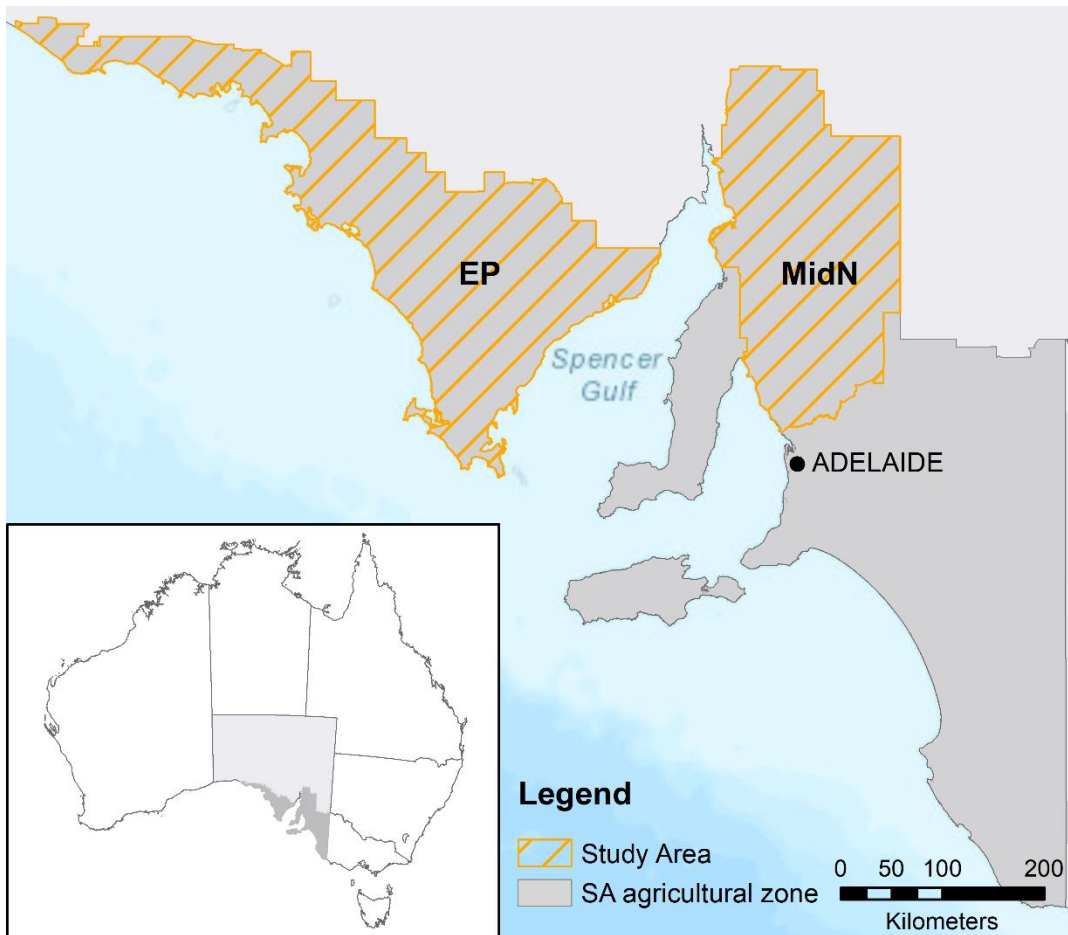


Figure 4.1 Location map and presentation of the study area (Eyre Peninsula & Mid-North) within the South Australian cropping region.

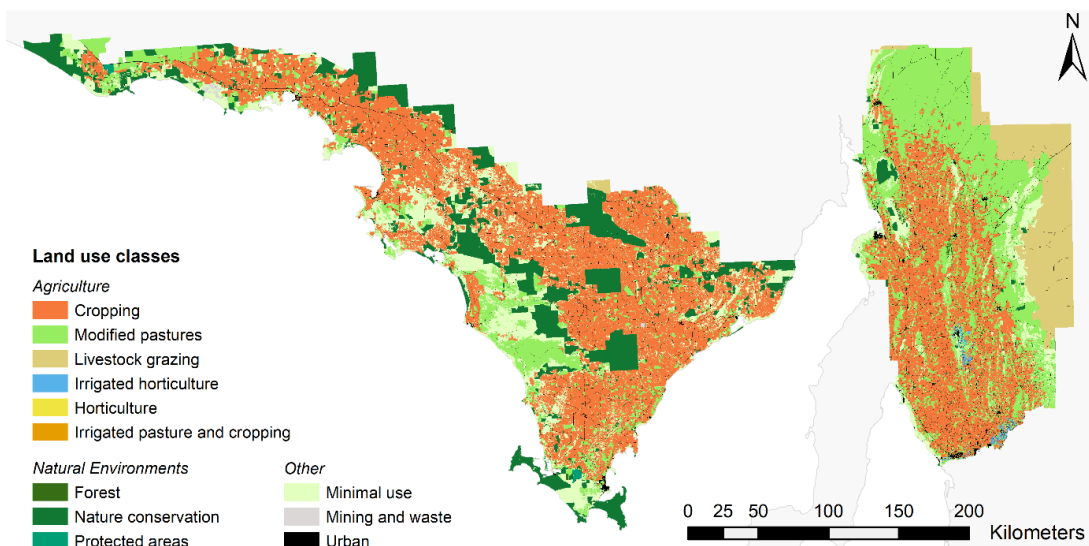


Figure 4.2 Land-use classes for the Eyre Peninsula and Mid-North regions. Source: (ABARES, 2016)

The two regions are characterised by a Mediterranean climate, with cool wet winters and hot dry summers with occasional summer storms and exhibit diverse soils and land uses, providing an excellent study site to demonstrate the utility of erosion modelling for land management. Mean annual rainfall ranges from 200mm in the north to 500mm in the south, with a mean of 350mm (BoM, 2016a). The average daily temperature varies between 12 and 19°C (BoM, 2016b). The dominant soil types in the Eyre Peninsula region range from sandy to clay-loam soils (Figure 4.3). On the other hand, soil types throughout the Mid-North region are more diverse and predominantly loam or clay-loam soils, with some sandy-loam patches (Figure 4.3). Elevation in the Eyre Peninsula region ranges between 0m and 480m, and from south-west to north-east. For the Mid-North region, altitude ranges between 0m and 950m above sea level with the highest elevations found in the centre of the region. The topography is complex in this area, and some parts have very steep slopes with gradients ranging from 0% to 60%.

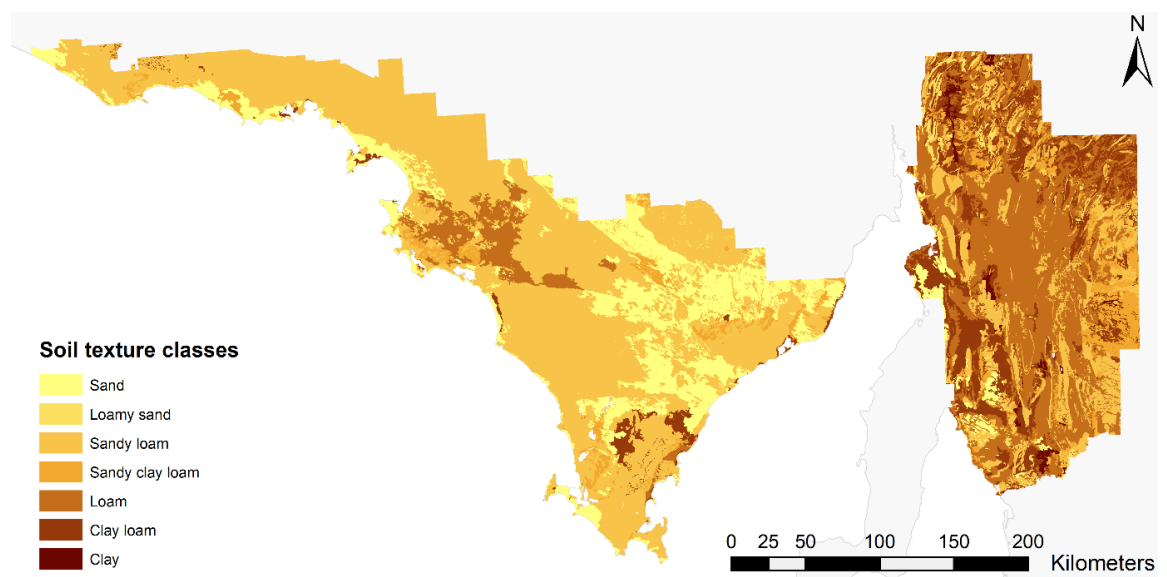


Figure 4.3 Dominant soil texture classes for the Eyre Peninsula and Mid-North regions. Source: DEW (2016).

4.2.2 Description of the data sources

All the datasets used in this study have been acquired from open-source databases. Data description (e.g. type, resolution, sources) can be found in Table A.1. Climate and weather data were obtained from the Australian Bureau of Meteorology Atmospheric

high-resolution Regional Reanalysis dataset for Australia (BARRA) (Su et al., 2019). More details about the dataset, product description and resolution can be found in (Su et al., 2019). For our modelling exercise, we used the hourly maximum gust wind speed at 10m and the soil moisture content in the top-most layer (0-10cm) datasets for the wind erosion model and the precipitation accumulation dataset for the water erosion model. These three datasets are available at a spatial resolution of 1.5km and an hourly temporal resolution for the State of South Australia.

Land-use and land cover classes were derived from the South Australian Land Cover dataset (Willoughby et al., 2018). This dataset modelled land cover throughout the state of South Australia based on a combination of satellite imagery (Landsat), aerial photography and land-use classification from National inventory (ABARES, 2016), and is available for six epochs (1987-90, 1990-95, 1995-2000, 2000-05, 2005-10, 2010-15) at a spatial resolution of 25m.

Ground cover was derived from Moderate Resolution Imaging Spectroradiometer (MODIS) fractional cover dataset for Australia (Guerschman et al., 2015). Guerschman et al. (2015) have developed an algorithm to isolate MODIS signal in three fractions representing the proportion of photosynthetic vegetation (PV), non-photosynthetic vegetation (NPV) and bare soil (BS). The spatiotemporal distribution of land surface properties can be evaluated with bidirectional reflectance distribution function (BRDF) of the surface and albedo. Chappell and Webb (2016) have demonstrated that MODIS BRDF/albedo products can be used reliably to derive land surface functions involved in wind erosion modelling. Here we programmatically downloaded the MODIS MCD43A1 and MCD43A3 products (band 1) with the *MODISrsp*: R package (Busetto and Ranghetti, 2016) to extract the isotropic (f_{iso}) and directional hemispherical reflectance (or black-sky albedo ω) parameters required to derive the normalised albedo factor for the wind erosion model. More details about the datasets can be found in Chappell and Webb (2016) and Chappell et al. (2018). Both MODIS datasets (Fractional Cover and

MODIS BRDF/albedo) provide daily data available at 500m resolution from the year 2000.

We extracted soil properties information from the Soil and Landscape Grid of Australia (SLGA) digital soil maps to estimate the ideal threshold friction velocity and soil erodibility. This dataset contains information about soil texture composition as a mass fraction at a depth of 0-5cm (clay < 2 μ m, silt < 50 μ m, sand < 2000 μ m, coarse fragments > 2000 μ m), soil organic carbon (SOC) and bulk density of the soil. The SLGA dataset is available at a resolution of 90m for the whole continent and can be automatically downloaded through the *slga*:: R package (O'Brien, 2019), more information about the range of soil properties and landscape attributes can also be found at www.csiro.au/soil-and-landscape-grid. We also downloaded additional soil properties datasets from the Australian Soil Resource Information System (ASRIS) (ASRIS, 2011) such as hydraulic conductivity and surface stone cover for the refinement of the soil erodibility factor.

Topography for the regions of interest was derived from the Advanced Land Observing Satellite (ALOS) Digital Surface Model (DSM) version 2.1 at a resolution of 30m (Tadono et al., 2014).

4.2.3 The water erosion model

To estimate hillslope erosion, we adapted the G2 model from Panagos et al. (2014) to Australian conditions. This model produces monthly maps predicting sheet and interrill erosion caused by rainfall and water runoff at a resolution of 500m. The structure of the G2 model is derived from the RUSLE, where five input parameters are combined in a multiplicative equation.

$$E_j = \frac{R_j}{V_j} \times S \times \frac{T}{L} \quad (22)$$

where E_j is the soil loss for the month j (t ha⁻¹), R_j is the rainfall erosivity for the month j (MJ mm ha⁻¹ h⁻¹), V_j represents the vegetation retention for the month j (dimensionless, analogous to the USLE's C-factor), S represents the soil erodibility

($\text{t ha h MJ}^{-1} \text{ ha}^{-1} \text{ mm}^{-1}$), T is the terrain influence and represents the influence of slope length and slope steepness (dimensionless, analogous to the USLE's LS factor), and L is the slope-intercept factor representing the effect of landscape alteration (dimensionless, corrective effect on T). More details about each erosion factor and the adaptation to local conditions can be found in Chapter 2.

4.2.4 The wind erosion model

Chappell and Webb (2016) proposed a new approach for wind erosion modelling simplifying the drag partition scheme of Raupach et al. (1993) while combining the use of remote sensing satellite imagery. The authors established a relationship between the sheltered area in the wake of plants and the proportion of shadow over a given area (Figure 4.4). This proportion of shadow can be derived from the inverse of the direct beam directional hemispherical reflectance (or black sky albedo ω) viewed at nadir, normalised by the surface reflectance and rescaled (or rescaled normalised albedo ω_{ns}). ω_{ns} is equivalent to the proportion of shadow described in Figure 4.4 and the empirical relationships required to estimate this parameter were calibrated against wind tunnel and field measurements of key aerodynamic properties which influence wind erosion. Chappell and Webb (2016) demonstrated that there was a strong relationship between the rescaled normalised albedo and the wind shear stress at the soil surface (u_{s*} , m s^{-1}) scaled by the freestream wind velocity (U_f , m s^{-1} , Figure 4.4a).

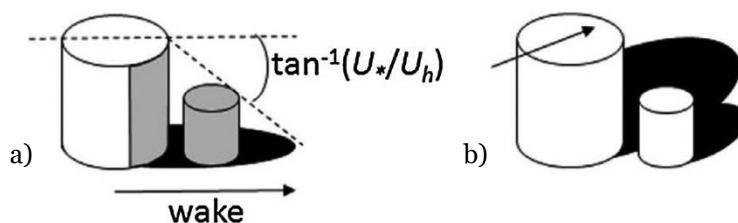


Figure 4.4 a) Concept representation of the sheltering effect of vegetation from Raupach et al. (1993), b) concept of the shadow effect of vegetation proposed by Chappell et al. (2010) to derive vegetation structure from remote sensing. Source: Chappell and Webb (2016)

This approach preserves the principles of previous wind erosion models, and the horizontal sediment flux can then be expressed as follow

$$Q_h = c_{shao} \frac{\rho_a \times u_{S*}^3}{g} \times \left(1 - \frac{u_{*ts}^2 \times H(w)^2}{u_{S*}^2} \right) \quad (23)$$

Where c_{shao} (0.006) represents a tuning factor adjusted to the magnitude of the model output, ρ_a is the density of the air (1.23 kg m^{-3}), g is the acceleration due to gravity (9.81 m s^{-2}), u_{*ts} is the soil threshold shear stress of bare soil below which sediment transport does not occur (Shao et al., 1996), and $H(w)$ is a soil moisture correction function which reduces sediment transport through the increase of cohesive forces in the soil (Fecan et al., 1999). The model is also adjusted by the influence of the total wind energy (shear stress) that is applied at the soil surface (u_{S*}).

To estimate wind erosion for the two regions of interest, we converted the horizontal sediment flux ($Q_h, \text{ g m}^{-1} \text{ s}^{-1}$), representing transport in one dimension, to an areal quantity ($E, \text{ t ha}^{-1} \text{ y}^{-1}$). First, we estimated the horizontal sediment flux on an hourly basis (finest temporal resolution) for each pixel in the archive (2001-2017). Then, we calculated the median value of daily horizontal sediment flux for each day in the time-series. Finally, we converted the median daily horizontal flux to an areal quantity to obtain the daily erosion rate ($E_{day}, \text{ t ha}^{-1} \text{ day}^{-1}$). To apply the conversion, we drew inspiration from Chappell et al. (2019) and used similar assumptions. We assumed that (i) the area of transport was defined by the size of a pixel (500m) and (ii) heterogeneity of transport within a pixel was captured by the albedo response of each pixel. Based on these assumptions, the median daily sediment transport in one dimension ($Q_{h_day}, \text{ g m}^{-1} \text{ s}^{-1}$) was converted to a surface quantity by dividing Q_{h_day} with the MODIS pixel size of 500m ($\text{g m}^{-2} \text{ s}^{-1}$). We further assumed wind erosion to be non-selective over a day and multiplied this quantity by the number of seconds in one day ($\text{g m}^{-2} \text{ day}^{-1}$) and then divided by 100 to convert the units to $\text{t ha}^{-1} \text{ day}^{-1}$. The daily erosion rate (E_{day}) was then summed by months and years for the analysis. More details about the model and its application to the Eyre Peninsula and Mid-North regions can be found in Chapter 3.

4.2.5 Description of the fire events

To investigate whether the wind and water erosion models could capture the impact of fires on soil erosion, we compared the erosion estimates for ten major fires in the study area. To narrow down the number of wildfire events for the analysis, we applied the following selection criteria: natural fire (bushfire), surface affected > 6,000 ha, the event occurred between 2001 and 2017. A complete list of the fire events and their characteristics can be found in Table 4.1.

Table 4.1 Description of the wildfire events used in the analysis.

Fire name	Type of event	Vegetation type	Fire date	Fire year	Season	Area affected (ha)
Pinery	Bushfire	Crops and pasture	2015-11-25	2015	Spring	78,434
Burra	Bushfire	Scrubs and pasture	2005-12-23	2005	Summer	6,147
Pinkawillinie Conservation Reserve	Bushfire	Mallee woodland	2005-12-27	2005	Summer	28,146
Wangary	Bushfire	Crops and pasture	2005-01-10	2005	Summer	77,964
Woolundunga	Bushfire	Scrubs and pasture	2012-01-04	2012	Summer	8,203
Kiana	Bushfire	Scrubs and pasture	2014-01-14	2014	Summer	6,711
Yumbarra Complex	Bushfire	Scrubs and pasture	2014-01-15	2014	Summer	7,744
Bangor	Bushfire	Eucalypts forest, pine plantation and pasture	2014-01-15	2014	Summer	33,373
Tulka	Bushfire	Scrubs and coastal vegetation	2001-02-01	2001	Summer	11,000
Pureba Conservation Park	Bushfire	Scrubs and pasture	2007-02-19	2014	Summer	11,801

These wildfire events affected very diverse landscapes and occurred at different stages of the fire season (November – March in Southern Australia). Most of these events affected scrubs and pasture landscapes (six out of ten), while two others burnt forests and woodlands (Pinkawillinie CR and Bangor). The Pinery and Wangary fires were the only two events to predominantly affect annual crops and pastures. This information is especially critical as annual vegetation responds differently to fires compared to perennials (Panico et al., 2020). Indeed, Australian native vegetation and forests evolved to adapt to wildfires and developed mechanisms to quickly recover after wildfires (Hill et al., 2016). However, annual plant communities (sown crops and annual pastures)

will not recover once they have burnt entirely and the soil will remain exposed to weathering elements until seasonal rain promotes pasture germination or enables a new crop to be sown. Therefore, more scrutiny needs to be applied to assess the impact of wildfires in a cropped environment.

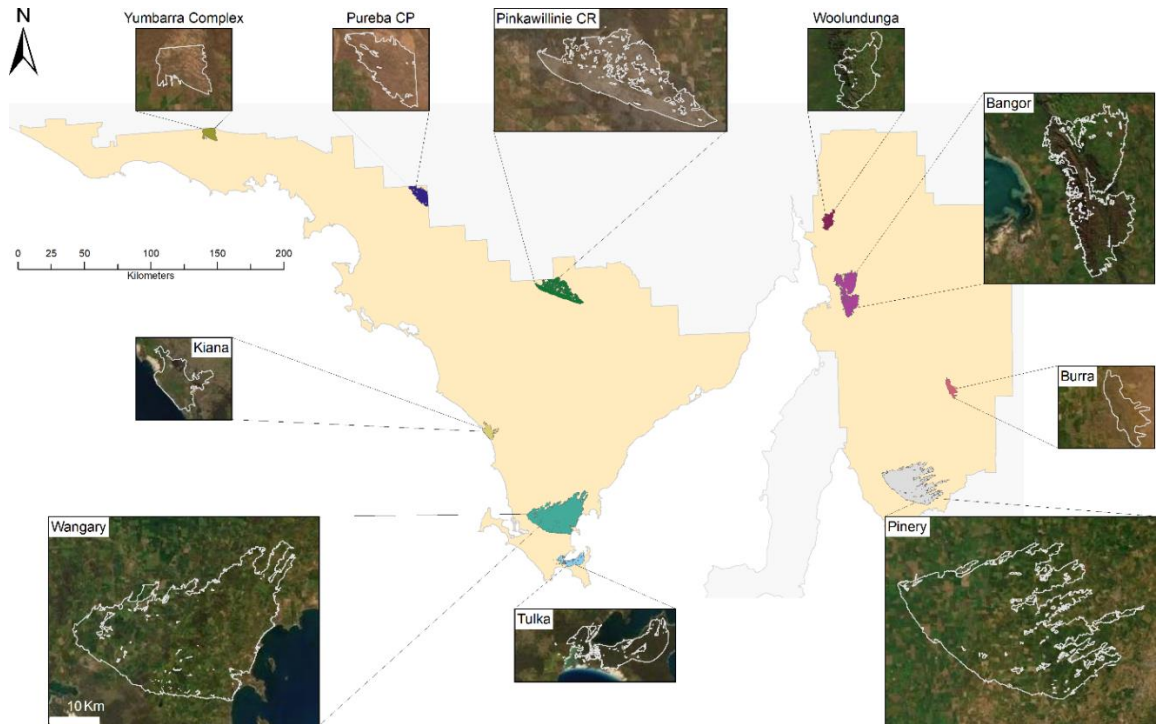


Figure 4.5 Fire location map for the Eyre Peninsula and the Mid-North region. All the fire scar inserts are displayed at the same scale and the reference scale bar is located in the Wangary insert (bottom-left corner).

Apart from the type of landscapes affected, it is essential to consider when a wildfire occurs as this can significantly influence soil erosion risk. For instance, the Pinery fire occurred very early in the fire danger season (Spring) and predominantly burnt crops and pastures. This event left the affected area more exposed to soil erosion for longer as new crops weren't sown before the end of summer (March) and pastures did not immediately recover from the fire. Although a number of mitigation measures were put in place shortly after the event, these were only temporary and could not prevent erosion entirely (Hall, 2017). The other wildfire events occurred between late December and February.

4.2.6 Analysis of the model results

The main focus of this study was to identify where wind or water erosion was the dominant process and where the two co-existed on the Eyre Peninsula and Mid-North regions, for the study period (2001-2017). For this reason, we performed an overlay analysis of the long-term wind and water erosion severity maps produced in Chapter 2 And 3 First, we classified the two maps in ten categories representing erosion severity deciles. Then we only selected the records representing the highest erosion severity (as falling within the 10th decile) for the overlay analysis. Finally, we estimated the proportion of the land where wind or water erosion was the dominant process and where the two co-existed.

The second objective of this study was to investigate whether the wind and water erosion models could capture the impact of fires on soil erosion. The fire disturbance was included in the model through the fractional vegetation cover (Guerschman et al., 2015) and MODIS albedo input datasets. For simplification of the method, no other model parameters were changed. We then estimated the mean monthly wind and water erosion for each fire events (Er_j) and for the first six months immediately after the event (Er_{j+1} to Er_{j+6}). To evaluate the relative change in monthly erosion due to the fires, we compared these results with their respective average monthly erosion values (\overline{Er}_j to \overline{Er}_{j+6}). The percentage of change in monthly erosion (ΔEr_j) is then estimated as follow,

$$\Delta Er_j = \frac{Er_j - \overline{Er}_j}{\overline{Er}_j} \times 100 \quad (24)$$

Therefore, a positive ΔEr_j represents an increase in monthly erosion compared to monthly averages for the month j , while a negative ΔEr_j represents a decrease in monthly erosion compared to monthly standards for the month j .

Finally, we wanted to test whether Aerosol Optical Depth (AOD) measurements could be used as a proxy for post-fire wind erosion monitoring. For this reason, we estimated the frequency of dust days from MODIS Multi-Angle Implementation of Atmospheric Correction (MAIAC) algorithm (Lyapustin et al., 2011a; Lyapustin et al., 2011b;

Lyapustin et al., 2012b). The MAIAC algorithm retrieves aerosol parameters over land daily at 1km resolution (MCD19A2v006) simultaneously with parameters of a surface bidirectional reflectance distribution function (BRDF). Compared to other MODIS Dark/Blue Target aerosol datasets (MOD04_3K and MYD04_3K), the MCD19A2 dataset provides the best estimate of AOD measurements over dark and vegetated surfaces, but also brighter surfaces including most urban areas. The cloud masking algorithm is also more performant than the other approaches and contains information about smoke injection height in the atmospheric column (Lyapustin et al., 2012a; Lyapustin et al., 2008). The monthly frequency of dust days was then calculated as the number of days in a month for which $AOD > 0.1$ and wind speed at 10m $> 6 \text{ m s}^{-1}$ following the method of von Holdt et al. (2017). The threshold friction velocity of 6 m s^{-1} represents the minimum wind speed for which dust can be detected with MODIS (von Holdt et al., 2017). We then compared the frequency of dust days for each fire events ($Fdust_j$) and for the first six months immediately after the event ($Fdust_{j+1}$ to $Fdust_{j+6}$) with their respective average monthly frequency values (\overline{Fdust}_j to \overline{Fdust}_{j+6}) to estimate the percentage of change (see equation (24)).

4.3 Results

4.3.1 Spatial distribution of water and wind erosion

The spatial patterns of hillslope erosion are presented in Figure 4.6. The areas where hillslope erosion was the most severe are located in the central part of the Mid-North region, and parts of the western and southern-most border of the Mid-North region. On the other hand, erosion severity was very low for most of the Eyre Peninsula, except for the south-eastern coast and parts of the north-east coast of the Eyre Peninsula. All these zones are characterised by steeper slopes and are more susceptible to extreme rainfall events. The mean annual soil loss rate was of 0.007 vs $0.017 \text{ t ha}^{-1} \text{ y}^{-1}$ for the Eyre Peninsula and Mid-North respectively. Approximately 68% of the study area was classified as having moderate (up to $0.021 \text{ t ha}^{-1} \text{ y}^{-1}$) to very low erosion susceptibility,

whereas 28% of the territory was classified with moderate to high ($0.021\text{--}0.069\text{ t ha}^{-1}\text{ y}^{-1}$) erosion severity (Table 4.2). The remaining 3.9% of the region presented very high ($0.069\text{--}1.36\text{ t ha}^{-1}\text{ y}^{-1}$) erosion susceptibility. Overall, soil erosion by water was very low in the study area compared to other parts of Australia (Teng et al., 2016; Yang, 2020).

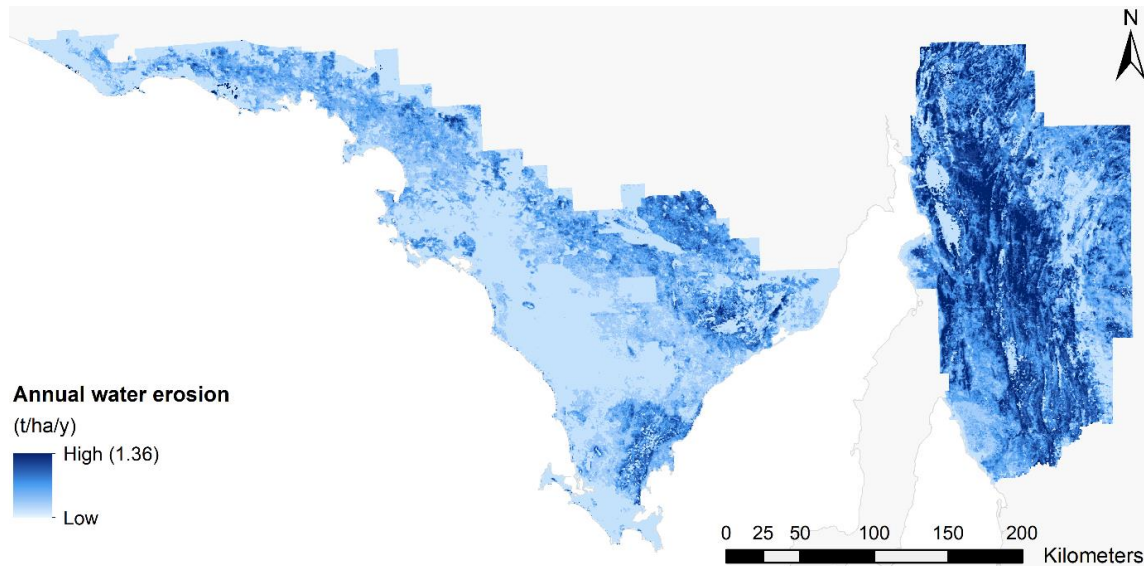


Figure 4.6 Modelled average annual water erosion severity (2001-2017).

Figure 4.7 presents the spatial patterns of wind erosion severity derived from the “albedo” Wind Erosion Model. Areas classified as moderate to very slight ($0.0\text{--}0.0025\text{ t ha}^{-1}\text{ y}^{-1}$) erosion covered $\sim 50\%$ of the total area (Table 4.3). Moderate to high erosion severity ($0.0025\text{--}0.0041\text{ t ha}^{-1}\text{ y}^{-1}$) covered about 41% of the study area. The remaining 9.3% of the land was classified as very high erosion severity ($0.0041\text{--}0.025\text{ t ha}^{-1}\text{ y}^{-1}$). These regions highly susceptible to wind erosion were predominantly located on the coastal areas of the Eyre Peninsula and Mid-North regions (Figure 4.8). A large proportion of the north-western half of the Eyre Peninsula, and some lowland plains in the central ranges and eastern plains of the Mid-North also experienced high to very erosion. This higher erosion susceptibility is mainly driven by high climatic erosivity (strong coastal winds), high soil erodibility (sandier soils) and low vegetation cover.

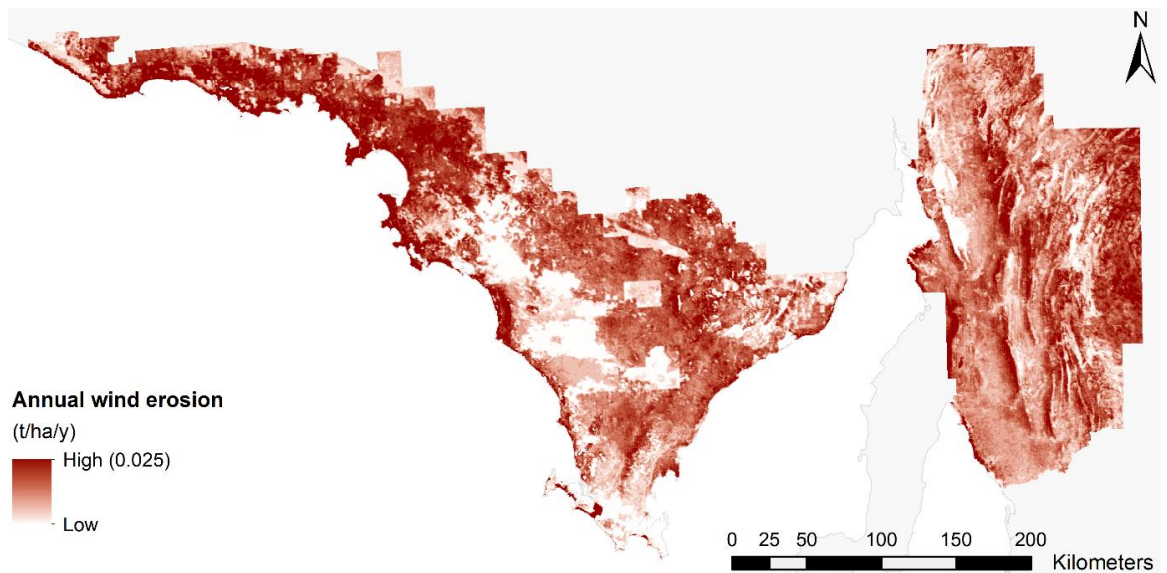


Figure 4.7 Modelled average annual wind erosion severity (2001-2017).

Table 4.2 Modelled hillslope erosion severity classes by total land area.

Soil erosion severity		Area	
decile	t ha ⁻¹ y ⁻¹	Thousands ha	%
1	0 - 0.000001	0.0025	0.0003
2	0.000001 - 0.005	2485.7	30.6
3	0.005 - 0.011	1174.0	14.4
4	0.011 - 0.016	1066.3	13.1
5	0.016 - 0.021	833.6	10.3
6	0.021 - 0.027	606.0	7.5
7	0.026 - 0.037	769.5	9.5
8	0.037 - 0.048	441.6	5.4
9	0.048 - 0.069	429.1	5.3
10	0.069 - 1.36	320.9	3.9
Total		8127	

Table 4.3 Modelled wind erosion severity classes by total land area.

Soil erosion severity		Area	
decile	t ha ⁻¹ y ⁻¹	Thousands ha	%
1	0 - 0.00059	727.4	8.9
2	0.00059 - 0.0013	787.9	9.7
3	0.0013 - 0.0017	817.4	10.1
4	0.0017 - 0.0022	905.5	11.1
5	0.0022 - 0.0025	798.7	9.8
6	0.0025 - 0.0028	801.0	9.9
7	0.0028 - 0.0031	975.4	12.0
8	0.0031 - 0.0035	789.3	9.7
9	0.0035 - 0.0041	766.1	9.4
10	0.0041 - 0.0251	758.3	9.3
Total		8127	

The overlay analysis of the wind and water erosion severity maps revealed that a very small portion of the study area (56 thousand ha, 0.7% of the total area) experienced very high erosion by wind and water simultaneously (Figure 4.8). These hotspots were mainly detected in the central ranges of the Mid-North region (west-facing foothills) and the north-west of the Eyre Peninsula. Figure 4.6 to 4.8 highlight that spatial patterns of erosion by wind and water were highly variable throughout the study area. This spatial variability could be explained by the diversity of landscapes, topography and climatic conditions of the two regions.

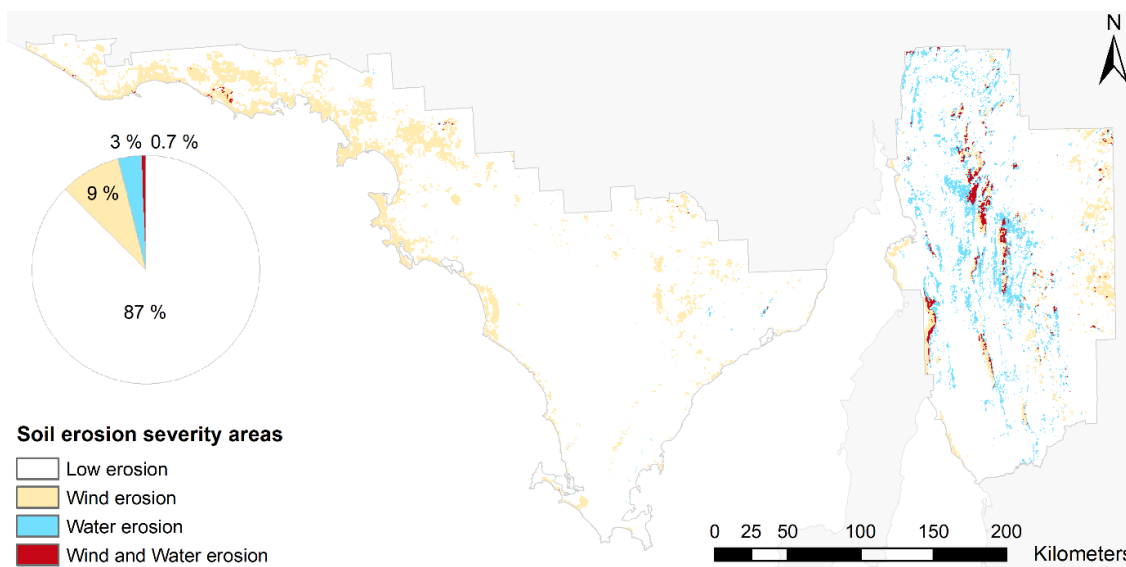


Figure 4.8 Spatial distribution of the predicted most severe soil erosion classes (top decile) in the Eyre Peninsula and Mid-North regions and dominant erosion process.

4.3.2 *The impact of fires on erosion*

The second objective of this study was to investigate whether the wind and water erosion models could capture the impact of wildfires on soil erosion immediately after the fire event and up to six months later. For this reason, we estimated the percentage of change in monthly erosion for each month after the fire event (up to 6-months) from their respective long-term mean with equation (24). The percentage of change in monthly water and wind erosion are presented in Figure 4.9 and 4.10. An increase in erosion of 100% for a month j is equivalent to a two-fold increase compared to an “unburnt”

month j , while a decrease of 50% is equivalent to half the average erosion rate of an “unburnt” month j .

The results from Figure 4.9 indicate that water erosion significantly increased in the months immediately after the Pinery, Bangor and Tulka wildfires and that the fires influenced erosion severity for at least 6 months. After these events, soil erosion was between two to 12 times higher than their respective monthly averages. Although the landscapes of the Pinery and Bangor regions were very different, the increase in water erosion following the wildfires was correlated to a reduction in ground cover combined with erosive rainfall events (Table E.1). However, it is worth noting that even though the model recorded a 600% increase in erosion in the Tulka region after the fire, the actual amount of erosion remained very low (0.1 kg ha^{-1}) (Table E.1).

Water erosion dramatically increased in the month following the Kiana fire event (February 2014) with a 12-fold increase compared to monthly averages (7.8 kg ha^{-1} vs 0.5 kg ha^{-1} for “unburnt” years). However, this increase was reduced in the following three months to a two-fold increase. This surge in monthly erosion for February 2014 could be explained by a combination of intense rainstorms and very low ground cover for the Kiana region (Table E.1). On the other hand, water erosion did not increase immediately after the Burra, Pinkawillinie CR, and Yumbarra Complex fires, but a spike in erosion was recorded for at least one of the following months. This increase was about an order of magnitude higher compared to monthly averages and concurred with a spike in monthly rainfall erosivity (Table E.1). However, there was no sustained increase nor decrease in water erosion following the Wangary, Woolundunga, Pureba Conservation Park fires.

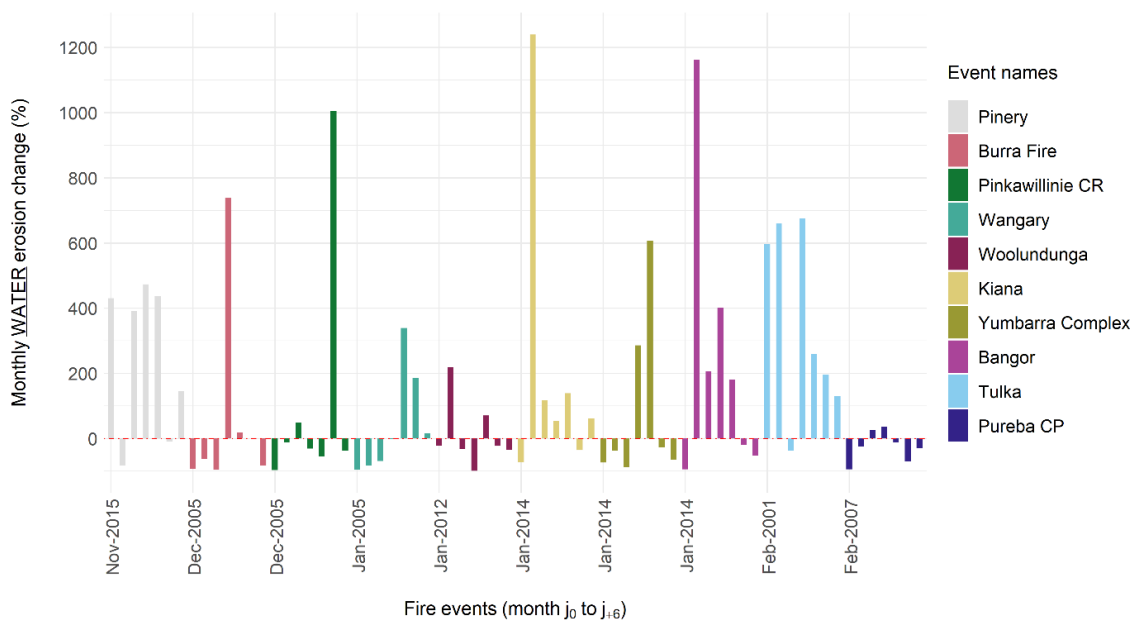


Figure 4.9 Modelled monthly water erosion change for months m_0 (start of the fire) to m_{+6} for each fire event. The y-axis represents the percent change in erosion for the month m_j compared to monthly averages. Bar graphs over the dotted line = increase in erosion compared to monthly averages, bar graphs below the dotted line = decrease in erosion compared to monthly averages.

Wind erosion significantly increased shortly after the Pinkawillinie, Wangary, and Tulka fires and this increase was sustained for at least six months. Monthly erosion was between two to five times higher than their respective monthly averages, except for the Tulka fire, where erosion rates were consistently higher, reaching up to 10 times the monthly averages. Nonetheless, even if this increase seems spectacular for the Tulka region, the actual erosion rates remained very low (c.a. 0.08 kg ha^{-1} vs 0.008 kg ha^{-1} for “unburnt” years) (Table E.1). The spikes in erosion for these three regions were all correlated to a low ground cover ($< 55\%$) and strong average wind velocities ($> 8.5 \text{ m s}^{-1}$).

Wind erosion did not immediately increase after the Pinery, Yumbarra Complex and Pureba CP fires, but was recorded six or seven months after the fire events. Monthly erosion for these periods was 3- to 4-times higher than seasonal averages, and can be correlated with consistently stronger winds and limited ground cover as well. The Yumbarra and Pureba regions are located in zones where wind erosion is generally moderate (Figure 4.8); however, with the removal of vegetation by wildfires these semi-arid regions can become more vulnerable to wind erosion with stronger wind gusts.

On the contrary, we did not observe any significant increase in wind erosion for the Woolundunga, Kiana, Bangor wildfires. This could be explained by the nature of the landscape affected (shrubs or forests), weather conditions (wetter conditions than average), and the fact that ground cover remained moderate (> 65%).

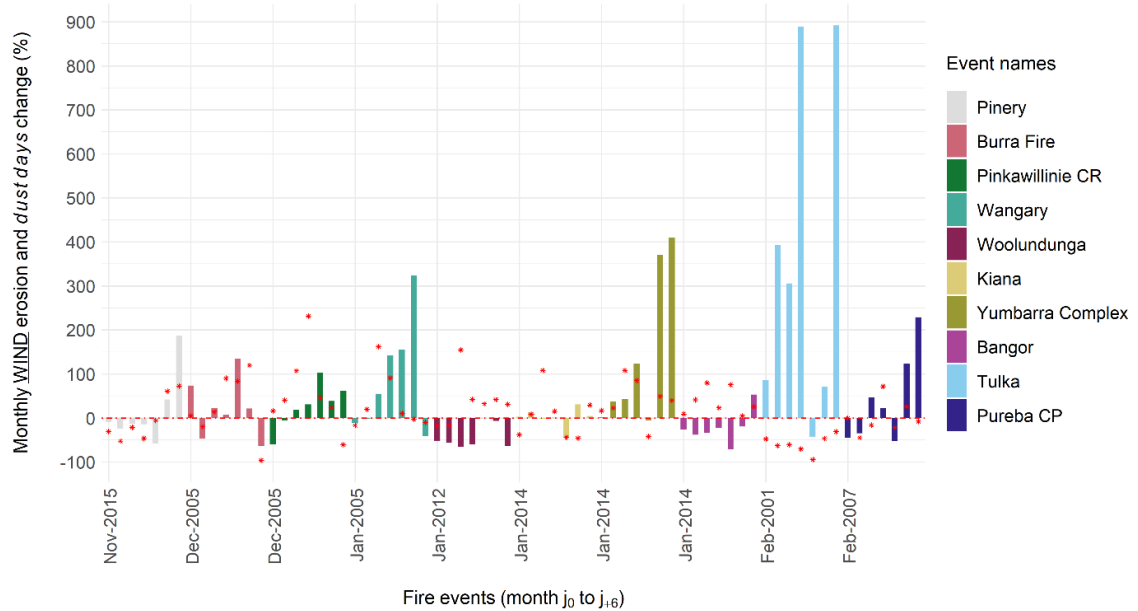


Figure 4.10 Modelled monthly wind erosion change for months m_0 (start of the fire) to m_{+6} for each fire event (bar graphs) and change in dust days from MODIS MAIAC (red dots). The y-axis represents the percent change in erosion for the month m_j compared to monthly averages. Bar graphs over the dotted line = increase in erosion compared to monthly averages, bar graphs below the dotted line = decrease in erosion compared to monthly averages.

Out of the ten wildfire events, only parts of the Pinery and Burra regions were located in zones highly susceptible to both wind and water erosion processes (Figure 4.8). However, the increase in wind and water erosion was not recorded simultaneously for these two events. For instance, in the Pinery region, a significant increase in water erosion was recorded by the models from the month following the fire, while there was only a slight increase in wind erosion six months after the event. This observation correlates well with regional weather records (Table E.1) and local observations (Hall, 2017; Lim, 2016).

Although the wind and water erosion severities were very low in the Wangary and Yumbarra Complex regions, both experienced an increase in severe wind erosion a couple of months after the fires (from February to March) and up to six months. However, the rise in water erosion was only predicted from April, May which coincides

with the first major rainfall events in the two regions (Table E.1). So, for April to June following these events, the two regions experienced a joint increase in wind and water erosion about 2.5 to 5 times their respective monthly averages.

4.3.3 Using AOD measurements for post-fire wind erosion monitoring

Although this work was preliminary, we attempted to test whether the MODIS MAIAC AOD dataset could be used in complement to the “albedo” Wind Erosion Model to monitor post-fire erosion. The change in the frequency of dust days seemed to agree with the wind erosion model for the Pinery, Burra, Kiana, and Yumbarra fires. However, the agreement was only partial for the Pinkawillinie, Wangary, and Pureba events. The Pinkawillinie Conservation Reserve is situated in a dry landscape where dust haze might be more common than predicted by the “albedo” erosion model, which could explain some of the discrepancies. For both, the Wangary and Pureba areas, the divergence between the number of dust days and monthly wind erosion occurred on two to three months out of seven. Dust haze might have been more common in the Wangary region shortly after the fire, which was not perceived by the erosion model. In contrast, there is no explicit agreement between the “albedo” Wind Erosion Model and the MODIS AOD for the Woolundunga, Bangor, Tulka wildfires. The discrepancies between the satellite-derived dust days and the wind erosion model for the Tulka fire could be correlated to the very small amount of actual soil erosion (Table E.1). The lack of fine dust observed by the MODIS AOD, could also be linked to the fact that the Tulka region consists of sandhills and coastal dunes. Indeed, the generation of finer particles would be limited in such environments even if a large portion of the protective ground cover was gone. The Bangor and Woolundunga events occurred in forested landscapes and ground cover remained moderate after the fires (> 65%), hence the limited change in wind erosion. Although the frequency of dust days derived from MODIS AOD correlates well with the spatial distribution of long-term modelled wind erosion severity (Chapter 3), this product might not be adequate for the detection of post-fire erosion. Therefore, the

frequency of dust days derived from MODIS AOD might not be correlated to localised erosion from the fire-affected region, but dust sources could originate from outside the burnt area.

4.4 Discussion

4.4.1 The performance of the models

This study demonstrated how soil erosion modelling could help in predicting the impact of wildfires on erosion by wind and water at the regional scale. Overall, the patterns identified here by the models correlated well with local observations (Hall, 2017; Lim, 2016), which highlights the benefit of an automated method to complement local observations. Even though post-fire erosion studies generally consider wind or water erosion processes separately, this joint investigation proved to be valuable for the study area. Indeed, for some of the events (Pinery, Wangary and Yumbarra Complex) the fire-affected regions experienced an increase in both wind and water erosion either sequentially or simultaneously. Therefore, considering only one of the two processes would only provide half of the post-fire erosion picture. This information is even more critical for dryland agricultural regions where severe wind and water erosion events can occur under undisturbed conditions (Field et al., 2011b).

Nonetheless, soil erosion vulnerability was probably higher after the fires than predicted by the models. Wildfires increase soil surface erodibility (Prats et al., 2016; Varela et al., 2010) and water repellence (Neary, 2011; Shakesby, 2011) due to the destruction of organic and chemical bonds between soil particles and aggregates. Unfortunately, this element was not taken into account in the models and might have led to a misclassification of post-fire erosion change.

Even if the removal of protective vegetation cover by wildfires increases erosion, the amount of post-fire erosion is also dependent on the presence of an erosive event. Therefore, even if the ground remains bare for an extended period, little to no erosion would be recorded if no intense rainstorm or wind event occurred. This could explain

why water erosion was so low after the Pureba Conservation Park event, and for the first few months after the Wangary fire, and why wind erosion remained low after the Kiana event (Table E.1).

As post-fire wind erosion modelling is not so common, further work could be implemented to compare on-ground measurements and modelling outputs to improve predictions. Simple dust sampling methods (Webb et al., 2016) could be easily put in place following wildfire events to monitor post-fire erosion (Jeanneau et al., 2019).

4.4.2 The opportunity of using AOD datasets for wind erosion monitoring

Although the use of the MODIS AOD dataset for post-fire wind erosion monitoring was preliminary work, the frequency of dust days approach presented potential. However, further validation and correlation analysis is needed to apply this technique with more confidence.

The change in monthly dust days correlated well with some of the “albedo” Wind Erosion Model records, but the results were not consistent. This could be because the MODIS MAIAC algorithm captures the presence of suspended dust particles (clays and silts) while the wind model predicts the movement of coarser fragments on the ground (saltation). Another limitation of the MODIS MAIAC dataset could be the lack of contrast between the colour of wind-blown sediments and soil background. Although this algorithm performs well over dark and vegetated surfaces, and bright surfaces (Lyapustin et al., 2011b), it might not be optimised for Australian red soils yet. Nonetheless, using the “albedo” Wind Erosion Model in conjunction with MODIS AOD could give a better understanding of post-fire wind erosion for organisations with limited resources.

This exploratory work showed promising results and supported the argument for more research to be developed in assessing the potential of satellite and remote-sensing data for post-fire erosion assessment.

4.4.3 The implication of predicted soil erosion severity for land management

It is essential to understand how wildfires can influence the increase in erosion susceptibility, to be more prepared in the future. Modelling has proven to be a valuable tool to prioritise remediation measures on areas the most at risk of post-fire erosion (Basso et al., 2020; Hosseini et al., 2018; Lanorte et al., 2019; Wagenbrenner et al., 2017), but a lot of research is still focussing on wind or water erosion separately. Here, we demonstrated that considering wind and water erosion together provided a better picture of post-fire erosion severity in the Eyre Peninsula and Mid-North regions. Even though the fire-affected sub-regions presented in this paper were not highly susceptible to erosion under undisturbed conditions (Figure 4.8), fires significantly increased erosion rates for the majority of the events within the first six months (Figure 4.9 and 4.10).

Although remediation measures are generally put in place in conservation parks and forests to reduce soil erosion risk (Fernández et al., 2011; Vieira et al., 2018), not much can be done on a large scale by land managers on farmlands. Some short-term measures can be applied for remediation, such as clay spreading on sandy soils if clay is available (Egan, 2006; GRDC, 2015; May, 2006), and deep cultivation of loam or heavier soils to roughen the soil surface (Lawson, 2015; Young et al., 2017). Still, in the long term, land managers will have to wait for rainfall to allow pasture regeneration, crops to be sown or native vegetation to recover. Nonetheless, an integrated erosion modelling approach combined with satellite ground cover, soil properties and various scenarios for levels of wind and rainfall events could then be used to predict where the worst erosion is likely to occur following a fire. This information could then be used to target remedial (on-ground) activities to reduce soil loss and protect water courses, dams, and livelihood of the community.

Even if this information would be of interest for land managers, we did not investigate the influence of post-fire erosion factors in this study. Nevertheless, statistical correlation analysis between erosion rates, time of the burn, type of vegetation burnt,

and scale effect could also be investigated to understand the implication of the modelling results better.

4.5 Conclusion

This research applied the G2 and “albedo” erosion models to identify regions that were the most severely affected by wind, water or both erosion types in the Eyre Peninsula and Mid-North agricultural zones of South Australia. We also tested the applicability of a joint wind-water erosion approach to assessing post-fire erosion in the region and investigated whether AOD products could provide complementary information to post-fire wind erosion assessment.

Districts with the most severe erosion susceptibility covered 4% and 9% of the total area for water and wind respectively. However, a very small fraction of the region (0.7%) was severely impacted by both wind and water erosion.

The G2 and “albedo” erosion models satisfactorily captured the spatial and temporal variability of post-fire erosion. All fire-affected regions suffered an increase in erosion either immediately after the wildfires or within the first six months. These results correlated well with anecdotal observations. Although post-fire erosion studies generally consider wind or water erosion processes separately, this joint investigation proved to be valuable for the study area. In fact, an increase in both wind and water erosion was predicted in consecutive months or at the same time for some of the wildfire events (Pinery, Wangary and Yumbarra Complex). Therefore, considering only one of the two processes would only provide half of the post-fire erosion picture. This information is even more critical for dryland agricultural regions where severe wind and water erosion events can occur under undisturbed conditions.

Even though this work was preliminary, the MODIS AOD dataset complemented well wind erosion predictions for post-fire erosion assessment. AOD measurements provide information on suspended dust particles (clays and silts) while the wind model predicts

the movement of coarser fragments on the ground (saltation). Therefore, these results support that further research could use satellite and remote-sensing data more broadly for post-fire erosion assessment, providing more validation and correlation work is undertaken before applying this technique with more confidence.

Therefore, this research demonstrated the importance of using an integrated modelling approach to estimate the impact of wind and water erosion in dryland agricultural regions. This information is critical for land managers and policy-makers as wind and water erosion is likely to increase in the face of climate change (Edwards et al., 2019). The G2 and “albedo” erosion models could be combined with satellite ground cover, soil properties and various scenarios for levels of wind and rainfall events to predict where the worst erosion is likely to occur following a fire. This knowledge could then be used to target remedial (on-ground) activities to reduce soil loss and protect watercourses, dams, and livelihood of the community.

4.6 References

- ABARES, 2016. The Australian Land Use and Management Classification Version 8. Australian Bureau of Agricultural and Resource Economics and Sciences (ABARES), http://data.daff.gov.au/anrdl/metadata_files/pe_alumc9aal20161017.xml?convertlinks=0
- ABARES, 2018. Catchment scale land use of Australia - Commodities - Version 2. Australian Bureau of Agricultural and Resource Economics and Sciences (ABARES), <https://www.agriculture.gov.au/abares/aclump/land-use/catchment-scale-land-use-of-australia-commodities-update-december-2018>
- ASRIS, 2011. ASRIS - Australian Soil Resource Information System, <http://www.asris.csiro.au>
- Basso, M., Vieira, D.C.S., Ramos, T.B., Mateus, M., 2020. Assessing the adequacy of SWAT model to simulate postfire effects on the watershed hydrological regime and water quality. *Land Degradation & Development* 31, 619-631, doi: <https://doi.org/10.1002/ldr.3476>.

- Belnap, J., Munson, S.M., Field, J.P., 2011. Aeolian and fluvial processes in dryland regions: the need for integrated studies. *Ecohydrology* 4, 615-622, doi: <https://doi.org/10.1002/eco.258>.
- Blake, D., Nyman, P., Nice, H., D'Souza, F.M.L., Kavazos, C.R.J., Horwitz, P., 2020. Assessment of post-wildfire erosion risk and effects on water quality in southwestern Australia. *International Journal of Wildland Fire* 29, 240-257, doi: <https://doi.org/10.1071/WF18123>.
- BoM, 2016a. Average annual, seasonal and monthly rainfall. Bureau of Meteorology, http://www.bom.gov.au/jsp/ncc/climate_averages/rainfall/index.jsp?period=an&area=sa#maps
- BoM, 2016b. Decadal and multi-decadal temperature. Bureau of Meteorology, http://www.bom.gov.au/jsp/ncc/climate_averages/decadal-temperature/index.jsp?maptype=6&period=7605&product=max#maps
- Borrelli, P., Alewell, C., Alvarez, P., Anache, J.A.A., Baartman, J., Ballabio, C., Bezak, N., Biddoccu, M., Cerda, A., Chalise, D., Chen, S., Chen, W., Girolamo, A.M.D., Gessesse, G.D., Deumlich, D., Efthimiou, N., Erpul, G., Fiener, P., Freppaz, M., Gentile, F., Gericke, A., Haregeweyn, N., Hu, B., Jeanneau, A., Kaffas, K., Kiani-Harchegani, M., Villuendas, I.L., Li, C., Lombardo, L., López-Vicente, M., Lucas-Borja, M.E., Märker, M., Matjaž, M., Miao, C., Modugno, S., Möller, M., Naipal, V., Nearing, M., Owusu, S., Panday, D., Patault, E., Patriche, C.V., Poggio, L., Portes, R., Quijano, L., Rahdari, M.R., Renima, M., Ricci, G.F., Rodrigo-Comino, J., Saia, S., Samani, A.N., Schillaci, C., Syrris, V., Kim, H.S., Spinola, D.N., Oliveira, P.T., Teng, H., Thapa, R., Vantas, K., Vieira, D., Yang, J.E., Yin, S., Zema, D.A., Zhao, G., Panagos, P., 2020. Soil erosion modelling: A global review and statistical analysis, *Earth-Science Reviews*,
- Borrelli, P., Robinson, D.A., Fleischer, L.R., Lugato, E., Ballabio, C., Alewell, C., Meusburger, K., Modugno, S., Schütt, B., Ferro, V., Bagarello, V., Oost, K.V., Montanarella, L., Panagos, P., 2017. An assessment of the global impact of 21st century land use change on soil erosion. *Nature Communications* 8, 2013, doi: <https://doi.org/10.1038/s41467-017-02142-7>.
- Breshears, D.D., Whicker, J.J., Johansen, M.P., Pinder, J.E., 2003. Wind and water erosion and transport in semi-arid shrubland, grassland and forest ecosystems: Quantifying dominance of horizontal wind-driven transport. *Earth Surface Processes and Landforms* 28, 1189-1209, doi: <https://doi.org/10.1002/esp.1034>.
- Busetto, L., Ranghetti, L., 2016. MODISstp: An R package for automatic preprocessing of MODIS Land Products time series. *Computers & Geosciences* 97, 40-48, doi: <https://doi.org/10.1016/j.cageo.2016.08.020>.
- Chappell, A., Van Pelt, S., Zobeck, T., Dong, Z., 2010. Estimating aerodynamic resistance of rough surfaces using angular reflectance. *Remote Sensing of Environment* 114, 1462-1470, doi: <https://doi.org/10.1016/j.rse.2010.01.025>.

- Chappell, A., Webb, N., 2016. Using albedo to reform wind erosion modelling, mapping and monitoring. *Aeolian Research* 23, 63-78, doi: <https://doi.org/10.1016/j.aeolia.2016.09.006>.
- Chappell, A., Webb, N.P., Guerschman, J.P., Thomas, D.T., Mata, G., Handcock, R.N., Leys, J.F., Butler, H.J., 2018. Improving ground cover monitoring for wind erosion assessment using MODIS BRDF parameters. *Remote Sensing of Environment* 204, 756-768, doi: <https://doi.org/10.1016/j.rse.2017.09.026>.
- Chappell, A., Webb, N.P., Leys, J.F., Waters, C.M., Orgill, S., Eyres, M.J., 2019. Minimising soil organic carbon erosion by wind is critical for land degradation neutrality. *Environmental Science & Policy* 93, 43-52, doi: <https://doi.org/10.1016/j.envsci.2018.12.020>.
- Clarke, H.G., Smith, P.L., Pitman, A.J., 2011. Regional signatures of future fire weather over eastern Australia from global climate models. *International Journal of Wildland Fire* 20, 550-562, doi: <https://doi.org/10.1071/WF10070>.
- CSIRO, Bureau of Meteorology, 2015. Climate Change in Australia Information for Australia's Natural Resource Management Regions: Technical Report. CSIRO and Bureau of Meteorology, Australia, https://www.climatechangeinaustralia.gov.au/media/ccia/2.1.6/cms_page_media/168/CCIA_2015_NRM_TechnicalReport_WEB.pdf
- DEW, 2016. Surface Soil Texture. Government of South Australia, Department for Environment and Water, <https://data.sa.gov.au/data/dataset/3ee7c63d-cae6-4076-a394-4db4a158e740>
- Du, H.Q., Dou, S.T., Deng, X.H., Xue, X., Wang, T., 2016. Assessment of wind and water erosion risk in the watershed of the Ningxia-Inner Mongolia Reach of the Yellow River, China. *Ecological Indicators* 67, 117-131, doi: <https://doi.org/10.1016/j.ecolind.2016.02.042>.
- Dukes, D., Gonzales, H.B., Ravi, S., Grandstaff, D.E., Van Pelt, R.S., Li, J., Wang, G., Sankey, J.B., 2018. Quantifying Postfire Aeolian Sediment Transport Using Rare Earth Element Tracers. *Journal of Geophysical Research: Biogeosciences* 123, 288-299, doi: <https://doi.org/10.1002/2017JG004284>.
- Edwards, B.L., Webb, N.P., Brown, D.P., Elias, E., Peck, D.E., Pierson, F.B., Williams, C.J., Herrick, J.E., 2019. Climate change impacts on wind and water erosion on US rangelands. *Journal of Soil and Water Conservation* 74, 405-418, doi: <https://doi.org/10.2489/jswc.74.4.405>.
- Egan, J., 2006. Technical Resource Manual for Farm Fire Recovery, https://agex.org.au/wp-content/uploads/2016/03/Technical_Resource_Manual_for_Farm_Fire_Recovery.pdf

- FAO, 2019. Soil erosion: the greatest challenge to sustainable soil management, Rome, p. 100 pp,
- Fecan, F., Marticorena, B., Bergametti, G., 1999. Parametrization of the increase of the aeolian erosion threshold wind friction velocity due to soil moisture for arid and semi-arid areas. *Annales Geophysicae-Atmospheres Hydrospheres and Space Sciences* 17, 149-157, doi: <https://doi.org/10.1007/s005850050744>.
- Fernández, C., Vega, J.A., 2018. Evaluation of the rusle and disturbed wepp erosion models for predicting soil loss in the first year after wildfire in NW Spain. *Environmental Research* 165, 279-285, doi: <https://doi.org/10.1016/j.envres.2018.04.008>.
- Fernández, C., Vega, J.A., Jiménez, E., Fonturbel, T., 2011. Effectiveness of three post-fire treatments at reducing soil erosion in Galicia (NW Spain). *International Journal of Wildland Fire* 20, 104-114, doi: <http://dx.doi.org/10.1071/WF09010>.
- Field, J.P., Breshears, D.D., Whicker, J.J., 2009. Toward a more holistic perspective of soil erosion: Why aeolian research needs to explicitly consider fluvial processes and interactions. *Aeolian Research* 1, 9-17, doi: <http://dx.doi.org/10.1016/j.aeolia.2009.04.002>.
- Field, J.P., Breshears, D.D., Whicker, J.J., Zou, C.B., 2011a. Interactive effects of grazing and burning on wind- and water-driven sediment fluxes: rangeland management implications. *Ecological Applications* 21, 22-32, doi: <https://doi.org/10.1890/09-2369.1>.
- Field, J.P., Breshears, D.D., Whicker, J.J., Zou, C.B., 2011b. On the ratio of wind- to water-driven sediment transport: Conserving soil under global-change-type extreme events. *Journal of Soil and Water Conservation* 66, 51A-56A, doi: <https://doi.org/10.2489/jswc.66.2.51A>.
- Flanagan, D.C., Ascough, J.C., Nieber, J.L., Misra, D., Douglas-Mankin, K.R., 2013. *Advances in Soil Erosion Research: Processes, Measurement, and Modeling*. Transactions of the ASABE 56, 455-463, doi: <https://doi.org/10.13031/2013.42666>.
- Fryrear, D.W., Bilbro, J.D., Saleh, A., Schomberg, H., Stout, J.E., Zobeck, T.M., 2000. RWEQ: Improved wind erosion technology. *Journal of Soil and Water Conservation* 55, 183-189, <http://www.jswnonline.org/content/55/2/183.abstract>
- Gonçalves, A.B., Vieira, A., Leite, F.F., Martins, J., Silva, D., Soares, V., 2011. ADAPTA CLIMA: adaptation to the effects from climate change in the AVE, 3rd International Meeting of Fire Effects on Soil Properties. Nigp-Univ. Minho e Cegot, pp. 175-180, <http://hdl.handle.net/1822/19983>
- GRDC, 2015. Clay spreading and delving in light, sandy soils, in: Corporation, G.R.D. (Ed.), https://grdc.com.au/_data/assets/pdf_file/0017/142550/grdc-fs-clayspreadingdelving-south_hr-pdf.pdf

- Guerschman, J.P., Scarth, P.F., McVicar, T.R., Renzullo, L.J., Malthus, T.J., Stewart, J.B., Rickards, J.E., Trevithick, R., 2015. Assessing the effects of site heterogeneity and soil properties when unmixing photosynthetic vegetation, non-photosynthetic vegetation and bare soil fractions from Landsat and MODIS data. *Remote Sensing of Environment* 161, 12-26, doi: <https://doi.org/10.1016/j.rse.2015.01.021>.
- Hagen, L., 1991. A wind erosion prediction system to meet user needs. *Journal of Soil and Water Conservation* 46, 106-111,
- Hall, N., 2017. Reflections on the Pinery fire. Department for Communities and Social Inclusion, Government of South Australia, https://dcsi.sa.gov.au/data/assets/pdf_file/0019/53119/Reflections-on-the-Pinery-fire-web.pdf
- Hill, R.S., Beer, Y.K., Hill, K.E., Maciunas, E., Tarran, M.A., Wainman, C.C., 2016. Evolution of the eucalypts – an interpretation from the macrofossil record. *Australian Journal of Botany* 64, 600-608, doi: <https://doi.org/10.1071/BT16117>.
- Hosseini, M., Nunes, J.P., Pelayo, O.G., Keizer, J.J., Ritsema, C., Geissen, V., 2018. Developing generalized parameters for post-fire erosion risk assessment using the revised Morgan-Morgan-Finney model: A test for north-central Portuguese pine stands. *CATENA* 165, 358-368, doi: <https://doi.org/10.1016/j.catena.2018.02.019>.
- Jeanneau, A.C., Ostendorf, B., Herrmann, T., 2019. Relative spatial differences in sediment transport in fire-affected agricultural landscapes: A field study. *Aeolian Research* 39, 13-22, doi: <https://doi.org/10.1016/j.aeolia.2019.04.002>.
- Jiang, C., Zhang, H.Y., Zhang, Z.D., Wang, D.W., 2019. Model-based assessment soil loss by wind and water erosion in China's Loess Plateau: Dynamic change, conservation effectiveness, and strategies for sustainable restoration. *Global and Planetary Change* 172, 396-413, doi: <https://doi.org/10.1016/j.gloplacha.2018.11.002>.
- Lanorte, A., Cillis, G., Calamita, G., Nolè, G., Pilogallo, A., Tucci, B., De Santis, F., 2019. Integrated approach of RUSLE, GIS and ESA Sentinel-2 satellite data for post-fire soil erosion assessment in Basilicata region (Southern Italy). *Geomatics, Natural Hazards and Risk* 10, 1563-1595, doi: <https://doi.org/10.1080/19475705.2019.1578271>.
- Lawson, A., 2015. Managing bare soils following a fire. Grains Research & Development Corporation, <https://grdc.com.au/news-and-media/news-and-media-releases/south/2015/12/managing-bare-soils-following-a-fire>
- Leys, J., McTainsh, G., Strong, C., Heidenreich, S., Biesaga, K., 2008. DustWatch: using community networks to improve wind erosion monitoring in Australia. *Earth Surface Processes and Landforms* 33, 1912-1926, doi: <https://doi.org/10.1002/esp.1733>.
- Leys, J.F., Butler, H.J., Yang, X., Heidenreich, S., 2010. CEMSYS modelled wind erosion.

- Lim, J., 2016. Huge dust storm as cool change sweeps South Australia, The Advertiser, <https://www.adelaidenow.com.au/news/south-australia/storms-forecast-as-cool-change-set-to-sweep-adelaide/news-story/073e8661a6273c8560a45961ceb0e115>
- Lu, H., Shao, Y.P., 2001. Toward quantitative prediction of dust storms: an integrated wind erosion modelling system and its applications. *Environmental Modelling & Software* 16, 233-249, doi: [https://doi.org/10.1016/s1364-8152\(00\)00083-9](https://doi.org/10.1016/s1364-8152(00)00083-9).
- Lyapustin, A., Korokin, S., Wang, Y., Quayle, B., Laszlo, I., 2012a. Discrimination of biomass burning smoke and clouds in MAIAC algorithm. *Atmos. Chem. Phys.* 12, 9679-9686, doi: <https://doi.org/10.5194/acp-12-9679-2012>.
- Lyapustin, A., Martonchik, J., Wang, Y., Laszlo, I., Korokin, S., 2011a. Multiangle implementation of atmospheric correction (MAIAC): 1. Radiative transfer basis and look-up tables. *Journal of Geophysical Research: Atmospheres* 116, doi: <https://doi.org/10.1029/2010JD014985>.
- Lyapustin, A., Wang, Y., Frey, R., 2008. An automatic cloud mask algorithm based on time series of MODIS measurements. *Journal of Geophysical Research: Atmospheres* 113, doi: <https://doi.org/10.1029/2007JD009641>.
- Lyapustin, A., Wang, Y., Laszlo, I., Kahn, R., Korokin, S., Remer, L., Levy, R., Reid, J.S., 2011b. Multiangle implementation of atmospheric correction (MAIAC): 2. Aerosol algorithm. *Journal of Geophysical Research: Atmospheres* 116, doi: <https://doi.org/10.1029/2010JD014986>.
- Lyapustin, A.I., Wang, Y., Laszlo, I., Hilker, T., G.Hall, F., Sellers, P.J., Tucker, C.J., Korokin, S.V., 2012b. Multi-angle implementation of atmospheric correction for MODIS (MAIAC): 3. Atmospheric correction. *Remote Sensing of Environment* 127, 385-393, doi: <https://doi.org/10.1016/j.rse.2012.09.002>.
- May, R., 2006. Clay spreading and delving on Eyre Peninsula: a broadacre clay application manual for farmers, contractors and advisors. South Australian Research Development Institute,
- Neary, D.G., 2011. Impacts of wildfire severity on hydraulic conductivity in forest, woodland, and grassland soils (Chapter 7), *Hydraulic Conductivity Issues, Determination, and Applications*, New York, NY, pp. 123-142, https://www.fs.fed.us/rm/pubs_other/rmrs_2011_neary_d006.pdf
- O'Brien, L., 2019. slga: Data Access Tools for the Soil and Landscape Grid of Australia, R package version 1.0.1 ed, <https://github.com/obrl-soil/slga>
- Panagos, P., Borrelli, P., Meusburger, K., Lugato, E., Ballabio, C., Poesen, J., Alewell, C., Montanarella, L., 2018. Soil erosion in Europe: current status, future climate and land use scenarios, in: Zlatic, M., Kostadinov, S. (Eds.), *Soil and Water Resources Protection in the Changing Environment*, pp. 1-13, <Go to ISI>://WOS:000464898800001

- Panagos, P., Christos, K., Cristiano, B., Ioannis, G., 2014. Seasonal monitoring of soil erosion at regional scale: An application of the G2 model in Crete focusing on agricultural land uses. *International Journal of Applied Earth Observation and Geoinformation* 27, 147-155, doi: <https://doi.org/10.1016/j.jag.2013.09.012>.
- Panagos, P., Katsoyiannis, A., 2019. Soil erosion modelling: The new challenges as the result of policy developments in Europe. *Environmental Research* 172, 470-474, doi: <https://doi.org/10.1016/j.envres.2019.02.043>.
- Panico, S.C., Ceccherini, M.T., Memoli, V., Maisto, G., Pietramellara, G., Barile, R., De Marco, A., 2020. Effects of different vegetation types on burnt soil properties and microbial communities. *International Journal of Wildland Fire*, -, doi: <https://doi.org/10.1071/WF19081>.
- Prats, S.A., Malvar, M.C., Vieira, D.C.S., MacDonald, L., Keizer, J.J., 2016. Effectiveness of Hydromulching to Reduce Runoff and Erosion in a Recently Burnt Pine Plantation in Central Portugal. *Land Degradation & Development* 27, 1319-1333, doi: <https://doi.org/10.1002/ldr.2236>.
- Raupach, M., Gillette, D., Leys, J., 1993. The effect of roughness elements on wind erosion threshold. *Journal of Geophysical Research: Atmospheres* 98, 3023-3029,
- Santín, C., Doerr, Stefan H., Otero, Xosé L., Chafer, C.J., 2015. Quantity, composition and water contamination potential of ash produced under different wildfire severities. *Environmental Research* 142, 297-308, doi: <https://doi.org/10.1016/j.envres.2015.06.041>.
- Shakesby, R.A., 2011. Post-wildfire soil erosion in the Mediterranean: Review and future research directions. *Earth-Science Reviews* 105, 71-100, doi: <http://dx.doi.org/10.1016/j.earscirev.2011.01.001>.
- Shakesby, R.A., Wallbrink, P.J., Doerr, S.H., English, P.M., Chafer, C.J., Humphreys, G.S., Blake, W.H., Tomkins, K.M., 2007. Distinctiveness of wildfire effects on soil erosion in south-east Australian eucalypt forests assessed in a global context. *Forest Ecology and Management* 238, 347-364, doi: <https://doi.org/10.1016/j.foreco.2006.10.029>.
- Shao, Y., Raupach, M., Leys, J., 1996. A model for predicting aeolian sand drift and dust entrainment on scales from paddock to region. *Soil Research* 34, 309-342, doi: <http://dx.doi.org/10.1071/SR9960309>.
- Shillito, R., Miller, J., Etyemezian, V., Mizell, S., 2012. Wind and Water Erosion Potential of Fire-Affected Soils: Immediate and Short-Term Effects in a Desert Ecosystem, *World Environmental and Water Resources Congress 2012*, pp. 1727-1736, doi: <https://doi.org/10.1061/9780784412312.171>.
- Su, C.-H., Eizenberg, N., Steinle, P., Jakob, D., Fox-Hughes, P., White, C., Rennie, S., Franklin, C., Dharssi, I., Zhu, H., 2019. BARRA v1.0: The Bureau of Meteorology Atmospheric high-resolution Regional Reanalysis for Australia. *Geoscientific*

Model Development 12, 2049-2068, doi: <https://doi.org/10.5194/gmd-12-2049-2019>.

Tadono, T., Ishida, H., Oda, F., Naito, S., Minakawa, K., Iwamoto, H., 2014. Precise Global DEM Generation by ALOS PRISM. ISPRS Ann. Photogramm. Remote Sens. Spatial Inf. Sci. II-4, 71-76, doi: <https://doi.org/10.5194/isprsannals-II-4-71-2014>.

Teng, H., Viscarra Rossel, R.A., Shi, Z., Behrens, T., Chappell, A., Bui, E., 2016. Assimilating satellite imagery and visible–near infrared spectroscopy to model and map soil loss by water erosion in Australia. Environmental Modelling & Software 77, 156-167, doi: <https://doi.org/10.1016/j.envsoft.2015.11.024>.

Varela, M., Benito, E., Keizer, J., 2010. Wildfire effects on soil erodibility of woodlands in NW Spain. Land degradation & development 21, 75-82, doi: <https://doi.org/10.1002/ldr.896>.

Vega, S.P., Williams, C.J., Brooks, E.S., Pierson, F.B., Strand, E.K., Robichaud, P.R., Brown, R.E., Seyfried, M.S., Lohse, K.A., Glossner, K., Pierce, J.L., Roehner, C., 2020. Interaction of wind and cold-season hydrologic processes on erosion from complex topography following wildfire in sagebrush steppe. Earth Surface Processes and Landforms 45, 841-861, doi: <https://doi.org/10.1002/esp.4778>.

Vieira, D.C.S., Serpa, D., Nunes, J.P.C., Prats, S.A., Neves, R., Keizer, J.J., 2018. Predicting the effectiveness of different mulching techniques in reducing post-fire runoff and erosion at plot scale with the RUSLE, MMF and PESERA models. Environmental Research 165, 365-378, doi: <https://doi.org/10.1016/j.envres.2018.04.029>.

von Holdt, J.R., Eckardt, F.D., Wiggs, G.F.S., 2017. Landsat identifies aeolian dust emission dynamics at the landform scale. Remote Sensing of Environment 198, 229-243, doi: <https://doi.org/10.1016/j.rse.2017.06.010>.

Wagenbrenner, N., Chung, S., Lamb, B., 2017. A large source of dust missing in Particulate Matter emission inventories? Wind erosion of post-fire landscapes. Elementa: Science of the Anthropocene. 5: 2. 5, doi: <http://doi.org/10.1525/elementa.185>.

Wagenbrenner, N.S., Germino, M.J., Lamb, B.K., Robichaud, P.R., Foltz, R.B., 2013. Wind erosion from a sagebrush steppe burned by wildfire: Measurements of PM10 and total horizontal sediment flux. Aeolian Research 10, 25-36, doi: <https://doi.org/10.1016/j.aeolia.2012.10.003>.

Wang, X.X., Liu, T.X., Li, F.L., Gao, R.Z., Yang, X.M., Duan, L.M., Luo, Y.Y., Li, R., 2014. Simulated soil erosion from a semiarid typical steppe watershed using an integrated aeolian and fluvial prediction model. Hydrological Processes 28, 325-340, doi: 10.1002/hyp.9579.

Webb, N.P., Herrick, J.E., Van Zee, J.W., Courtright, E.M., Hugenholtz, C.H., Zobeck, T.M., Okin, G.S., Barchyn, T.E., Billings, B.J., Boyd, R., Clingan, S.D., Cooper, B.F.,

Duniway, M.C., Derner, J.D., Fox, F.A., Havstad, K.M., Heilman, P., LaPlante, V., Ludwig, N.A., Metz, L.J., Nearing, M.A., Norfleet, M.L., Pierson, F.B., Sanderson, M.A., Sharratt, B.S., Steiner, J.L., Tatarko, J., Tedela, N.H., Toledo, D., Unnasch, R.S., Van Pelt, R.S., Wagner, L., 2016. The National Wind Erosion Research Network: Building a standardized long-term data resource for aeolian research, modeling and land management. *Aeolian Research* 22, 23-36, doi: <http://dx.doi.org/10.1016/j.aeolia.2016.05.005>.

Willoughby, N., Thompson, D., Royaland, M., Miles, M., 2018. South Australian Land Cover Layers: an Introduction and Summary Statistics. Government of South Australia, Department for Environment and Water (DEW), Adelaide, Australia, <https://data.environment.sa.gov.au/Content/Publications/SA-Land-Cover-Layers-1987-2015-Technical-Summary.pdf>

Woodruff, N., Siddoway, F., 1965. A wind erosion equation. *Soil Science Society of America Journal* 29, 602-608,

Yang, X., 2020. State and trends of hillslope erosion across New South Wales, Australia. *CATENA* 186, 104361, doi: <https://doi.org/10.1016/j.catena.2019.104361>.

Young, M.-A., Woodard, D., Hughes, B., Masters, B., 2017. Emergency measures to curb wind erosion, in: Australia, P.I.a.R.S. (Ed.). Rural Solutions SA,

Appendix E

Table E.1 Zonal stats results post-fire (continued). The values in bold represent an increase in erosion compared to monthly averages.

Fire name	Fire date	Date	Water erosion (kg ha ⁻¹ month ⁻¹)		Wind erosion (kg ha ⁻¹ month ⁻¹)		Rainfall erosivity (MJ mm ha ⁻¹ h ⁻¹)	Ground cover (%)	Wind speed (m s ⁻¹)
			Post-fire	2001-2017 average	Post-fire	2001-2017 average			
Pinery	2015-11-25	Nov-2015	7.4	1.4	0.317	0.350	160.7	84	9.5
		Dec-2015	0.3	1.6	0.371	0.495	0.8	45	9.8
		Jan-2016	49.2	10.0	0.380	0.445	111.2	42	10.6
		Feb-2016	12.5	2.2	0.249	0.292	28.4	41	8.5
		Mar-2016	16.5	3.1	0.097	0.231	48.9	47	7.0
		Apr-2016	3.0	3.4	0.213	0.150	9.9	48	7.4
		May-2016	5.3	2.2	0.281	0.098	33.9	61	9.4
Butra	2005-12-23	Dec-2005	0.3	5.1	0.682	0.393	3.4	72	12.3
		Jan-2006	8.1	21.9	0.167	0.314	25.2	54	10.6
		Feb-2006	0.2	4.8	0.227	0.186	0.6	54	9.2
		Mar-2006	21.1	2.5	0.200	0.187	68.4	55	8.5
		Apr-2006	3.3	2.8	0.395	0.168	16.3	61	9.6
		May-2006	1.7	1.7	0.187	0.154	17.9	73	7.7
		Jun-2006	0.2	1.5	0.051	0.140	3.8	79	6.8
Pinkawillinie Conservation Reserve	2005-12-27	Dec-2005	0.0	1.1	0.144	0.357	3.9	72	10.0
		Jan-2006	1.6	1.8	0.351	0.374	18.0	48	9.8
		Feb-2006	1.6	1.1	0.325	0.277	11.7	40	9.1
		Mar-2006	1.5	2.1	0.258	0.197	10.4	41	8.2
		Apr-2006	0.1	0.3	0.227	0.112	1.0	40	7.8
		May-2006	6.4	0.6	0.100	0.072	25.2	41	6.5
		Jun-2006	0.1	0.1	0.064	0.040	1.4	58	5.7
Wangary	2005-01-10	Jan-2005	0.0	1.0	0.327	0.370	0.3	70	12.0
		Feb-2005	0.2	1.4	0.240	0.246	0.9	56	10.1
		Mar-2005	0.5	1.7	0.222	0.143	2.2	57	9.5
		Apr-2005	1.6	1.6	0.175	0.072	6.	58	8.6
		May-2005	11.4	2.6	0.087	0.034	45.6	58	7.3
		Jun-2005	7.5	2.6	0.065	0.015	79.0	77	9.5
		Jul-2005	2.0	1.8	0.003	0.005	34.9	84	7.6

	Jan-2012	5.9	7.6	0.088	0.182	41.1	70	11.5
	Feb-2012	15.7	5.0	0.053	0.121	153.1	67	9.9
	Mar-2012	1.2	1.8	0.039	0.114	14.7	74	9.5
Woolundunga	Apr-2012	0.0	0.8	0.037	0.091	0.1	74	8.9
	May-2012	1.9	1.1	0.063	0.064	21.9	73	9.0
	Jun-2012	1.1	1.4	0.038	0.041	17.6	77	9.6
	Jul-2012	0.6	1.0	0.009	0.025	11.3	80	8.1
	Jan-2014	0.2	0.6	0.419	0.408	13.1	71	10.4
	Feb-2014	7.8	0.6	0.322	0.287	202.7	56	10.2
	Mar-2014	0.9	0.4	0.223	0.225	30.4	59	9.3
Kiana	Apr-2014	0.4	0.3	0.178	0.176	20.0	62	8.1
	May-2014	0.5	0.2	0.090	0.163	48.5	74	7.2
	Jun-2014	0.2	0.4	0.191	0.146	53.2	87	10.0
	Jul-2014	0.2	0.1	0.138	0.133	57.8	88	10.6
	Jan-2014	0.1	0.4	0.263	0.258	9.1	65	12.2
	Feb-2014	0.2	0.3	0.265	0.193	9.0	53	10.3
	Mar-2014	0.0	0.3	0.161	0.113	1.1	52	8.5
Yumbarra Complex	Apr-2014	0.7	0.2	0.102	0.046	30.0	55	7.5
	May-2014	0.7	0.1	0.024	0.025	43.8	63	6.5
	Jun-2014	0.1	0.1	0.081	0.017	6.1	70	7.6
	Jul-2014	0.0	0.1	0.095	0.019	3.1	68	8.5
	Jan-2014	0.3	5.5	0.092	0.124	6.4	83	12.9
	Feb-2014	46.9	3.7	0.051	0.082	505.4	71	9.8
	Mar-2014	2.5	0.8	0.043	0.064	24.0	68	8.8
Bangor	Apr-2014	4.1	0.8	0.033	0.042	49.2	74	8.1
	May-2014	2.4	0.8	0.009	0.031	58.9	80	8.3
	Jun-2014	0.9	1.1	0.016	0.020	23.7	82	9.4
	Jul-2014	0.3	0.7	0.013	0.008	10.7	85	10.1

Fire name	Fire date	Date	Water erosion (kg ha ⁻¹ month ⁻¹)		Wind erosion (kg ha ⁻¹ month ⁻¹)		Rainfall erosivity (Mj mm ha ⁻¹ h ⁻¹)	Ground cover (%)	Wind speed (m s ⁻¹)
			Post-fire	2001-2017 average	Post-fire	2001-2017 average			
Tulka	2001-02-01	Feb-2001	0.059	0.008	0.055	0.029	17.4	65	9.9
		Mar-2001	0.072	0.009	0.082	0.017	15.8	60	9.2
		Apr-2001	0.003	0.004	0.056	0.014	0.8	60	7.6
		May-2001	0.128	0.016	0.072	0.007	48.6	65	7.4
		Jun-2001	0.029	0.008	0.001	0.003	21.0	70	7.2
		Jul-2001	0.02	0.007	0.003	0.002	64.0	81	6.8
		Aug-2001	0.014	0.006	0.086	0.009	28.2	77	10.4
		Aug-2007	0.1	0.2	0.321	0.097	1.1	43	7.8
Pureba Conservation Park	2007-02-19	Feb-2007	0.1	1.6	0.169	0.307	5.8	64	9.4
		Mar-2007	5.0	6.7	0.132	0.204	65.8	48	8.3
		Apr-2007	0.4	0.3	0.152	0.104	4.3	46	8.0
		May-2007	0.3	0.2	0.073	0.060	3.7	49	7.6
		Jun-2007	0.1	0.2	0.016	0.033	1.9	56	5.7
		Jul-2007	0.1	0.2	0.105	0.047	1.5	58	7.6
		Aug-2007	0.1	0.2	0.321	0.097	1.1	43	7.8
		Aug-2007	0.1	0.2	0.321	0.097	1.1	43	7.8

Chapter 5

Relative spatial differences in sediment transport in
fire-affected agricultural landscapes: A field study

Published in: Aeolian Research

Statement of Authorship

Title of Paper	Relative spatial differences in sediment transport in fire-affected agricultural landscapes: A field study
Publication Status	<input checked="" type="checkbox"/> Published <input type="checkbox"/> Accepted for Publication <input type="checkbox"/> Submitted for Publication <input type="checkbox"/> Unpublished and Unsubmitted work written in manuscript style
Publication Details	Jeanneau, A., Ostendorf, B. & Herrmann, T.(2019). Relative spatial differences in sediment transport in fire-affected agricultural landscapes: A field study. <i>Aeolian research</i> 39, 13-22, https://doi.org/10.1016/j.aeolia.2019.04.002


Principal Author


Name of Principal Author (Candidate)	Amelie Jeanneau	
Contribution to the paper	Conceptualization, methodology, data curation, formal analysis, writing – original draft preparation, writing – review and editing.	
Overall percentage (%)	70%	
Certification	This paper reports on original research I conducted during the period of my Higher Degree by Research candidature and is not subject to any obligations or contractual agreements with a third party that would constrain its inclusion in this thesis. I am the primary author of this paper.	
Signature		Date: 04/06/2020

Co-author Contributions

By signing the Statement of Authorship, each author certifies that:

- i. the candidate's stated contribution to the publication is accurate (as detailed above);
- ii. permission is granted for the candidate to include the publication in the thesis; and
- iii. the sum of all co-author contributions is equal to 100% less the candidate's stated contribution.

Name of Co-Author	Tim Herrmann	
Contribution to the Paper	Conceptualization, methodology, formal analysis, writing – review and editing.	
Signature		Date: 04/06/2020

Name of Co-Author	Bertram Ostendorf	
Contribution to the Paper	Conceptualization, methodology, formal analysis, writing – review and editing.	
Signature		Date: 04/06/2020

Abstract

Fires can considerably increase wind erosion risk in dryland agricultural regions. While wind erosion post-fire has been extensively studied in rangeland and grazing landscapes, limited work has considered post-fire erosion on annual plant communities and annual crops. Here we evaluated the relative spatial differences in patterns of sediment transport between burnt and unburnt crop stubble sites. Following a severe wildfire, we studied the spatio-temporal patterns of aeolian sediment transport with an array of Modified Wilson and Cooke (MWAC) dust samplers on adjacent burnt and unburnt wheat stubble. Sediment collection was conducted during nine weeks over an area of 3 hectares. Collection rates were converted to horizontal sediment flux to derive spatial distribution maps and perform statistical analysis. Compared to the unburnt plot, we observed that sediment transport was up to 1000 times higher within the burnt area. This could lead to damages to emerging annual crops sown after the fire if no management strategy was applied. There was only negligible sediment flux in areas with shallow and low-density stubble, which gradually increased with distance from the unburnt area. These results suggest that strips of remaining unburnt stubble could provide a potential benefit to adjacent burnt or bare plots. Patterns of sediment transport were consistent in all sampling periods and were observed at a spatial scale undetectable in wind tunnel studies, indicating that field observations could complement fine-scale experimental studies to assess environmental processes in real-life conditions.

5.1 Introduction

Wind erosion strongly impacts agricultural productivity and public health. It generates on-site disturbances such as loss of topsoil leading to a decline in nutrients, organic matter and soil carbon, or damages to crops and infrastructure through sandblasting and burial (Bennell et al., 2007; Kontos et al., 2018; Panebianco et al., 2016). Consequences include the cost of nutrient replacement, purchase of new grain seeds and lost

productivity. Wind erosion also generates off-site damages such as visibility limitation leading to road safety and transport issues, health impacts including asthma and other respiratory problems (Baddock et al., 2014; Li et al., 2018; Seinfeld and Pandis, 2012) as well as cleaning costs due to dust deposition and road maintenance. A substantial body of research have identified factors and parameters controlling wind erosion (Mayaud et al., 2017; Tatarko et al., 2013; Webb et al., 2016; Zobeck et al., 2003), but there is a paucity of studies relating soil erosion to consequences of extreme environmental disturbances like wildfires (Mayaud et al., 2017; Vermeire et al., 2005; Whicker et al., 2006).

Low rainfall agricultural regions in Mediterranean winter-rain climates are at high risk of soil loss due to a combination of low vegetation cover with potentially high wind events. Consequently, many studies have demonstrated that vegetation cover is the most effective way to control aeolian sediment transport (Chappell et al., 2019; McKenzie and Dixon, 2006; Shao, 2008; Vacek et al., 2018). Conservation agriculture is an increasingly common farming system in dryland agricultural regions as it aims to maintain vegetation cover for most of the year. In such areas, the erosion risk window generally occurs during autumn through to crop establishment or early winter. However, even with the best practices, catastrophic events and major types of disturbances such as wildfires can destroy the protective non-photosynthetic vegetation cover and increase erosion risk (Mayaud et al., 2017; Nordstrom and Hotta, 2004).

Fires are a dominant type of environmental disturbance, and they are unpredictable. They also remove protective vegetation cover of annual non-woody plants, increasing erosion risk in regions prone to wind erosion. Based on future climate forecast, in dryland agricultural regions, fires are expected to be more intense and more frequent, due to climate change, leading to an increase in erosion risk (Clarke et al., 2011; Gonçalves et al., 2011). In hot climates, even sparse vegetation can carry fires (Turner et al., 2011). Fires often occur during drier months, and if they occur early in the fire-danger season, they will leave soils bare for longer as summer rainfalls become more sporadic (CSIRO and Bureau of Meteorology, 2015; Williams et al., 2009).

Extensive research has studied wind erosion on agricultural croplands (Hagen, 1988; Retta et al., 1996; Tatarko et al., 2013; Zobeck et al., 2003), but there is limited evidence of the impact of fires in dryland agriculture on wind erosion (Breshears et al., 2003; Ravi et al., 2012). Only a few studies directly compared wind erosion from burnt and unburnt plots simultaneously (Dukes et al., 2018; Merino-Martín et al., 2014; Miller et al., 2012; Wagenbrenner et al., 2013) and most of them only considered desert or grazing landscapes. Vegetation reduces wind velocity by applying a sheltering effect on exposed soil as clearly demonstrated in wind tunnel experiments and some field studies (Billbro and Stout, 1999; Cornelis and Gabriels, 2005). However, there is a lack of information on the effect of unburnt vegetation patches on aeolian transport in cropped regions. Enhancing our predictive understanding of the link between erosion processes and catastrophic events such as wildfires is increasingly important in light of global climate change.

This study aims to assess the relative spatial differences in patterns of sediment transport between burnt and unburnt stubble patches after catastrophic wildfire events. Such information is challenging to obtain quantitatively because of their sizeable spatial extent and associated logistic difficulties to design controlled experiments, the rarity of wildfires in agricultural landscapes, and the emotional status of affected landholders after the fire. Here we report measurements taken after a severe wildfire that burnt 12,000 hectares of crops and pastures but left a small area of stubble unburnt which allowed for a paired sampling design.

5.2 Material and Method

5.2.1 Site description

The study site is located near Keith in southern South Australia, Australia (Lat. 36°01'S, Long. 140°34'E, 73m elevation) (Figure 5.1). Mean annual precipitation for this district generally ranges between 350-450mm with predominant autumn-winter rainfall from May through to September. At the town of Keith, located 20km west of the site, mean

annual maximum temperatures are of 22.3°C and mean annual minimum temperature of 9.1°C (Australian Bureau of Meteorology, <http://www.bom.gov.au/climate/data/>). Historically, most erosive and prevailing near-surface winds are from W to SW. Soils on the site are recorded as deep sands over clays, prone to wind erosion if unprotected.

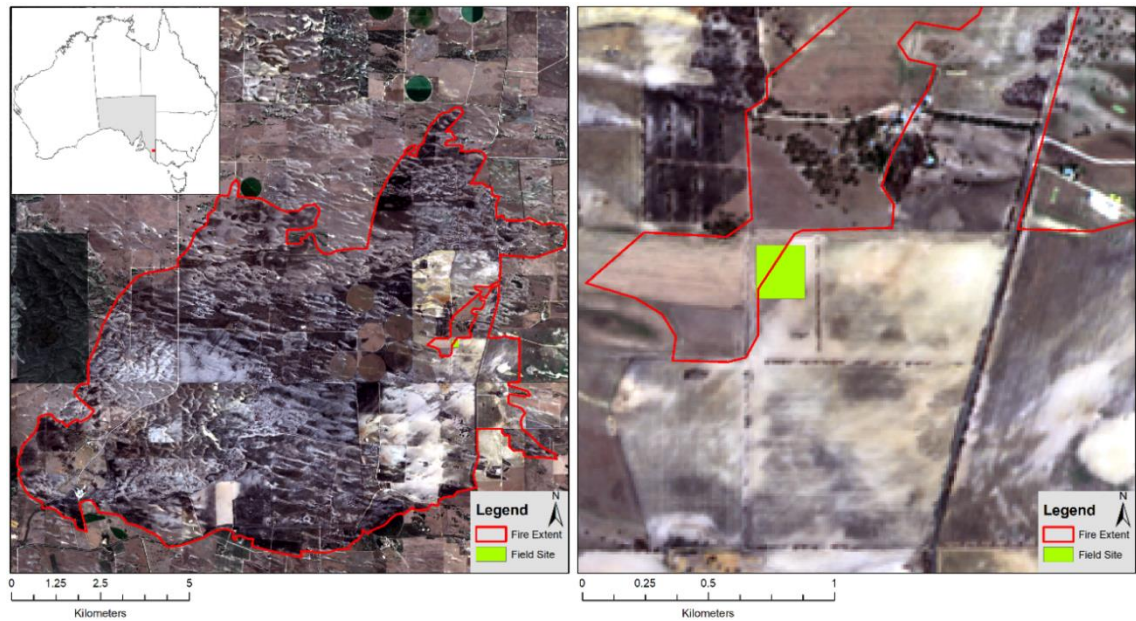


Figure 5.1 Location map and extent of the Sherwood fire, Sherwood, South Australia. The imagery was sourced from the European Space Agency (ESA) Copernicus – Sentinel 2 imagery, 03 February 2018. Within the fire boundary, darker colours represent charred vegetation; lighter cream colour represents exposed bare sands. Sand drifts can be observed predominantly in the south-eastern corner of fire extent.

The site was established on adjacent burnt and un-burnt wheat stubble following a severe fire that swept through the area between 6th and 7th January 2018. The study site was planted with a wheat crop with rows orientated North to South under no-till farm management. The field was harvested three weeks before the fire. To enhance water-holding capacity and improve the soil, this paddock was spread with clay five years ago. The land around the study site was also affected by the fire and spread with clay between the 9th and 23rd of March by the landholder as a recovery measure to increase surface roughness in an attempt to limit wind erosion.

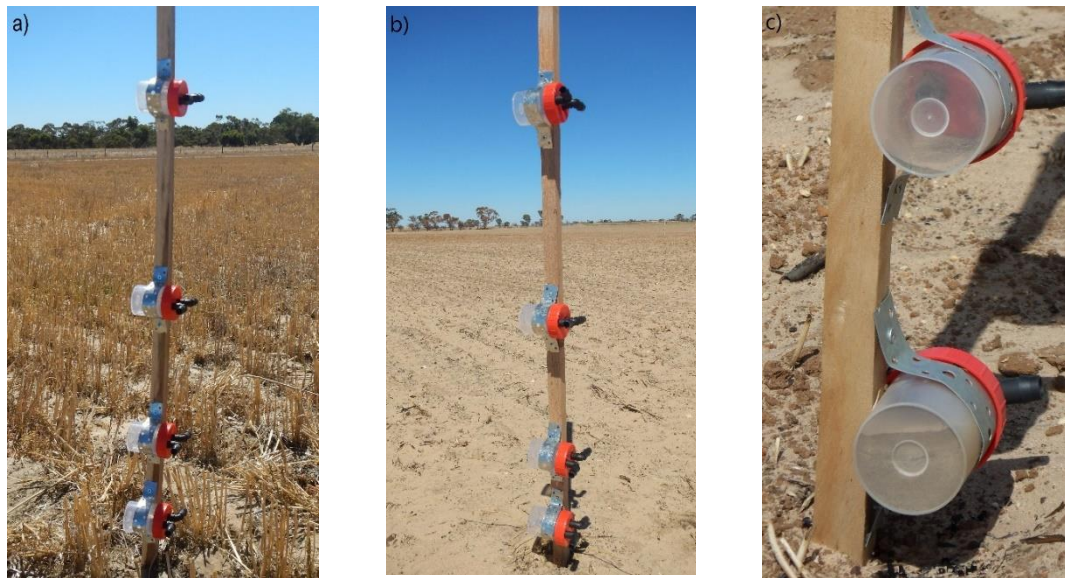


Figure 5.2 Dust samplers in the field, a) sediment sampler on unburnt wheat stubble, b) sediment sampler on the burnt bare ground, c) lower collecting cups filled with deposited sediment.

5.2.2 Monitoring design

Our monitoring design was adapted from the USDA (United States Department of Agriculture) wind erosion monitoring standardised methods (Webb et al., 2015). To monitor spatial variability in sediment transport influenced by fires, we established two 100m x 100m study plots within the same partly burned paddock. We set one site on unburnt wheat stubble (Figure 5.2a) and another on the adjacent bare ground (Figure 5.2b) with an exposed open fetch of about 300m by 150m extending to the south-west of the site. We will then refer to the treatments as unburnt and burnt. To improve the assessment of spatial patterns of sediment transport, we also installed sediment sampler every 40 m along a transect between the burnt and unburnt plots (Figure 5.3).

Horizontal sediment flux represents a measure of the wind-driven mass of sediments moving horizontally along the Earth surface at a particular height measured by a single sampler. Sediment transport was monitored with Modified Wilson and Cooke (MWAC) dust samplers (Wilson and Cooke, 1980). Preference was given to this type of equipment as they are efficient sediment traps, cost-effective and relatively easy to use and maintain. MWACs have a simple design: collection chambers are mounted on a rotating pole at four different sampling heights (0.1, 0.25, 0.5, 0.85m) with a wind vane that orients

sampler inlets to face the wind. Due to manufacturing and time constraints, we decided to position the collector inlets to face the most dominant winds' direction (south-westerly winds). We acknowledge that this design has affected the efficiency of the MWAC collectors as they were not calibrated to collect airborne sediments in a single direction, however, this approach has been successfully applied by others to estimate the order of magnitude and spatial variability in local sediment transport (Farrell et al., 2012; Sherman et al., 2014; Van Jaarsveld, 2008).

In the standardised methods of Webb et al. (2015), the monitoring sites are divided into a 3x3 grid with three randomly located sediment samplers in each of the nine cells (total of 27 masts per site). The standard design was adopted in the burnt area, but due to the limited size of the unburnt patch, we could only establish a 2x3 grid with 18 masts in the unburnt section (Figure 5.3).

Due to emergency work required to limit soil erosion and land management constraints, monitoring commenced six weeks after the fire (26/Feb/2018), and samples were collected at three-week intervals over the next nine weeks (20/March, 12/April, 4/May). Half-hourly wind data was obtained from a local weather station in Keith (20km west of the site). Vegetation height and soil surface cover were estimated at site establishment on each plot along three 100m transects intersecting at 50m in the centre of the plot spaced by a 60° angle (Figure 5.3). Soil samples were taken following standard methods of Webb et al. (2015), and soil texture was defined by a hand texturing method (National Committee on Soil Terrain Committee, 2009).

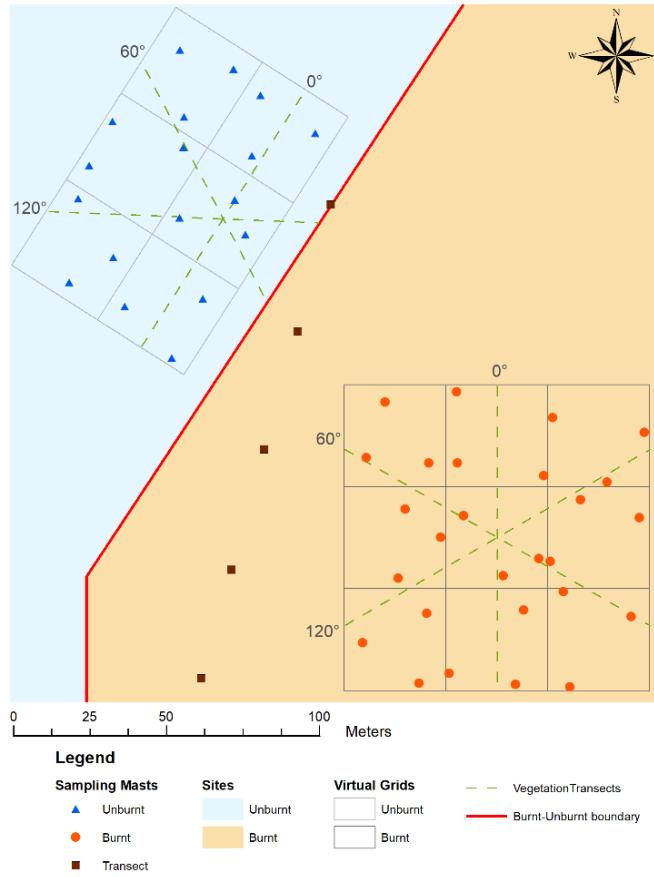


Figure 5.3 Experimental layout showing the spatial distribution of sampling masts and the position of the vegetation transects.

5.2.3 Sediment analysis

5.2.3.1 Horizontal sediment flux

After collection, sediments were dried in the lab and weighed on a high precision scale (0.0001 g). We then converted the measurements to horizontal sediment mass flux by normalising the weight with tube inlet area (0.7854 cm²) and the time of collection to obtain a time-averaged horizontal mass flux $q_{(z)}$ as

$$q_{(z)} = mass \times area^{-1} \times time^{-1} \quad (25)$$

where $mass$ is in g of sediments collected, $area$ is the size of the tube inlet area in m² and $time$ is the sampling interval in days. The units $q_{(z)}$ are expressed in grams per square metre opening per day.

The total observed horizontal sediment flux (Q_i) for a sampling mast i was estimated as the mean of time-averaged horizontal mass flux $q_{(z)i}$ over all collection heights using the following expression:

$$Q_i = \sum (q_{(10cm)i} + q_{(25cm)i} + q_{(50cm)i} + q_{(85cm)i})/4 \quad (26)$$

where Q_i is expressed in grams per square metre opening per day.

This simple averaging approach has been used in similar settings (Belnap et al., 2009; Breshears et al., 2009; Duniway et al., 2015; Miller et al., 2012) but differs from standard methods using exponential decay functions to vertically integrate horizontal sediment flux estimates (Bergametti and Gillette, 2010; Gillette and Ono, 2008). However, sediment flux on the unburnt plot in our study area could not be described with an exponential decay function because the highest fluxes occurred at 50 cm and 85 cm height. Such pattern is likely due to the dust samplers being located in stable settings (wheat stubble) and primarily collected sediments generated far upwind or from the adjacent burnt area. Therefore, we chose to apply equation (26) to estimate the vertically averaged total horizontal sediment flux.

5.2.3.2 Spatial interpolation

In order to visualise how spatial patterns of sediment transport changed in time and with height, we generated maps of horizontal sediment mass flux (Q) for each collection period (Figure 5.5) and maps of time-averaged mass flux ($q_{(z)}$) for each sampling height over the total nine weeks (Figure 5.6). These maps were derived from sediment flux point data using Kriging (ArcGIS 10.5 Interpolation Toolbox with default parameters: spherical semi-variogram, variable search radius with 12 points, and output cell size of 0.9m). Kriging is a standard method of interpolation and was shown to be one of the most reliable two-dimensional spatial estimator (Chappell et al., 2003). We applied a mask to dim areas of high kriging uncertainty in the maps to aid visual interpretation of patterns. This mask was subjectively based on visual identification of areas with high kriging variance at the different sampling periods.

5.2.3.3 Statistical analysis

We used regression modelling to examine the relative influence and interactions of experimental parameters (horizontal and vertical dimensions, burnt/unburnt treatment, time) on horizontal sediment transport. Data preparation for the statistical analysis included the estimation of the shortest distance from each sampling mast to the burnt/unburnt boundary measured with the Proximity Toolbox (Near tool, ArcGIS 10.5). We employed linear mixed-effect models (*nlme* package, Pinheiro et al. (2018), R Development Core Team (2010)) for the regression analysis. In addition, we visualised the effect of distance to the burnt/unburnt boundary on sediment flux using LOESS regression.

Initial testing of regression modelling of horizontal sediment transport showed that residuals did not meet model assumptions of normality and constant variance. Normality of residuals was obtained through log-transformation of horizontal sediment flux. Variance changed within the study area, leading to a wide-tailed distribution of residuals that needed to be considered in the model structure.

Such a high variance was not surprising in an environment of high natural spatio-temporal variability of environmental factors (i.e. wind, soils, topography, canopy surface). The *nlme* mixed-effects models allow non-constant variance among sampling units. We initially used two models to explore if variance differed amongst grids, or whether those differences occurred among sampling locations at the within-grid scale. Examination of residuals and quantile-quantile plots indicated that the two linear mixed-effect models satisfied normality assumptions and hence the final model choice was based on the Akaike Information Criterion (AIC) (Akaike, 1973). This exercise revealed that finer scale sampling (point observations) better explained the variance in total horizontal sediment flux than grid level sampling ($AIC_{mod1} = 596.5$, $AIC_{mod2} = 681.7$). Similar method considerations were employed by Chappell et al. (2003) who observed that nested point sampling of airborne sediments outperformed grid and random sampling layouts.

Therefore, the final model structure used log-transformed horizontal sediment transport with the fixed effects treatment type (unburnt, burnt), direct distance to the burnt/unburnt boundary, collection period and height (with interactions between parameters) including all possible two-, three-, and four-way interactions. As random effects, we used the sampling grid location within the plots and the specific dust sampler's position within each grid of each plot.

5.3 Results

5.3.1 Meteorological conditions and surface cover

Wind direction was not constant in the region throughout the experiment. It predominately originated from the South and South-West in the first collection period with speeds up to 12.8 m s^{-1} (46 km h^{-1}), from the West-South-West and South-West in the second collection period with velocities up to 15 m s^{-1} (54 km h^{-1}) and from West to North with speeds up to 18.6 m s^{-1} (67 km h^{-1}) (Figure 5.4). Winds were the strongest in the final collection period. However, the weather remained mostly dry with less than 41mm of rain between 24/Feb/2018 and 04/May/2018, almost half of the precipitation has been recorded during a single event on 04/May/2018 (19 mm). The average maximum daily temperature was recorded at 26.4°C for the length of our monitoring study.

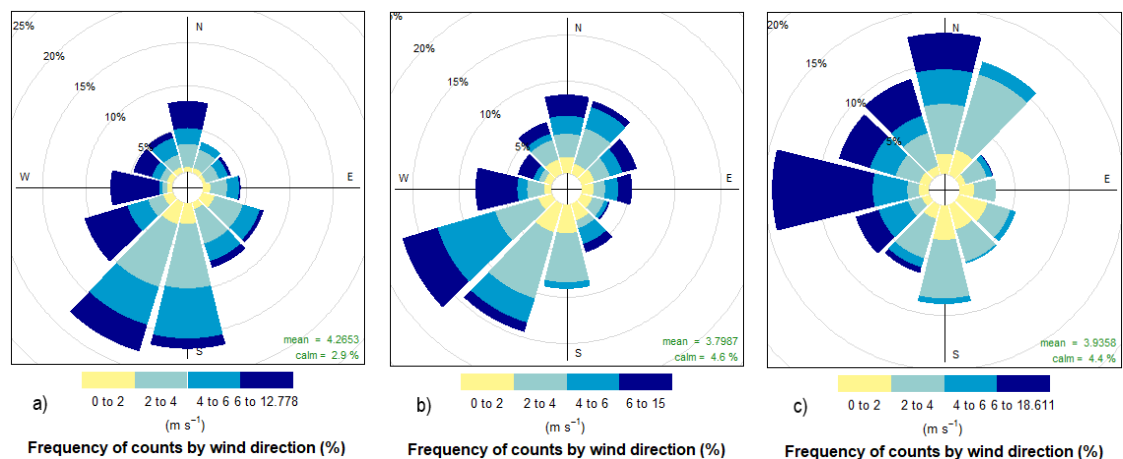


Figure 5.4 Wind roses representing wind speed and direction for the study area. a) collection weeks 1-3, b) collection weeks 4-6, c) collection weeks 7-9. Note the different frequency scale for collection week 7-9.

Wheat stubble on the unburnt patch had an average height of 20cm (± 2 cm) with a 20cm row spacing, and an average bare surface of 4.7% ($\pm 0.9\%$). Soil texture across the unburnt plot was sandy loam, and no soil crusting was observed at site establishment (Table 5.1). On the burnt plot, the fire consumed all of the vegetation (wheat stubble), only charred roots remained (1.3cm height ± 0.7 cm), and no regrowth was detected between February and May 2018. We recorded an average bare surface of 54% ($\pm 9.5\%$). Soil texture within the burnt plot was sandy loam, and soil crusting was observed on 47.6% ($\pm 2.9\%$) of the plot (Table 5.1).

5.3.2 Spatial distribution of sediment flux

When comparing the spatial distribution of total horizontal sediment flux (Q) between the three sampling dates, we can observe a recurring pattern common to all collection periods (Figure 5.5). Sediment transport was higher in the south-eastern corner of the burnt plot, which was the furthest away from the unburnt stubble boundary. There was also more spatial variability in horizontal sediment flux within the burnt plot compared to the unburnt patch. Total horizontal sediment flux in the last collection period (weeks 7-9) has almost decreased by half. Even if winds were the strongest during this collection period, the low sediment transport recorded could be explained by the fact that dust samplers were facing South-West and North-East directions while winds mostly originated from West to Northerly angles. Additionally, the last collection period recorded wetter conditions than the other two (37mm as opposed to 1.5mm) which could have also impacted the quantity of sediment collected.

Table 5.1 Summary of the soil surface conditions and vegetation states for the burnt and unburnt study plots, based on measurements collected

	Unburnt		
	<i>Transect 0°</i>	<i>Transect 60°</i>	<i>Transect 120°</i>
Soil texture	SL	SL	SL
Vegetation state	Crop Stubble	Crop Stubble	Crop Stubble
Average vegetation height (cm)	20.2	19.7	20.2
Soil surface type	S, L, FG, GR	S, L, FG, GR	S, L, FG, GR
Proportion of BS (%)	4	6	4
Proportion with PC surface type (%)	0	0	0
Proportion with FG surface type (%)	33	40	33
Proportion with GR surface type (%)	30	33	31

(SL: sandy loam, BS: bare soil, S: soil, PC: physical crust, L: litter, FG: fragments size 2-5mm, GR: 5mm < fragments size < 76mm)

	Burnt		
	<i>Transect 0°</i>	<i>Transect 60°</i>	<i>Transect 120°</i>
Soil texture	SL	SL	SL
Vegetation state	Charred Roots, BS	Charred Roots, BS	Charred Roots, BS
Average vegetation height (cm)	1.4	1.4	1.2
Soil surface type	PC, S, L, FG, GR	PC, S, L, FG, GR	PC, S, L, FG, GR
Proportion of BS (%)	49	54	59
Proportion with PC surface type (%)	51	48	44
Proportion with FG surface type (%)	38	33	31
Proportion with GR surface type (%)	33	32	33

(SL: sandy loam, BS: bare soil, S: soil, PC: physical crust, L: litter, FG: fragments size 2-5mm, GR: 5mm < fragments size < 76mm)

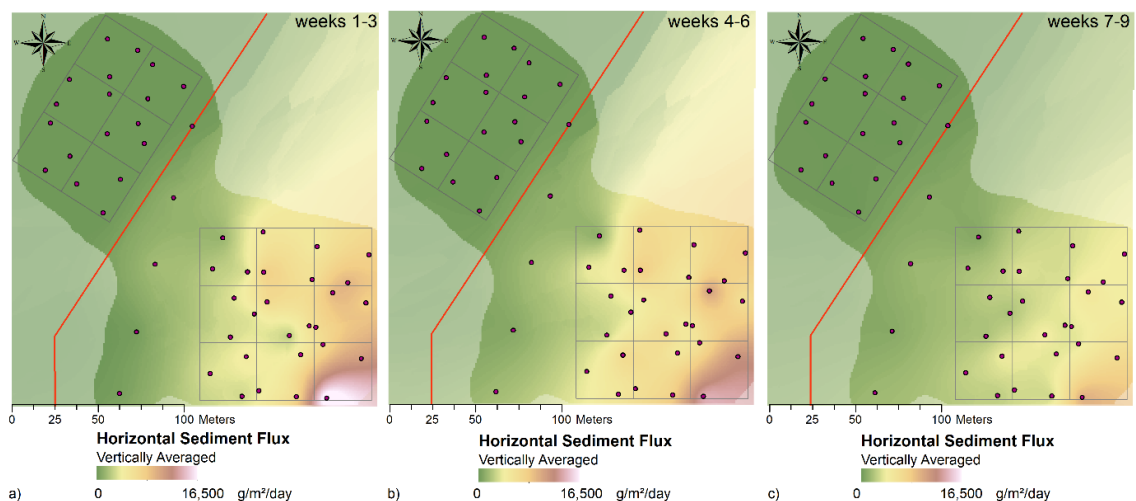


Figure 5.5 Vertically averaged horizontal sediment flux spatial distribution maps. a) collection weeks 1-3, b) collection weeks 4-6, c) collection weeks 7-9. The dots represent the MWAC dust sampler, and the two virtual sampling grids are outlined in grey.

Height-resolved time-averaged horizontal sediment flux: $q_{(z)}$ (mean of all collection periods) indicates similar spatial distribution patterns for each sampling height (Figure 5.6). These maps illustrate that total horizontal sediment flux increased with the direct distance from the unburnt stubble into the exposed part and reached its highest value in the south-eastern corner of the burnt plot.

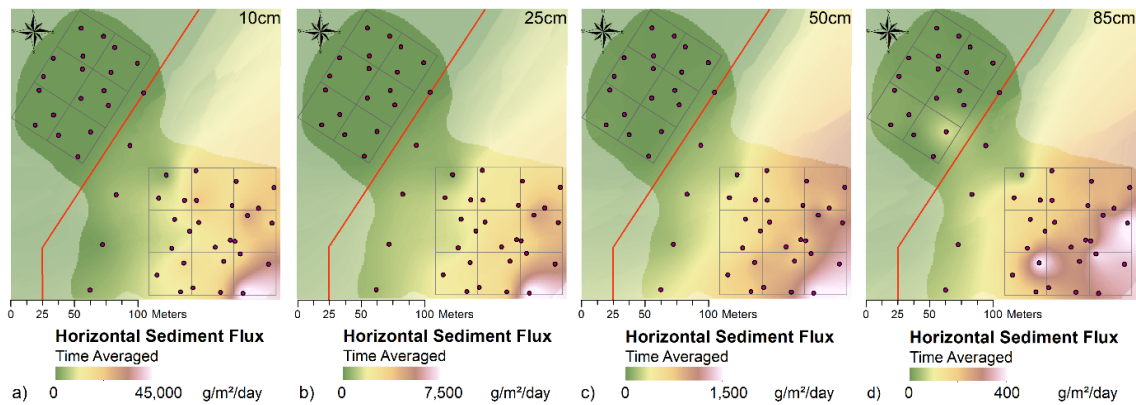


Figure 5.6 Mean horizontal sediment flux for the study at a) 10cm, b) 25cm, c) 50cm and d) 85cm sampling height. The purple dots represent the position of each MWAC dust samplers. Note large differences in sediment flux with height as indicated by different colour scales, ranging from 0 to maximum value.

Sediment movement was low in the unburnt plot and within the first 25-50m from the unburnt stubble, but steadily intensified with direct distance from the burnt-unburnt boundary (Figure 5.6 and 5.7).

As previously reported in other wind erosion studies, we observed that sediment transport rapidly decreased with height. Additionally, we can notice from the legend scale of Figure 5.6 and 5.7 that there is a very large difference in horizontal sediment flux between the collection height of 10cm and the other sampling heights.

5.3.3 Factors influencing horizontal sediment flux

The mixed-effects model allowed detailed examination of main effects and interactions between all the experimental factors (Treatment: unburnt/burnt; direct Distance to the burnt-unburnt boundary; sampling Height; Time: collection period, Table 5.2). Our results indicate that all four variables had a significant impact on total horizontal sediment flux ($p < 0.001$). More specifically, the interaction between treatment type and other individual factors had a significant effect on sediment transport ($p \leq 0.0001$). This

information reflects that the magnitude of sediment transport on the burnt plot compared to the unburnt part of the site varies independently from the collection period or collection height (Figure 5.5 and 5.6). The strongest interaction is that of Treatment x Height. In the burnt area, sediment flux follows an exponential decline, whereas, in the stubble, sediment is lowest in the bottom collection containers. The strong significance underpins this observation. We also observed that the interaction between sampling height and collection period had a significant impact of on total horizontal sediment flux ($p < 0.001$). This finding supports visual patterns in Figure 5.7 where horizontal sediment flux is lower during the third collection period (week 7-9) for all sampling heights, particularly for the 10cm sampling height. This can be expected due to changes in wind speed and direction throughout the experiment. The only significant three-way interaction identified in our model was between treatment type, collection height and time ($p < 0.001$). This indicates that the strongest two-way interaction (*Treatment x Height*) also differs in time. This observation also reflects the stochastic nature of wind causing a significant spatial variability in sediment flux with height.

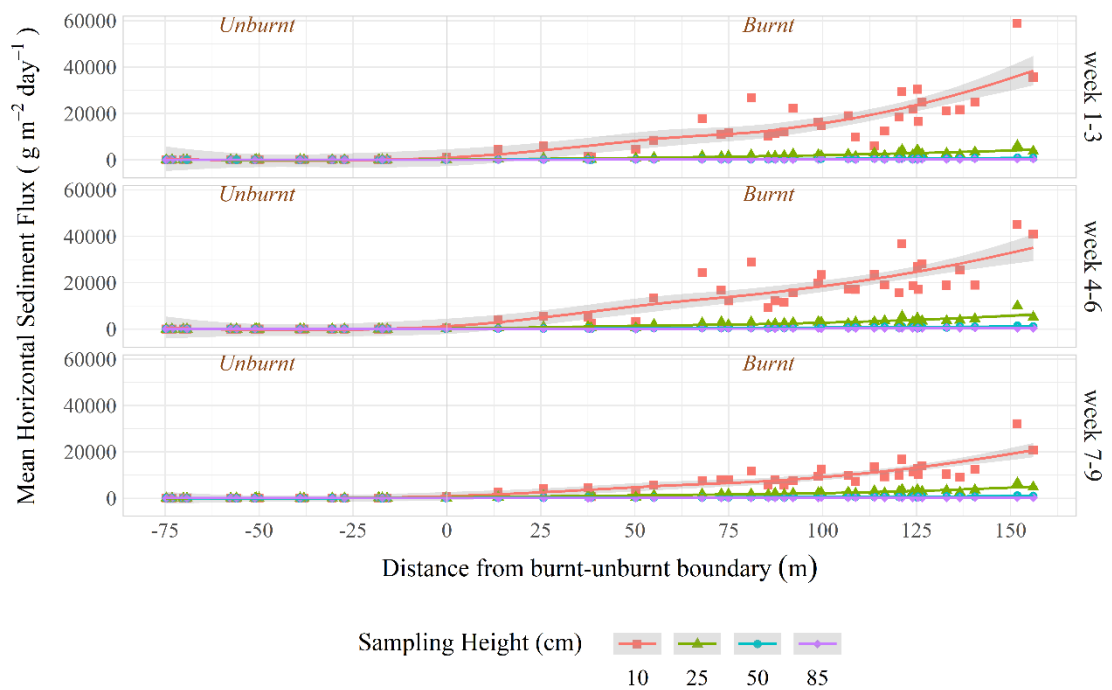


Figure 5.7 Observed horizontal sediment flux distribution with sampling distance from the burnt-unburnt boundary. 95% confidence interval of the LOESS regressions are shown as shaded grey bands.

Table 5.2 Estimated effect of experimental variables on sediment transport, obtained from linear mixed-modelling and Anova Wald Chi-square test, type II.

Source	χ^2	d.f	p-value	Significance
Treatment (unburnt/burnt)	248.0444	1	< 0.0001	***
Dist (distance to burnt-unburnt boundary)	43.7216	1	< 0.0001	***
Height (dust sampling height)	16966.8615	3	< 0.0001	***
Time (collection period)	342.7610	2	< 0.0001	***
Treatment*Dist	14.7704	1	0.0001	***
Treatment*Height	895.4564	3	< 0.0001	***
Treatment*Time	17.7556	2	0.0001	***
Dist*Height	8.2086	3	0.0419	ns
Dist*Time	9.3862	2	0.0092	**
Height*Time	83.3022	6	< 0.0001	***
Treatment*Dist*Height	2.5118	3	0.4731	ns
Treatment*Dist*Time	4.7756	2	0.0918	ns
Treatment*Height*Time	24.8422	6	0.0004	***

(d.f = degree of freedom, ns = not significant, ** = $p < 0.01$, *** = $p < 0.001$)

This significance was investigated further by a comparison of the estimated marginal means of sediment flux grouped by treatment, height, and time (Figure 5.8). Mean horizontal sediment flux was low for all collection periods and all heights on the unburnt plot ($\sim 16 \text{ g m}^{-2} \text{ d}^{-1}$) (Figure 5.8). Conversely, sediment transport was consistently higher on the burnt part of the site ($100 - 8,000 \text{ g m}^{-2} \text{ d}^{-1}$). Flux on the burnt plot was about 300 times larger than on the unburnt part of the site and within a similar order of magnitude of results published by Miller et al. (2012). Within the first four months of their post-fire study, the authors reported mean horizontal sediment fluxes of $\sim 24 \text{ g m}^{-2} \text{ d}^{-1}$ on unburnt sites and $\sim 2,400 \text{ g m}^{-2} \text{ d}^{-1}$ on burnt monitoring sites.

Mean collection rates from our experiment ranged from 0.001 g d^{-1} on the unburnt plot to 0.39 g d^{-1} on the burnt part of the site. These values are comparable to findings from Whicker et al. (2002) where they recorded median collection rates ranging from 0.1 g d^{-1} on unburnt sites to 0.3 g d^{-1} on burnt sites.

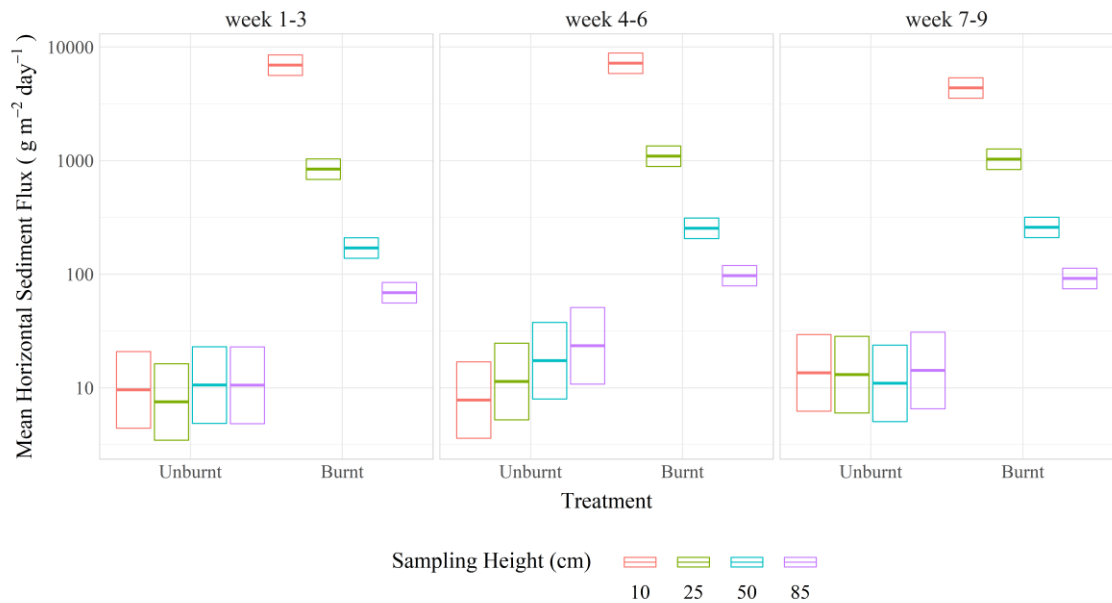


Figure 5.8 Mean horizontal sediment flux derived from modelled estimated marginal means for the three collection periods on burnt and unburnt plots. Estimates are based on log-scale predictions from the model. The mean horizontal sediment flux on the burnt plot rapidly decreased with sampling height for all three collection periods (Figure 5.8), which is consistent in space and time (Figure 5.6 and 5.7). This observation also supports results reported in other wind erosion studies (Bergametti and Gillette, 2010; Gillette and Ono, 2008). Additionally, the difference in sediment transport between the burnt and unburnt plots was highly significant, even at the upper sampling point. We detected a 10-fold difference at 85cm, a 100-fold difference at 50cm and a 1,000-fold difference at 10cm for all collection periods

5.4 Discussion

This work has detected a significant difference in spatial distribution patterns between burnt and unburnt stubble plots after a severe wildfire event. Under the experimental conditions and throughout the three collection periods, we consistently observed a large aeolian sediment transport on the burnt part of the site and minimal sediment flux within the unburnt plot.

Our experimental design was limited by the nature and the pattern of the wildfire, as well as the land management actions required for remediation and erosion mitigation. Finding collaboration partners proved to be challenging given the emotional status of affected landholders. Furthermore, to increase the number of sampling locations, we decided to compromise on sampling directionality. In order to assess spatial patterns of sediment transport in burnt and unburnt areas, we used a simple unidirectional design and focussed on the prevailing wind direction in the region during that time of the year. The performance of our MWAC sediment samplers was thus limited by the fact that they could not face the wind during each wind event causing a potential underestimation of our sediment flux estimates. Based on the literature, the efficiency of our samplers might only be about 20 to 50% (Zobeck, 2002). While our approach reduced comparability with other studies, this proved to be successful for our study objectives, as we repeatedly collected a large amount of sediments on the burnt plot (Figure 5.2c and 5.5), and consistently observed significant spatial distribution patterns of sediment transport regardless of wind speed and wind direction (Figure 5.5 and 5.6)

There were substantial differences in sediment transport in the height profile between the burnt and unburnt plots (Figure 5.8). In the burnt area, our data show a 10-fold difference at 85cm, a 100-fold difference at 50cm and a 1,000-fold difference at 10cm for all collection period, over all wind directions compared to the unburnt patch. These large amounts of sediment observed on the burnt side consistently exhibited exponential decline with height, whereas, over the stubble, height response was flat or increased with height. This is underpinned by the significant three-way interaction of treatment, height, and time. In fact, during the second collection period (weeks 4-6), most sediments were collected in the highest samplers. This indicates a potential influence of stubble on sediment flux as sediments captured on the unburnt part of the site may have originated from the burnt site. The observed inversion of exponential decline detected on the unburnt plot hence supports the supposition that stubble prevented aeolian sediments from forming. Differences of wind speed and direction and sediment load from the burnt

site moving into the unburnt patch may also explain heteroscedasticity between observation points and the need to use mixed models.

The consistent increase of sediment flux with distance from the burnt/unburnt boundary further supports that sediment transport was generated in the burnt patch, while saltation was prevented in the stubble area. Given that the field length was about 300m long by 150m wide, we may not have reached maximum transport carrying capacity. According to Zobeck et al. (2003), a field length of approximately 300m is needed in open agricultural fields with fine sandy loam soils to approach saltation transport capacity and assess total soil loss. However, in their study, horizontal sediment flux continued to increase at distances greater than 350m. This implies that our experimental design may not have sampled the total soil loss from the burnt site, but mainly captured local sediment redistribution instead.

Sediments generated in the burned area may have implications for land management. Sandblasting after a wildfire event may damage emerging seedlings from subsequent annual crops. There is anecdotal evidence from farmers who observed growing tillers to be sheared off in similar settings. Therefore, remediation and crop growth efficiency could be significantly reduced if wind erosion events occur before crop establishment.

We observed patterns of sediments transport within our burnt plot at a scale that is unachievable in controlled experiments. This indicates that field observations, albeit under less controlled conditions, can complement fine-scale experimental studies using wind tunnels to assess environmental processes. Although aeolian transport was very high on the burnt part of the site, it might have approached even higher values outside of our sampling range when maximum transport carrying capacity was reached.

5.5 Conclusion

Wind erosion is a key factor causing land degradation in dryland agricultural regions around the world. In such regions, soil cover is a critical erosion control factor and

conservation agriculture is contributing to erosion mitigation. However, unpredictable extreme environmental disturbances such as wildfires can remove protective vegetation cover and consequently increase soil erosion risk.

In this study, an array of aeolian sediment samplers was established on adjacent burnt and unburnt sections of a paddock to assess relative spatial differences in patterns of sediment transport. This spatial array could be rapidly installed after a severe wildfire and proved to capture the spatial variability of aeolian sediment transport within the sites, regardless of wind velocity and direction.

Our findings indicate that sediment transport was very high and variable within the burnt and bare plots. These results could imply that annual crops sown after the fire may be at risk of sandblasting if one or several erosion events occurred before crop establishment, leading to serious implications for land management and productivity. However, we estimated that sediment transport was greatly reduced within the unburnt stubble plot and its vicinity into the burnt area. Based on our results, we can suggest that strips of remaining unburnt stubble could provide a beneficial effect on adjacent burnt or bare plots. Therefore, any management strategy that adds or maintains roughness elements, such as conservation farming and no-tillage, could reduce the risk of soil loss in degraded environments. Some of these may include strip cropping or soil treatments (e.g. clay spreading, soil mixing), particularly on light sandy soils. Nonetheless, such options may not always be practical or economically viable in agricultural production systems. There will thus be a need to find a balance between soil conservation, agricultural productivity and practicality when it comes to wind erosion management.

Our study also supports the argument that field observations can complement fine-scale experimental studies to assess environmental processes in real-life conditions. Indeed, we measured a large sediment transport on the burnt part of the site, but the scale at which we observed these distribution patterns would not have been detected in wind tunnel experiments.

While our study focused on fire as a cause of soil exposure, extended drought and overgrazing may also produce large patches of bare soils. Here, small areas of remnant vegetation may substantially reduce soil losses.

Acknowledgements

We wish to thank Stephen Jaeschke and his family for their involvement in the project and for supporting our monitoring study on their land despite being personally impacted by the fire. We also want to express our gratitude to Claire Dennerley for her assistance in the field, Steven Delean for his advice on statistical analysis, and the anonymous reviewers, whose suggestions significantly improved the quality of the manuscript. This research was supported by an International Postgraduate Scholarship Award.

5.6 References

- Akaike, H., 1973. Information theory and an extension of the maximum likelihood principle, in: Petrov, B.N., Csaki, F. (Eds.). Akadémiai Kiadó, Budapest, Hungary, pp. 267-281, doi: https://doi.org/10.1007/978-1-4612-1694-0_15.
- Baddock, M.C., Strong, C.L., Leys, J.F., Heidenreich, S.K., Tews, E.K., McTainsh, G.H., 2014. A visibility and total suspended dust relationship. *Atmospheric Environment* 89, 329-336, doi: <https://doi.org/10.1016/j.atmosenv.2014.02.038>.
- Belnap, J., Reynolds, R.L., Reheis, M.C., Phillips, S.L., Urban, F.E., Goldstein, H.L., 2009. Sediment losses and gains across a gradient of livestock grazing and plant invasion in a cool, semi-arid grassland, Colorado Plateau, USA. *Aeolian Research* 1, 27-43, doi: <https://doi.org/10.1016/j.aeolia.2009.03.001>.
- Bennell, M.R., Leys, J.F., Cleugh, H.A., 2007. Sandblasting damage of narrow-leaf lupin (*Lupinus angustifolius* L.): a field wind tunnel simulation. *Soil Research* 45, 119-128, doi: <https://doi.org/10.1071/SR06066>.
- Bergametti, G., Gillette, D., 2010. Aeolian sediment fluxes measured over various plant/soil complexes in the Chihuahuan desert. *Journal of Geophysical Research: Earth Surface* 115, doi: <https://doi.org/10.1029/2009JF001543>.
- Bilbro, J.D., Stout, J.E., 1999. Wind velocity patterns as modified by plastic pipe windbarriers. *Journal of Soil and Water Conservation* 54, 551-556,

- Breshears, D.D., Whicker, J.J., Johansen, M.P., Pinder, J.E., 2003. Wind and water erosion and transport in semi-arid shrubland, grassland and forest ecosystems: Quantifying dominance of horizontal wind-driven transport. *Earth Surface Processes and Landforms* 28, 1189-1209, doi: <https://doi.org/10.1002/esp.1034>.
- Breshears, D.D., Whicker, J.J., Zou, C.B., Field, J.P., Allen, C.D., 2009. A conceptual framework for dryland aeolian sediment transport along the grassland–forest continuum: effects of woody plant canopy cover and disturbance. *Geomorphology* 105, 28-38, doi: <https://doi.org/10.1016/j.geomorph.2007.12.018>.
- Chappell, A., McTainsh, G., Leys, J., Strong, C., 2003. Simulations to optimize sampling of aeolian sediment transport in space and time for mapping. *Earth Surface Processes and Landforms* 28, 1223-1241, doi: doi:10.1002/esp.1036.
- Chappell, A., Webb, N.P., Leys, J.F., Waters, C.M., Orgill, S., Eyres, M.J., 2019. Minimising soil organic carbon erosion by wind is critical for land degradation neutrality. *Environmental Science & Policy* 93, 43-52, doi: <https://doi.org/10.1016/j.envsci.2018.12.020>.
- Clarke, H.G., Smith, P.L., Pitman, A.J., 2011. Regional signatures of future fire weather over eastern Australia from global climate models. *International Journal of Wildland Fire* 20, 550-562, doi: <https://doi.org/10.1071/WF10070>.
- Cornelis, W.M., Gabriels, D., 2005. Optimal windbreak design for wind-erosion control. *Journal of Arid Environments* 61, 315-332, doi: <https://doi.org/10.1016/j.jaridenv.2004.10.005>.
- CSIRO, Bureau of Meteorology, 2015. Climate Change in Australia Information for Australia's Natural Resource Management Regions: Technical Report. CSIRO and Bureau of Meteorology, Australia, https://www.climatechangeinaustralia.gov.au/media/ccia/2.1.6/cms_page_media/168/CCIA_2015_NRM_TechnicalReport_WEB.pdf
- Dukes, D., Gonzales, H.B., Ravi, S., Grandstaff, D.E., Van Pelt, R.S., Li, J., Wang, G., Sankey, J.B., 2018. Quantifying Postfire Aeolian Sediment Transport Using Rare Earth Element Tracers. *Journal of Geophysical Research: Biogeosciences* 123, 288-299, doi: <https://doi.org/10.1002/2017JG004284>.
- Duniway, M.C., Palmquist, E., Miller, M.E., 2015. Evaluating rehabilitation efforts following the Milford Flat Fire: successes, failures, and controlling factors. *Ecosphere* 6, art80, doi: <https://doi.org/10.1890/ES14-00318.1>.
- Farrell, E.J., Sherman, D.J., Ellis, J.T., Li, B., 2012. Vertical distribution of grain size for wind blown sand. *Aeolian Research* 7, 51-61, doi: <https://doi.org/10.1016/j.aeolia.2012.03.003>.
- Gillette, D.A., Ono, D., 2008. Expressing sand supply limitation using a modified Owen saltation equation. *Earth Surface Processes and Landforms* 33, 1806-1813, doi: <https://doi.org/10.1002/esp.1736>.

- Gonçalves, A.B., Vieira, A., Leite, F.F., Martins, J., Silva, D., Soares, V., 2011. ADAPTA CLIMA: adaptation to the effects from climate change in the AVE, 3rd International Meeting of Fire Effects on Soil Properties. Nigp-Univ. Minho e Cegot, pp. 175-180, <http://hdl.handle.net/1822/19983>
- Hagen, L., 1988. New wind erosion model developments in the USDA, 1988 Wind Erosion Conference Proceedings. Texas Tech. University, Lubbock, pp. 11-13,
- Kontos, S., Liora, N., Giannaros, C., Kakosimos, K., Poupkou, A., Melas, D., 2018. Modeling natural dust emissions in the central Middle East: Parameterizations and sensitivity. Atmospheric Environment 190, 294-307, doi: <https://doi.org/10.1016/j.atmosenv.2018.07.033>.
- Li, J., Kandakji, T., Lee, J.A., Tatarko, J., Blackwell, J., Gill, T.E., Collins, J.D., 2018. Blowing dust and highway safety in the southwestern United States: Characteristics of dust emission “hotspots” and management implications. Science of The Total Environment 621, 1023-1032, doi: <https://doi.org/10.1016/j.scitotenv.2017.10.124>.
- Mayaud, J.R., Bailey, R.M., Wiggs, G.F.S., 2017. A coupled vegetation/sediment transport model for dryland environments. Journal of Geophysical Research-Earth Surface 122, 875-900, doi: <https://doi.org/10.1002/2016jf004096>.
- McKenzie, N., Dixon, J., 2006. Monitoring soil condition across Australia. Recommendations from expert panels. Prepared for the National Committee on Soil and Terrain for the National Land and Water Resources Audit, <http://lwa.gov.au/products/pn21340>
- Merino-Martín, L., Field, J.P., Villegas, J.C., Whicker, J.J., Breshears, D.D., Law, D.J., Urgeghe, A.M., 2014. Aeolian sediment and dust fluxes during predominant “background” wind conditions for unburned and burned semiarid grassland: Interplay between particle size and temporal scale. Aeolian Research 14, 97-103, doi: <https://doi.org/10.1016/j.aeolia.2014.02.004>.
- Miller, M.E., Bowker, M.A., Reynolds, R.L., Goldstein, H.L., 2012. Post-fire land treatments and wind erosion – Lessons from the Milford Flat Fire, UT, USA. Aeolian Research 7, 29-44, doi: <https://doi.org/10.1016/j.aeolia.2012.04.001>.
- National Committee on Soil Terrain Committee, 2009. Australian Soil and Land Survey Field Handbook. CSIRO PUBLISHING, Victoria,
- Nordstrom, K.F., Hotta, S., 2004. Wind erosion from cropland solutions in the USA: a review of problems, and prospects. Geoderma 121, 157-167, doi: <https://doi.org/10.1016/j.geoderma.2003.11.012z>.
- Panebianco, J.E., Mendez, M.J., Buschiazzi, D.E., 2016. PM10 Emission, Sandblasting Efficiency and Vertical Entrainment During Successive Wind-Erosion Events: A Wind-Tunnel Approach. Boundary-Layer Meteorology 161, 335-353, doi: <https://doi.org/10.1007/s10546-016-0172-7>.

- Pinheiro, J., Bates, D., DebRoy, S., Sarkar, D., Team, R.D.C., 2018. nlme: Linear and Nonlinear Mixed Effects Models, R package version 3.1-137 ed, <https://CRAN.R-project.org/package=nlme>
- R Development Core Team, 2010. R: A Language and Environment for Statistical Computing. R Foundation for Statistical Computing, Vienna, Austria, <http://www.R-project.org>
- Ravi, S., Baddock, M.C., Zobeck, T.M., Hartman, J., 2012. Field evidence for differences in post-fire aeolian transport related to vegetation type in semi-arid grasslands. *Aeolian Research* 7, 3-10, doi: <http://dx.doi.org/10.1016/j.aeolia.2011.12.002>.
- Retta, A., Armbrust, D.V., Hagen, L.J., 1996. Partitioning of biomass in the crop submodel of WEPS (wind erosion prediction system). *Transactions of the ASAE* 39, 145-151,
- Seinfeld, J.H., Pandis, S.N., 2012. Atmospheric chemistry and physics: from air pollution to climate change. John Wiley & Sons,
- Shao, Y., 2008. Physics and modelling of wind erosion. Springer Science & Business Media,
- Sherman, D.J., Swann, C., Barron, J.D., 2014. A high-efficiency, low-cost aeolian sand trap. *Aeolian Research* 13, 31-34, doi: <https://doi.org/10.1016/j.aeolia.2014.02.006>.
- Tatarko, J., Sporcic, M.A., Skidmore, E.L., 2013. A history of wind erosion prediction models in the United States Department of Agriculture prior to the Wind Erosion Prediction System. *Aeolian Research* 10, 3-8, doi: <https://doi.org/10.1016/j.aeolia.2012.08.004>.
- Turner, D., Lewis, M., Ostendorf, B., 2011. Spatial indicators of fire risk in the arid and semi-arid zone of Australia. *Ecological Indicators* 11, 149-167, doi: <https://doi.org/10.1016/j.ecolind.2009.09.001>.
- Vacek, Z., Rehacek, D., Cukor, J., Vacek, S., Khel, T., Sharma, R.P., Kucera, J., Kral, J., Papaj, V., 2018. Windbreak Efficiency in Agricultural Landscape of the Central Europe: Multiple Approaches to Wind Erosion Control. *Environmental Management* 62, 942-954, doi: <https://doi.org/10.1007/s00267-018-1090-x>.
- Van Jaarsveld, F., 2008. Characterising and mapping of wind transported sediment associated with opencast gypsum mining. Stellenbosch: Stellenbosch University, <http://hdl.handle.net/10019.1/2352>
- Vermeire, L.T., Wester, D.B., Mitchell, R.B., Fuhlendorf, S.D., 2005. Fire and Grazing Effects on Wind Erosion, Soil Water Content, and Soil Temperature. *Journal of Environmental Quality* 34, 1559-1565, doi: <https://doi.org/10.2134/jeq2005.0006>.
- Wagenbrenner, N.S., Germino, M.J., Lamb, B.K., Robichaud, P.R., Foltz, R.B., 2013. Wind erosion from a sagebrush steppe burned by wildfire: Measurements of PM10

and total horizontal sediment flux. *Aeolian Research* 10, 25-36, doi: <https://doi.org/10.1016/j.aeolia.2012.10.003>.

Webb, N., Herrick, J., Van Zee, J., Hugenholtz, C., Zobeck, T., Okin, G., 2015. Standard Methods for Wind Erosion Research and Model Development: Protocol for the National Wind Erosion Research Network. USDA-ARS Jornada Experimental Range, Las Cruces, New Mexico,

<https://winderosionnetwork.org/files/NetworkManual.pdf>

Webb, N.P., Herrick, J.E., Van Zee, J.W., Courtright, E.M., Hugenholtz, C.H., Zobeck, T.M., Okin, G.S., Barchyn, T.E., Billings, B.J., Boyd, R., Clingan, S.D., Cooper, B.F., Duniway, M.C., Derner, J.D., Fox, F.A., Havstad, K.M., Heilman, P., LaPlante, V., Ludwig, N.A., Metz, L.J., Nearing, M.A., Norfleet, M.L., Pierson, F.B., Sanderson, M.A., Sharratt, B.S., Steiner, J.L., Tatarko, J., Tedela, N.H., Toledo, D., Unnasch, R.S., Van Pelt, R.S., Wagner, L., 2016. The National Wind Erosion Research Network: Building a standardized long-term data resource for aeolian research, modeling and land management. *Aeolian Research* 22, 23-36, doi: <http://dx.doi.org/10.1016/j.aeolia.2016.05.005>.

Whicker, J.J., Breshears, D.D., Wasiolek, P.T., Kirchner, T.B., Tavani, R.A., Schoep, D.A., Rodgers, J.C., 2002. Temporal and Spatial Variation of Episodic Wind Erosion in Unburned and Burned Semiarid Shrubland. *Journal of Environmental Quality* 31, 599-612, doi: <https://doi.org/10.2134/jeq2002.5990>.

Whicker, J.J., Pinder, J.E., Breshears, D.D., 2006. Increased wind erosion from forest wildfire: Implications for contaminant-related risks. *Journal of Environmental Quality* 35, 468-478, doi: <https://doi.org/10.2134/jeq2005.0112>.

Williams, R.J., Bradstock, R.A., Cary, G.J., Enright, N.J., Gill, A.M., Liedloff, A.C., Lucas, C., Whelan, R.J., Andersen, A.N., Bowman, D.M.J.S., Clarke, P.J., Cook, G.D., Hennessy, K.J., York, A., 2009. Interactions between climate change, fire regimes and biodiversity in Australia - a preliminary assessment. Department of Climate Change,

Department of the Environment, Water, Heritage and the Arts, Canberra, <http://researchrepository.murdoch.edu.au/id/eprint/14926>

Wilson, S., Cooke, R., 1980. Wind erosion, Kirby, M.J, Morgan, R.P.C. (Eds.), *Soil erosion*. Wiley, Chichester, pp. 217-251,

Zobeck, T., 2002. Field measurement of erosion by wind, *Encyclopedia of Soil Science*, Marcel Dekker, Inc., New York, pp. 503-507,

Zobeck, T.M., Sterk, G., Funk, R., Rajot, J.L., Stout, J.E., Van Pelt, R.S., 2003. Measurement and data analysis methods for field-scale wind erosion studies and model validation. *Earth Surface Processes and Landforms* 28, 1163-1188, doi: <https://doi.org/10.1002/esp.1033>.

Chapter 6

Discussion

Soil erosion modelling is a valuable tool for decision-makers as it can be tested under a wide range of conditions. Prediction models for wind and water erosion assessment differ in the complexity of the processes examined and the type of input data required. The high spatial and temporal variability of factors causing erosion and the difficulty to source model drivers that realistically represent these factors in its spatial and temporal complexity make the prediction of erosion trends very difficult. To overcome these limitations, we need detailed data and access to high spatio-temporal datasets to be able to give the best assessment of soil losses and identify regions at risk of erosion in the future. Especially in low rainfall zones, where erosion rates may be affected by the combined impact of wind and water erosion (Field et al., 2011). However, the impact of these two environmental processes is still widely assessed separately (Borrelli et al., 2020). Dryland ecosystems are highly sensitive to environmental disturbances (e.g. droughts, overgrazing, fires) which can dramatically increase soil erosion susceptibility. Unfortunately, these threats, particularly wildfires, are likely to be more frequent in the future due to climate change, land management practices and planning. Fire is recognised as a significant driver of erosion, requiring model-based tools for assessing post-fire erosion and for decision support management.

This thesis aims to demonstrate the benefits of a joint wind-water-erosion modelling approach to identify the spatio-temporal variability of extreme erosion events in the South Australian agricultural zone and the likely increase of variability in the face of climate change and the recurrence of wildfires.

The Eyre Peninsula and Mid-North agricultural regions of South Australia are an ideal study area for such an investigation due to their historical susceptibility to wind and water erosion and because the climatic conditions make this region a fire-prone landscape. This allowed us to demonstrate that erosion models capture the relative spatio-temporal variability of extreme wind and water erosion events for a wide range of land cover over large regions (Chapter 2 and 3). This research also demonstrates the importance of using an integrated modelling approach to estimate the impact of wind

and water erosion for post-fire assessment as an increase in both erosion types was predicted either sequentially or simultaneously after catastrophic wildfires (Chapter 4).

6.1 Key findings

Empirical erosion models can capture spatial and temporal variability of extreme erosion events

With the best spatio-temporal climate, ground cover, soils and elevation datasets for Australia, Chapter 2 and 3 (i) explored the spatio-temporal variability of extreme wind and water erosion events for a wide range of land cover and (ii) described the complex interactions between erosion processes and influencing factors (e.g. climate conditions, and vegetation cover). To the best of our knowledge, this study is the first one to examine the relative assessment of wind and water erosion frequency for agricultural regions of Australia. It provides valuable insight on erosion severity for the management of natural and dryland agricultural environments. Our results can now be used to set land management targets tailored to specific Local Government Areas of South Australia. The most relevant findings of our study were as follows.

- The G2 and “albedo” erosion models satisfactorily captured the spatial and temporal variability of extreme erosion events for the Eyre Peninsula and Mid-North regions. Severe monthly water erosion generally occurred during the summer months (December - February) and late autumn (May and June) for both regions (Figure 2.7). On the other hand, extreme monthly soil loss from wind occurred during the autumn (May-June) and winter months (July-September) for the Eyre Peninsula, and during the summer (Dec-Feb) and late autumn (May-June) for the Mid-North (Figure 3.10). For both processes, annual severe soil loss was extremely variable between the years and did not occur in the same years for the two regions (Figure 2.8 and 3.11). Nonetheless, more extreme erosion events were recorded at the beginning and the very end of the Australian ‘Millennium Drought’.

- We identified that these extreme events consistently occurred with a combination of low ground cover (< 50%) and extreme weather events (erosive rainfall or strong wind gusts) (Figure 2.8 and 3.13).
- The variability in erosion severity was consistent with locally recorded events and land at risk of erosion (DEW, 2017a, b). However, absolute erosion rates still require validation.

An integrated wind-water erosion modelling approach is critical for dryland ecosystems

Parts of the Eyre Peninsula and Mid-North regions are historically prone to wind and water erosion, so it is essential to consider both processes simultaneously to inform land management decisions. Based on results from Chapters 2 and 3, Chapter 4 identified regions that were the most severely affected by wind, water or both erosion types. Although the South Australian government already produced soil erosion susceptibility maps (based on inherent soil susceptibility, terrain and topography) (DEW, 2017a, b), this new version included seasonal changes in vegetation and climate variables. Chapter 4 also characterised changes in relative wind and water erosion severity post-fire in dryland agricultural landscapes. The key findings for this study were the following.

- Considering wind and water erosion simultaneously provided the opportunity to realistically assess the regional erosion susceptibility and enabled the identification of regions where the two processes overlapped. Erosion susceptibility was low for the vast majority of the study area, while 4% and 9% of the total area suffered severe erosion by water and wind respectively. However, a very small fraction of the region (0.7%) was severely impacted by both erosion types (Figure 4.8).
- Soil erosion severity generally increased within the first six months following a fire event. We also identified that regions with low wind or water erosion severity could experience an increase in both erosion types in consecutive months or at

the same time (Figure 4.9 and 4.10). Therefore, considering the two processes simultaneously was essential to get a complete picture of the total erosion severity in fire-affected regions.

Unburnt stubble patches can limit sediment transport in fire-affected landscapes

Dead, shallow vegetation cover distinctly influences aeolian sediment transport (McKenzie et al., 2017; Vacek et al., 2018). However, even with the best management practices, catastrophic events and major types of disturbances such as wildfires are uncontrollable and can destroy the protective non-photosynthetic vegetation cover and increase erosion risk (Edwards et al., 2019; Mayaud et al., 2017). Using a simple sediment sampling set-up (Webb et al., 2016) Chapter 5 examined the influence of unburnt stubble patches on adjacent burnt or bare plots. This field study allowed a quantitative assessment of spatial and temporal patterns of wind erosion and sediment transport after a catastrophic wildfire event. The most relevant findings of our study were as follows.

- The results showed very high levels of spatial variability of erosion processes between burnt and bare patches (Figure 5.5 and 5.6) regardless of wind speed and direction (Figure 5.4).
- Sediment transport was very high and variable in the burnt and bare plot. At the same time, it was significantly reduced within the unburnt stubble and its vicinity into the burnt area (Figure 5.7). Although we focussed on fire as a cause of soil exposure, extended drought and overgrazing may also produce large patches of bare soils. Here, small areas of remnant vegetation may substantially reduce soil losses on adjacent burnt or bare plots.
- This study also supports the argument that field observations can complement fine-scale experimental studies to assess environmental processes in real-life conditions. We measured large sediment transport on the burnt part of the site,

but the scale at which we observed these distribution patterns would not have been detected in wind tunnel experiments.

6.2 Significance and broader implications

Findings from this thesis highlight that soil erosion models are valuable tools to test the influence of climate change and extreme environmental conditions scenarios on soil erosion for a wide range of land cover over large regions. Results from these models can then inform corrective measures for future land management.

The identification of the inter- and intra-regional variability in erosion severity (Chapter 2 and 3) can help management authorities to focus on problem areas and set specific erosion control targets for each Local Government Areas tailored to their unique landscape and sub-regional conditions. This knowledge is particularly useful for land management under future uncertainty.

Given the current predictions on the frequency and severity of future fire weather, there is a strong demand for model-based tools for predicting post-fire erosion response. The models tested here provided encouraging results and proved to capture well changes in post-fire erosion by wind and water. However, further testing and validation are required to ensure the models integrate post-fire change correctly (e.g. changes in soil erodibility for fire-affected sites). This method could then be used to target remedial (on-ground) activities to reduce soil loss and protect watercourses, dams, and livelihood of the community.

The integrated modelling approach presented in this thesis is automated and could be easily modified to test a variety of future scenarios (e.g. changes in land management, drier climate, extended droughts, more recurrent rain-storm events, advances in precision agriculture or other innovative technology). This flexibility also allows for the adjustment of major contributing factors such as inherent soil and landscape properties, land management practices, and climatic and weather events, to test their contribution

towards regional wind and water erosion rates. This knowledge could then be used by management authorities to inform corrective measures for future land management.

Although we focussed on the Eyre Peninsula and Mid-North regions, the modelling approach could be expanded to the rest of the Australian agricultural zone and the Australian Rangelands. All the input data can be freely sourced Australia-wide, and similar datasets are available globally.

6.3 Key assumptions and limitations

As the statistician George Box quoted: “All models are wrong, but some are useful. The practical question is how wrong do they have to be to not be useful” (Box, 1976). Being able to describe relative spatial differences, trends over times and systems reactions to processes and management is critical for erosion modelling (Alewell et al., 2019). The role of modelling at the regional scale cannot be to accurately predict point (or field) measurements of erosion but rather to test hypotheses about process understanding to develop scenarios to assist in policy and strategy development.

The models' results from this study, corresponded well with previous observations (Figure 2.10). This corroborates the benefit of soil erosion modelling for land management and scenario testing, and supports that the models provide a realistic estimate of the spatial and temporal variability. However, error in absolute rates of erosion magnitude could not be quantitatively assessed.

The “albedo” Wind Erosion Model was previously tested under Australian conditions (Chappell and Webb, 2016; Chappell et al., 2018) and validated with field data from standard plots in the US (Chappell and Webb, 2016; Webb et al., 2016). We were also able to demonstrate correspondence of predicted pattern with independent observations of MODIS satellite Aerosol Optical Depth (AOD) (Figure 3.16). On the other hand, the G2 water erosion was not tested under Australian conditions, but we applied corrections

to model parameters based on recommendations from published literature (Yang, 2015; Yang et al., 2017), where these parameters were correlated against field measurements.

6.4 Future research and general recommendations

Modelled soil erosion magnitudes strongly depend on how the influence of erosion controlling parameters is implemented in the models, making it difficult to set absolute quantitative soil loss targets for land management. However, the need for spatial validation of modelled outputs remains.

For instance, Bayesian validation methods could be employed to correlate qualitative field observations (presence/absence of erosion) with modelled erosion estimates. Fantappie et al. (2019) used local records of the presence or absence of erosion from 6,150 sites in Sicily (Italy) to validate their USLE model outputs. The authors reclassified their erosion maps to create maps of predicted presence/absence of erosion and correlated them with the local observations. Using the Bayes theorem (Lesaffre and Lawson, 2012), they estimated the model's positive predictivity, meaning the probability for erosion to occur where the model predicted it, and the model's negative predictivity, meaning the probability for erosion absence where the model predicted the absence of erosion. Their analysis showed that the model performed well, with a capacity to predict the presence of erosion 80% of the time. In comparison, the absence of erosion was correctly estimated 60% of the time. A similar method could be applied in South Australia with the Soil Erosion Protection Field Surveys conducted four times a year by the Department for Environment and Water (Forward, 2011). These road-side surveys document the extent of erosion features and spatial patterns of inherent risk. Using this data to validate erosion models will be further investigated.

Another way to validate quantitative predictions of soil erosion at a smaller scale would be to use simple set-ups such as those presented in Chapter 5. Similar standardised sampling methods are already broadly adopted in the US (Webb et al., 2016; Webb et al., 2017), parts of Australia (Leys et al., 2008) and Germany (Nerger et al., 2017).

Monitoring results have then been compared with prediction modelling for calibration and validation of erosion models (Chappell and Webb, 2016; Edwards et al., 2018; Leys et al., 2010; Nerger et al., 2017). In Australia, the DustWatch community project (Leys et al., 2008) has been used for development and validation of the CEMSYS model (Leys et al., 2010) to predict annual wind erosion and dust concentration over large areas (spatial resolution: 50km). This project was initiated in 2002 by the NSW Office of Environment and Heritage. It consists of instrumented sites: Dust Watch Nodes (DWN) scattered across New South Wales (40 locations, including 2 in South Australia and 3 in Victoria), operated and maintained by community volunteers (DustWatchers). Observers report the date and time of the observation, type of dust event (i.e. local or regional), visibility, the colour of the dust, wind direction and speed, and make other comments and take photographs. Each DWN also records PM₁₀ levels with DustTrak® sensors and sample total suspended sediments with high-volume air samplers. All these observations are then compiled into monthly reports which can be accessed through the NSW Department of Planning, Industry and Environment website (NSW DPI, 2020). Although the current network is limited to the state of NSW, other initiatives could see the light of day if there was a proven need for aeolian sediment transport monitoring in other parts of Australia. As the DWN instrumentation is quite costly, simpler sampling devices such as those presented in Chapter 5 could prove to be a good compromise. However, such an undertaking would still be relying on community volunteers and on a project coordinator to ensure that all measurements follow standardised procedures (Webb et al., 2016).

Remote sensing technologies (i.e. satellite sensors and Unmanned Aerial Vehicles (UAVs)) are developing rapidly, and so are their spatial and temporal resolutions. In a world where precision agriculture and smart-technologies are fast-expanding, these could potentially be used as proxies to validate erosion patterns at local and regional scales. For instance, Aerosol Optical Depth (AOD) has been used extensively to locate dust sources (Ginoux et al., 2010; Li and Sokolik, 2018) and estimate PM₁₀ and PM_{2.5} concentrations (Chudnovsky et al., 2014; Shin et al., 2020). However, limited research

has considered AOD as a proxy for wind erosion assessment (Najafpour et al., 2018; Pu et al., 2020; Rayegani et al., 2020) or wind erosion model validation (Fenta et al., 2020). In this thesis, we tested the applicability of a MODIS AOD product to validate spatial patterns of wind erosion (Chapter 3), and investigated whether AOD measurements could provide complementary information to post-fire wind erosion assessment (Chapter 4). We demonstrated that the frequency of dust storms derived from MODIS AOD can provide a satisfactory level of model validation (Figure 3.16) and compared well with previous erosion susceptibility maps (DEW, 2017b). Although the use of the MODIS AOD dataset for post-fire wind erosion monitoring was preliminary work, the frequency of dust days method correlated well with locally observed dust events following major wildfires (Figure 4.10). However, more validation and correlation analysis are needed to apply this technique with more confidence. Based on these promising results, further work could be implemented to investigate the applicability of AOD measurements for models validation and post-fire erosion monitoring.

UAVs mounted with high-resolution cameras can produce very high-resolution (< 1cm) Digital Surface Models (DSMs). Researchers have already investigated the use of such technology to monitor soil erosion at the field scale (d'Oleire-Oltmanns et al., 2012; Peternel et al., 2017; Pineux et al., 2017). However, these very high-resolution DSM could also be beneficial to estimate changes in surface conditions after catastrophic events (e.g. wildfires, landslides) when sites are not easily accessible. These estimates could also be correlated to post-fire erosion predictions and contribute to the validation of erosion models in such conditions.

In conclusion, this thesis has provided a proof of concept for an integrated wind-water erosion modelling approach for agricultural landscapes of South Australia and demonstrated that models are valuable tools to test the influence of climate change and extreme environmental conditions scenarios on soil erosion. With further development and validation, this integrated approach can be expanded to other parts of Australia or other regions of the globe as all input data can be freely sourced Australia-wide, and similar datasets are available globally.

6.5 References

- Alewell, C., Borrelli, P., Meusburger, K., Panagos, P., 2019. Using the USLE: Chances, challenges and limitations of soil erosion modelling. *International Soil and Water Conservation Research* 7, 203-225, doi: <https://doi.org/10.1016/j.iswcr.2019.05.004>.
- Borrelli, P., Alewell, C., Alvarez, P., Anache, J.A.A., Baartman, J., Ballabio, C., Bezak, N., Biddoccu, M., Cerda, A., Chalise, D., Chen, S., Chen, W., Girolamo, A.M.D., Gessesse, G.D., Deumlich, D., Efthimiou, N., Erpul, G., Fiener, P., Freppaz, M., Gentile, F., Gericke, A., Haregeweyn, N., Hu, B., Jeanneau, A., Kaffas, K., Kiani-Harchegani, M., Villuendas, I.L., Li, C., Lombardo, L., López-Vicente, M., Lucas-Borja, M.E., Märker, M., Matjaž, M., Miao, C., Modugno, S., Möller, M., Naipal, V., Nearing, M., Owusu, S., Panday, D., Patault, E., Patriche, C.V., Poggio, L., Portes, R., Quijano, L., Rahdari, M.R., Renima, M., Ricci, G.F., Rodrigo-Comino, J., Saia, S., Samani, A.N., Schillaci, C., Syrris, V., Kim, H.S., Spinola, D.N., Oliveira, P.T., Teng, H., Thapa, R., Vantas, K., Vieira, D., Yang, J.E., Yin, S., Zema, D.A., Zhao, G., Panagos, P., 2020. Soil erosion modelling: A global review and statistical analysis, *Earth-Science Reviews*,
- Box, G.E.P., 1976. Science and Statistics. *Journal of the American Statistical Association* 71, 791-799, doi: <https://doi.org/10.1080/01621459.1976.10480949>.
- Chappell, A., Webb, N., 2016. Using albedo to reform wind erosion modelling, mapping and monitoring. *Aeolian Research* 23, 63-78, doi: <https://doi.org/10.1016/j.aeolia.2016.09.006>.
- Chappell, A., Webb, N.P., Guerschman, J.P., Thomas, D.T., Mata, G., Handcock, R.N., Leys, J.F., Butler, H.J., 2018. Improving ground cover monitoring for wind erosion assessment using MODIS BRDF parameters. *Remote Sensing of Environment* 204, 756-768, doi: <https://doi.org/10.1016/j.rse.2017.09.026>.
- Chudnovsky, A.A., Koutrakis, P., Kloog, I., Melly, S., Nordio, F., Lyapustin, A., Wang, Y.J., Schwartz, J., 2014. Fine particulate matter predictions using high resolution Aerosol Optical Depth (AOD) retrievals. *Atmospheric Environment* 89, 189-198, doi: <https://doi.org/10.1016/j.atmosenv.2014.02.019>.
- d'Oleire-Oltmanns, S., Marzloff, I., Peter, K.D., Ries, J.B., 2012. Unmanned Aerial Vehicle (UAV) for Monitoring Soil Erosion in Morocco. *Remote Sensing* 4, 3390-3416, doi: <https://www.doi.org/10.3390/rs4113390>.
- DEW, 2017a. Soil Water Erosion Potential. Government of South Australia, Department for Environment and Water, <https://data.sa.gov.au/data/dataset/water-erosion-grid>

- DEW, 2017b. Soil Wind Erosion Potential. Government of South Australia, Department for Environment and Water, <https://data.sa.gov.au/data/dataset/wind-erosion-grid>
- Edwards, B.L., Nicholas, W., McCord, S.E., 2018. AERO: A wind erosion modeling framework with applications to monitoring data, 73rd Soil and Water Conservation Society Annual Conference, Albuquerque, USA,
- Edwards, B.L., Webb, N.P., Brown, D.P., Elias, E., Peck, D.E., Pierson, F.B., Williams, C.J., Herrick, J.E., 2019. Climate change impacts on wind and water erosion on US rangelands. *Journal of Soil and Water Conservation* 74, 405-418, doi: <https://doi.org/10.2489/jswc.74.4.405>.
- Fantappie, M., Costantini, E.A.C., Priori, S., 2019. Calibration and validation of an USLE model to map soil erosion by water in the Sicilian Region (Italy), Global Symposium on Soil Erosion, FAO headquarters, Rome, Italy,
- Fenta, A.A., Tsunekawa, A., Haregeweyn, N., Poesen, J., Tsubo, M., Borrelli, P., Panagos, P., Vanmaercke, M., Broeckx, J., Yasuda, H., Kawai, T., Kurosaki, Y., 2020. Land susceptibility to water and wind erosion risks in the East Africa region. *Science of The Total Environment* 703, 135016, doi: <https://doi.org/10.1016/j.scitotenv.2019.135016>.
- Field, J.P., Breshears, D.D., Whicker, J.J., Zou, C.B., 2011. On the ratio of wind- to water-driven sediment transport: Conserving soil under global-change-type extreme events. *Journal of Soil and Water Conservation* 66, 51A-56A, doi: <https://doi.org/10.2489/jswc.66.2.51A>.
- Forward, G., 2011. Soil Erosion Protection Field Survey Manual - Agricultural cropping districts. Government of South Australia, Department of Environment Water and Natural Resources - Landscape Conservation Branch,
- Ginoux, P., Garbuzov, D., Hsu, N.C., 2010. Identification of anthropogenic and natural dust sources using Moderate Resolution Imaging Spectroradiometer (MODIS) Deep Blue level 2 data. *Journal of Geophysical Research: Atmospheres* 115, doi: <https://doi.org/10.1029/2009jd012398>.
- Lesaffre, E., Lawson, A.B., 2012. Bayesian biostatistics. John Wiley & Sons,
- Leys, J., McTainsh, G., Strong, C., Heidenreich, S., Biesaga, K., 2008. DustWatch: using community networks to improve wind erosion monitoring in Australia. *Earth Surface Processes and Landforms* 33, 1912-1926, doi: <https://doi.org/10.1002/esp.1733>.
- Leys, J.F., Butler, H.J., Yang, X., Heidenreich, S., 2010. CEMSYS modelled wind erosion.
- Li, L., Sokolik, I.N., 2018. Analysis of Dust Aerosol Retrievals Using Satellite Data in Central Asia. *Atmosphere* 9, 288, <https://www.mdpi.com/2073-4433/9/8/288>

- Mayaud, J.R., Bailey, R.M., Wiggs, G.F.S., 2017. A coupled vegetation/sediment transport model for dryland environments. *Journal of Geophysical Research-Earth Surface* 122, 875-900, doi: <https://doi.org/10.1002/2016jf004096>.
- McKenzie, N., Hairsine, P., Gregory, L.J., Austin, J., Baldock, J., Webb, M., Mewett, J., Cresswell, H., Welti, N., Thomas, M., 2017. Priorities for improving soil condition across Australia's agricultural landscapes, Report prepared for the Australian Government Department of Agriculture and Water Resources. CSIRO, Australia,
- Najafpour, N., Afshin, H., Firoozabadi, B., 2018. The 20–22 February 2016 Mineral Dust Event in Tehran, Iran: Numerical Modeling, Remote Sensing, and In Situ Measurements. *Journal of Geophysical Research: Atmospheres* 123, 5038-5058, doi: <https://doi.org/10.1029/2017jd027593>.
- Nerger, R., Funk, R., Cordsen, E., Fohrer, N., 2017. Application of a modeling approach to designate soil and soil organic carbon loss to wind erosion on long-term monitoring sites (BDF) in Northern Germany. *Aeolian Research* 25, 135-147, doi: <https://doi.org/10.1016/j.aeolia.2017.03.006>.
- NSW DPI, 2020. DustWatch publications. NSW Department of Planning, Industry and Environment, NSW Government, <https://www.environment.nsw.gov.au/Topics/Land-and-soil/Soil-degradation/Wind-erosion/Community-DustWatch/DustWatch-publications>
- Peternel, T., Kumelj, S., Ostir, K., Komac, M., 2017. Monitoring the Potoska planina landslide (NW Slovenia) using UAV photogrammetry and tachymetric measurements. *Landslides* 14, 395-406, doi: <https://doi.org/10.1007/s10346-016-0759-6>.
- Pineux, N., Lisein, J., Swerts, G., Biielders, C.L., Lejeune, P., Colinet, G., Degre, A., 2017. Can DEM time series produced by UAV be used to quantify diffuse erosion in an agricultural watershed? *Geomorphology* 280, 122-136, doi: <https://doi.org/10.1016/j.geomorph.2016.12.003>.
- Pu, B., Ginoux, P., Guo, H., Hsu, N.C., Kimball, J., Marticorena, B., Malyshev, S., Naik, V., O'Neill, N.T., Pérez García-Pando, C., Paireau, J., Prospero, J.M., Shevliakova, E., Zhao, M., 2020. Retrieving the global distribution of the threshold of wind erosion from satellite data and implementing it into the Geophysical Fluid Dynamics Laboratory land-atmosphere model (GFDL AM4.0/LM4.0). *Atmos. Chem. Phys.* 20, 55-81, doi: <https://doi.org/10.5194/acp-20-55-2020>.
- Rayegani, B., Barati, S., Goshtasb, H., Gachpaz, S., Ramezani, J., Sarkheil, H., 2020. Sand and dust storm sources identification: A remote sensing approach. *Ecological Indicators* 112, 106099, doi: <https://doi.org/10.1016/j.ecolind.2020.106099>.
- Shin, M., Kang, Y., Park, S., Im, J., Yoo, C., Quackenbush, L.J., 2020. Estimating ground-level particulate matter concentrations using satellite-based data: a review. *GIScience & Remote Sensing* 57, 174-189, doi: <https://doi.org/10.1080/15481603.2019.1703288>.

- Vacek, Z., Rehacek, D., Cukor, J., Vacek, S., Khel, T., Sharma, R.P., Kucera, J., Kral, J., Papaj, V., 2018. Windbreak Efficiency in Agricultural Landscape of the Central Europe: Multiple Approaches to Wind Erosion Control. *Environmental Management* 62, 942-954, doi: <https://doi.org/10.1007/s00267-018-1090-x>.
- Webb, N.P., Herrick, J.E., Van Zee, J.W., Courtright, E.M., Hugenholtz, C.H., Zobeck, T.M., Okin, G.S., Barchyn, T.E., Billings, B.J., Boyd, R., Clingan, S.D., Cooper, B.F., Duniway, M.C., Derner, J.D., Fox, F.A., Havstad, K.M., Heilman, P., LaPlante, V., Ludwig, N.A., Metz, L.J., Nearing, M.A., Norfleet, M.L., Pierson, F.B., Sanderson, M.A., Sharratt, B.S., Steiner, J.L., Tatarko, J., Tedela, N.H., Toledo, D., Unnasch, R.S., Van Pelt, R.S., Wagner, L., 2016. The National Wind Erosion Research Network: Building a standardized long-term data resource for aeolian research, modeling and land management. *Aeolian Research* 22, 23-36, doi: <http://dx.doi.org/10.1016/j.aeolia.2016.05.005>.
- Webb, N.P., Van Zee, J.W., Karl, J.W., Herrick, J.E., Courtright, E.M., Billings, B.J., Boyd, R., Chappell, A., Duniway, M.C., Derner, J.D., Hand, J.L., Kachergis, E., McCord, S.E., Newingham, B.A., Pierson, F.B., Steiner, J.L., Tatarko, J., Tedela, N.H., Toledo, D., Scott Van Pelt, R., 2017. Enhancing Wind Erosion Monitoring and Assessment for U.S. Rangelands. *Rangelands* 39, 85-96, doi: <https://doi.org/10.1016/j.rala.2017.04.001>.
- Yang, X., 2015. Digital mapping of RUSLE slope length and steepness factor across New South Wales, Australia. *Soil Research* 53, 216-225, doi: <http://dx.doi.org/10.1071/SR14208>.
- Yang, X., Gray, J., Chapman, G., Zhu, Q., Tulau, M., McInnes-Clarke, S., 2017. Digital mapping of soil erodibility for water erosion in New South Wales, Australia. *Soil Research* 56, 158-170, doi: <https://doi.org/10.1071/SR17058>.